

UNIVERSITÀ DEGLI STUDI DI MILANO

CORSO DI DOTTORATO

MEDICINA TRASLAZIONALE

DIPARTIMENTO DI SCIENZE BIOMEDICHE PER LA SALUTE

TESI DI DOTTORATO DI RICERCA

INVESTIGATING THE INVOLVEMENT OF β -GLUCOCEREBROSIDASE DEFICIENCY
IN THE ONSET OF NEURODEGENERATION

BIO/10

DOTTORANDA

Emma Veronica CARSANA

TUTOR

Prof. Massimo AURELI

COORDINATORE DEL DOTTORATO

Prof.ssa Chiarella SFORZA

A.A.

2021/2022

INDEX

1. ABSTRACT	- 5 -
2. INTRODUCTION	- 8 -
2.1. Lipids in the Central Nervous System	- 9 -
2.1.1. Cholesterol and Phospholipids	- 9 -
2.1.2. Sphingolipids	- 9 -
2.1.2.1. Structure and chemical-physical properties	- 9 -
2.1.2.2. Sphingolipids' metabolism	- 13 -
2.1.2.2.1. Sphingolipids biosynthesis	- 14 -
2.1.2.2.1.1. De novo biosynthesis of ceramide	- 14 -
2.1.2.2.1.2. Ceramide obtained from the sphingosine recycling/ salvage pathway	- 15 -
2.1.2.2.1.3. Complex sphingolipid biosynthesis	- 15 -
2.1.2.2.2. Trafficking of sphingolipids	- 16 -
2.1.2.2.3. Catabolism of sphingolipids at lysosomal and PM level	- 17 -
2.1.2.2.3.1. Sphingolipid hydrolases	- 19 -
2.1.2.2.3.1.1. β - galactosidases	- 20 -
2.1.2.2.3.1.2. β - hexosaminidases	- 21 -
2.1.2.2.3.1.3. Sialidases	- 23 -
2.1.2.2.3.1.4. β - glucocerebrosidases	- 24 -
2.1.2.2.3.1.5. Mannosidases	- 25 -
2.2. Sphingolipids in neuronal differentiation	- 26 -
2.3. Lysosomal storage disorders	- 29 -
2.3.1. <i>GBA</i> - related pathologies	- 33 -
2.3.1.1. Gaucher Disease	- 33 -
2.3.1.2. <i>GBA</i> - dependent Parkinson's Disease	- 34 -
2.4. <i>In vitro</i> models for Parkinson's Disease and neuronopathic Gaucher Disease	- 35 -
2.5. Brain metabolism	- 36 -
2.5.1. Glucose metabolism	- 37 -
3. AIM	- 38 -
4. METHODS	- 40 -
4.1. Brain areas isolation	- 41 -
4.2. Cell culture of induced pluripotent stem cells (iPSCs)	- 41 -
4.3. IPSC characterization	- 41 -
4.3.1. Real-time PCR (qPCR)	- 41 -
4.3.1.1. RNA extraction	- 41 -
4.3.1.2. Quantification of extracted RNA by UV absorption	- 42 -
4.3.1.3. RT-PCR	- 42 -

4.3.1.4.	qPCR	_____	- 42 -
4.3.2.	Karyotype analysis	_____	- 43 -
4.4.	IPSCs differentiation into dopaminergic neurons	_____	- 43 -
4.5.	Primary culture of mouse cerebellar granule neurons	_____	- 44 -
4.6.	Cell treatment with conduritol B epoxide	_____	- 45 -
4.7.	Cell treatment with glucosylsphingosine	_____	- 45 -
4.8.	Treatment of CGNs with [³H (sphingosine)]- GM1	_____	- 46 -
4.9.	Cell viability assays	_____	- 46 -
4.9.1.	Calcein assay	_____	- 46 -
4.9.2.	MTT assay	_____	- 47 -
4.10.	Samples preparation	_____	- 47 -
4.11.	Identification of the protein content	_____	- 47 -
4.11.1.	Determination of protein content through DC protein assay	_____	- 48 -
4.11.2.	Indirect immunofluorescence experiments	_____	- 48 -
4.11.3.	Immunoblotting	_____	- 49 -
4.11.4.	Detection of biotinylated proteins	_____	- 50 -
4.11.5.	Proteomic analysis	_____	- 50 -
4.11.6.	Nuclear purification from DA neurons and CGNs	_____	- 52 -
4.11.7.	LysoTracker staining	_____	- 52 -
4.12.	Evaluation of enzymatic activities	_____	- 53 -
4.12.1.	Evaluation of enzymatic activities in total lysates	_____	- 53 -
4.12.1.1.	GCase and NLGase	_____	- 53 -
4.12.1.2.	β- galactosidase, β- hexosaminidase α- and β- mannosidase	_____	- 54 -
4.12.2.	Evaluation of enzymatic activities at the cell surface of living cells	_____	- 54 -
4.13.	Evaluation of the lipid content	_____	- 54 -
4.13.1.	Total lipid extraction	_____	- 54 -
4.13.2.	Two- phase partitioning and alkaline methanolysis reaction	_____	- 55 -
4.13.3.	Cell sphingolipid labelling with [1- ³ H]- sphingosine	_____	- 55 -
4.13.4.	Lipid analysis by High- Performance Thin Layer Chromatography (HPTLC)	_____	- 56 -
4.13.5.	Analysis of glucosylceramide and glucosylsphingosine content by LC ESI- MS/ MS	_____	- 57 -
4.13.6.	Svennerholm assay	_____	- 57 -
4.14.	Evaluation of the protein and lipid content of the plasma membrane	_____	- 58 -
4.14.1.	Cell surface protein biotinylation and isolation of PM proteins by streptavidin pulldown assay	_____	- 58 -
4.14.2.	Cell surface protein biotinylation and isolation of detergent- resistant membrane fractions	_____	- 59 -
4.15.	Evaluation of cell metabolites	_____	- 59 -
4.15.1.	Targeted metabolomics by LC- MS/ MS	_____	- 59 -
4.16.	Evaluation of the energetic metabolism of the cell	_____	- 61 -
4.16.1.	Agilent Seahorse XF Real- Time ATP Rate Assay	_____	- 61 -
4.16.2.	Agilent Seahorse XF Cell Mito Stress Test	_____	- 62 -
4.17.	Statistics	_____	- 62 -

5. RESULTS	- 63 -
5.1. Characterization of human brain areas of a patient affected by <i>GBA</i> - dependent Parkinson's disease	- 64 -
5.2.1. Development and biochemical characterization of <i>in vitro</i> models of GCase deficiency exploiting human iPSCs-derived dopaminergic neurons and mouse cerebellar granule neurons	- 69 -
5.2.2. Analysis of metabolites and ATP production in <i>iPSCs</i> derived dopaminergic neurons	- 96 -
6. DISCUSSION	- 104 -
7. BIBLIOGRAPHY	- 111 -
8. ANNEX I	- 121 -
9. PUBLISHED MANUSCRIPT	- 128 -

1. ABSTRACT

β -glucocerebrosidase (GCase) is the enzyme responsible for the catabolism of glucosylceramide (GlcCer) mainly at lysosomal level. The deficiency of this enzyme causes the onset of so called GCase-related pathologies such as Gaucher (GD) and Parkinson's Disease (PD), which share neurodegenerative features. GD is a lysosomal storage disorder characterized by a broad spectrum of phenotypes, ranging from the lethal neuropathic type-II form to type-I, which is characterized by a more favorable prognosis. Interestingly, patients with GD type-I have a 10- fold increased risk of developing PD. On the other hand, PD is a progressive neurodegenerative disorder characterized by the primary selective and progressive loss of dopaminergic neurons. Nowadays, mutations affecting *GBA1*, the gene coding for GCase, represent the major inherited recessive risk factor for the development of PD.

Unfortunately, the molecular mechanism leading from GCase deficiency to the onset of neuronal damage in GD and PD is still unclear. One of the main drawbacks in the study of neurodegenerative disorders in general and in particular in studies involving GD and PD is the lack of suitable *in vitro* models.

Based on these considerations, for my PhD project I have focused on i) performing: the biochemical characterization of different brain areas obtained from healthy subjects and from a patient affected by GCase- dependent PD and ii) developing suitable *in vitro* models able to recapitulate the pathological features, with the aim to dissect the molecular mechanisms relating GCase deficiency to the onset of neurodegeneration.

Related to the first part I found that in the frontal and parietal cortex, substantia nigra, *cerebellum* and *hippocampus* of GCase- PD patients, GCase activity was decreased of about 50% and in case of the parietal cortex and the *hippocampus* the reduction was even of greater entity. On the other hand, in almost all areas I observed an increased activity of the non- lysosomal β - glucoceramidase when compared to healthy areas, which could be a compensatory effect that hinders GlcCer accumulation in the GCase- PD brain areas.

To figure out the possible molecular mechanism linking GCase loss of function with the onset of neuronal damage I developed two *in vitro* models of the neuronal form of GD, which are represented by mouse cerebellar granule neurons and iPSCs-derived dopaminergic neurons differentiated from healthy subject's fibroblasts. Both models were treated with conduritol B epoxide to suppress GCase activity. These models correctly recapitulate the pathological phenotype by presenting a time- dependent accumulation of GlcCer and onset of neuronal damage. I demonstrated that the aberrant accumulation of GlcCer induces alterations of the endolysosomal

compartment, with consequent accumulation of GlcCer at the plasma membrane, where it alters PM architecture and functioning. Furthermore, GCCase deficiency induces several alterations in terms of cell metabolites, in particular involving amino acids, but seems to have no effect on the overall energetic balance of the neurons.

These *in vitro* models help to identify the existence of new possible mechanisms involving the PM and metabolism in the onset of the neuronal degeneration occurring in GD and GCCase-PD.

Taken together the obtained data allow a better characterization of the effects of a partial reduction of GCCase activity in PD brain, while the developed *in vitro* models help to shed light on some molecular mechanisms involved in the neuronal degeneration occurring upon the almost complete deficiency of GCCase activity as it occurs in GD patients.

2. INTRODUCTION

2.1. Lipids in the Central Nervous System

2.1.1. Cholesterol and Phospholipids

Phospholipids (PLs) are important membrane constituents and in mammalian cells the most abundant species is phosphatidylcholine (PC). Other phospholipids include phosphatidylethanolamine (PE), phosphatidylserine (PS), sphingomyelin (SM), cardiolipin (CL), phosphatidylinositol (PI) and its phosphorylated derivatives. Among these, in neuronal tissues the most enriched PL is PS which is localized at the inner layer of the plasma membrane (PM)¹.

The PL composition is essential for the correct functioning of membrane proteins. Among the different cell types there are differences in PL composition, which are mainly in terms of quantity than quality².

Cholesterol is the principal sterol synthesized by animal cells. It serves as biosynthetic precursor for molecules as steroid hormones, vitamin D and bile acids, which make the prevalent human body localization of cholesterol clear. Cholesterol is also an important membrane component involved in the regulation of the membrane architecture and fluidity. In the CNS the cholesterol levels are regulated by *de novo* biosynthesis or through the trafficking from the blood brain barrier³. Furthermore, cholesterol is known to be packed in the PL bilayer accounting for almost 45 % of membrane lipids and modifying some of its properties, including membrane permeability and fluidity⁴.

Within the central nervous system (CNS), PLs and cholesterol content of the cortical portion of the brain decreases linearly along aging, while considering the white matter it has a curve-shaped diminishing trend with a slight peak around 50 years of age⁵. Alterations in PLs and cholesterol content are associated with alterations in the PM composition described in hypomyelinating pathologies with are associated to neurodegeneration⁶.

2.1.2. Sphingolipids

2.1.2.1. Structure and chemical-physical properties

Sphingolipids (SLs) are essential components of cell membranes and are particularly enriched in the PM where they define the structure, integrity, and fluidity of the PL bilayer. In addition, many SL are considered bioactive molecules since they are directly involved in cell development, signaling, and cell- to- cell or cell- to- matrix adhesion.

All SLs are amphiphilic molecules, with a hydrophilic headgroup that extrudes in the extracellular compartment and a hydrophobic tail, called ceramide, inserted in the membrane lipid core. Ceramide is composed of a long chain amino alcohol, the sphingosine (D- erythro- (2S, 3R)- sphingosine or trans- D- erythro- 2- amino- 4- ottadecen- 1, 3- diol), simply known as sphingosine, bound through an amidic linkage to a long chain fatty acid (Figure 1).

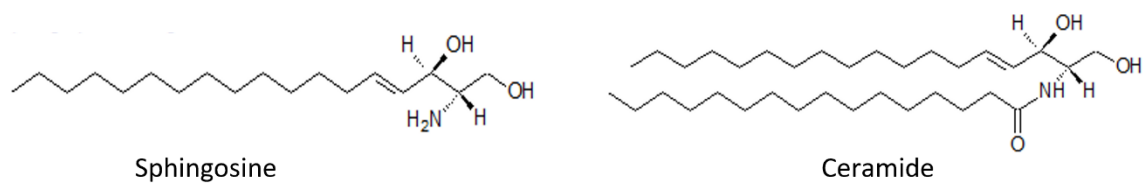
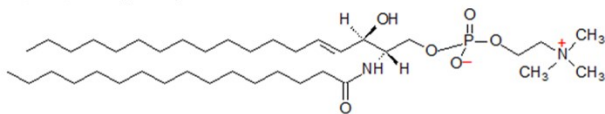


Figure 1. Chemical structure of sphingosine [sphingosine (D- erythro- (2S, 3R)- sphingosine or trans- D- erythro- 2- amino- 4- ottadecen- 1, 3- diol)] and ceramide

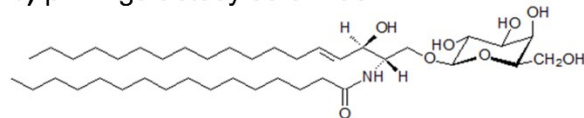
The presence of the amidic bond allows it to be both donor and acceptor for hydrogen bonds formation allowing the self- segregation of these lipids forming the so- called “SL- enriched membrane domains”, also known as detergent- resistant membrane domains.

Ceramide backbone can have a different length based on the carbon chain, but it is constitutive in all SLs. On the other hand, the polar portion varies among the different SLs’ classes: in case of SM it is represented by phosphocholine; for glycosphingolipids (GSL) it is a saccharide moiety, which can be either a monosaccharide as it occurs for cerebrosides or a polysaccharide giving origin to more complex GSL. In all cases, the polar head group is bound to the first hydroxy group of the ceramide backbone through a β - glycosidic linkage.

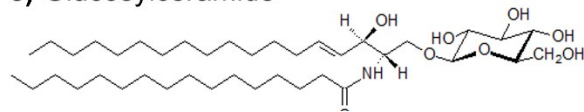
a) Sphingomyelin



b) β - D- galactosylceramide



c) Glucosylceramide



d) Ganglioside GM1

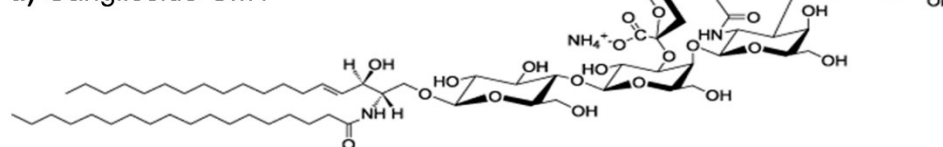


Figure 2. Chemical structure of the principal sphingolipids

The first hydroxy group of the ceramide can be bound to **a)** a phosphocholine residue generating sphingomyelin, a monosaccharide molecule as for example galactose or glucose to give origin to either **b)** galactosylceramide or **c)** glucosylceramide **d)** a longer oligosaccharide chain to which one or more sialic acid residues are attached forming gangliosides as the ganglioside GM1

Through the sequential addition of saccharide residues such as glucose or galactose, GSLs glucosylceramide (GlcCer) or galactosylceramide (GalCer) are formed. As reported in Figure 2, these are the simplest GSL and they are also known as cerebrosides, which together with globosides (SLs containing two or more sugar moieties among glucose, galactose, and N- acetyl- galactosamine) compose the class of neutral glycolipids.

Cerebrosides are prevalently located at encephalic level and in the peripheral nervous tissue, with particular regards for myelin sheaths.

Among the SLs those containing the sialic acid are classified as gangliosides⁷. They were firstly identified by the German scientist Ernest Klenk in 1942 in the brain. Indeed, gangliosides are mainly located in gangliar cells of the CNS and particularly at nervous terminals. Gangliosides are sialic acid containing GSLs constituted by an oligosaccharide portion made from a minimum of 3 up to 15-20

monosaccharides residues among which there are neutral hexoses (D- glucose, D- galactose, and seldomly D- fucose) and N- acetylated hexosamines (N- acetylglucosamine, N- acetylgalactosamine). The presence of one or more sialic acid residues in the oligosaccharide chain increases the acidic properties and the negative charge of gangliosides. Sialic acid residues are linked to the oligosaccharide core through an α - glycosidic linkage.

Gangliosides were originally classified according to the amount and position of the hexoses and of sialic acid residues accordingly to the IUPAC nomenclature⁸ (Figure 3).

The polar head of gangliosides extrudes from the outer layer of membranes, prevalently of the PM where it can work as receptor or it can be involved in cell- to- cell or cell- to- substrate recognition as it occurs during cell growth. Alterations in the ganglioside pattern reflect in alterations in the listed processes⁹.

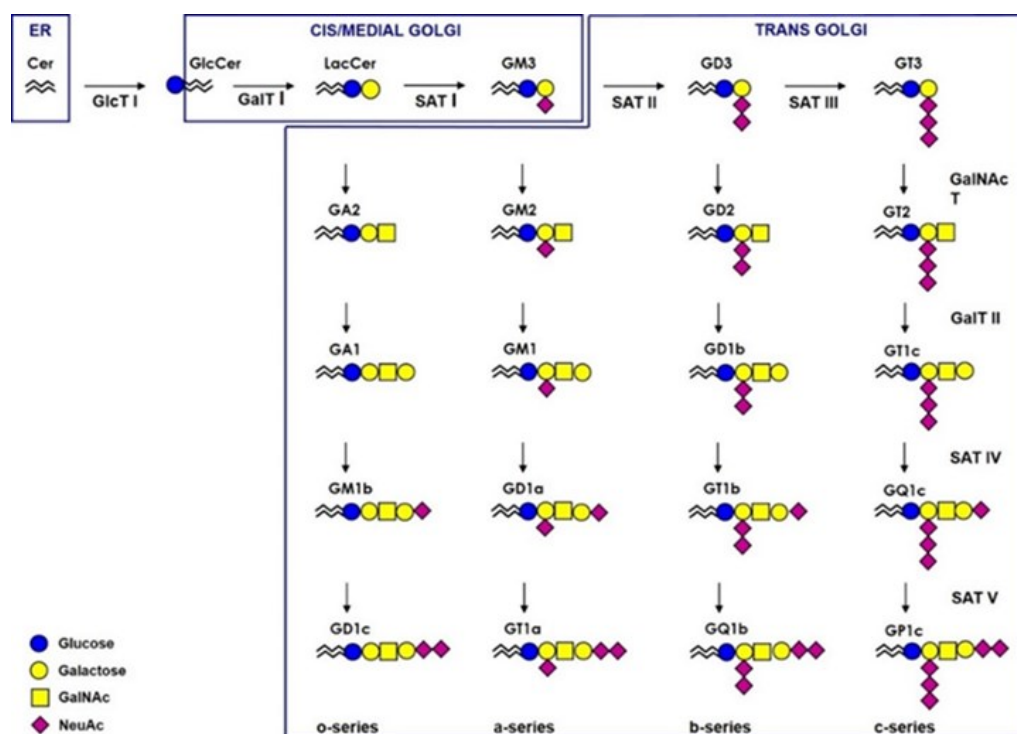


Figure 3. Schematic representation of the gangliosides series biosynthesis

Another class of SLs is represented by the sulfatides. These are esters of GalCer and sulfuric acid, which confers acidic properties and a highly negative charge at physiological pH. Sulfatides are inserted in the outer leaflet of the membrane and are particularly enriched in kidney,

gastrointestinal tract, erythrocytes and in the nervous tissue, in detail they are mainly present in oligodendrocytes and Schwann cells membranes, where they contribute to the proper structuring and functioning of myelin¹⁰. Sulfatides are also involved in cell recognition and adhesion processes, in protein trafficking and cellular aggregation, but the involved molecular mechanisms are not elucidated so far.

2.1.2.2. Sphingolipids' metabolism

GSLs' metabolism is a complex process that needs the contribution of many enzymes working in different subcellular compartments as shown in Figure 4. In the different cell types, GSLs' composition and content associated with the PM can vary according to the developmental stage, to the cell functions, and to pathological conditions. All these processes are connected and controlled by intracellular and extracellular signaling pathways aimed to define the SL pattern controlling SLs' trafficking, biosynthesis, and catabolism.

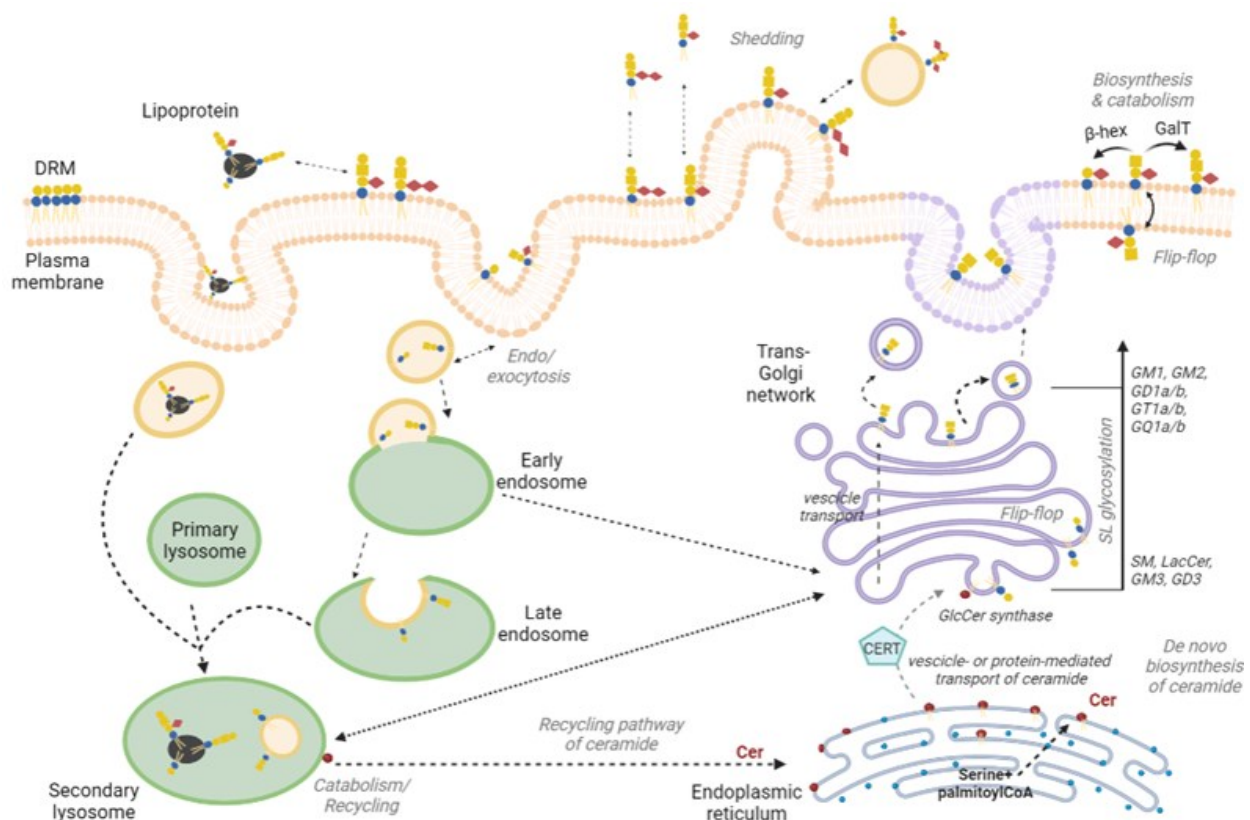


Figure 4. Schematic representation of the pathways involved in the SL metabolism (biosynthesis, trafficking, and catabolism) both at intracellular and at plasma membrane level (Cer= ceramide, SM= sphingomyelin; LacCer= lactosylceramide; GlcCer= glucosylceramide; β-hex= β- hexosaminidase; GalT= galactosyltransferase; DRM= detergent- resistant membrane portion)

2.1.2.2.1. Sphingolipids biosynthesis

Biosynthesis of GSLs requires the availability of ceramide, which can be synthesized *de novo* in the smooth endoplasmic reticulum, or it can be obtained by the addition of acyl groups to sphingosine recovered from the lysosomal catabolism of complex SLs, the so- called *sphingosine recycling/salvage pathway*. The oligosaccharide chain of GSLs is formed through the sequential addition of monosaccharides to the ceramide backbone or to the growing saccharide chain.

2.1.2.2.1.1. De novo biosynthesis of ceramide

This pathway is described in Figure 5 and involves four steps. The first step of ceramide biosynthesis is the condensation of L- serine and palmitoylCoA through the serine palmitoyltransferase and pyridoxal phosphate, which leads to the formation of 3- keto- sphinganine. This is then reduced to dihydrosphinganine by a NADPH- dependent reductase^{11,12}. The ceramide synthase, which uses acylic chains activated with Coenzyme A, adds a fatty acid in position 2 forming dihydroceramide¹³. Dihydroceramide is then desaturated in position 4,5 by a dihydroceramide desaturase, which probably acts at endoplasmic reticulum level¹⁴.

In the CNS there is a second proposed mechanism for ceramide synthesis, that involves ATP hydrolysis and uses as substrate long chain free fatty acids¹⁵.

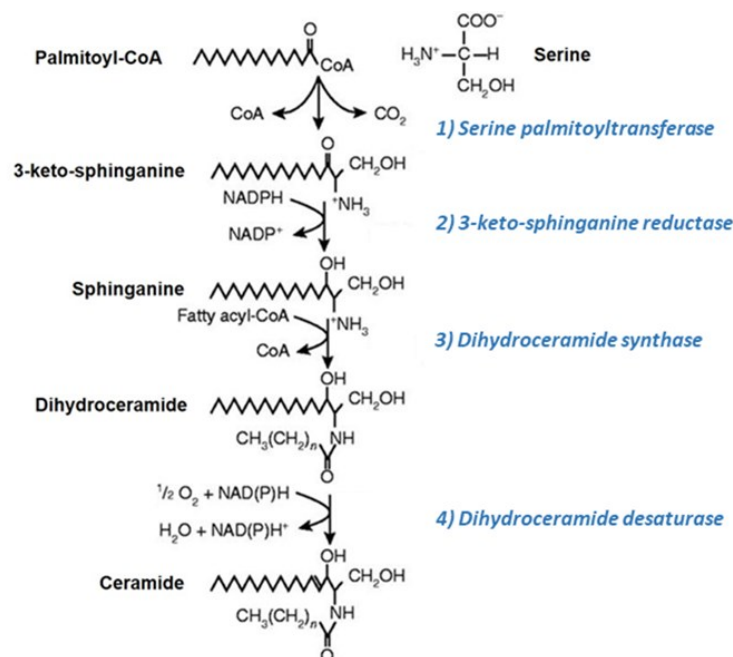


Figure 5. Pathway representing the *de novo* biosynthesis of ceramide starting from L- serine in the endoplasmic reticulum

2.1.2.2.1.2. Ceramide obtained from the sphingosine recycling/ salvage pathway

Ceramide in the ER can be also formed by the direct N- acylation of sphingosine because ceramide synthases are able to work with a similar affinity both on sphinganine and sphingosine. Sphingosine derives from the degradation of more complex SLs. Since this pathway doesn't need the action of ceramide desaturases, considered as the "gatekeeper" of ceramide synthesis, it is responsible for a massive production of cell SLs^{16,17}. The newly synthesized ceramide can undergo diverse metabolic fates: it can be transported to the PM, or it can be used to synthesize SM. The use of catabolic molecules for biosynthesis is the so-called metabolic salvage pathway.

2.1.2.2.1.3. Complex sphingolipid biosynthesis

The GLS biosynthesis is mediated by a multienzyme system of glycosyltransferases present at the Golgi cisterns but also at PM level, where the newly produced ceramide is transported by both vesicular- dependent transport and protein- dependent transport via CERT protein to synthesize complex SLs¹⁸.

Biosynthesis of phosphosphingolipids

Ceramide is firstly converted into SM both on the PM and on the Golgi apparatus, respectively by SM synthase (SMS) 2 and 1. These enzymes transfer phosphorylcholine from PC to the 1- hydroxyl group of ceramide, releasing diacylglycerol (DAG). If DAG accumulates, phosphorylcholine can be transferred from SM to DAG to form phosphatidylcholine and ceramide again.

SMS2 is also able to catalyze the synthesis of CerPE, transferring phosphatidylethanolamine to ceramide, while Cer1P is synthesized by ceramide kinase, which is selective for ceramide with at least 12 carbon acyl chains.

Biosynthesis of glycosphingolipids

Concerning the GSL synthesis, ceramide is subjected to the sequential addition of saccharide residues by the action of specific membrane- bound glycosyltransferases, which transfer specific carbohydrates from a sugar nucleotide to an acceptor.

First step of the GSL biosynthesis is the formation of GlcCer by the UDP- Glc: Cer glucosyltransferase which transfers the glucose moiety from UDP to ceramide at the cytosolic leaflet of the Golgi apparatus. GlcCer can reach the PM or it can be translocated to the luminal side of the Golgi apparatus, where it can be further glycosylated by lactosylceramide (LacCer) synthase to form

LacCer¹⁹. Gangliosides are synthesized, starting from LacCer, in the lumen of the Golgi apparatus by the stepwise addition of neutral sugars and sialic acids, and are then incorporated into the outer leaflet of the membrane through a vesicle- mediated transport (Figure 6).

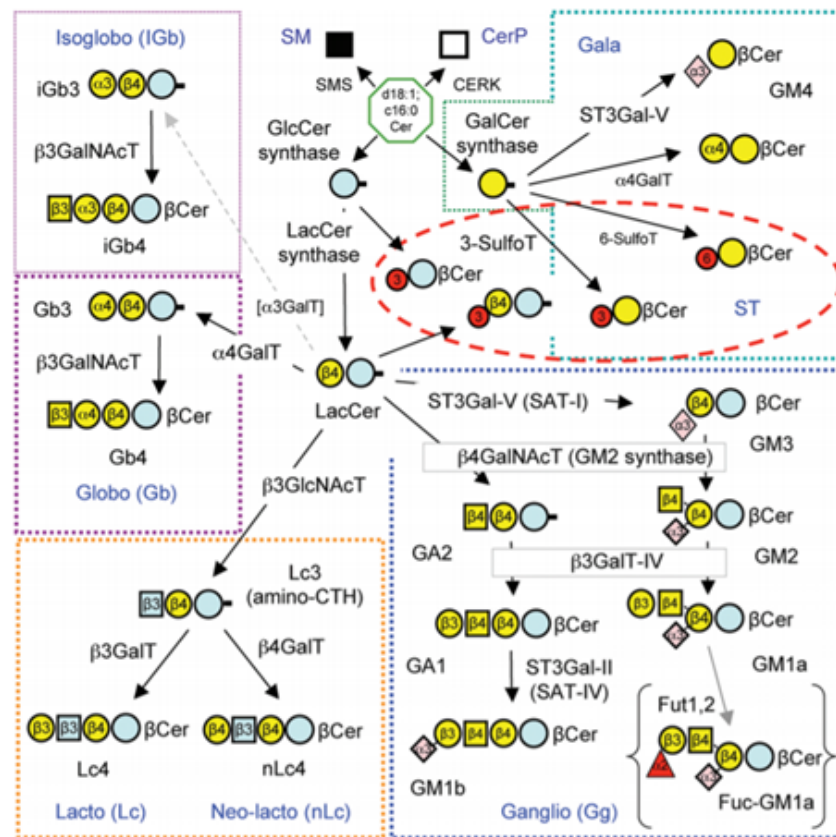


Figure 6. Biosynthesis of sphingolipids

Scheme representing the major headgroups addition in the Golgi apparatus during the biosynthesis of complex sphingolipids. Each section represents a GSL category. Green dashed area: ala- series; red dashed area: sulfatides; blue dashed area: gangliosides; yellow dashed area: lactosides and neolactosides; purple dashed area: globo and isoglobo series. Cer= ceramide; LacCer= alctosylceramide, GalCer= galactosylceramide; GlcCer= glucosylceramide; GalNAc= N-acetylgalactosamine; Fuc= fucosyl; T= transferase²⁰.

2.1.2.2.2. Trafficking of sphingolipids

Complex SLs are moved via vesicle- dependent or protein- dependent pathways from their site of synthesis, the endoplasmic reticulum, to the Golgi apparatus, the PM, and the endolysosomal system²¹.

In the Golgi apparatus SLs, undergo several glycosylation steps necessary to form complex GSLs. The endolysosomal compartment is responsible for the catabolism and recycling of SLs' components.

The ability of lipids to move from one membrane leaflet to the other, spontaneously or helped by proteins known as flippases, is called "flip- flop" and allows the generation and definition of specific

lipid profiles in cell membranes. Based on the differences in profiles, membranes change their physical- chemical properties. This becomes particularly relevant considering the PM. At this level SLs can cluster together forming so- called detergent- resistant membrane portions (DRM) which change the organization order of the PM. Lipoproteins or extracellular vesicles can exchange SLs with the PM. Lipoproteins or directly PM portions can also be internalized and be directed to the endolysosomal system for their complete degradation or recycling. Vice versa, vesicles can be shed from the endolysosomal compartment and fuse with the PM, a process known as lysosomal exocytosis. This can lead to altered SL composition of the PM or to the release of SL- containing vesicles in the extracellular space. The PM is also a site for SL modifications, both involving catabolic and biosynthetic enzymes (Figure 4).

2.1.2.2.3. Catabolism of sphingolipids at lysosomal and PM level

Degradation of GLSs occurs prevalently in acid cellular compartments such as in the endosomes and lysosomes. These are cytoplasmic organelles delimited by a lipid membrane and contain enzymes involved in the catabolism of the main macromolecules (lipids, carbohydrates, nucleic acids, and proteins). These organelles are considered to be the “digestive system” of the cell, since they degrade both materials imported from the outer environment and intracellular damaged structures.

PM portions containing GSLs, which are destined to degradation are internalized via endocytosis and the vesicles pass through endosomes to reach lysosomes, where the vesicles fuse with the organelles’ membrane becoming part of the intralysosomal membrane. Lysosomes appear as sphere- shaped vacuoles with a diameter around 0.5 μm . The lysosomal membrane protects the surrounding environment from hydrolytic enzymes present in the lysosomal lumen, since the optimal working condition for these enzymes is at acid pH (pH 5) and not at neutral cytoplasmic pH. For this reason, lysosomes need the activity of proton pumps (V- ATPases) to maintain the lysosomal pH acid.

Lysosomal hydrolases are synthesized in the endoplasmic reticulum, modified in the Golgi apparatus through addition of mannose- 6- phosphate residues, and then at the trans-Golgi level they are packed into clathrin- covered vesicles which allow their trafficking to the endolysosomal compartments.

Once they have docked the mannose- 6- phosphate receptors on the late endosome, the hydrolases are separated from the receptors, which are transported back to the trans Golgi network through

retrograde transport. The acidification by V-ATPases of the late endosome to pH 4- 5.0, determines the maturation of the late endosomes to lysosomes, the loss of the phosphate group attached to the mannose, and the activation of the hydrolases^{22,23}. At this level, each specific glycohydrolases catalyzes the sequential removal of saccharide residues starting from the non- reducing extremity of the oligosaccharide chain (Figure 7). Short chain GSLs (1 to 4 residues) on the intralysosomal membrane are not accessible to hydrolases. For this reason, specific proteins called saposins (Sap A, Sap B, Sap C, and Sap D) and the GM2 activator protein, help to obtain the complete removal of the oligosaccharide chain forming ceramide. At the end, ceramide is catabolized into sphingosine and a fatty acid. All the obtained molecules (sphingosine, fatty acid, monosaccharides, and sialic acid) can leave the lysosome and be recycled for biosynthetic purposes. *In vivo* saponins have different substrates specificity²⁴: Sap A favors the degradation of GalCer, Sap B stimulates the catabolism of sulfatides and the removal of galactose, Sap C helps in GlcCer degradation, and Sap D is involved in ceramide catabolism. GM2 activator protein (GM2AP) helps removing the N- acetyl-galactosamine residue from GM2 ganglioside.

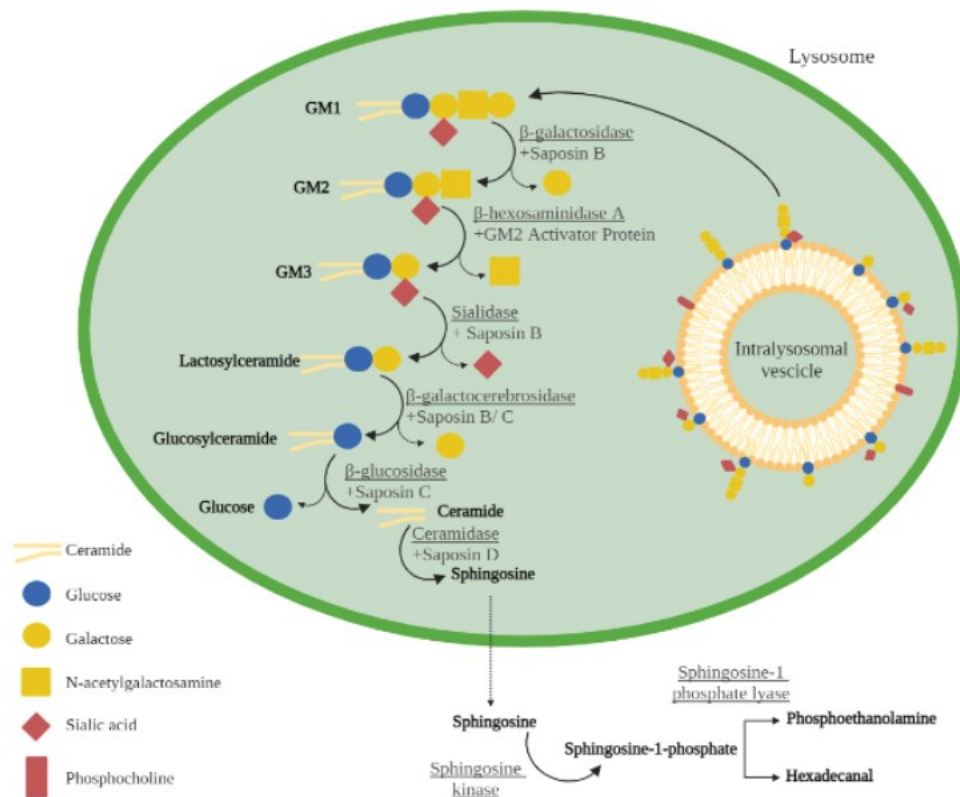


Figure 7. Schematic representation of the catabolism of complex glycosphingolipids

The representation refers to the catabolism of ganglioside GM1 through the action of lysosomal glycohydrolases helped by their specific saposin or activator protein.

2.1.2.2.3.1. *Sphingolipid hydrolases*

During neuronal development the GSL pattern undergoes important changes, which are reflected on the reorganization of GSL- enriched membrane domains. As emerges from the literature, important players are the glycohydrolases associated with the PM but also with the lysosome. Generally, there is a strong modulation of the glycohydrolases' activity during neuronal differentiation, suggesting their role in defining a proper local PM composition necessary for the different stages occurring during the neuronal life. The main glycohydrolases, are: β - galactosidases, β - hexosaminidases, sialidases, α - mannosidases, β - mannosidases, β - glucocerebrosidases (GCCase) and the non- lysosomal β - glucoceramidases (NLGase) which, contrary to the other mentioned enzymes, works prevalently at PM level.

Almost all SLs hydrolases are N- glycoproteins. Proteins are produced in the ER and extrude in its lumen. The synthesis of the glycan portion starts in the ER membrane with the formation of the core oligosaccharide (Glc₃Man₅GlcNAc₂) by the action of nucleotide sugars on dolichol phosphate.

A flippase allows the translocation across the ER membrane of the dolichol- glycan structure, making it accessible to enzymes present in the ER lumen.

Sugars are sequentially added to the glycan (4 mannose and 3 glucose). Dol- P- Man is the mannose residue donor (Dol- P + GDP- Man \rightarrow Dol- P- Man + GDP) and Dol- P- Glc is the glucose residue donor (Dol- P + UDP- Glc \rightarrow Dol- P- Glc + UDP). Many dolichols translocate multiple sugars simultaneously, which leads to the formation of Dolichol- GlcNAc₂- Man₉- Glc₃.

The complete saccharide portion is then transferred to an asparagine residue of the peptide sequence by oligosaccharyltransferases. At this point the saccharide portion has to be processed to reach the correct folding degree of the protein. Two glucose residues are removed from the non-reducing end of the glycan. The signal to transfer the glycoprotein from the ER to the cis-Golgi is the removal of the third and last glucose moiety by a glucosidase. This step doesn't occur if the folding degree of the protein is not proper, and in this case, chaperone proteins as calnexin or calreticulin bind the unfolded protein to assist it in the folding process. In the cis- Golgi the further addition and removal of sugar residues occurs by glycosyltransferases and glycosidases. Mannosidases remove some or all the four mannose residues, whereas in the medial Golgi, sugar residues are added to the glycan structure, giving rise to the three main types of glycans: high mannose, hybrid and

complex glycans. Depending on the substrate specificity and accessibility the addition of sugars to the glycan can vary. A UTP- GlcNac1P- transferase binds a GlcNac to the mannose moieties signalling the transfer of the protein to the trans- Golgi. Here a GlcNac hydrolase removes the GlcNac causing the exposition of the mannose phosphate residues (Man6P). On endosomes there are receptors for Man6P which allow to target the protein to the endolysosomal compartment.

Some glycohydrolases can escape this pathway and are released in the cytosol to enter the secretory pathway. That is why in the cytosol and on the PM there are some Man6PR able to scavenge the escaped molecules and target them back to the lysosome.

Mutations in the UTP- GlcNac1P- transferase lead to the absent phosphorylation of mannose in the Golgi and to the onset of the lysosomal storage disorder Inclusion- cell (I- cell) disease, classified as mucopolipidosis II. Studies concerning this pathology have demonstrated that patients do not show activity of many glycohydrolases, but still present a functioning GCCase. Indeed, GCCase is transported to lysosomes in a M6P- independent way, by exploiting the lysosomal integral membrane protein (LIMP- 2). Deficiencies in LIMP- 2 cause the onset of the myoclonus- renal failure syndrome which shares some hallmarks with Gaucher disease.

2.1.2.2.3.1.1. β - galactosidases

Two different forms of this enzymes are known to be involved in lysosomal GSLs' metabolism: β - galactocerebrosidases (β - gal) is involved in the catabolism of GalCer, LacCer, and galactosylsphingosine, while β - galactosidases (GAL) remove galactose from glycoproteins and GM1 ganglioside (Figure 8)²⁵.

The β - galactosidase (β - D- galactohydrolase; EC 3.2.1.23) is encoded by *GLB1* gene localised at chromosomal region 3p21.33²⁶. This gene is composed of 16 exons each of 62.5 kb. Alternative splicing can give rise to two products: the 85 kDa precursor of the lysosomal β - galactosidase and the elastin binding protein (EBP). Once in the lysosome, the enzymatic precursor is cleaved to its mature form of 64 kDa^{27,28} and binds cathepsin A, an essential protein for intracellular transport, stability, and enzyme activity. EBP binds to PPCA and to neuraminidase Neu1, forming the receptor complex of elastin, which is a key structure for the formation of elastic fibres of the connective tissue²⁹.

The β - galactocerebrosidase or β - galactosylceramidase (GALC; EC 3.2.1.46) is encoded by *GALC* gene, localized on 14q31 and composed by 17 exons, each of 60 kb. The enzyme works

predominantly at lysosomal level, but recent data report its activity also at PM level. These enzymes, beside playing a catabolic role, could be involved also in cellular senescence and neurodegeneration³⁰.

β - galactosidase activity associated with the cell surface has been measured in several cell lines. Nevertheless, the identity of the proteins responsible for the enzymes activity at PM level is unknown so far^{31,32}. In human fibroblasts the existence of a PM associated β -galactosidase showing a *trans*- activity has been demonstrated. In the same cells, it has been demonstrated that the β -galactosidases expression is upregulated by the overexpression of Neu3 sialidases and this correlates with the ectopic production of ceramide and the onset of apoptosis³³.

Changes in the β - galactosidase activity associated both at the cell surface of the lysosomes were described also in cultures of rat granule cells both during *in vitro* differentiation and aging³⁴. The total activity remains constant during differentiation and increases four folds at the onset of aging. Whereas the activity associated with the cell surface increases of ten folds during differentiation and duplicates during neuronal senescence. A similar behavior was described for the PM β -galactosidase activity during neuronal differentiation of neural stem cells^{30,35,36}. Concerning all this information, it seems that β - galactosidase activity, besides being a marker of senescence, could be also used as marker of neuronal differentiation and of apoptosis in human fibroblasts. There are not many data regarding the functional role of β - galactosidases on the cell surface, probably they have an involvement as receptor molecules involved in cell- to- cell or cell-to -matrix interactions, which lead the cell migration, differentiation, and axonal outgrowth.

2.1.2.2.3.1.2. β - hexosaminidases

The β - hexosaminidases (β - N- acetyl-hexosaminidase; EC 3.3.1.52) are responsible for the catabolism of GM2 to GM3, removing the residue of N- acetylgalactosamine (GalNac) from the oligosaccharide chain of GM2 ganglioside (Figure 7). There are three isoforms of this enzyme: β -hexosaminidase A, B, and S. β - hexosaminidase A works at lysosomal level where together with GM2 activator protein (GM2AP), it catalyses the degradation of GM2 ganglioside and other molecules containing an N- acetyl- galactosamine (GalNac) residue at their reducing end. This isoform works as a heterodimer and is composed of two subunits, α and β , encoded by two different genes: *HEX-A* localized at chromosomal region 15q24.1 and *HEX-B* localized at 5q13.3.

β -hexosaminidase B and β -hexosaminidase S work as homodimers, the firsts' subunits are $\beta\beta$, while the latter' subunits are $\alpha\alpha$ ³⁷.

For what concerns the catabolism of GM2 to GM3 mediated by β -hexosaminidase A, it starts with the binding of GM2AP to the GM2 ganglioside to make it fit into the catalytic site of the enzyme. There are two catalytic sites, one for each enzyme's subunit and this means two GM2 molecules can be hydrolysed simultaneously.

The hydrolysis occurs because a glutamate residue present in the catalytic site creates a hydrogen bond with the GalNac, stabilising the GM2 and favouring the nucleophilic attack of an aspartate residue on the carbon atom bound to the GM2 moiety. The catabolism terminates with the release of GalNac with the formation of GM3 and the catalytic site returns to its basal state³⁸.

The presence of active β -hexosaminidase A in the outer membrane layer was demonstrated in cultured fibroblasts³⁹. Immunological and biochemical characterization of this enzyme associated with the PM has demonstrated it has the same structure of the lysosomal isoform. This suggests the existence of a specific transport mechanism of lysosomal enzymes to the plasma membrane, probably a direct fusion of the two membranes through vesicle release^{40,41}.

A genetic defect in both genes encoding for the subunit α and β of HexA or encoding for GM2AP can result in accumulation of GM2 in the nervous tissues, leading to three different GM2 gangliosidosis: Tay-Sachs disease (caused by a defect in the α subunit), Sandhoff disease (caused by a defect in the β subunit) and the AB variant of Sandhoff disease, where both subunits are deficient³⁷. The excessive storage of GM2 is followed by neurological deterioration which involves motor functions but also cerebral and spinocerebellar-related ones.

These enzymes could play an active role in GSL remodelling of the outer PM layer also during the neuronal differentiation (Figure 8). During differentiation of murine neural stem cells, PM β -hexosaminidase increases its activity and reaches its maximum when cells are at a fully differentiated state³⁴.

PM associated β -hexosaminidase activity results higher also in cells deriving from GD patients presenting the most severe form of the pathology that has also a neuronopathic involvement⁴².

2.1.2.2.3.1.3. Sialidases

Sialidases or neuraminidases are enzymes which hydrolyse the glycosidic linkage between sialic acid and the oligosaccharide chain. They are ubiquitous enzymes, presenting some highly conserved structural regions such as: i) the catalytic domain formed by three antiparallel β - sheets, ii) the active site hosting an arginine, a glutamate, and an aspartate molecule, iii) two “lectin- like” binding domains, the Asp box, formed by the aminoacidic sequence: X- Pro- Arg- Pro, and iv) several sites of N and O- glycosylation.

Sialidases are either soluble or associated with the PM. The soluble variant is the cytosolic isoform Neu2 encoded by *NEU2* gene located at 2q37.1. Neu2 is present also at PM level and takes part in myoblast and neuronal differentiation. The sialidase Neu1 is encoded by *NEU1 gene*, located on 6p21.33. Neu1 is localized mainly in the lysosomes and it is involved in the catabolism of sialyl-glycoconjugates, whereas its counterpart associated with the PM desialylates many receptors, playing a key role in many pathophysiological processes⁴³. Neu3 and Neu4 are both involved in neuronal differentiation, apoptosis, and cell adhesion. While Neu4 is prevalently found in the lysosomes or in the mitochondria, and the endoplasmic reticulum⁴⁴, Neu3 is instead at PM level. *NEU3* gene, encoded by the chromosomal region 11q13.5 allows the expression of a sialidase (EC 3.2.1.18), which is about 48.8 kDa and even if it is associated with the PM it has its best working condition in a pH range between 3.8- 4.6⁴⁵. Neu3 is a ubiquitous protein, situated in the PM of almost all healthy and pathological tissues (Figure 8)⁴⁵⁻⁴⁹.

This enzyme is mainly involved in the hydrolysis of α 2- 3 outer ketosidic linkages and is not able to remove internal sialic acid residues. An increase in Neu3s activity alters the ganglioside composition at PM level, transforming polysialylated species Gg4 and Gg3 into monosialo- derivatives and GM3 into LacCer. These alterations have deep consequences on the neuronal differentiation and apoptosis, both in healthy and pathologic cells^{33,50}.

It has been proven, that neuronal differentiation induced in neuroblastoma cell line is accompanied by an increased expression of Neu3 sialidases⁵¹. Neurite outgrowth was also obtained through transfection with *NEU3* gene and the increased activity of Neu3 determines a higher degree of neurites outbranching⁵². These data have been sustained by experiments on rat granule cells, where it had been observed that Neu3 activity increases during differentiation³⁴ and is responsible for GM1 content regulation through hydrolysis of GD1a, having an important effect, following axotomy, on axonal growth and regeneration⁵³. At PM level Neu3 is associated with the SL enriched domains⁵⁴

and therefore it can be hypothesized that the biological effects of this enzyme could be attributed to the local reorganization of signalling units based on the modulation of the glycolipid content. Furthermore, it has been demonstrated that Neu3 is able to modulate the surface glycolipid composition of neighbouring cells⁵⁵.

2.1.2.2.3.1.4. β - glucocerebrosidases

β - glucosidases (β - D- glucopyranoside glucohydrolases) are a family of enzymes able to hydrolyse β (1- 4) or β (1- 1) linkages involving glucose. These enzymes are conserved from *Archea* to eukaryotes. Data report the existence of at least three different enzymes with β - glucocerebrosidase activity able to catalyse the glucosylceramide in glucose and ceramide: i) the lysosomal β - glucocerebrosidases GCCase (EC 3.2.1.45) encoded by *GBA1* gene, sensitive to conduritol B epoxide (CBE) inhibition, ii) the non- lysosomal β - glucoceramidases NLGase (EC 3.2.1.45), encoded by *GBA2* gene and irreversibly inhibited by N- (5- adamantane- 1- yl- methoxy-pentyl)- Deoxynojirimycin (AMP- DNM), and iii) the cytosolic β - glucosidase (EC 3.2.1.21) encoded by *GBA3* gene^{56,57}.

GBA1 gene, localized at the chromosomal region 1q21, encodes for a (β/α)₈- barrel protein that presents a highly conserved catalytic site containing two residues of carboxylic acid, which are settled in the fourth and seventh β - strand and are indispensable for the occurrence of the nucleophilic attack and the acid- base reaction⁵⁸. *GBA1* gene has 7000 bp and contains 11 exons. The enzyme GCCase is not only associated with the lysosomal membrane, but it works also at PM level (Figure 9). The association with the PM probably relates to an involvement of these enzymes in signalling cascades related to apoptosis and neuronal differentiation³¹.

It has been demonstrated as expected that GCCase activity at PM level of human fibroblast obtained from Gaucher Disease patients is strongly reduced with respect to the fibroblasts derived from healthy subjects. These data confirm that GCCase at the cell surface is the same enzyme located in the lysosome⁴². In addition, it has been demonstrated that an increase in PM β - glucosidase activity (GCCase and NLGase) is responsible for cell cycle arrest and apoptosis^{31,33,41}.

GBA2 gene is instead located on chromosome 9q13.3 and encodes for a transmembrane protein whose N- terminal domain is intracellular and whose C- terminal domain is on the extracellular side. *GBA2* sequence is conserved in many species, from *Drosophila* to vertebrates, which indicates the functional importance of the protein. NLGase is a transmembrane protein associated predominantly with the PM (Figure 8), but partly also with the endoplasmic reticulum and endosomal vesicles.

NLGase has a controversial localization, which according to literature data, seems to vary together with cell types. Expression studies show that NLGase is highly expressed at brain level, in the heart, in skeletal muscle, and in kidneys^{59,60}, while main expression sites in mice are the testis and the brain. A study on NLGase knock-out mice has shown an abnormal accumulation of GlcCer in several tissues including brain, liver, and testis. These knock-out mice have an impairment in the repair of liver damage and male infertility, but they do not show any compromise of the CNS⁵⁹. Whereas, in humans, biallelic loss of function mutations of *GBA2* lead to the accumulation of GlcCer in the lysosomes affecting particularly the liver, the spleen, the brain, and the testis: specifically, this last district reflects into aberrant spermatogenesis, acrosomal vesicles, and reduced fertility in males^{59,61} and correlates with cerebellar spastic ataxia⁶².

Furthermore, the use of morpholino antisense oligonucleotides targeting *GBA2* gene in zebrafish, determines an abnormal motor behavior and a reduced motoneurons ramification and extension. These can be only restored transfecting the animal with human wildtype *GBA2* mRNA⁶².

The discrepancies observed among the mouse model, zebrafish, and humans could be explained by the differences in the cortico- spinal tract between these species. It could also be due to a compensation mechanism by other enzymes exerting β - glucosidase activity, set on during the first development stages⁶³. It is notable of remarks that even if *GBA2* knockout mice lack 5 to 10 exons, they conserve 50 % of their normal β - glucosidase activity. On this basis, it has been hypothesized that the accumulation of GlcCer in the endoplasmic reticulum or at PM level, doesn't reach the threshold level needed to develop neurological signs and symptoms.

It has been demonstrated that NLGase activity increases of three folds during neuronal differentiation³⁴ of mouse granule cells as well as during the *in vitro* differentiation of murine stem cells³⁴. In addition, in fully differentiated neurons NLGase is the prevalent β - glucosidase activity.

Furthermore, it has been demonstrated that in fibroblasts derived from GD patients, a reduction in GCase activity correlates with an increase in NLGase activity. This becomes particularly evident in patients affected by the neuronopathic GD, which affects the nervous system severely⁴². Thus, the link between NLGase, the neuronal differentiation, and the neurodegeneration has been hypothesized, nevertheless further studies are needed.

2.1.2.2.3.1.5. Mannosidases

Mannosidases are a group of enzymes involved in the hydrolysis of α - or β - linked mannose.

α -mannosidases (α -D-mannoside mannohydrolase; EC 3.2.1.24) are present in two isoforms, the acid- and the basic α -mannosidase. They are both encoded by *MANB* gene, located at the chromosomal region 19p13,2- q129. These hydrolases are responsible for the lysosomal catabolism of N-linked glycoproteins by breaking the $\alpha(1-2)$, $\alpha(1-3)$ and $\alpha(1-6)$ mannosidic linkage from the non-reducing extremity of the saccharide chain⁶⁴.

β -mannosidases (β -D-mannoside mannohydrolase EC 3.2.1.25) hydrolyse the β -mannosidic linkage present at the branching point of the pentasaccharide core of N-glycoproteins allowing the fully degradation of the protein' glycoalyx⁶⁵.

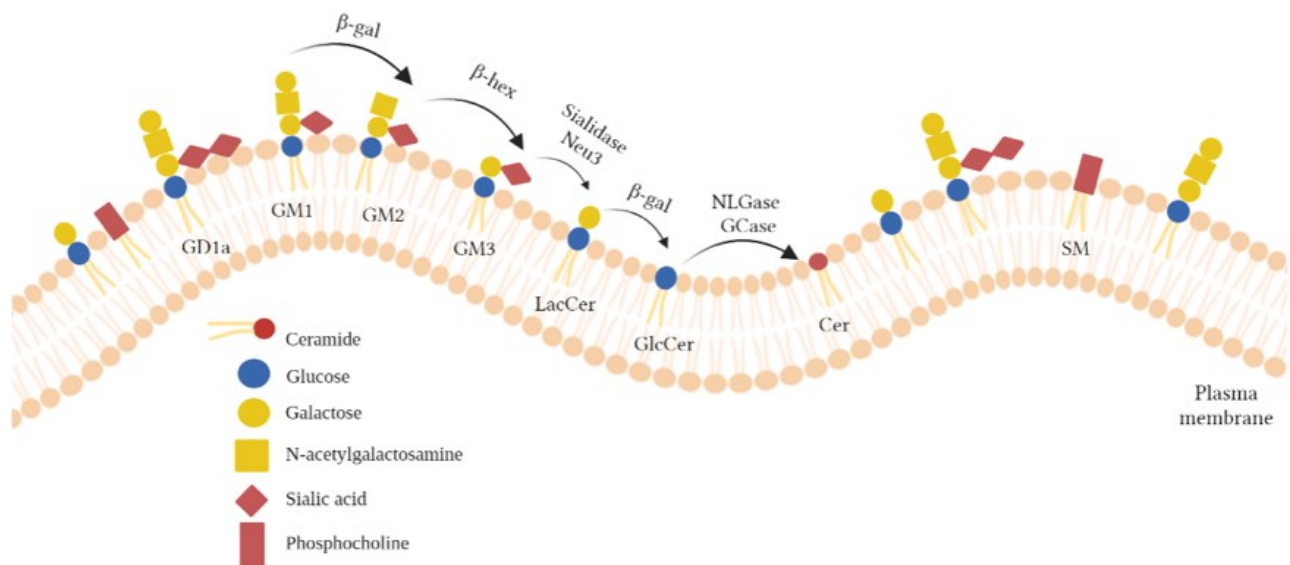


Figure 8. Catabolism of sphingolipids at PM level

HexA= β - hexaminidase A; β - Gal= β - galactosidase; GCCase= β - glucosidase; NLGase= β - glucosidase; SMase= sphingomyelinase; Neu3= sialidase 3; Cer= ceramide; GlcCer= glucosylceramide; LacCer= lactosylceramide; SM=sphingomyelin, GD1a, GM1, GM2, GM3 = gangliosides .

2.2. Sphingolipids in neuronal differentiation

SLs and in particular GSLs were demonstrated to play an essential role during embryonic development and neural differentiation⁶⁶. A particular role is played by gangliosides. Indeed, in particular during the neuronal differentiation, a significative switch from globoside species to gangliosides ones occurs and has been demonstrated fundamental for the correct brain function⁶⁷. Among ganglioside species there is a quantitative change from simple gangliosides towards more complex species⁶⁸. GD3 and GM3 gangliosides are expressed mainly during the neural tube

formation and neuronal stem cell proliferation phase⁶⁹, and their expression decreases during the later phases of development. During the development, the brain GSL content increases, and the simpler gangliosides are replaced by the more complex ones, suggesting an important role of the oligosaccharide chains in the process. GM1, GD1a, GD1b, and GT1b gangliosides characterize the neurogenesis, axonal and dendritic arborization, and synaptogenesis phases⁷⁰ (Figure 9). In humans, the rapid increase of ganglioside content starts from the 6th month of gestational life and reaches its maximum peak at about 5 years of age⁷¹.

During adult life there is a progressive loss of brain gangliosides. The trend of variation is complex, and it diverges according to the different brain areas, the ganglioside species, and the subjects' age. Gender doesn't seem to affect these differences. The major change occurring along aging is the increase in simple gangliosides (GM3 and GD3), the decrease in complex gangliosides of the a-pathway (GD1a and GT1a) and the increase of GD1b^{72,73}.

Together with these changes a strict regulation of the expression of GalCer and sulfatides was described. As mentioned before these lipids are abundant in central and peripheral myelin. Their synthesis starts during embryonal development along with the terminal differentiation of oligodendrocytes and is upregulated during postnatal extension of the myelin sheath⁷⁴. In the grey matter, the presence of lipids constituting myelin, starts decreasing around 20 years of age⁷².

Modifications in the concentration or in the pattern of GSLs at PM level harshly influence the behavior of neuronal cells, modulating PM proteins activity through direct GSL- proteins interactions or indirectly through lateral interactions mediated by detergent- resistant membrane portions.

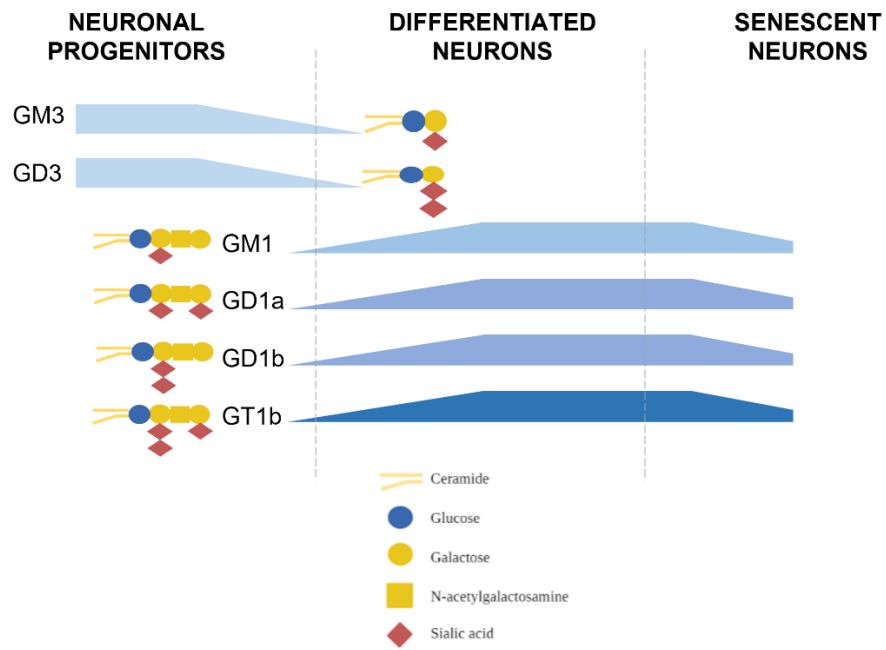


Figure 9. Modifications of the ganglioside pattern in neurons during neuronal differentiation -modified from⁶⁸

2.3. Lysosomal storage disorders

Inherited or acquired defects in the lysosomal catabolism of macromolecules (saccharides, glycogen, and peptides) are classified as lysosomal storage disorders (LSDs). They are distinguished into five classes based on the type of the primary accumulated compound in lysosomes: mucopolysaccharidoses, sphingolipidoses, glycoprotein, and glycogen storage diseases. The accumulation of uncatabolized material can change the lysosomal shape and size, impairing the whole endolysosomal compartment.

In particular, the incidence of sphingolipidoses is around 1: 10,000 individuals but it becomes higher in geographically or culturally isolated populations e.g., Ashkenazi Jewish. LSDs present clinical manifestations in different organs, ranging from the compromission of the cardiovascular system or immunological manifestations to bone disease and neurodegenerative phenotypes. Indeed, lysosome-associated neurodegeneration is induced by a combination of mechanisms, most importantly, the accumulation of undegraded material⁷⁵ and dysregulated signalling⁷⁶. These events cause cellular stress and ultimately lead to apoptosis, which results mainly dangerous in neuronal tissues since these post-mitotic cells have little regenerative capacity. An example of lysosomal-associated neurodegeneration is represented by so-called GCase-related pathologies, which present defects in lysosomal catabolism and the onset of a neurodegenerative phenotype. A list of the LSDs identified so far is reported in Table 1, where LSDs are separated accordingly to the accumulated substrate.

Defects in glycosphingolipid degradation				
Disorder	Defect	Effect on degradation of glycoprotein	Effect on degradation of glycolipid	Clinical symptoms
α - Mannosidosis (type I and II)	α - mannosidase	major	none	Type I: infantile onset, intellectual disability, hepatomegaly, death betw. 3- 12 yr Type II: juvenile/ adult onset, milder
β - Mannosidosis	β - mannosidase	major	none	Severe quadriplegia, death by 15 mo, mild cases have

				intellect. disability + facial dysmorphism and angiokeratoma
Aspartylglucosaminuria	Aspartyl- glucosaminidase	major	none	Progressive, coarse facies, intel. disability
Sialidosis (mucopolipidosis I)	Sialidase	major	minor	Progressive, severe mucopolysaccharidosis- like features, intel. disability
Schindler (types I and II)	α - N- acetyl- galactosaminidase	yes	?	Type I: infantile onset, neuroaxonal dystrophy, severe psychomotor and intel. Disability, cortical blindness, neurodegeneration Type II: mild intel. Impairment, angiokeratoma, corpus diffusum
Galactosialidosis	protective protein/ cathepsin A	major	minor	Coarse facies, skeletal dysplasia, early death
Fucosidosis	α - fucosidase	major	minor	Psychomotor delay, coarse facies, growth retardation
GM1 gangliosidosis	β - galactosidase	minor	major	Progressive neurological disease + skeletal dysplasia
GM2 gangliosidosis	β - hexosaminidase	minor	major	Severe form: neurodegeneration with death by 4 yr Less severe: slower onset of symptoms and variable, all related to CNS

Defects in glycosaminoglycan (GAG) degradation → the mucopolisaccharidosis

Disorder	Number	Defect	GAG affected	Clinical symptoms
Hurler; Hurler-Scheie; Scheie	MPS I H	α - L- iduronidase (IDUA)	DS, HS	<i>Hurler</i> : corneal clouding, organomegaly, heart disease, intel disability, detach in childhood

				<i>Hurler-Scheie/ Scheie</i> : less severe, survive longer
Hunter	MPS II	Iduronic acid- 2-sulfatase (IDS)	DS, HS	Severe: organomegaly, no corneal clouding, intel. Disability, death before 15 yr Less severe: normal intelligence, short stature, survival 20- 60 yr
I- Cell disease	MPS II	N- acetylglucosamine- 1-phosphotransferase		
San Filippo A	MPS III A	Heparan N- sulfatase (SGSH)	HS	Profound mental deterioration, hyperactivity, relatively mild somatic manifestations
San Filippo B	MPS III B	α - N- acetylglucosaminidase (NAGLU)	HS r	Similar to III A
San Filippo C	MPS III C	acetyl CoA: α - glucosaminide N- acetyltransferase (HGSNAT)	HS	Similar to III A
San Filippo D	MPS III D	N- acetyl- glucosamine- 6- sulfatase (GNS)	HS	Similar to III A
Morquio A	MPS IV A	N- acetyl- galactosamine- 6- sulfatase (GALNS)	KS, CS	Distinctive skeletal abnormalities, corneal clouding, odontoid hypoplasia, milder forms known to exist
Morquio B	MPS IV B	β - galactosidase (GLB1)	KS	Same as IV A
Maroteaux- Lamy	MPS VI	N- acetyl- galactosamine- 4- sulfatase (ARSB)	DS	Corneal clouding, normal intelligence, survival to teens, milder forms exist
Sly	MPS VII	β - glucuronidase (GUSB)	DS, HS, CS	Wide spectrum of severity, including hydrops fetalis and neonatal form

Natowicz	MPS IX	hyaluronidase (HYAL-1)	Hyaluronan	Periarticular soft tissues masses, short stature, mild facial changes
Multiple sulphatase deficiency (MSD)	SUMF-1	FGE converts cysteine → formyl glycine (SUMF1)	All sulphated glycans	Hypotonia, developmental delay, neurodegeneration

Defects in glycosphingolipids degradation

Disorder	Defect	Clinical symptoms
Tay- Sachs	β -hexosaminidase A	<i>Severe:</i> neurodegeneration, death by 4yr <i>less severe:</i> slower onset of symptoms, variable symptoms all relating to parts of the nervous system)
Sandhoff	β - hexosaminidase A and B	Same as Tay- Sachs
GM1 gangliosidosis	β - galactosidase	-
Sialidosis	sialidase	-
Fabry	α - galactosidase	Severe pain, angiokeratoma, corneal opacities, death from renal or cerebrovascular disease
Gaucher's	β - glucocereamidase	<i>See paragraph 2.1.1.</i>
Krabbe	β - galactoceramidase	Early onset with progression to severe mental and motor deterioration
Metachromatic leukodystrophy	arylsulfatase A (cerebroside sulfatase)	Infantile, juvenile and adult forms can include mental regression, peripheral neuropathy, seizures, dementia
Saposin deficiency	saposin precuros	Similar to Tay- Sachs and Sandhoff
Farber	acid ceramidase	<i>Severe:</i> death by age 2-3 yr; Lipogranulomatosis, moderately impaired mental ability and difficulty with swallowing
Niemann Pick type A and B	sphingomyelinase	Accumulation of sphingomyelin, symptoms and signs similar to Gaucher disease

Multiple enzyme deficiency

Disorder	Defect	Clinical signs
Wolman's/ cholesterol ester storage disease	Acid lipase	Accumulation of cholesterol esters
Niemann- Pick	NPC1	Accumulation of cholesterol, sphingomyelin
Pyknodystosis	Cathepsin K	Accumulation of bone proteins
Cystinosis	Cystine	Cystinosis

Salla disease (infantile free sialic acid storage disease)	Sialin	Sialic acid, glucuronic acid
Infantile neuronal ceroid lipofuscinosis	Palmitoyl- protein thioesterase	Accumulation of palmitoylated proteins
Late infantile neuronal ceroid lipofuscinosis	Pepstatin- insensitive lysosomal peptidase	Accumulation of pepstatin- insensitive lysosomal peptidase

Table 1. Classification of lysosomal storage disorders based on the typology of defect

2.3.1. *GBA*- related pathologies

GBA1 gene localized at 1q22, encodes for the GCCase enzyme, responsible for the catabolism of GlcCer into glucose and ceramide prevalently at lysosomal level. Nowadays more than 300 different loss of function mutations were described, nevertheless the two most frequent disease- causing mutations are the L444P and N370S. Interestingly, these two mutations are found in almost 85 % of GD patients as well as in the 95 % of *GBA*- dependent PD patients, which are the two *GBA*- related pathology described so far⁷⁷.

2.3.1.1. Gaucher Disease

GD is the most common LSD, and it is of autosomic recessive inheritance. GD has a frequency of manifestation of about 1:40,000 newborns with the highest incidence in the Jewish Ashkenazi population, where the frequency of manifestation reaches 1:500- 1:2,000.

This disorder is caused by the deficiency of GCCase activity and the consequent accumulation of the uncatabolized substrate at lysosomal level of the: i) reticulate endothelial system, ii) nervous system, and iii) skeletal apparatus. GD was described for the first time by Doctor Philippe C. E. Gaucher in 1882 and the accumulated substrate was identified only in the 1934 and classified as cerebroside or GlcCer. GlcCer accumulates in many organs and therefore GD is characterized by a continuum of clinical phenotypes, which have been conventionally classified in 3 main types: Type 1 GD is the most common non- neuronopathic form and is characterized by a high variability of symptoms including: anemia, platelet deficiency, splenomegaly, and bone disease. Type 2 GD is the

most severe neuronopathic form, which has its onset in the first years of life and besides the symptoms of GD type 1, it shows also neurological impairment which leads to death in the first years of life. Type 3 GD is the neuronopathic chronic subacute form which presents the same symptomatology as GD type 1 together with progressively invalidating neurological symptoms⁷⁸.

Therapeutical strategies are aimed to reduce GlcCer content by Enzyme Replacement Therapy (ERT) which is based on the intravenous administration of small amounts of recombinant GCCase (known as *Cerezyme*)⁷⁹. *Cerezyme* contains two Man6P residues which allow its recognition by Man6PR in the endolysosomal compartment. This strategy allows to increase the amount of GCCase present at lysosomal level to catabolize the accumulated GlcCer.

Another possible therapeutic tool is based on *the Substrate Reduction Therapy* (SRT) using *N-butyldeoxy-nojirimycin (NB-DNJ: Zavesca)*⁸⁰ as inhibitor of the GlcCer synthase, the enzyme responsible for GlcCer synthesis. *Zavesca*, respect to *Cerezyme*, is able to cross the blood brain barrier, partially resolving the symptoms of patients affected by GD type 2 and 3. Unfortunately, due to an important side effect of the drug, its administration is prescribed only to those patients which are not suitable for ERT therapy⁸¹.

2.3.1.2. *GBA*- dependent Parkinson's Disease

PS is a progressively neurodegenerative pathology characterized by the selective loss of dopaminergic neurons in the *pars compacta* of the *substantia nigra*. These neurons are responsible for the performance of voluntary movements, and they ensure a correct functioning of the automatic movements as the walking. The main regulatory pathway involved in this process is the one coordinated by the neurotransmitter dopamine, which is deficient in PD.

Typical feature of PD is the presence inside neurons of inclusion bodies called Lewy Bodies, whose principal component is α -synuclein, a small protein involved in synaptic functioning. Due to this feature, PD is also classified as synucleinopathy.

The pathology affects both males and females, with a slight prevalence towards males. Usually, the onset is around 58- 60 years of age, but 10 % of the patients can develop it before the 50 years of age. PD affects approximately the 0.3 % of the general population, more than 1 % of individuals above 65 years old and this portion increases to 3- 5 % in people above 85 years of age.

Association studies have identified at least 15 loci and 13 genes involved in PD⁸², among which there are the α -synuclein gene *SNCA*, *PARK2*, *PINK1*, *LRKK2*, and others.

Until 2004, *GBA1* gene was thought to be just responsible for GD. Recently it has been observed that GD type 1 is often associated with PD onset including various forms of parkinsonism. Type 1 GD patients have a 20- folds increased risk to develop PD with respect to the healthy population⁸³, while individuals carrying monoallelic mutations of *GBA1*, have a 5- folds higher risk to develop the pathology⁸⁴. A reduced GCase activity has been observed in the brain of PD patients carrying *GBA1* mutations as well as in sporadic PD patients⁸⁵. Studies on iPSCs- derived neurons obtained from *GBA*- PD patients, have led to hypothesize that the accumulated GlcCer could function as a scaffold for the oligomerization of α - synuclein, which on its turn forms a complex that furtherly inhibits GCase activity. This suggests auto- propagation features of the pathology⁸⁶. Unless the great effort, the molecular mechanisms linking *GBA1* loss of function mutations with the onset of neurological damage in GD and PD are not elucidated so far.

2.4. *In vitro* models for Parkinson's Disease and neuronopathic Gaucher Disease

The study of neuronal differentiation mechanisms has been limited by the difficulties in obtaining biological samples and by the lack of suitable *in vitro* models recapitulating the pathology. Until now the most frequently used models are fibroblasts derived from biopsies of patients, differentiated neuroblastoma cell lines, immortalized murine neurons, mouse cerebellar granule cells, and only recently, models exploiting human induced pluripotent stem cells (iPSCs). Up to now, iPSCs are the only models that allow to obtain human neurons presenting the same genetic features of patients. This is an important aspect, because the main drawbacks in the study of neurodegenerative pathologies, are the inaccessibility to the human brain *in vivo* and the difficulties in working on the *post-mortem* human brain.

The ability to generate pluripotent stem cells starting from completely committed adult cells as the skin fibroblasts, has revolutionized the study of neurodegenerative disorders. Fibroblasts have to be extracted from the patient they are then reprogrammed to pluripotent stem cells through transfection with a linear DNA fragment containing a polycistronic reprogramming cassette made of a CAG promotor that leads the expression of four factors: Oct4, Sox2, Klf4, and c-Myc. These cells can then undergo an *in vitro* differentiation process to obtain a specific neuronal commitment: they can become a population of dopaminergic, glutamatergic or GABAergic neurons or motoneurons⁸⁷.

These 2D models help having a better insight into the molecular mechanisms involved in the pathological onset and development but do not give any information about the surrounding environment which could influence the neuronal population growth and development, playing an important role in the pathogenesis. For this reason, during the last years particular attention was paid on the development of 3D cultures, called organoids, that could give better insights into the complexity and maturity of the studied organ or of its compartments. The advent of self-organized, 3D midbrain organoids has opened a new research opportunity to better investigate the molecular mechanisms, the influence of surrounding cells and in general to better recapitulate the pathological features occurring *in vivo*. Midbrain organoids are generated starting from induced pluripotent stem cells obtained from patients or healthy subjects' fibroblasts, cultured on a polymeric matrix with high support of nutrients and differentiation factors to yield embryoid bodies and allow the development of the neuroepithelium up to the generation of a fully differentiated organoid expressing neuronal differentiation markers and dopaminergic markers as tyrosine hydroxylase and neuromelanin⁸⁸.

2.5. Brain metabolism

The brain occupies about 2 % of the total body weight, but in resting conditions it uses the 20 % of the total energy available. In particular, neurons account for about 90 % of ATP consumption of the brain⁸⁹. Based on literature data it is known that neurons consume prevalently glucose to sustain their energetic demand, but in case of needs they can also take advantage of other substrates. For instance, during fasting or during the physiological brain development neurons also metabolize ketone bodies, while in case of intense physical activity they can also use lactate as energetic substrate⁹⁰. Lactate is massively produced by astrocytes and then transferred to neurons according to their needs. This process is defined as the Astrocyte- to- Neuron Lactate Shuttle (ANLS) and was described for the first time by Pierre Magistretti and Luc Pellerin⁹¹. According to previously reported evidence, astrocytes exploit more anaerobic glycolysis than neurons which are more prone to use oxidative phosphorylation, probably also related to the fact that neurons need a higher energy production⁹²⁻⁹⁴.

2.5.1. Glucose metabolism

The brain does not have sufficient energy storages as for example glycogen and for this reason it highly depends on the blood supply of metabolites with particular regards for glucose. This can change depending on the brain area, on the cell type, on the class of glucose transporter and so on its affinity and specificity to glucose.

Glucose metabolism doesn't serve only for energetic purposes, it produces several metabolic intermediates which are then used for the synthesis of macromolecules such as fatty acids and other lipids, which are essential components of cell membranes and myelin sheaths, or amino acids for the protein synthesis and for the production of neurotransmitters, or it can be used for the synthesis of sugars, nucleotides, and to produce glycogen in astrocytes.

Focusing on neurons, the main pathways responsible for glucose metabolism are the glycolysis, the pentose phosphate pathway (PPP), the tricarboxylic acid (TCA) cycle, and the oxidative phosphorylation. Glucose enters the cell and is converted to glucose- 6- phosphate by the hexokinase. Glucose- 6- phosphate can be further processed via glycolysis or PPP or can be used for glycogen synthesis. For what concerns glycolysis, glucose is converted to pyruvate, which can be either transported into the mitochondria to give acetyl coenzyme A, which after being bound to citrate, is subjected to several enzymatic reactions with the aim to produce reduced nicotinamide adenine dinucleotide (NADH) and flavin adenine dinucleotide (FADH₂) in the TCA cycle. The NADH and FADH₂ are oxidized in the electron transport chain, which exploits the energy produced by the transfer of electrons through the four complexes, to generate a proton gradient in the intermembrane space. This gradient is then used by the ATP synthase (complex V) to generate ATP from ADP pushing protons back into the mitochondrial matrix.

Glucose- 6- phosphate in neurons is preferentially metabolized through the PPP, where it is converted into 5- carbon sugars for the biosynthesis of nucleotides at the expenses of NADP which gets reduced to nicotinamide adenine dinucleotide phosphate (NADPH). Based on the requirements, an intermediate of the PPP can be converted into intermediates of the glycolytic pathway in order to supply it. The physiologically PPP is highly active in neurons, since NADPH is essential for synthesis of fatty acids and myelin, for neurotransmitter turnover, and to maintain redox homeostasis, by assisting in the reduction of the oxidized glutathione. On the other hand, astrocyte use glucose in a complementary way to neurons where its conversion through glycolysis into lactate is the predominant pathway⁹⁵.

3. AIM

SLs are components of all cell membranes and are mainly associated with the external leaflet of the PM of all eukaryotic cells. In particular, they are highly represented in neurons, with a specific role played by gangliosides, a class of complex GSLs that contain one or more residues of sialic acid in the hydrophilic chain. During the neuronal differentiation and maturation, the SL composition undergoes profound quantitative and qualitative modifications. The fine regulation of the SL's PM pattern is the result of a complex metabolic machinery, including the biosynthesis in the endoplasmic reticulum and Golgi apparatus, the catabolism in the endolysosomal compartment, and the trafficking of SLs to several cell districts. The information concerning the onset of pathological phenotypes due to deficiency of the biosynthetic enzymes is scant. On the other hand, the loss of function of catabolic enzymes is widely studied and leads to the onset of LSDs. Among these pathologies, the most common is the GD, which is caused by biallelic loss of function mutations in *GBA1* gene. This gene encodes for GCCase, an enzyme involved in the catabolism of GlcCer. In addition, monoallelic mutations of this enzyme have been associated to the development of PD, named therefore *GBA*-dependent PD, which is characterized by the progressive and selective loss of dopaminergic neurons. Despite the recent findings reported in literature, no data are available on the effect of monoallelic *GBA1* mutations on the human brain as well as on the molecular mechanism linking GCCase loss of function with the onset of neuronal degeneration.

My PhD project was mainly focused on dissecting the molecular mechanism linking the aberrant lysosomal accumulation of GlcCer, due to GCCase deficiency, with the onset of neurodegeneration. First, I have investigated *post-mortem* brain areas derived from a patient affected by *GBA*-PD in order to understand the biochemical features behind the pathology. Afterwards, I have exploited the use of two *in vitro* models developed in our laboratory and based on mouse cerebellar granule neurons and dopaminergic neurons derived from human iPSCs. Both models were treated with conduritol b epoxide to suppress GCCase activity and mimic the pathological features of GD. The data related to the development and characterization of these *in vitro* models, described in *section 5.2.1* have already been published on *Cells* journal⁹⁶. The manuscript and the related supporting information are attached in *section 9* of the present work.

4. METHODS

4.1 Brain areas isolation

Fresh brain areas such as frontal cortex, *substantia nigra*, parietal cortex, *cerebellum*, *hippocampus* from one male affected by *GBA*- PD and three healthy males of age comprised from 50 to 60 years, dead for accidental reasons and without clinical history of disorders affecting the CNS, were collected within 6 hours post- mortem and immediately immersed in liquid nitrogen. Each individual snap frozen sample was sealed in an air- tight bag and stored at -80 °C.

4.2 Cell culture of induced pluripotent stem cells (iPSCs)

Induced pluripotent stem cells were generated starting from fibroblasts of a healthy subject at IRCCS Foundation Ca' Granda Ospedale Maggiore Policlinico. Fibroblasts were derived from a skin punch biopsy and cultured in DMEM supplemented with 15 % foetal bovine serum and 100 U/ ml penicillin, and 100 µg/ ml streptomycin. Cells were cultured in a humidified atmosphere at 37 °C, 5 % CO₂. They were reprogrammed using a commercial kit (CytoTune™- iPS 2.0 Sendai Reprogramming Kit, ThermoFisher) according to manufacturer's instructions. Fibroblasts were incubated with the virus for 24 hours. After 6 days of culture, cells were detached, plated in 6- well plates and maintained in culture with the specific medium (Essential 8™ Medium, ThermoFisher) to obtain the formation of iPSCs colonies. iPSCs were grown on Geltrex- coated supports (1 % for 1 hour at 37 °C) and passaged once reached the 80 % of confluence using Accutase® (3 minutes, 37 °C) for the detachment. Cells were plated at a density of 10⁴ cells/ cm² and cultured in Essential 8™ Medium supplemented with 10 µM Rock inhibitor, the latter was removed after 24 hours and replaced with fresh Essential 8™ Medium.

4.3 IPSC characterization

4.3.1. Real-time PCR (qPCR)

4.3.1.1. RNA extraction

RNA extraction was achieved by TRIzol™ Reagent (Invitrogen). After a mechanical homogenization of the sample with 1 mL of TRIzol™ Reagent, 200 µL of ice- cold CHCl₃ was added. Samples were vortexed to form an emulsion and then centrifuged for 10 minutes at 4°C at 13,500 rpm. The aqueous phase containing RNA was collected in a new tube and ice-cold isopropanol was added in

1: 1 ratio, mixing gently. The RNA was precipitated overnight at -20 °C. Samples were then centrifuged for 20 minutes at 4 °C at 13,500 rpm. RNA pellets were then washed two or three times with 1 mL of ice-cold 70 % ethanol. For every wash, samples were centrifuged for 5 minutes at 6,000 rpm at 4 °C. After the last wash, RNA pellets were dried in fume hood for a few minutes until they become transparent. RNA pellets were then resuspended in RNase- free water based on the RNA pellet dimension (usually 20- 30 µL for 5×10^6 cells) and kept at -80 °C until further use.

4.3.1.2. Quantification of extracted RNA by UV absorption

RNA was quantified using UV absorption at 260 nm through a spectrophotometer. The linear relationship between absorbance and concentration of an absorbing specie was determined by the Beer- Lambert law, $A = \log (I_0/I) = \epsilon \times C \times l$, which predicts a linear change in absorbance along with concentration. The NanoDrop 1000 Spectrophotometer (Thermo Fisher Scientific) was used to perform the analyses. The ratios of the absorbance 260/ 280 nm (~2.0) and 260/ 230 (~1.8-2.2) were used to assess the RNA purity. RNA samples were diluted to reach 500 ng/ µL and after every dilution the RNA concentrations were quantified again.

4.3.1.3. RT-PCR

The iScript cDNA Synthesis Kit (Bio-Rad) was used to perform the retrotranscription. This kit contains oligo (dT), random hexamer primers and a reverse transcriptase enzyme. To perform retrotranscription, 500 ng of RNA were transferred in a PCR RNase- free tube and nuclease- free water was added up to 15 µL volume. Then 5 µL of mix solution (4 µL 5X iScript Reaction Mix/ Buffer, 1 µL iScript Reverse Transcriptase) were added and the PCR tube containing complete reaction mix was incubated in a thermal cycler using the RT-PCR protocol. cDNA was stored at -20 °C until use.

4.3.1.4. qPCR

The qPCR mix used was the SsoFast™ EvaGreen® Supermix 2X (Bio-Rad). Retrotranscribed cDNA from RT- PCR was further diluted (1: 10) and 5 µL of diluted cDNA for each sample were loaded in triplicate in a Hard-Shell® 96-Well PCR Plates (Bio-Rad). 15 µL of SsoFast™ EvaGreen® Supermix diluted with nuclease- free water and with the specific primers for the target of interest (Table 2), were added. In this final qPCR reaction volume, Supermix reached the right dilution and primers got 10 µM concentration. Routine qPCR negative controls were included in the plate and the qPCR protocol was performed using a CFX96™ Real- Time System (Bio-Rad) coupled with a C1000™

Thermal Cycler (Bio-Rad). Once qPCR was carried out, data were analysed with the CFX Manager Software (BioRad) and excel data sheet tool. Gene expression was achieved through the use of Δ CT as relative gene expression analysis using a reference gene. Δ CT was calculated through Ct normalization of the target gene to the reference YWHAZ gene.

$$2^{(Ct(\text{ref})-Ct(\text{sample}))} = \text{Expression}$$

PRIMER	SEQUENCE 5'>3'
YWHAZ-FW	ACTTTTGGTACATTGTGGCTTCAA
YWHAZ-RV	CCGCCAGGACAAACCAGTAT
OCT4-FW	AGGCTCTGAGGTGTGGGGGAT
OCT4-RV	TGAGAGGTCTCCAAGCCGCCT
NANOG-FW	CATGAGTGTGGATCCAGCTTG
NANOG-RV	CCTGAATAAGCAGATCCATGG

Table 2. List of primers used for qPCR

4.3.2. Karyotype analysis

After incubation with colchicine for 3 hours, iPSCs were incubated with 0.6 % sodium citrate and 0.13 % potassium chloride, fixed with CH₃OH/ CH₃COOH, and incubated with Quinacrine solution to obtain Q- banding. Metaphases were acquired and analyzed with MetaSyste- Ikaros.

4.4. iPSCs differentiation into dopaminergic neurons

iPSCs were differentiated into dopaminergic (DA) neurons according to the protocol developed by Zhang *et. al.*⁹⁷. Cells were cultured in a humidified atmosphere at 37 °C, 5 % CO₂ using different media supplemented with specific factors:

-Day in culture (DIC) 0: KSR differentiation medium (82 % DMEM high glucose with sodium pyruvate, 15 % KSR, 100X non- essential amino acids, 100X mercaptoethanol, 100 U/ ml penicillin, 100 µg/ ml streptomycin; and 100X L- glutamine) supplemented with 100 nM LDN- 193189 and 10 µM SB431542.

-DIC 1 and DIC 2: DIC 0 medium supplemented with 0.25 µM SAG, 2 µM purmorphamine, and 50 ng/ ml FGF8b.

- DIC 3 and DIC 4: DIC 1 and DIC 2medium supplemented with 3 µM CHIR99021.

- DIC 5 and DIC 6: 75 % KSR differentiation medium combined to 25 % of N2 differentiation medium (98 % DMEM high glucose with sodium pyruvate, 100X N2 supplement, 100 U/ ml penicillin, 100 µg/

ml streptomycin, and 100X L- glutamine) supplemented with 50 ng/ ml FGF8b, 100 nM LDN- 193189, 2 μ M purmorphamine, 0.25 μ M SAG, and 3 μ M CHIR99021.

-DIC 7 and DIC 8: A combination of 50 % of KSR differentiation medium and 50 % N2 differentiation medium supplemented with 3 μ M CHIR99021 and 100 nM LDN- 193189.

- DIC 9 and DIC 10: A combination of 25 % KSR differentiation medium and 75 % of N2 differentiation medium supplemented with 3 μ M CHIR99021 and 100 nM LDN- 193189.

- DIC 11 and DIC 12: B27 differentiation medium (96 % Neurobasal Medium 1x, 50X B27 supplement, 100 U/ ml penicillin and 100 μ g/ ml streptomycin, 100X glutamax) integrated with 10 ng/ ml BDNF, 10 ng/ ml GDNF, 3 μ M CHIR99021, 1 ng/ ml TGF3 β , 0.1 mM cAMP, and 0.2 mM ascorbic acid.

- DIC 13 and following DIC: B27 differentiation medium integrated with 10 ng / ml BDNF, 10 ng/ ml GDNF, 1 ng/ ml TGF3 β , 0.1 mM cAMP, and 0.2 mM ascorbic acid.

At DIC 20 cells were enzymatically detached using Accutase[®] solution (3 minutes, 37 °C) and replated on different Geltrex- coated supports (1 % for 1 hour at 37 °C) at lower cell density based on experimental needs: 2×10^5 cells/ cm². The cell culture medium was changed daily.

4.5. Primary culture of mouse cerebellar granule neurons

Pregnant C57BL/ 6J mice were provided by Charles River- Research Models and Services (Calco, Lecco, Italy). Animal procedures were approved by the Ethics Committee of the Università degli Studi di Milano, Italy and were performed in accordance with the National Institute of Health Guide for the Care and Use of Laboratory Animals (Directive 2010/ 63/ EU) (project numbers FD611.N.TAQ).

Cerebellar granule neurons (CGNs) were obtained from cerebella of 5 postnatal days pups of C57BL/ 6 mice as previously described⁹⁸. Briefly, mice pups were sacrificed by decapitation, cerebella were extracted under sterile conditions and then transferred into a Petri dish containing Ca²⁺ Mg²⁺ free PBS supplemented with 0.2 % (w/ v) glucose (CMF- PBS-glucose). After the removal of meninges, cerebella were mechanically triturated and using CMF- PBS-glucose solution they were then transferred in a sterile 15 ml tube. After the sedimentation of triturated cerebella and the removal of supernatant, 1 ml of CMF- PBS-glucose containing trypsin (1 % w/ v) and DNase (0.1 % w/ v) was added to obtain the enzymatic lysis of the tissue. To note, DNase allows to digest the DNA possibly released by the damaged cells after the lysis process. The suspension was incubated for 3.5 minutes RT and then centrifuged for 10 seconds at 1,000 x g to remove the supernatant. Afterwards, 1 ml of

CMF-PBS-glucose containing trypsin inhibitor (0.04 % w/ v) and DNase (0.1 % w/ v) was added to the pellet. To obtain a single cell suspension, cells were passed through glass Pasteur pipettes with decreasing diameter; in detail, 60 times trituration with the biggest calibre, 30 times trituration with the medium calibre, and 15 times with the smallest calibre. Cell suspension was then centrifuged at 1,000 x g for 5 minutes and supernatant was discarded. Cell pellet was subsequently resuspended in 6 ml of CMF- PBS-glucose; then cell suspension was further centrifuged at the above- mentioned conditions. Finally, supernatant was discarded, and the cell pellet was resuspended in 10 ml of complete culture medium (Neurobasal A supplemented with B27 (1 % v/ v), L-glutamine, 25 mM KCl, 2 mM, 100 U/ ml penicillin e 100 µg/ ml streptomycin). Cerebellar granule cells were plated at the cell density of 3.15×10^5 cells/ cm² in different poly- L- lysine- coated (10 µg/ ml 2 hours, 37 °C) supports based on experimental needs. Cells were cultured in a humidified atmosphere at 37 °C, 5 % CO₂. The day after plating, cytosine β- D- arabinofuranoside was added directly to the cell medium at the final concentration of 2.5 µg/ ml to prevent replication of non- neuronal cells. Half of the cell culture medium was changed every 48 hours.

4.6. Cell treatment with conduritol B epoxide

Human DA neurons at DIC 31 and CGNs at DIC 3 were treated respectively for 14 or 29 days and for 7 or 14 days with 0.5 mM conduritol B epoxide (CBE), a specific and irreversible inhibitor of GCase enzyme. CBE was dissolved in H₂O and daily administered to the differentiation medium to reach the concentration of 0.5 mM. For DA neurons cell culture medium was changed every 24 hours keeping cells in the presence of CBE. For CGNs half of the cell medium was changed every 48 hours keeping cells in the presence of CBE. Cells under the same experimental conditions without CBE administration were used as control condition.

4.7. Cell treatment with glucosylsphingosine

Glucosylsphingosine (GlcSph) was administered to DA neurons and CGNs, respectively at DIC 40 and 14. At DIC 37, prior to GlcSph administration, DA neurons needed to be detached (Accutase, 3 minutes, 37 °C) and replated at 200, 000 cells/ cm².

GlcSph was solubilized directly in the culture medium of CGNs or DA neurons at the concentrations of 0.1 µM or 10 µM. Concerning DA neurons cell medium was changed daily

keeping cells in the presence of GlcSph. For CGNs, half of the cell medium was changed every 48 hours keeping cells in the presence of GlcSph.

4.8. Treatment of CGNs with [³H (sphingosine)]- GM1

Isotopically labelled [³H(sphingosine)]- GM1 was administered to both control and CBE-treated mouse cerebellar granule neurons. [³H(sphingosine)]- GM1 dissolved in CH₃CH₂CH₂OH: H₂O (7: 3, v: v) was transferred in a sterile glass tube and dried under nitrogen flow and the residue was solubilised in the cell culture medium. To follow the catabolism of [³H(sphingosine)]- GM1 in the lysosomes, after removal of the medium and rapid washing of cells, 1.5 ml of the medium containing the radioactive lipid were added to each well of 6-well plates and the cells were incubated at 37 °C for 4 hours (0.1 µCi/ well). At the end of incubation, cells were washed three times with complete cell culture medium and incubated in the same medium for 5 minutes. Finally, cells were harvested with water containing protease inhibitor cocktail and processed for lipid analysis as described below in the sample preparation paragraph.

Radioactive lipids were extracted as described below and separated by HPTLC using the solvent system CHCl₃: CH₃OH: 0.2 % CaCl₂ 50: 42: 11 (v: v: v). Visualization and quantification were carried out as described below.

4.9. Cell viability assays

4.9.1. Calcein assay

Calcein assay is a cell viability assay based on the use of the calcein- acetoxymethyl ester (Calcein-AM), a highly lipophilic cell- permeant dye which rapidly crosses the PM of viable cells. Once internalized, cellular esterases remove the acetoxymethyl ester group from calcein which thus can emit fluorescence.

DA neurons and CGNs were seeded in a 96- well microplate at the density of 3,15x 10⁵ cells/ cm². After the removal of culture medium, cells were washed once with HEPES-buffered solution (135 mM NaCl, 10 mM KCl, 0.4 mM MgCl₂, 10 mM HEPES) and then incubated with Calcein- AM solution at the final concentration of 0.005 µg/ µl in HEPES- buffered solution (15 minutes, 37 °C). At the end of incubation, Calcein- contained solution was discarded, and cells were lysed by the addition of 1 % Triton X- 100 in TNEV buffer. The microplate was incubated in mild agitation for 10 minutes and

then the reaction volume was transferred to a black microplate (Black, 96- well, OptiPlate- 96 F, Perkin Elmer) for the fluorescence detection by a Victor microplate reader (Perkin Elmer) (ex/ em 495/ 515 nm).

4.9.2. MTT assay

MTT assay is a colorimetric assay for assessing mitochondrial activity. The mitochondrial enzymes can reduce the tetrazolium dye MTT 3- (4,5- dimethylthiazol- 2- yl)- 2,5- diphenyltetrazolium bromide to insoluble formazan, which has a purple colour.

DA neurons and CGNs were seeded in a 96- well microplate at a density of $3,15 \times 10^5$ cells/ cm². After the removal of culture medium, cells were washed once with HEPES-buffered solution (135 mM NaCl, 10 mM KCl, 0.4 mM MgCl₂, 10 mM HEPES) and then incubated with MTT solution diluted in cell culture medium (0.1 % w/ v MTT final concentration). After 2 hours of incubation (37 °C, 5 % CO₂), MTT solution was discarded and lysis buffer (95 % isopropanol, 5 % formic acid) was added to each well. The microplate was incubated in mild agitation for 10 minutes at RT and then absorbance at 570 nm was detected by a Victor microplate reader (Perkin Elmer).

4.10. Samples preparation

To obtain cell lysates DA neurons and CGNs were washed two times with PBS and then harvested in PBS by mechanical scraping. After 10 minutes centrifugation at 2,000 x g at 4 °C, cellular pellets were resuspended in Milli- Q water supplemented with protease inhibitor cocktail (SigmaAldrich) and transferred to 2 ml tubes.

For what concerns post- mortem human brain samples, each brain sample was weighted and additioned with an amount of water supplemented with protease inhibitor cocktail equivalent to 15 folds the weight of the sample.

Both cell pellets and brain samples were then homogenized using an ultrasonic pulse homogenizer at 25 db for 10 seconds.

4.11. Identification of the protein content

4.11.1. Determination of protein content through *DC* protein assay

Samples protein content was determined in triplicate through *DC* protein assay (Bio-Rad). The assay was performed in a 96-wells plate using: 5 μ l for the background, 5 μ l of BSA with increasing concentration for the standards and 5 μ l of each sample lysate properly diluted in H₂O to be in the range of linearity of the assay which is between 0.2 and 2 mg proteins/ ml. After the sequential addition of 25 μ l of Reagent A (an alkaline copper tartrate solution) and 200 μ l of Reagent B (a diluted Folin reagent) the plate was put on gently agitation for 15 minutes at RT and then absorbance evaluated by a spectrophotometer (Victor, Perkin- Elmer). Protein content was calculated interpolating the average absorbance value of each sample within the calibration curve obtained from the standards' absorbance values.

4.11.2. Indirect immunofluorescence experiments

iPSCs, DA neurons and CGNs for immunofluorescence experiments were seeded in 12-well plates on sterilized and delipidated coverslips of 13 mm diameter to allow visualization of the cells following immunofluorescence by inverted wide field microscope. Cells were plated at a concentration of 10⁵ cells/ well. After 14 DIC for CGNs, 60 DIC for DA neurons and when iPSCs colonies reached about 60 % confluence, cells were washed 2 times in PBS and fixed in a 4 % paraformaldehyde solution in PBS at RT for 20 minutes for neurons and 30 minutes for iPSCs. Cells were rinsed twice with PBS and permeabilized using 0.2 % triton X- 100 in PBS 1X for 10 minutes at RT and after one wash in PBS, non- specific binding sites were blocked for 1 hour at RT in blocking solution which consisted of PBS containing 1 % BSA, 2 % donkey serum for neurons and PBS + 3% BSA + goat serum (Vector) 5 % + Triton X- 100 0.3 % for iPSCs. Incubation with primary antibodies has occurred in semidry condition for 2 hours at RT for neurons and overnight at 4 °C for iPSCs. Antibodies were diluted in 0.25X blocking solution and combined as follows to allow a concomitant staining of the antigens: anti- β 3- tubulin (mouse, CellSignaling; 1: 200) together with anti- TH (rabbit, Millipore; 1: 1000), anti- MAP2 (rabbit, SigmaAldrich; 1: 50) together with anti- Nestin (mouse, SantaCruz; 1: 250) and anti- Neurofilament H (mouse, CellSignaling; 1: 400) in combination with anti- PSD95 (rabbit, CellSignaling; 1: 100), and anti- LAMP1 (mouse, DSHB, dilution: 1: 50), anti- Sox2 (rabbit, CellSignaling, 1: 200), anti- TRA- 1- 60 (mouse, CellSignaling, 1: 500), anti- TRA-1- 81 (mouse, CellSignaling, 1: 500), anti- Oct4 (rabbit, CellSignaling, 1: 100), anti- SSEA4 (mouse, CellSignaling, 1: 200), anti- Nanog (rabbit, CellSignaling, 1: 200). After the staining with the primary antibody cells were washed in PBS and incubated 1 hour at RT with the respective secondary

antibody: anti- mouse AlexaFluor488 (Invitrogen, 1: 2000) and anti- rabbit AlexaFluor568 (Invitrogen, 1: 500). Finally, cells were washed two times with PBS and incubated 10 minutes at RT with Hoechst in PBS (1: 500) for nuclear staining. After three washings, coverslips were mounted on glass slides using Fluoromount-G™ mounting medium to guarantee anaerobic conditions. Images were acquired using a Nikon Eclipse 90i Ni microscope at 20X magnification.

4.11.3. Immunoblotting

Aliquots of lysates obtained from iPSCs derived DA neurons, CGNs, and human brain areas were denatured with 5X Laemmli Buffer and heated at 95°C for 5 minutes; proteins were separated by SDS- PAGE using a 4- 20 % polyacrylamide gradient gel (Mini- PROTEAN® TGX™ Precast Gels (Bio- Rad) in a Mini- Protean- IV Cell electrophoretic cell. Electrophoretic run was performed at constant voltage (80 V in stacking gel and 180 V in running gel) in running buffer (Tris- HCl 25 mM, glycine 19 mM and 0.1 % SDS). Separated proteins were transferred on Turbo Polyvinylidene difluoride (PVDF) Mini-membrane (Bio-Rad) using the Bio- Rad Trans- Blot® Turbo™ Blotting System for 7 minutes at a constant voltage of 25 V and current intensity of 1.3 A. To verify the protein transfer, PVDF membranes were stained using Red Ponceau dye (Ponceau Red dye 0.1 %, Acetic Acid 5% in H₂O) for 5 minutes under mild agitation. Membranes were then rinsed in Milli- Q H₂O and then in Tris- buffered Solution (Tris- HCl 10 mM, NaCl 150 Mm) with 0.1 % Tween- 20 pH 8 (TBS- T 0.1 %) three times and blocked with blocking solution (5 % non- fat dry milk/ TBS- T 0.1 %) for 2 hours RT, in order to block unspecific binding sites.

PVDF membranes were incubated with primary antibodies diluted in blocking solution or in a 5 % BSA solution in TBS- T 0.1 %; specifically the following primary antibodies were used: Polyclonal rabbit anti- PSD95 (Cell Signaling , dilution: 1: 1,000), polyclonal rabbit anti- MAP2 (Immunological Sciences, dilution: 1: 1,000), monoclonal mouse anti- Tau (Immunological Sciences, dilution: 1: 1,000), monoclonal mouse anti- Neurofilament H (Cell Signaling, dilution: 1: 1,000), monoclonal mouse anti- LAMP1 (Developmental Studies Hybridoma Bank, dilution: 1: 100), monoclonal mouse non- phospho- Src Tyr416 (Cell Signaling, dilution 1: 1,000), monoclonal mouse phospho- Src family Tyr416 (Cell Signaling, dilution 1: 1,000), polyclonal mouse anti- GAPDH (Immunological Sciences, dilution: 1: 10,000), monoclonal mouse anti- β3- tubulin (Cell Signaling, dilution: 1: 1,000), monoclonal rabbit anti- histone H3 antibody (Cell Signaling, dilution 1: 20,000), polyclonal goat- anti TFEB (Bethyl Laboratories, dilution 1: 500), monoclonal mouse anti- Prp antibody (Cayman, dilution 1: 5,000).

After overnight incubation at 4 °C, the excess of antibody was removed washing the PVDFs three times in TBS- T 0.1 %. Then membranes were incubated for 1 hour at RT with the appropriate secondary antibody goat- anti- rabbit horseradish peroxidase (HRP)- conjugated (Immunological Sciences, dilution: 1: 10,000), goat- anti- mouse HRP conjugated (ThermoFisher: dilution: 1: 2,000 or 1: 10,000 for highly diluted primary antibodies i.e. anti- GAPDH), or anti- goat HRP conjugated antibody (Pierce, dilution: 1: 10,000). Both secondary antibodies were conjugated to HRP and were diluted in blocking solution. After removal of the secondary antibody solutions, membranes were washed three times in TBS- T 0.1 % and incubated with a commercial solution containing luminol (WESTAR ηC, Cyanagen) for 2 minutes in dark conditions. The chemiluminescent signal was revealed through Alliance Mini HD9 (UV TECH Cambridge) digital system and quantified by Alliance 1D software. The chemiluminescent signal revealed was normalized on the signal of the housekeeping protein glyceraldehyde- 3- phosphate dehydrogenase (GAPDH).

4.11.4. Detection of biotinylated proteins

For what concerns the visualization of the biotin pattern of the supernatant after precipitation (SN) and the precipitated fraction (P), I followed the same protocol described for immunoblotting but after incubation with the blocking solution, PVDF membranes were directly incubated with streptavidin conjugated to HRP (Pierce, dilution: 1: 2,000) for 2 hours at RT, which was followed by three washes in TBS- T 0.1 % and by the incubation with the commercial luminol solution as previously described.

4.11.5. Proteomic analysis

All chemicals and reagents used for sample preparation and LC- MS/ MS analysis were purchased from Aldrich (Milano, Italy). Digestion buffer was obtained by dissolving NH_4HCO_3 in Milli- Q water at the final concentration of 50 mM. The reducing solution was 100 mM dithiothreitol in digestion buffer, the alkylating solution was 100 mM iodoacetamide in digestion buffer. Trypsin from porcine pancreas was used for protein digestion: the powder was reconstituted in 40 μL of water + 0.1 % formic acid.

A volume corresponding to 50 μg of proteins was transferred to a new Eppendorf tube. Disulfide bonds were reduced by adding 10 μL of reducing solution and incubating samples at 56 °C for 30

minutes. Cysteine residues were alkylated by adding 30 μL of alkylating solution, vortexing and incubating at RT for 20 minutes in the dark. After spinning the tubes, proteins were precipitated by adding 1 mL of cold acetone and incubating samples at $-20\text{ }^\circ\text{C}$ overnight. Samples were then centrifuged at $20,000 \times g$ for 30 minutes at $4\text{ }^\circ\text{C}$, the supernatant was removed, and the pellet was washed with 100 μL of cold methanol, vortexed for 10 minute and centrifuged at $20,000 \times g$ for 30 minutes at $4\text{ }^\circ\text{C}$. The supernatant was discarded, and protein pellets dried under the fume hood. The pellet was then redissolved 200 μL of digestion buffer (50 mM NH_4HCO_3), and 2 μL of Trypsin (0.5 $\mu\text{g}/\mu\text{L}$) were added. The samples were incubated at $37\text{ }^\circ\text{C}$ in a shaker at 600 rpm overnight for protein digestion. Sample tubes, now containing peptides, were then centrifuged at $20,000 \times g$ for 30 minutes at $4\text{ }^\circ\text{C}$. The supernatant was transferred to new Eppendorf tubes and dried down under vacuum. Peptides were then resuspended in 50 μL of 3 % acetonitrile added with 0.1 % formic acid for LC- MS analysis.

Tryptic peptides were analysed by high- resolution LC- MS using a UPLC NanoAcquity chromatographic system (Waters, Milford, MA, USA) coupled with a TripleTof 5600+ mass spectrometer (Sciex, Warrington, UK) equipped with an electrospray ion source. Peptides were desalted using a trapping column (Guard column YMC- Triart C18, 3 μm particle size, 0.5 x 5 mm, 1/32") then moved on a reversed- phase C18 column (Eksigent C18, 3 μm particle size, 0.3 x 150 mm format) and eluted with a gradient of CH_3CN in H_2O . Both eluents were added with 0.1 % formic acid. Samples were acquired both in DIA (data independent acquisition) and DDA (data dependent acquisition) acquisition modes.

The eluents used were: A (H_2O + 0.1 %) and B (CH_3CN + 0.1 % formic acid). Injection volume was 5 μL (Full Loop), the flow rate was set to 5 $\mu\text{L}/\text{min}$, the column temperature was kept at $45\text{ }^\circ\text{C}$. After trapping the sample on the trap column (at 1 % CH_3CN for 5 minutes), samples were eluted with the following gradient program: 0,0 - 1,0 minutes 5 % B; 1,0 - 60,0 minutes 5 to 40 % B; 60,0 – 63,0 minutes 40 to 95 % B; 63,0 – 68,0 minutes 95 % B and 68,0 – 68,1 minutes 95 back to 5 % B. The column was then reconditioned for 11,9 min. The total run time was 80 min.

Acquisition in SWATH DIA (data independent acquisitions), ESI+ was performed. A TOF MS Scan was set from 350 to 1,250 m/ z. 100 SWATH experiments were collected in high sensitivity mode, each with an accumulation time of 25 ms, from 100 to 1500 m/ z. The total cycle time was ~ 2.8 sec. Collision energy for each window was automatically calculated by the acquisition software using the equation: $\text{CE} = 0.063 (\text{m}/\text{z}) - 3.24$ (parameter recommended by the vendor). The ion source

parameters were: ion spray voltage floating at 5,300 V, ion source gas 1 at 30, curtain gas at 30, declustering potential at 80 V.

The spectra were acquired in ESI+. The scan range was set from 300 to 1250 m/z for MS and from 100 to 1,500 m/z for MS/MS. Precursor ions with charge states 2 and 5 with intensity greater than 150 counts were selected for MS/MS. Collision energy profiles were set according to SCIEX recommended settings. The ion source parameters were: ion spray voltage floating at 5,000 V, ion source gas 1 at 20, curtain gas at 30, declustering potential at 80 V.

The raw data files were analysed by using the SWATH Acquisition MicroApp 2.0.1.2133 of PeakView software 2.2 (SCIEX). The quantification was performed applying the following filters: Number of peptides per protein at 6, number of transition per peptide at 6, peptide confidence threshold at 99 %, FDR threshold at 1 %, maximum mass tolerance at 50 ppm, maximum RT tolerance at 20 minutes, modified peptides were excluded. Multivariate data analysis and other statistics were performed by using the free online software MetaboAnalyst⁹⁹.

Raw data were analysed using Protein Pilot software (SCIEX). The Paragon Method used for protein identification employed an UniProt reviewed human database, the confidence cut-off was set on 0.05, running the false discovery rate (FDR) analysis. Only protein identified with at least two peptides were retained.

4.11.6. Nuclear purification from DA neurons and CGNs

Nuclear purification was performed as previously described¹⁰⁰. Briefly, cells were lysed with 0.5 ml of 50 mM Tris- HCl (pH 7.5), 0.5 % Triton X- 100, 137.5 mM NaCl, 10 % glycerol, and 5 mM EDTA supplemented with protease inhibitor Cocktail and 1 mM Na₃VO₄ (lysis buffer) for 15 minutes in ice under gentle shaking. Lysates were centrifuged at 15,700 x g for 15 minutes at 4 °C. The nuclear pellet was rinsed 3 times with 0.5 ml of lysis buffer, resuspended in 0.1 ml of lysis buffer supplemented with 0.5 % SDS, and sonicated in ice. Upon centrifugation at 15,700 x g for 15 minutes at 4 °C nuclear extracts were collected.

4.11.7. LysoTracker staining

LysoTracker Red DND- 99 (Molecular Probes) is a red-fluorescent dye for labelling and tracking acidic organelles in living cells. CGNs were seeded in a 24-well plate at a density of 3,15 x 10⁵ cells/ cm² and were treated or not with CBE for 17 days. After 20 days in culture, neurons were incubated with LysoTracker diluted directly in the cell media at the final concentration of 50 nM (30 minutes, 37 °C,

5 % CO₂). After one wash in HEPES-buffered solution (135 mM NaCl, 10 mM KCl, 0.4 mM MgCl₂, 10 mM HEPES), images were acquired with Olympus IX50 Inverted Fluorescence Microscope equipped with a halogen lamp directly on live cells.

4.12. Evaluation of enzymatic activities

4.12.1. Evaluation of enzymatic activities in total lysates

Enzyme activities of glycohydrolases were determined in lysates of DA neurons, CGNs, and human brain samples using an already published method by Aureli et al.³² Evaluated enzymes were the following: β - glucocerebrosidase (GCase), non- lysosomal β -glucosylceramidase (NLGase), β - galactosidase (β - Gal), β - hexosaminidase (β - Hex), α - mannosidase (α - Man) and β - mannosidase (β - Man). The method exploits fluorogenic substrates specific for each glycohydrolase. Enzymatic activity determines the release of methylumbelliferone conjugated to the substrate. In this condition methylumbelliferone at alkaline pH emits a fluorescent signal, which can be detected by a fluorimeter (Victor, Perkin- Elmer) (ex/ em 365/ 460 nm).

Each sample has been assayed in triplicate and as background for each enzymatic assay, wells have been set up with the same experimental conditions without the sample, to evaluate substrates auto-hydrolysis. Each reaction mixture has been put at 37 °C on gently agitation for at least 1,5 hours, then 10 μ l of the reaction mixture were transferred to a black 96- well plate (Black, 96- well, OptiPlate 96 F, Perkin Elmer) and added with 190 μ l of 0.25 M glycine pH 10.7 to stop the reaction and reach the maximum fluorescence emission peak of the free MUB. Plates were analysed through a microplate reader (Victor, Perkin Elmer). Nanomoles of converted substrate were calculated with the help of a free MUB standard at known concentration. Specific activity of the enzymes was expressed as picomoles of converted substrate/ hours/ mg of proteins.

4.12.1.1. GCase and NLGase

Aliquots of the lysates corresponding to 20 μ g of proteins were pre-incubated for 30 minutes at RT in a 96- well plate with a reaction mixture composed of: 25 μ l of McIlvaine buffer 4X (0.4 M citric acid, 0.8 M Na₂HPO₄) pH 5.2 to assay GCase or pH 6 to assay NLGase, the specific inhibitor of the other counter- enzyme to discriminate either GCase or NLGase activity and H₂O to a final volume of 75 μ l. Lysates were pre-incubated for 30 minutes at RT with the inhibitors, CBE used at the final concentration of 0.5 mM to inhibit GCase; while AMP- DNM (Adamantane- pentyl- dNM;N- (5- adamantane- 1- yl- methoxy- pentyl)- Deoxynojirimycin) has been used at the final concentration of

5 nM to inhibit NLGase. The enzymatic reaction was then started adding 25 μ l of the specific fluorogenic substrate 4-Methylumbelliferyl- β -D-glucopyranoside (MUB- β -Glc) (Glycosynth) at a final concentration of 6 mM.

4.12.1.2. β -galactosidase, β -hexosaminidase α - and β -mannosidase

Aliquots of the lysates corresponding to 5 μ g (for β -galactosidase and β -hexosaminidase) or 10 μ g (for α - and β -mannosidase) of proteins were incubated with a reaction mixture composed of: 25 μ l of McIlvaine buffer 4X pH 5.2, 50 μ l of the specific fluorogenic substrate 4-Methylumbelliferyl- β -D-galactopyranoside (MUB- β -Gal) for β -Gal, 4-Methylumbelliferyl- β -D-glucosaminide (MUG) for β -Hex, Methylumbelliferyl- α -D-mannopyranoside (MUB- α -Man) for α -Man and 4-Methylumbelliferyl- β -D-mannopyranoside (MUB- β -Man) for β -man at a final concentration of 500 μ M and H₂O to a final volume of 100 μ l.

4.12.2. Evaluation of enzymatic activities at the cell surface of living cells

DA neurons and CGNs were plated in a 96-well plate respectively at a density of 2×10^5 and $3,15 \times 10^5$ cells / cm². Respectively at DIC 60 and 17 PM-associated β -galactosidase and β -hexosaminidase were determined using the artificial fluorogenic substrates MUB- β -Gal and MUG solubilized in DMEM/ F-12 without phenol red at the final concentrations of 0.25 mM and 1 mM respectively. The pH of medium was adjusted at pH 6. Cell medium was discarded and cells were washed twice with DMEM /F-12. The specific substrates were then added to the cell monolayers and the incubation was performed at 37 °C under gentle shaking. After 2 hours aliquots of the medium were transferred in a black microplate and 20 volumes of 0.25 M glycine pH 10.7 was added. The fluorescence was evaluated using a Victor microplate reader (Perkin Elmer). Data were expressed as nmoles of converted substrate/ hour/ 10^6 cells³⁴.

4.13. Evaluation of the lipid content

4.13.1. Total lipid extraction

To perform lipid extraction, cell and brain lysates were subjected to lyophilisation to remove water. Lyophilised pellets were resuspended in CHCl₃: CH₃OH: H₂O (2: 1: 0.1, v: v: v). After each addition, the samples were vortexed, sonicated in a H₂O bath for 5 minutes and then mixed at 1,400 rpm for

10 minutes at RT using ThermoMixer® (Eppendorf). The samples were centrifuged at 13,000 x g for 10 minutes at 4 °C. The supernatant, containing the total lipid extraction (TLE), was collected in Eppendorf of 2 ml, while the pellet was subjected to a second extraction with CHCl₃: CH₃OH (2: 1, v: v). The supernatant of the second extraction was joined to the first one.

4.13.2. Two- phase partitioning and alkaline methanolysis reaction

Aliquots of the TLE were then subjected to a two- phase partitioning, resulting in the separation of an aqueous phase containing gangliosides and an organic phase containing all other lipids¹⁰¹. Aliquots of TLE were dried under nitrogen flow and then resuspended in CHCl₃: CH₃OH (2: 1, v: v) and 20 % of Milli- Q H₂O. The samples were vortexed, sonicated in a H₂O bath of 5 minutes and mixed at 1,400 rpm for 10 minutes at RT using ThermoMixer® (Eppendorf).

The samples were centrifuged at 500 x g for 10 minutes at RT. The upper aqueous phase (AP) was collected in Eppendorf of 1.5 ml while the lower organic phase (OP) was subjected to a second extraction with 400 µl of CHCl₃: CH₃OH: H₂O (3: 48: 47, v: v: v), vortexed, sonicated in a H₂O bath of 5 minutes and then mixed at 1,400 rpm for 10 minutes at RT using ThermoMixer® (Eppendorf). After centrifugation at 500 x g for 10 minutes at 4 °C, the upper phase was joined to the first AP.

AP was subjected to H₂O dialysis to remove the salts, lyophilized, and resuspended in the appropriate volume of CHCl₃: CH₃OH (2: 1, v: v).

Aliquots of the endogenous OP were dried and resuspended in 800 µl of CHCl₃ and 800 µl of 0.5 M NaOH in CH₃OH; the mixture was then incubated overnight at 37 °C. This alkaline treatment allows to remove glycerophospholipids from the OP, breaking their ester bonds and preserving the amide bonds of SLs. At the end of incubation, the reaction was blocked by adding 50 µl of 0.5 M HCl in CH₃OH. The samples were then dried under nitrogen flow and subjected again to the two- phase partitioning as described above to obtain the new alkali- stable OP resuspended in a known volume of CHCl₃: CH₃OH (2: 1, v: v).

4.13.3. Cell sphingolipid labelling with [1- ³H]- sphingosine

CGNs at DIC 2 and iPSCs derived DA neurons at DIC 29 were fed with [1- ³H]- sphingosine to metabolically label at the steady state cell's SLs and PE, a glycerophospholipid derived from the catabolism of [1- ³H]- sphingosine. Radioactive sphingosine is solubilized in CH₃OH and was therefore dried under nitrogen flow and solubilised in the complete culture medium at the concentration of 36 nM (specific radioactivity 1.06 Ci/ mmol), which is largely below the cytotoxic

one. An aliquot of the culturing medium was counted by liquid scintillation with beta- counter (PerkinElmer) to evaluate the percentage of solubilisation of the tritiated sphingosine. 24 hours after incubation, the radioactive medium was replaced with fresh culture medium.

At the end of the experimental plan, cells were harvested as described in the “sample preparation” paragraph to perform lipid analysis as described above.

4.13.4. Lipid analysis by High- Performance Thin Layer Chromatography (HPTLC)

For the analyses of the radioactive lipids the radioactivity associated with the TLE, AP, OP was evaluated by liquid scintillator and equal amounts of radioactivity were loaded on HPTLC (stationary phase) for lipid separation. In the case of endogenous lipid pattern, equal amounts in term of cell proteins of alkali- stable OP were loaded on HPTLC.

Generally, the following solvent systems were used:

- to separate lipids of the TLE and of the OP: CHCl₃: CH₃OH: H₂O (110: 40: 6, v: v: v);
- to separate lipids of the OP for the resolution of GlcSph content: CHCl₃: CH₃OH: NH₄OH (70: 30: 3, v: v: v);
- to separate lipids of the AP: CHCl₃: CH₃OH: 0.2 % CaCl₂ (50: 42: 11, v: v: v) in order to evaluate the ganglioside pattern.

The identification of lipids after separation was assessed by co- migration with authentic lipid standards.

Radioactive lipids were detected and quantified by radioactivity imaging performed with a Beta- Imager TRacer instrument (BioSpace) and the radioactivity associated with individual lipids was determined with M3 Vision software and normalized on both the samples’ radioactivity and protein content.

Endogenous lipids of the alkali- stable OP were detected by spraying the HPTLC with anisaldehyde reagent, quantified by ImageJ software and normalized on the samples’ protein content and expressed as fold change with respect to CBE- untreated cells.

4.13.5. Analysis of glucosylceramide and glucosylsphingosine content by LC ESI- MS/ MS

The analysis of GlcCer content was carried out on aliquots of the alkaline- stable OP used also for the HPTLC analyses.

On the contrary, to analyse GlcSph content it was used a specific method, already described in literature, to selectively extract and separate exosyl-sphingosines from the other GSLs¹⁰². Briefly, lyophilized cell lysates were extracted with acetone, the extracts were dried under nitrogen flow and then were resuspended in CHCl₃: CH₃OH (2: 1, v: v).

GlcCer and GlcSph were analysed by LC ESI- MS/ MS following the method published by Merrill AH Jr¹⁰³ with proper modifications.

Mass spectrometry (MS) analyses were carried out using a LCQDeca ion trap mass spectrometer (Thermo Fisher Scientific) equipped with an electrospray ionization source, an Xcalibur data system and a Jasco PU980 Pump HPLC.

GlcCer and GlcSph were separated and detected using an HPLC system (JASCO; Tokyo, Japan) equipped with a normal phase column LC- Si (Supelco 2.1 mm x 250 mm x 5 µm).

Elution was carried out at a flow rate of 0.700 ml/ min, with a gradient formed by solvent system A, consisting of CH₃CN: CH₃OH: H₃CCOOH (97: 2: 1, v: v: v) with 5 mM ammonium acetate and solvent system B, consisting of CH₃OH containing 5 mM ammonium acetate.

MS analyses were carried out at a positive ion mode MS/ MS, sheath gas flow of 60 arbitrary units, spray voltage of 5 kV, capillary voltage of 70 eV and capillary temperature of 300 °C. Mass spectra were acquired over a range of m/ z 200– 2000.

4.13.6. Svennerholm assay

AP of brain areas were used to quantify sialic acid.

The assay performed is a re- adaptation of Svennerholm's method¹⁰⁴ and was set up in triplicate in 2 ml Eppendorf tubes adding to 30 µl of sample, 7.6 µl of Milli- Q water, 37.6 µl of Resorcinol. Then the reaction mixes were heated to constant 100 °C for 15 minutes. After cooling in ice, 300 µl of extraction solvent butylene acetate: butanol (85: 15, v: v) were added. Samples were centrifuged at 12,000 x g for 15 minutes and the upper blue/ violet supernatant read at spectrophotometer (Jasco V-730) at 580 nm. The absorbance related to the extraction solvent was evaluated as background signal. Nanomoles of sialic acid were calculated interpolating the mean absorbance value of each

sample with the calibration curve obtained from the standards' absorbance values. As standards, AP at known growing concentration of sialic acid were used.

4.14. Evaluation of the protein and lipid content of the plasma membrane

4.14.1. Cell surface protein biotinylation and isolation of PM proteins by streptavidin pulldown assay

In order to evaluate lipid enrichment at PM level, at the end of CBE treatment PM proteins of DA neurons were precipitated exploiting a biotin/ streptavidin pulldown assay.

Cell medium was removed and cells washed 2 times with PBS 1X. Cells were treated with 4.7 mg/mL Sulfo- NHS- biotin in PBS 1X for 30 minutes at 4 °C. Biotin action was then blocked by rinsing cells 3 times with 100 mM glycine in PBS 1X at 4 °C. Cells were then mechanically harvested in PBS 1X, centrifuged at 270 x g for 10 minutes at 4 °C and pellets were lysed in 2 mL of 1 % Triton X- 100, 50 mM Tris- HCl pH 7.4, 150 mM NaCl, 2 mM NaF, 1 mM EDTA, 1 mM EGTA supplemented with protease inhibitor cocktail and 1 mM Na₃VPO₄ for 30 minutes in ice. Lysates were then mechanically passed 11 times in a Dounce homogenizer with tight pestle.

Nuclei and cell debris were removed upon centrifugation at 1,300 x g for 5 minutes at 4 °C and the post- nuclear supernatant (PNS) was transferred to a 2 ml Eppendorf tube. Equal amounts of the PNS' proteins from CBE- treated and untreated cells were subjected to streptavidine- coated magnetic beads (Dynabeads™ M- 280 Streptavidin) to separate the biotinylated protein fraction, and put on rotation overnight at 4 °C. Subsequently, with the help of a multimagnet, beads were removed from the sample and transferred to another tube representing the P fraction. The leftover part represents the SN.

Total radioactive lipids were extracted from the P twice with 400 µl CHCl₃: CH₃OH (2: 1, v: v) and from the PNS and SN fraction as described in the "lipid analysis" paragraph. Radioactivity associated with both fractions was determined by liquid scintillation counting. Lipids of the TLE were separated, detected, and quantified as described in the "lipid analysis" paragraph.

4.14.2. Cell surface protein biotinylation and isolation of detergent-resistant membrane fractions

After 29 days of CBE treatment, treated and untreated DA neurons were biotinylated as described in the previous paragraph, mechanically harvested in PBS and centrifuged at 270 x g for 10 minutes. Cells were then mechanically harvested in PBS 1X, centrifuged at 270 x g for 10 minutes at 4 °C and pellets were lysed in 2 mL of 1 % Triton X- 100 in 19 mM TNEV buffer [10 mM Tris- HCl, 150 mM NaCl, 5 mM EDTA (pH 7.5)] supplemented with protease inhibitor cocktail and 1 mM Na₃VPO₄ for 30 minutes in ice and lysates were then mechanically passed 11 times in a Dounce homogenizer with tight pestle.

The lysates were centrifuged at 1,300 x g for 5 minutes at 4 °C to remove nuclei and cellular debris and obtain the PNS. 1 mL of PNS was mixed with an equal volume of 85 % sucrose (w/ v) in TNEV buffer supplemented with 1 mM Na₃VO₄ and loaded at the bottom of a discontinuous sucrose gradient (30– 5 %). After ultracentrifugation at 200,000 x g at 4 °C for 17 hours, 12 fractions were collected starting from the top of the tube. In correspondence of fractions 5 and 6 the light scattering band representing the detergent- resistant membrane domains (DRM) fraction was collected, whereas fractions 10, 11, and 12 correspond to high- density fractions (HD). The entire procedure was performed at 0– 4 °C in ice. Radioactivity associated with PNS and with the fractions (HD and DRM) was determined by liquid scintillation counting¹⁰⁵. DRM fractions from CBE- treated and untreated cells were then subjected to precipitation of cell surface biotinylated proteins and lipids extraction as described in the previous paragraph. The pellets containing the biotinylated cell surface proteins represent the detergent-resistant PM domain fractions (PM- DRM). Radioactivity associated with PM- DRM and SN was determined by liquid scintillation counting. Lipids of the TLE were separated, detected, and quantified as described in the “lipid analysis” paragraph. Equal volumes of each fraction were diluted with 5X Laemmli buffer and used for immunoblotting analysis.

4.15. Evaluation of cell metabolites

4.15.1. Targeted metabolomics by LC- MS/ MS

Metabolomic data were obtained by liquid chromatography coupled to tandem mass spectrometry. An API- 3500 triple quadrupole mass spectrometer (AB Sciex, Framingham, MA, USA) coupled with an ExionLC™ AC System (AB Sciex) was used. Cells were smashed in a tissue lyser for 2 minutes at maximum speed in 250 µl of ice- cold CH₃OH: H₂O: CH₃CN, 55: 25: 20, (v: v: v) containing [U- ¹³C₆]-

glucose 1 ng/ μl and [U- $^{13}\text{C}_5$]- glutamine 1 ng/ μl as internal standards. Lysates were spun at 15,000 x g for 15 minutes at 4 °C and supernatants were then passed through a regenerated cellulose filter (4 mm \varnothing , Sartorius). Samples were then dried under nitrogen flow at 40 °C and resuspended in 125 μl of ice- cold CH_3OH : H_2O , 70: 30, (v: v) for subsequent analyses.

Amino acids, their derivatives, and biogenic amines' quantification was performed through previous derivatization. Briefly, 25 μl out of 125 μl of samples were collected and dried separately under nitrogen flow at 40 °C. Dried samples were resuspended in 50 μl of phenylisothiocyanate (PITC), ethanol, pyridine, and H_2O , 5 %: 31.5 %: 31.5 %: 31.5 %, (v: v: v: v) and then incubated for 20 minutes at RT, dried under nitrogen flow at 40 °C for 90 minutes and resuspended in 100 μl of 5 mM ammonium acetate in CH_3OH : H_2O , 50: 50, (v: v). Quantification of different amino acids was performed by using a C18 column (Biocrates, Innsbruck, Austria) maintained at 50 °C. The mobile phases for positive ion mode analysis were phase A: 0.2 % formic acid in H_2O and phase B: 0.2 % formic acid in CH_3CN . The gradient was T0: 100 % A, T5.5: 5 % A, T7: 100 % A with a flow rate of 500 $\mu\text{l}/\text{min}$. All metabolites analysed in the described protocols were previously validated by pure standards and internal standards were used to check instrument sensitivity.

Quantification of energy metabolites was performed by using a cyano- phase LUNA column (50 mm x 4.6 mm, 5 μm ; Phenomenex) by a 5- minute run in negative ion mode with two separated runs. Protocol A: the mobile phase A was: H_2O and phase B was: 5 mM $\text{NH}_4\text{CH}_3\text{COOH}$ in CH_3OH and the gradient was 10 % A and 90 % B for all the analysis with a flow rate of 500 $\mu\text{l}/\text{min}$. Protocol B: the mobile phase A was: H_2O and phase B was: 5 mM $\text{NH}_4\text{CH}_3\text{COOH}$ in CH_3OH and the gradient was 50 % A and 50 % B for all the analysis with a flow rate of 500 $\mu\text{l}/\text{min}$.

Acylcarnitines, glutathione (GSH), oxidized glutathione (GSSG), and S-adenosyl methionine (S-AME) quantification was performed on the same samples by using a Varian Pursuit XRs Ultra 2.8 Diphenyl column (Agilent). Samples were analysed by a 5- minute run in positive ion mode. Mobile phases were A: 0.1 % formic acid in H_2O B: 0.1 % formic acid in CH_3OH and the gradient was 15 % A and 85 % B for all the runs.

MultiQuant™ software (version 3.0.3, AB Sciex) was used for data analysis and peak review of chromatograms. Raw areas were normalized by the median of all metabolite areas in the same sample. Specifically, I defined the relative metabolite abundance (m_a^N) as:

$$m_a^N = \frac{X_n}{M_{a=1}^n a}$$

where x_n represents the peak area of metabolite n for samples a, b, \dots, z , and $M_{a=1}^n a$ represents the

median of peak areas of metabolite n for samples a, b, \dots, z . Obtained data were then transformed by generalized log-transformation and Pareto scaled to correct for heteroscedasticity, reduce the skewness of the data, and reduce mask effects¹⁰⁶. In detail, obtained values were transformed by generalized log ($glog$) as follows:

$$glog_2(x) = \log_2 \frac{x + \sqrt{x^2 + a^2}}{2}$$

where a is a constant with a default value of 1 and x is the sample area for a given metabolite¹⁰⁷. Then, obtained values underwent Pareto scaling as follows:

$$\bar{x}_{ij} = \frac{x_{ij} - \bar{x}_i}{\sqrt{s_i}}$$

where x_{ij} is the transformed value in the data matrix (i (metabolites), j (samples)) and s_i is the standard deviation of transformed metabolite values. Obtained values were considered as relative metabolite levels. Data processing and analysis were performed by MetaboAnalyst 5.0 web tool¹⁰⁸

4.16. Evaluation of the energetic metabolism of the cell

4.16.1. Agilent Seahorse XF Real- Time ATP Rate Assay

The measurements of glycolytic and mitochondrial ATP production were performed by using a Seahorse XF Real- time ATP Rate Assay Kit and an XFe24 Seahorse instrument, following the manufacturer's instructions. At DIC 56 DA neurons were detached using Accutase (3 minutes, 37°C) and 2×10^5 cells plated in each well of the Seahorse XF Microplate using the appropriate cell culture medium. A sensor cartridge was hydrated overnight at 37 °C in an incubator without CO₂. Sterile assay medium was prepared by supplementing 100 mL of Seahorse XF DMEM, pH 7.4 with 10 mM of XF glucose, 1 mM of XF pyruvate, 2 mM of XF glutamine.

Cell culture medium was removed, and cells were rinsed twice with the warmed assay medium. Then cells were transferred for 45- 60 minutes at 37 °C without CO₂. Before starting the assay, the medium was substituted with a fresh and warm one.

To measure glycolytic and mitochondrial ATP production, 1.5 μM oligomycin and 0.5 μM rotenone/ antimycin A were subsequently injected. Data were analyzed using the Seahorse XF Real- Time ATP Rate Assay Report Generator and normalized the data on the total amount of protein in the samples.

4.16.2. Agilent Seahorse XF Cell Mito Stress Test

The Seahorse XF Cell Mito Stress Test is used to measure mitochondrial function. 4 days prior to analysis, DA neurons were detached using Accutase (3 minutes, 37 °C) and 2×10^5 cells plated in each well of the Seahorse XF Microplate using the appropriate cell culture medium. A sensor cartridge was hydrated overnight at 37 °C in an incubator in the absence of CO₂. Assay media were prepared as above, by supplementing 100 mL of Seahorse XF DMEM, pH 7.4 with 10 mM of XF glucose, 1 mM of XF pyruvate, 2 mM of XF glutamine.

Cell culture medium was discarded, and cells were rinsed twice with a warmed assay medium and incubated for 45- 60 minutes at 37°C deprived of CO₂.

Oxygen Consumption Rate (OCR) was assessed under basal conditions and after sequential injection of 1.5 μM oligomycin, 1 μM FCCP, and 0.5 μM of rotenone/ antimycin A.

Seahorse XF Mito stress Test Assay was run, selecting the protocol from the available templates according to the manufacturer's instructions. Then, data were analysed using the Seahorse XF Mito Stress Test Assay Report Generator and normalized the data on the total amount of protein in the samples.

4.17. Statistics

All the experiments have been performed at least in triplicate and repeated three times and data were tested for significance using GraphPad Prism 8 (GraphPad Software Inc., La Jolla, CA, USA).

Data are expressed as mean ± SEM. For normally distributed data, two- tailed unpaired Student's t test was used. The level of significance was set at $p < 0.05$.

5. RESULTS

5.1. Characterization of human brain areas of a patient affected by *GBA*- dependent Parkinson's disease

GBA1 gene codes for GCCase, the enzyme involved in the lysosomal catabolism of GlcCer. Nowadays, monoallelic loss of function mutations of *GBA1* are considered to be the major genetic risk factor for the development of PD. GCCase is involved in the catabolism of SLs but scant is the information about the consequences of its deficiency on the SL pattern of the human brain. Thanks to a collaboration with the Movement Disorder Unit of the Policlinico hospital of Milan, I had the opportunity to characterize five brain areas (frontal cortex, *substantia nigra*, parietal cortex, *cerebellum*, and *hippocampus*) derived from a patient affected by *GBA*- PD carrying monoallelic L444P mutation in *GBA1* gene. Tissue samples were compared to the same areas derived from healthy subjects concerning activity of the main glycohydrolases and SL and ganglioside content.

Brain areas derived from the patient affected by *GBA*- PD presented a reduced GCCase activity with respect to the same areas derived from healthy subjects. In particular, in the *substantia nigra*, parietal cortex, *cerebellum*, and *hippocampus* GCCase activity was decreased of about 60- 70 % with respect to the healthy counterparts, while in the frontal cortex it decreased of about 40 %.

In GD it has been demonstrated that cells react to GCCase loss of function increasing the activity of the NLGase, an enzyme which is responsible for the same reaction as GCCase but prevalently at PM level. Interestingly, in all the tested areas, with exception for the parietal cortex and the *hippocampus*, I observed an increased activity of NLGase (Figure 10) of about 15- 20 % with respect to the one measured in healthy subjects. No changes among pathological and healthy areas were observed concerning β - galactosidase activity, except for the *cerebellum* where in PD patients β - galactosidase activity increased of about two folds. β - hexosaminidase presented the highest activity measured in all areas and it appeared to be lower in areas derived from the PD patient with respect to those derived from healthy subjects, the only exception was the *cerebellum* where β - hexosaminidase appeared to show the opposite trend.

In all PD patient's areas the activity of α - mannosidase seemed reduced with respect to healthy subjects, presenting comparable values (500 pmoles/ hour/ mg of tissue proteins) in all areas except for the *cerebellum*, which showed a halved activity. β - mannosidase showed a trend of reduction of about two-fold in all PD patient's- derived areas with respect to those of healthy subjects.

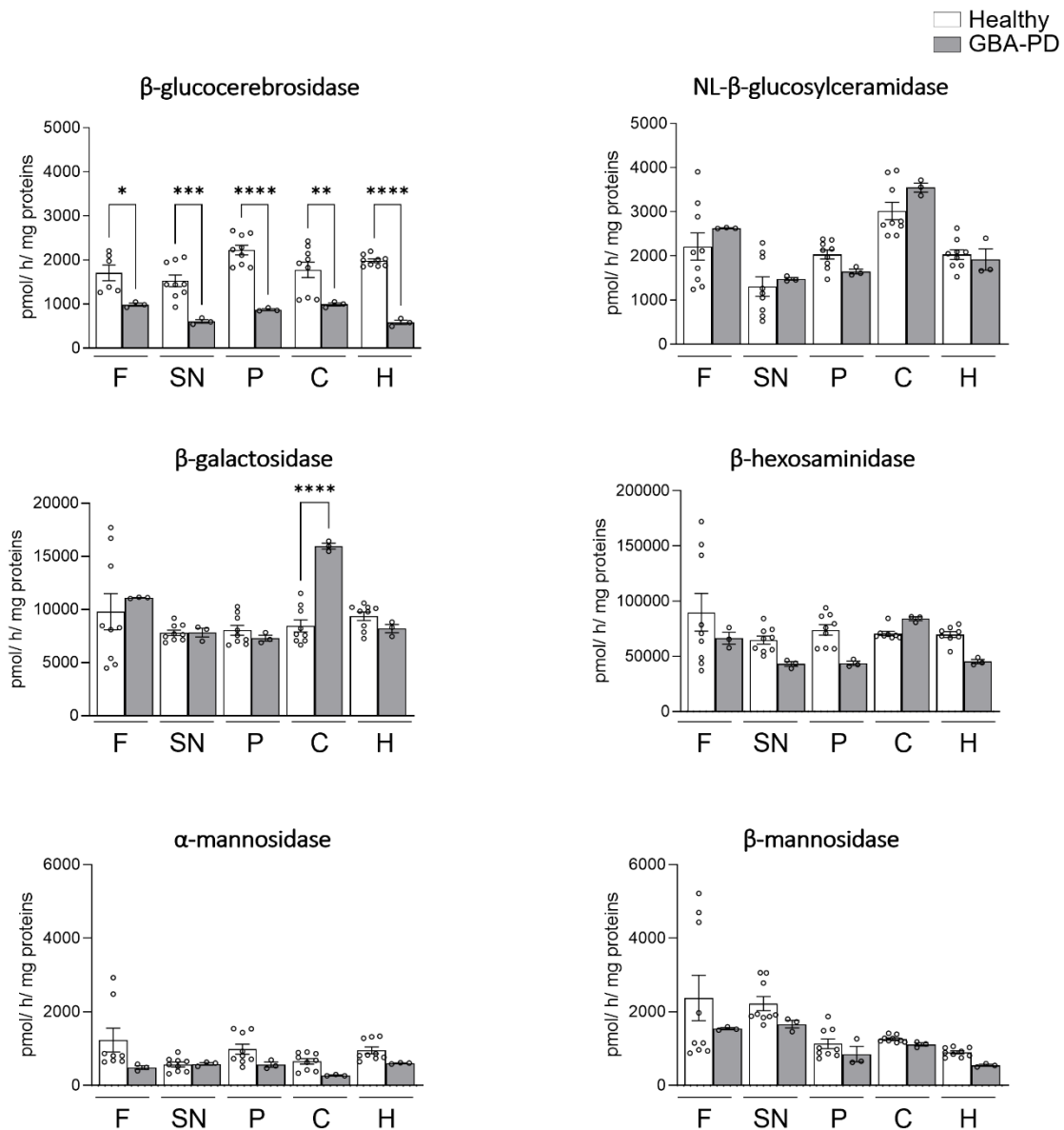


Figure 10 Enzymatic activities among brain areas derived from healthy subjects and from a patient affected by GBA-dependent Parkinson's disease

Enzymatic activities were measured on aliquots of lysate of *post-mortem* brain areas derived from healthy subjects (white bars) and from a patient affected by GBA- Parkinson's disease (GBA- PD) (grey bars). Analysed brain areas are F= frontal cortex; SN= *substantia nigra*; P=parietal cortex; C=*cerebellum*, and H= *hippocampus*. Activities were measured using specific fluorogenic substrates. To discriminate between β-glucocerebrosidase and NL-β-glucosylceramidase activity, lysates were preincubated with specific inhibitors AMP- DNM and CBE respectively. Each assay was performed in triplicate and enzymatic activity is expressed as pmoles of product/ hour/ mg of proteins. All data are shown as mean ± SEM of three different experiments, *p<0.05, **p<0.01, ***p=0.003, ****p<0.0001, One- way ANOVA- test vs areas derived from healthy subjects.

The content of neutral SLs of the different areas was also affected. In detail, there was a general decrease of GlcCer and LacCer content in all pathological brain areas with exception of the *cerebellum* where it was increased of about 2,5- fold. Whereas sulfatides' content strongly

decreased in all the analyzed pathological areas when compared with areas of healthy subjects, reaching the lowest amount in the frontal cortex and the *substantia nigra* (Figure 11).

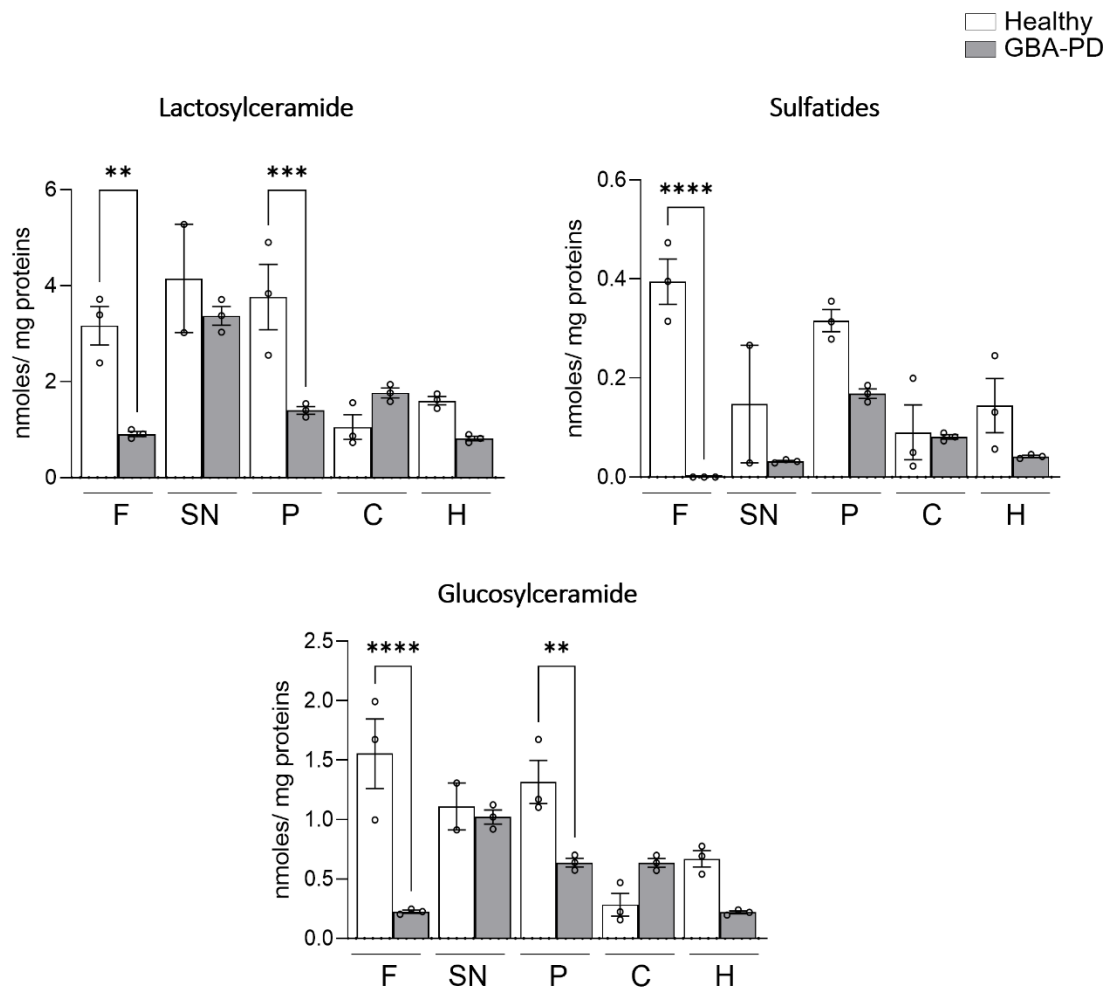


Figure 11 Main lipid pattern among brain areas derived from healthy subjects and from a patient affected by *GBA1*-dependent Parkinson's disease

Lipid content was measured on aliquots of lysate of post- mortem brain areas derived from healthy subjects (white bars) and from a patient affected by *GBA*- Parkinson's disease (*GBA*- PD) (grey bars). Analysed brain areas are F= frontal cortex; SN= *substantia nigra*; P=parietal cortex; C=cerebellum, and H= *hippocampus*. Total lipids were extracted and separated by HPTLC using as solvent system CHCl_3 : CH_3OH : H_2O (110:40:6, v: v: v) and analysed through ImageJ densitometric analysis. Lipid amount is expressed as nmoles / mg of proteins. All data are shown as mean \pm SEM of three different experiments, **p<0.01, ***p=0.003, ****p<0.0001, one- way ANOVA- test vs areas derived from healthy subjects.

For what concerns the ganglioside pattern, I observed that in *GBA*- dependent PD patient, the content of ganglioside GM1 was decreased of about 1.2- fold in the frontal cortex and in the *cerebellum*, of about 1.8- fold in the parietal cortex, while it increased respectively of about 1.5 and 2- folds in the *substantia nigra* and in the *hippocampus* with respect to the same areas derived from

the healthy subjects. The parietal cortex, *cerebellum*, and *hippocampus* of the PD patient presented a higher GD3 content with respect to healthy subjects. GD1a content was increased in all *GBA*- PD patient's areas (ranging from a 1.3- fold increase in the parietal cortex; a 2- fold increase in the *hippocampus*; a 3- fold increase in the frontal cortex, to a 3.6- fold increase in the *cerebellum*) with respect to those of healthy subjects, except for the *substantia nigra* where its level halved. I found a twofold increase in GD1b content in the frontal cortex, *substantia nigra*, and *cerebellum*, which was decreased in the parietal cortex and the *hippocampus*. GT1b was 6.5- fold higher in the frontal cortex, 2- fold higher in the *substantia nigra*, and 1.6- fold higher in the *cerebellum* and *hippocampus*, whereas it was decreased in the parietal cortex. The O- acetylated form of GT1b increased of 8- fold in the frontal cortex of PD patients, whereas it underwent a slight decrease in the parietal cortex and *cerebellum* (Figure 12).

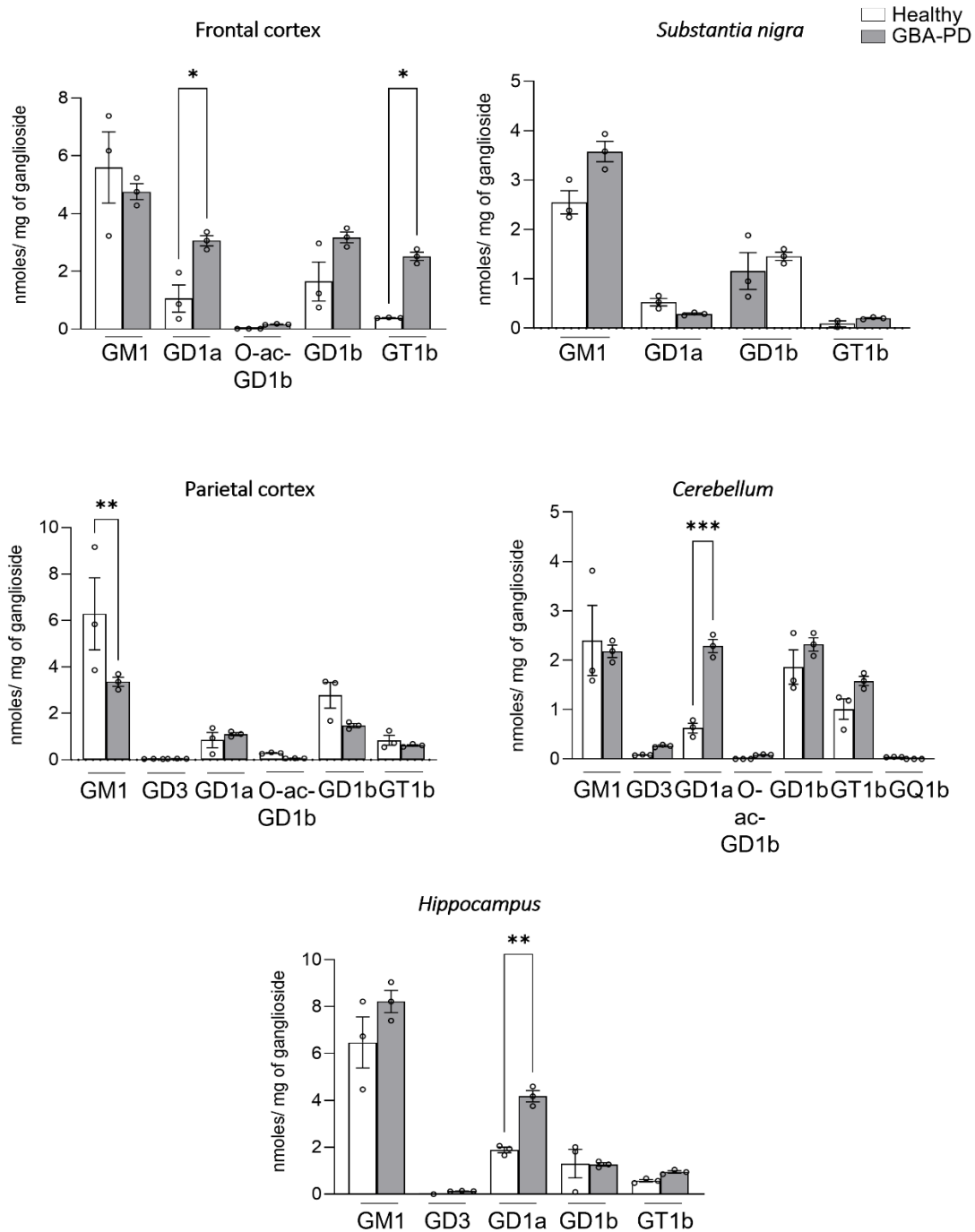


Figure 12 Ganglioside pattern among brain areas derived from healthy subjects and a patient affected by *GBA1*-dependent Parkinson's disease

Gangliosides content was measured on aliquots of lysates of post-mortem brain areas derived from healthy subjects (white bars) and from patient affected by *GBA1*- Parkinson's disease (*GBA1*- PD) (grey bars). Analysed brain areas are F= frontal cortex; SN= *substantia nigra*; P=parietal cortex; C=*cerebellum*, and H= *hippocampus*. Gangliosides were extracted and separated by HPTLC using as solvent system CHCl_3 : CH_3OH : CaCl_2 0.2% (50:42:11, v: v) and analysed through ImageJ densitometric analysis. Sialic acid content of each area was assayed according to Svennerholm's assay and used to quantify the content of the different ganglioside species. Gangliosides amount is expressed as nmoles of ganglioside/ mg proteins. All data are shown as mean \pm SEM of three different experiments, * $p < 0.05$, ** $p < 0.01$, *** $p = 0.003$, One-way ANOVA- test vs areas derived from healthy subjects.

5.2.1. Development and biochemical characterization of *in vitro* models of GCase deficiency exploiting human iPSCs- derived dopaminergic neurons and mouse cerebellar granule neurons

The molecular mechanism at the basis of the onset of neurodegeneration upon GCase deficiency is not entirely understood, mainly due to the lack of suitable *in vitro* models. In order to study the link between GCase deficiency and the onset of neuronal degeneration in GD and *GBA*- PD, I have developed two new cell models of GCase deficiency obtained by its inhibition with 0.5 mM CBE in dopaminergic (DA) neurons derived from iPSCs and mouse cerebellar granule neurons (CGNs). The data reported in this section were previously described in a published manuscript where I am first author together with Dr Lunghi⁹⁶. The manuscript and the related supplementary material are attached at the end (section 9. *Published manuscript*) of the present work.

The first cell model is represented by CGNs spontaneously differentiated from neuronal precursors isolated from postnatal day 5 C57BL/ 6 mouse cerebella. After 2 days in culture (DIC) cells were fed with [¹⁻³H]- sphingosine to label all cell SLs and PE at the steady state. At 4 DIC, neurons were treated with 0.5 mM CBE either for 7 days (short- term treatment) or 14 days (long- term treatment) (Figure 13a).

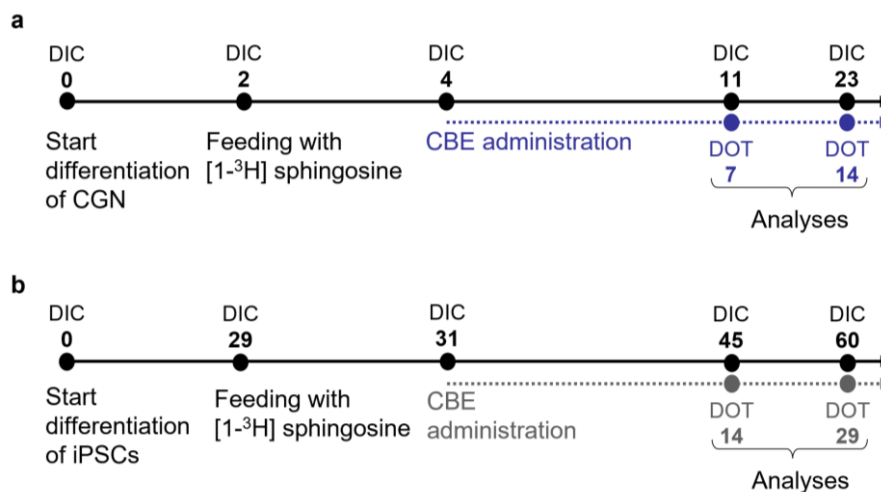


Figure 13. Generation of *in vitro* neuronal models of β - glucocerebrosidase deficiency

Schematic diagrams of the experimental protocols to induce β - glucocerebrosidase deficiency in two neuronal models: **a)** primary cultures of granule neurons from the post-natal mouse *cerebellum* (CGN); **b)** dopaminergic neurons from human-induced pluripotent stem cells (iPSCs). During differentiation of both the neuronal cultures, cell sphingolipids were metabolically labeled at the steady state with radioactive sphingosine; at the stage of mature neurons, cells were then treated with 0.5 mM conduritol B epoxide (CBE) to inhibit β - glucocerebrosidase. After different time points of CBE treatment, neurons were analyzed for β - glucocerebrosidase activity, neuronal marker expression and sphingolipid levels. DIC: days in culture; DOT: days of CBE treatment.

The second cell model exploited the use of human iPSCs (Figure 14) obtained from fibroblasts of a healthy subject and differentiated according to Zhang et al.⁸⁷ for 29 days into a neuronal population enriched in DA neurons. Briefly, skin fibroblasts of a healthy subject were reverted to pluripotent stem cells through a non-integrative reprogramming strategy based on the expression of OCT4, SOX2, KLF4, and c-Myc factors¹⁰⁹. These cells were obtained thanks to the collaboration with Dr Alessio Di Fonzo of the Policlinico hospital of Milan. Afterwards iPSCs were differentiated into neuronal populations enriched in DA neurons, which are the first neuronal population to degenerate in PD.

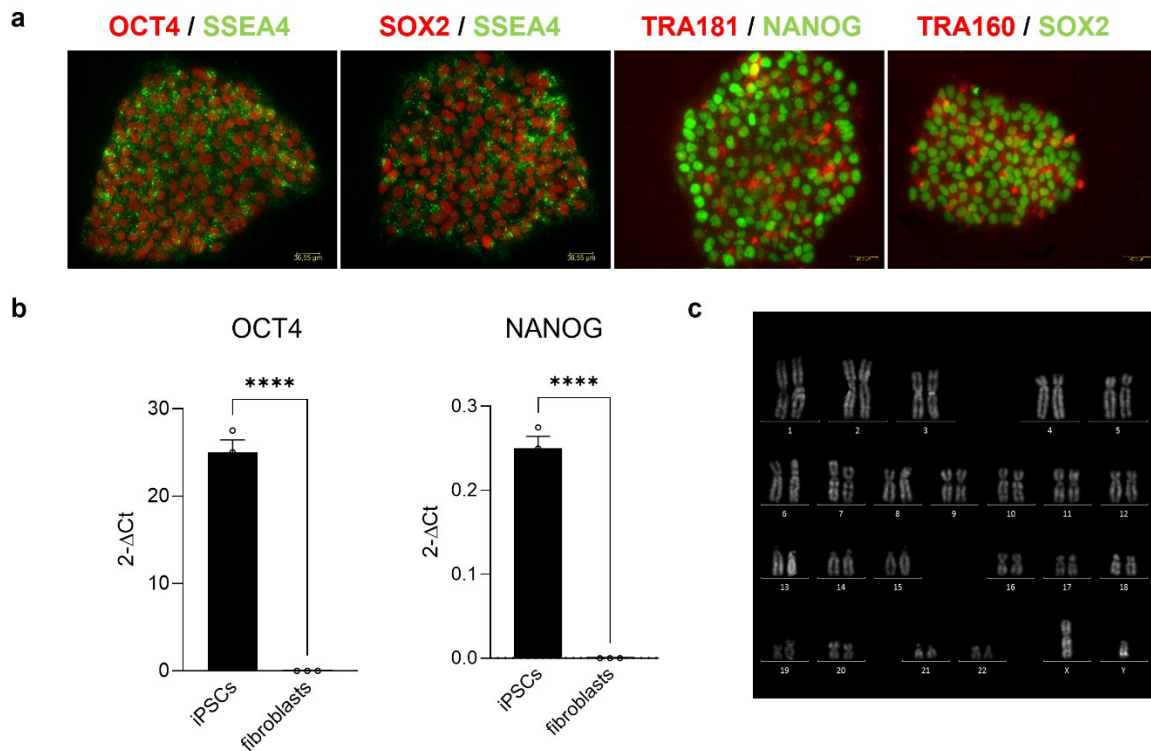


Figure 14. Characterization of iPSCs

a) Representative immunofluorescence images of iPSC colonies showing expression of stem cell markers (OCT4, SSEA4, SOX2, TRA181, TRA160, and NANOG). Images were acquired at 200X magnification. **b)** qPCR showing expression levels of stem cell genes OCT4 and NANOG in iPSCs compared with fibroblasts. Data are shown as absolute normalized amount of mRNA ($2^{-\Delta\text{Ct}}$) \pm SEM. (iPSCs N=8, Fibroblasts N=2; ***P < 0.001, *P < 0.05, Student's *t*-test). **c)** Karyotype analysis of a selected clone of the generated iPSC line.

iPSCs were differentiated into DA neurons using different culture medium formula described in the method chapter, which give a high efficiency of differentiation. The differentiation process has been evaluated by immunofluorescence staining with specific primary antibodies against the mature neuronal marker class III β -tubulin (Tuj1), which was expressed by almost the totality of neurons and the DA marker tyrosine hydroxylase (TH), an enzyme involved in dopamine synthesis to assess the DA commitment. As reported in Figure 15, the protocol of neuronal differentiation allows to obtain at least about 35 % of cells positive for the DA marker TH. I also assessed a relevant representation of mature neurons indicated by the expression of neuronal markers neurofilament H (NF-H), Microtubule-associated protein-2 (MAP2) and Tau. [1-³H]-sphingosine was administered to mature DA neurons at 29 DIC. At 31 DIC cells were treated with 0.5 mM CBE for either 14 days (short- term treatment) or 29 days (long- term treatment) (Figure 13b).

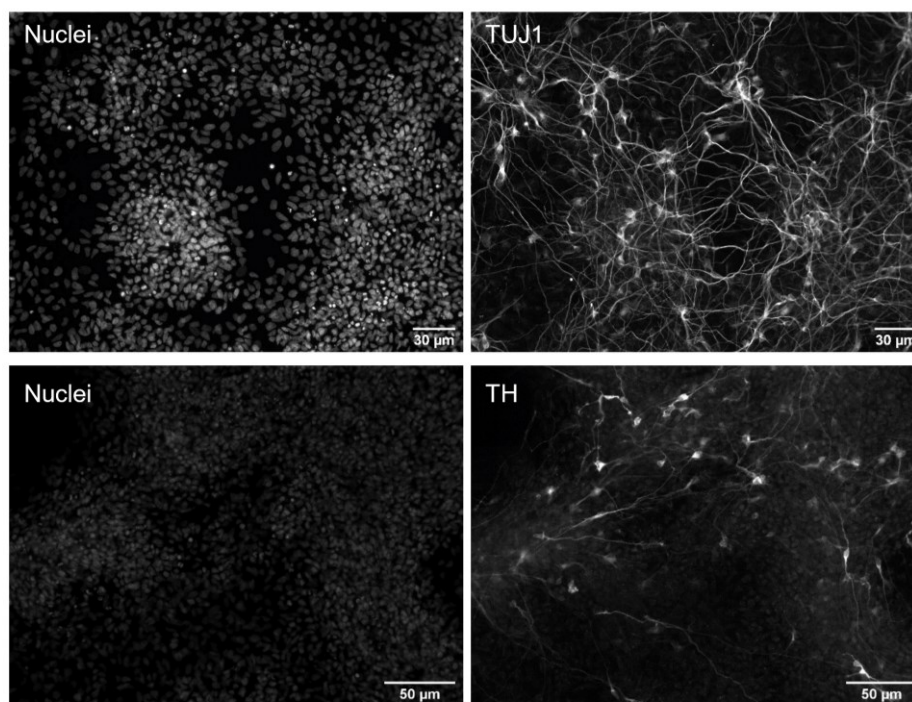


Figure 15. Evaluation of differentiation of iPSC- derived dopaminergic neurons by immunofluorescence analysis

Representative immunofluorescence images of human iPSCs-derived dopaminergic neurons after 29 days of differentiation. Cells were positive for neuron- specific class III β -tubulin (TUJ1) and for the dopaminergic marker Tyrosine Hydroxylase (TH). Cell nuclei were stained with Hoechst. Images were acquired at 400x magnification.

I assured that CBE treated DA neurons and CGNs were able to recapitulate GCase deficiency. Indeed, both short- and long- term treatment strongly reduced GCase activity to a residual activity of 4 % and 1 % in CGNs and DA neurons, respectively (Figure 16).

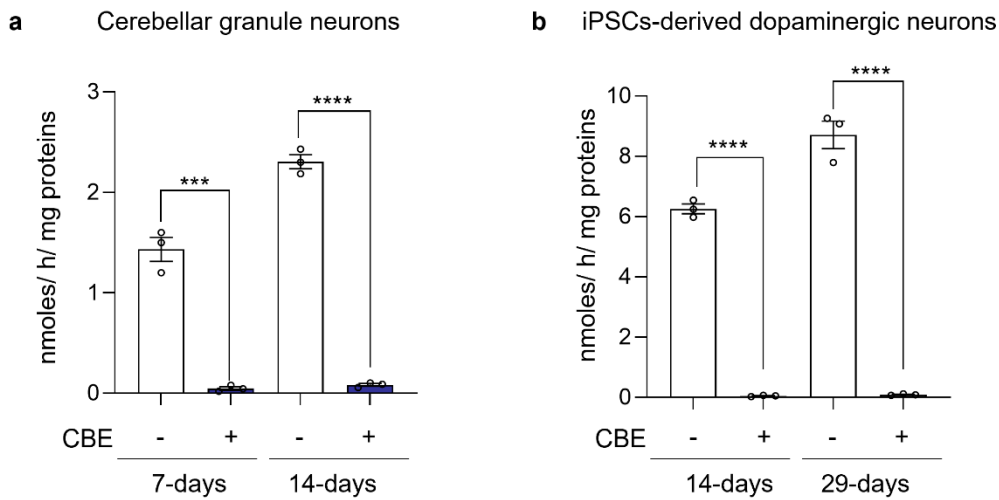


Figure 16. Effect of conduritil B epoxide treatment on β - glucocerebrosidase activity

β -glucocerebrosidase activity was evaluated in **a)** mouse cerebellar granule neurons treated or not with 0.5 mM CBE for 7 or 14 days and **b)** in human iPSC-derived dopaminergic neurons treated or not with 0.5 mM CBE for 14 or 29 days. β -glucocerebrosidase activity is expressed as nmoles of formed product/ hour/ mg cell proteins. All data are shown as mean \pm SEM of three different experiments. ***p=0.003, ****p<0.0001, two- tail Student's t- test vs CBE- untreated cells.

The presence of neuronal damage was evaluated analyzing the expression of neuron- specific markers by immunoblotting. As shown in Figure 17a, CGNs subjected to short- term treatment with CBE did not show any significant change in the protein levels of the neuronal markers NF- H, MAP2, TAU, and PSD95. On the other hand, long- term treated CGNs were characterized by a reduction in protein levels of about 50 % for NF-H, 60 % for MAP2, 50 % for TAU and 30 % for PSD95. On the other side, DA neurons presented neurodegenerative features at both time points. Upon short- term treatment with CBE, MAP2 was reduced of 40 % and TAU of 70 % (Figure 17b). Upon long- term treatment, the neuronal markers decreased even more, with a reduction of 50 % for NF- H, 60 % for MAP2, 65 % for TAU, and 35 % for PSD95 (Figure 17b). Moreover, I confirmed the degeneration of long- term CBE-treated DA neurons by immunofluorescence analyses against MAP2 and Tuj1, showing neurites fragmentation and degeneration (Figure 18a), and by the halving of the cell number compared to the untreated cells (Figure 18b).

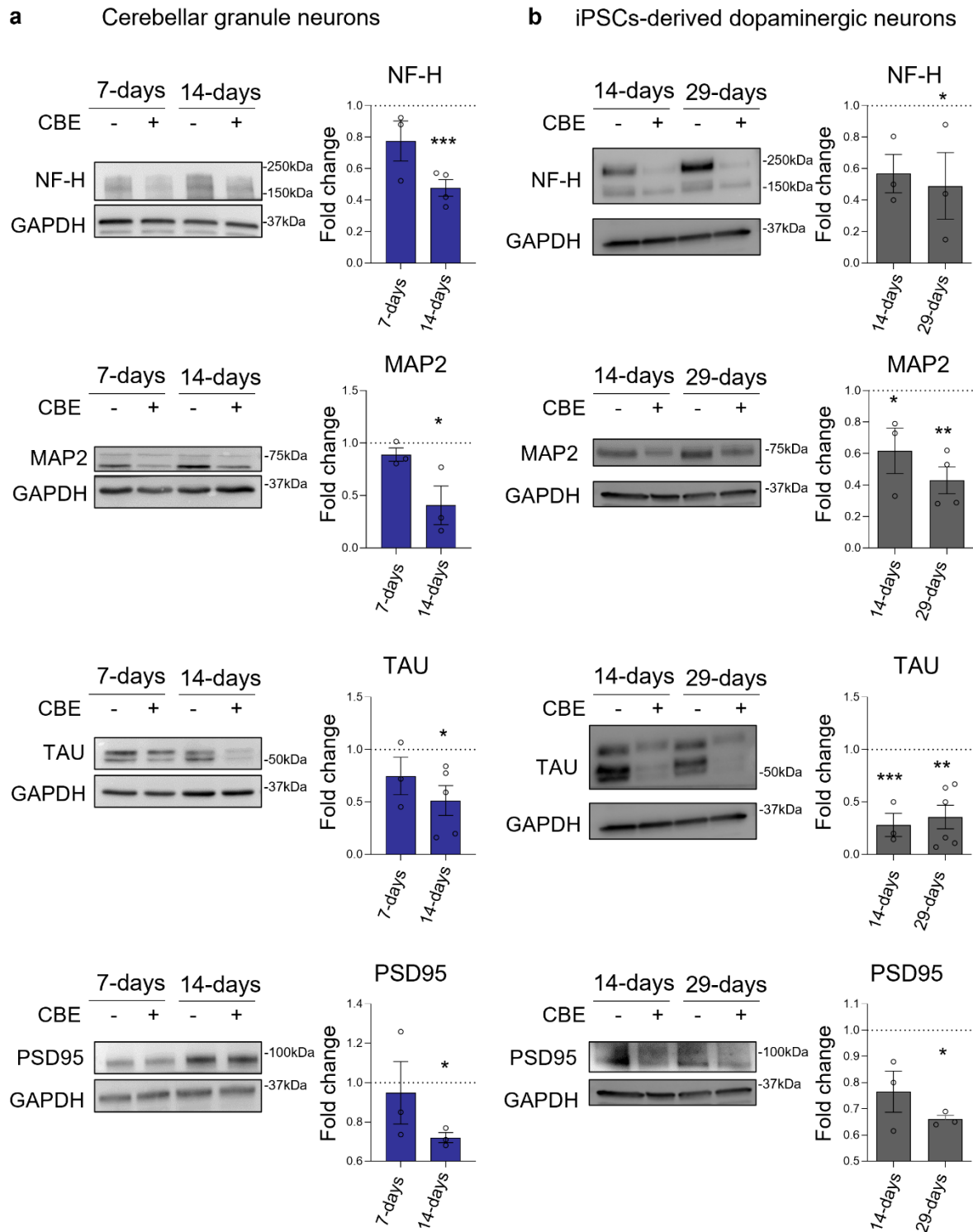


Figure 17. Effect of β - glucocerebrosidase inhibition on neuronal markers' expression

Immunoblotting analysis of the expression of Neurofilament H (NF- H), MAP2, TAU and PSD95 in: **a)** mouse cerebellar granule neurons (CGN) treated or not with conduritot B epoxide (CBE) 0.5 mM for 7 and 14 days and **b)** human iPSC-derived dopaminergic neurons treated or not with CBE 0.5 mM for 14 and 29 days. Optical densities of the individual bands were quantified using NIH ImageJ and normalized to GAPDH. Data are expressed as fold change with respect to CBE- untreated cells (dashed lined) and are the mean \pm SEM of three different experiments. * $p < 0.05$; ** $p < 0.01$; *** $p < 0.001$; **** $p < 0.0001$. Two- tail Student's t- test vs CBE- untreated cells.

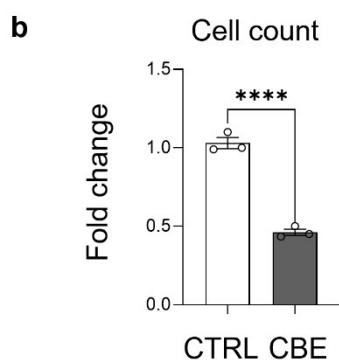
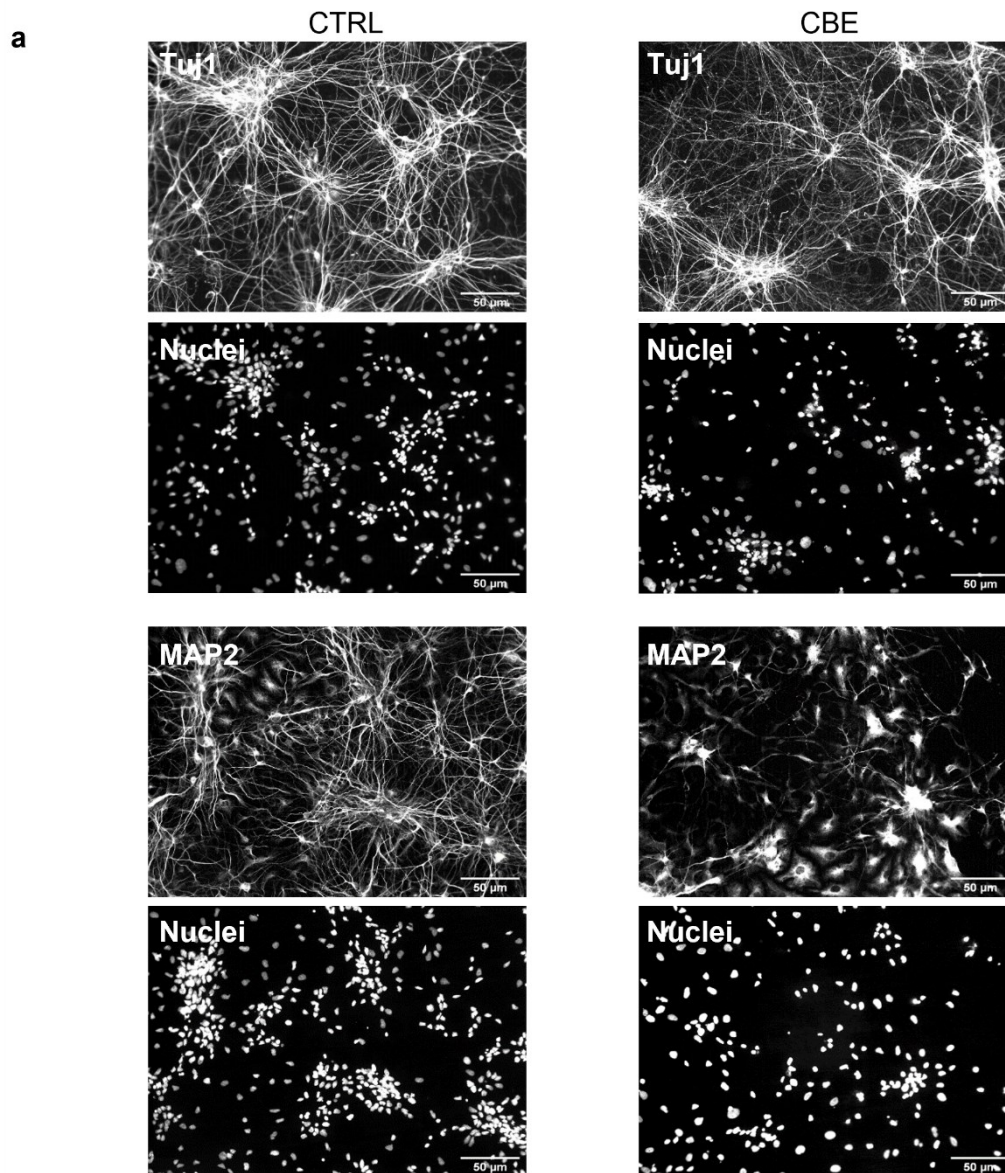


Figure 18. Effect of CBE treatment on dopaminergic neurons differentiation

a) Representative immunofluorescence images of human iPSCs-derived dopaminergic neurons treated or not with 0.5 mM CBE for 29 days. Cells were positive for the neuron- specific class III β -tubulin (TUJ1) and microtubule associated protein 2 (MAP2). Cell nuclei were stained with Hoechst. Images were acquired at 200x magnification. **b)** Cell counting of dopaminergic neurons derived from human iPSCs treated or not (CTRL) with CBE 0.5 mM for 29 days. The graph shows the mean \pm SEM of the fold change over control from three different experiments; **** $p < 0.001$, Student's t- test vs CBE- untreated cells.

Afterwards, I analyzed the radioactive lipids of CGNs and DA neurons, treated or not with CBE, by HPTLC. Both *in vitro* models showed a significant and time- dependent accumulation of GlcCer compared to untreated cells Figure 19. In detail, short- term CBE-treated CGNs and DA neurons showed a 7- and 5- fold increase in GlcCer compared to untreated cells. After long- term CBE treatment GlcCer content was about 10- times higher with respect to untreated cells in both models.

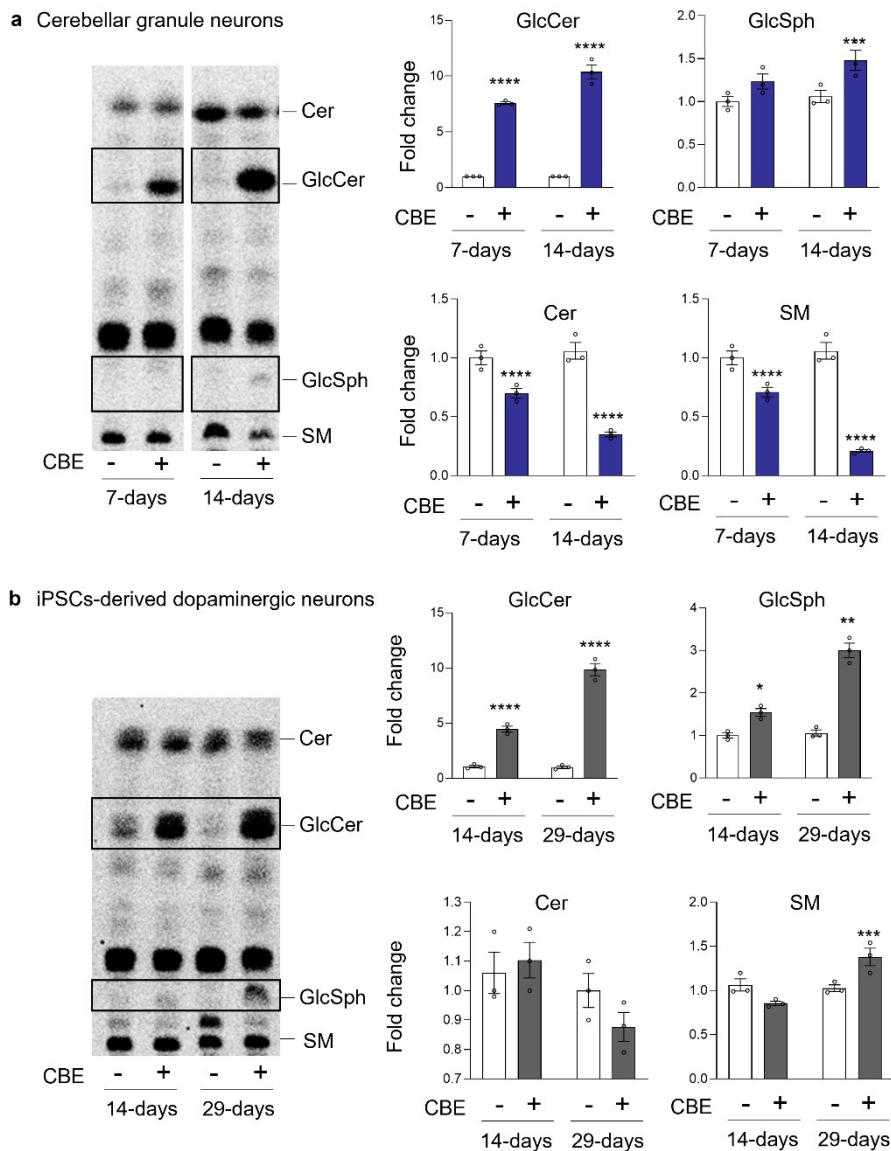
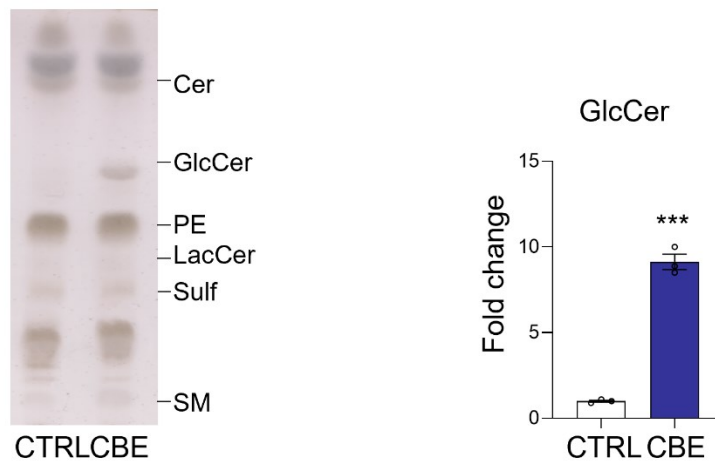


Figure 19. Effect of β -glucocerebrosidase inhibition on glucosylceramide and glucosylsphingosine levels

Representative digital autoradiography of sphingolipid pattern and quantification of the radioactivity associated with glucosylceramide (GlcCer), glucosylsphingosine (GlcSph), ceramide (Cer), and sphingomyelin (SM) in: **a)** mouse cerebellar granule neurons fed with radioactive sphingosine and treated or not (-) with 0.5 mM conduritol B epoxide (CBE) for 7 and 14 days and **b)** human iPSC- derived dopaminergic neurons fed with radioactive sphingosine and treated or not with CBE for 14 and 29 days. Data are expressed as fold change with respect to CBE- untreated cells (-) and are the mean \pm SEM of three different experiments. * $p < 0.05$; ** $p < 0.01$; *** $p < 0.001$; **** $p < 0.0001$, two- tail Student's t- test vs CBE- untreated cells.

To confirm these data, I analyzed the endogenous counterpart by HPTLC and HPLC elution profile followed by ESI- MS analysis (Figure 20 and 21), which affirmed GlcCer accumulation.

a Cerebellar granule neurons



b iPSCs-derived dopaminergic neurons

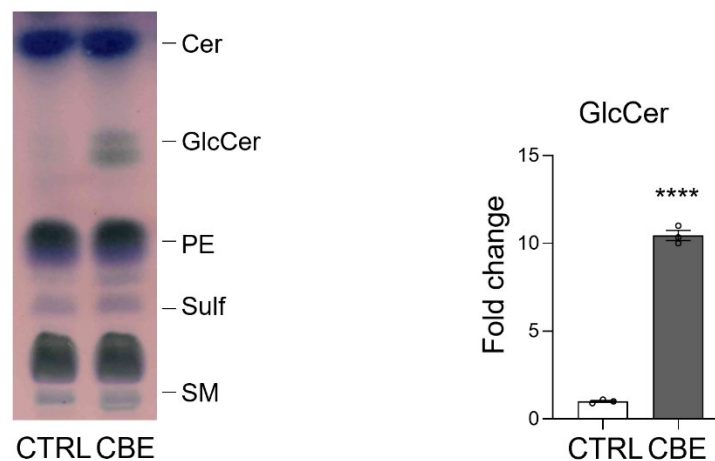


Figure 20. Effect of GCCase inhibition on GlcCer level

Representative HPTLC separation of endogenous lipids of the organic phases extracted from: **a**) mouse cerebellar granule neurons and **b**) human iPSCs-derived dopaminergic neurons treated or not with 0.5 mM CBE for 14 days and 29 days, respectively. Cer= ceramide; GlcCer= glucosylceramide; PE= phosphatidylethanolamine; Sulf= sulfatides; SM= sphingomyelin); GlcCer content was quantified by densitometric analysis; data are expressed as fold change with respect to CBE- untreated cells and are the mean \pm SEM of three different experiments; *** p <0.001; **** p <0.0001. Student's t-test vs CBE- untreated cells.

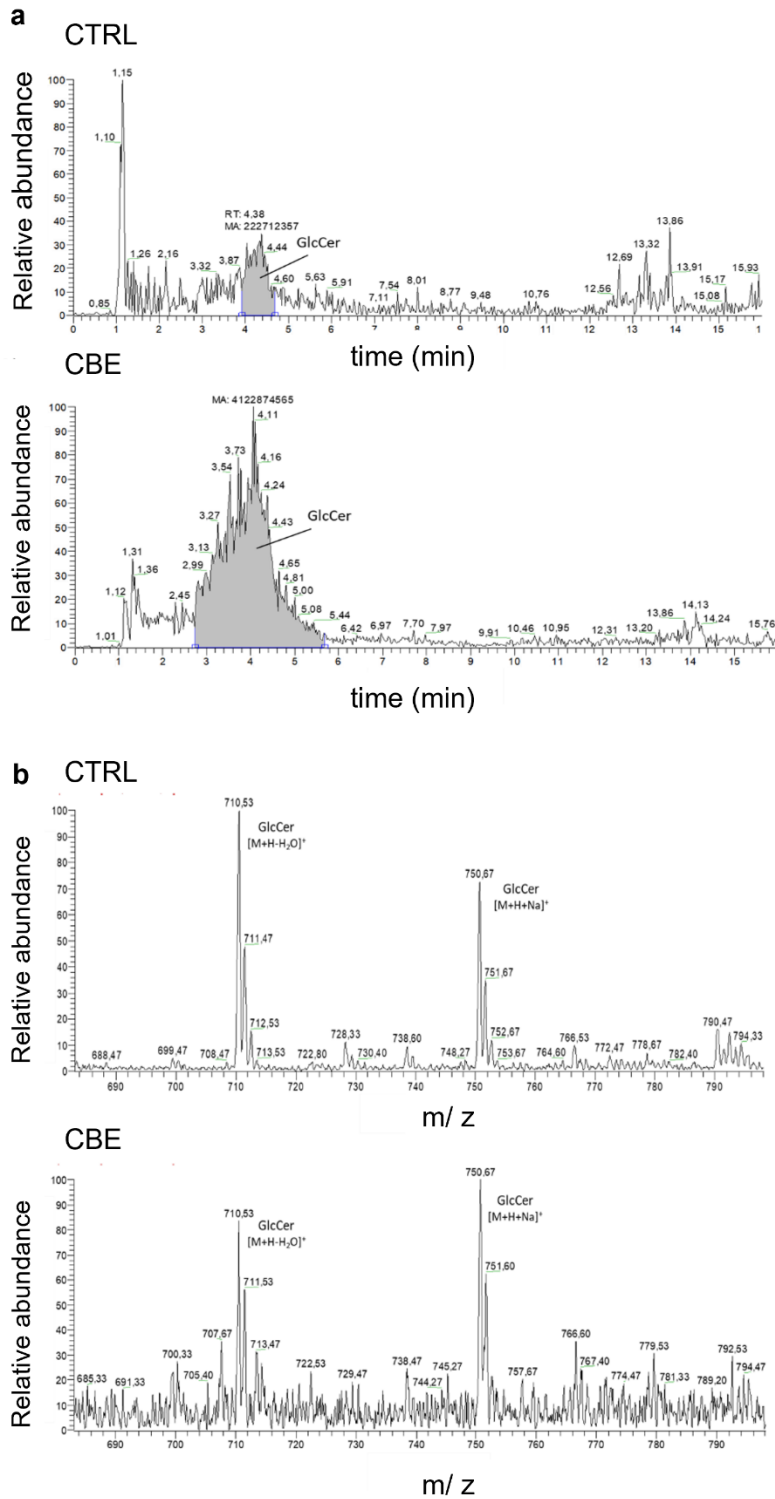


Figure 21. HPLC elution profiles of total lipid extracts and ESI-MS analyses of glucosylceramide

a) Representative chromatogram of the HPLC elution profile of total lipid extracts from mouse cerebellar granule neurons treated or not (CTRL) with 0.5 mM conduritol B epoxide (CBE); in grey is highlighted the peak corresponding to glucosylceramide (GlcCer) **b)** Mass spectrum of GlcCer content of mouse cerebellar granule neurons treated or not (CTRL) with 0.5 mM CBE.

Furthermore, as shown in Figure 20 and Figure 22, in both CBE- treated cell models, I observed an increased production of glucosylsphingosine (GlcSph) which is the deacylated form of GlcCer

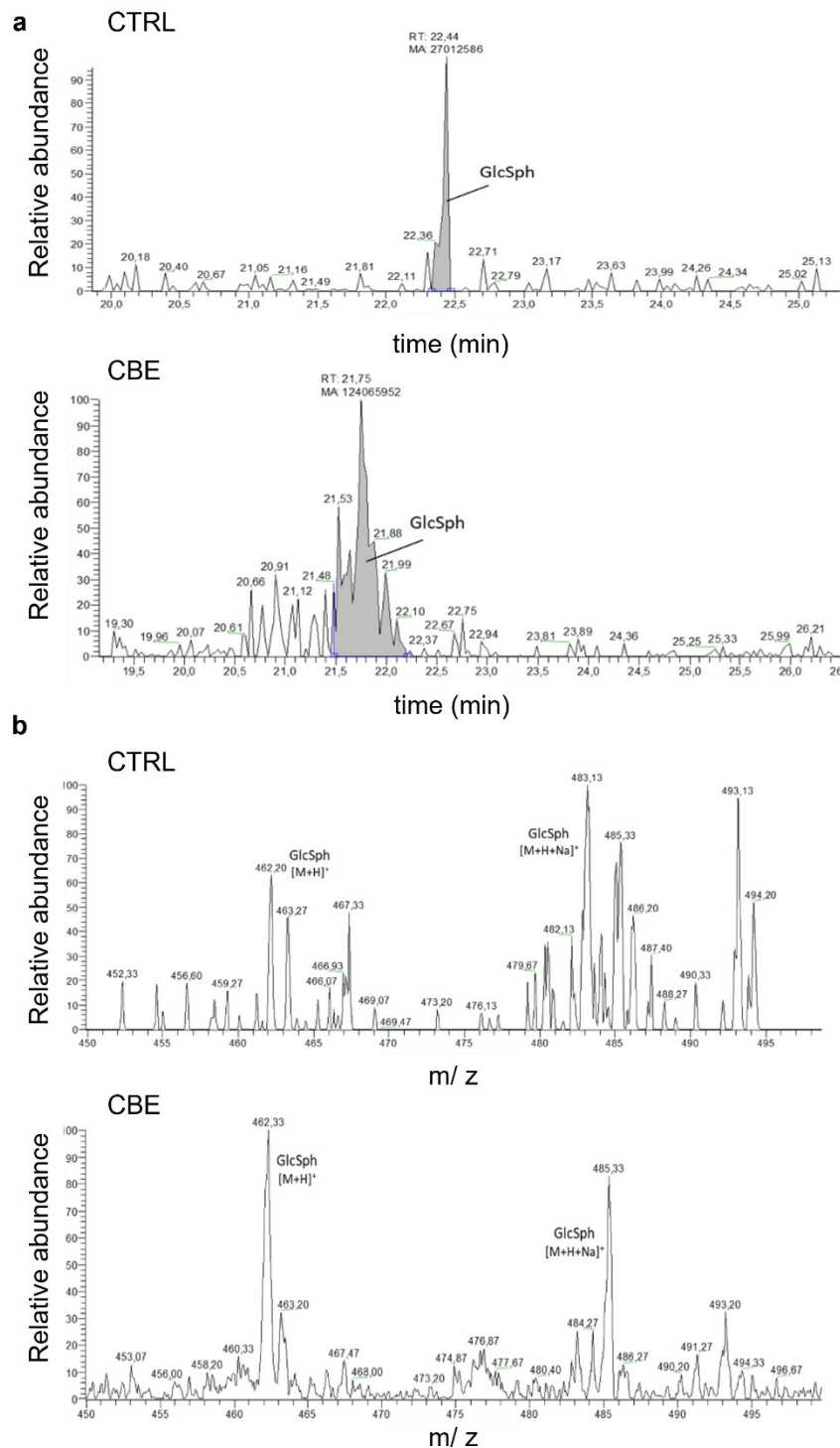


Figure 22. HPLC elution profiles of total lipid extracts and ESI-MS analyses of glucosylsphingosine

a) Representative chromatogram of the HPLC elution profile of total lipid extracts from mouse cerebellar granule neurons treated or not (CTRL) with 0.5 mM conduritol B epoxide (CBE); in grey is highlighted the peak corresponding to glucosylsphingosine (GlcSph) **b)** Mass spectrum of GlcSph content of mouse cerebellar granule neurons treated or not (CTRL) with 0.5 mM CBE.

The role of GlcSph in the onset of cell toxicity is a widely discussed topic^{110,111} and for this reason I investigated its effect on the viability of neurons administering it exogenously to both cell models. As shown in Figure 23a, no toxic effect was present upon administration of low concentrations of GlcSph to CGNs and DA neurons, whereas a 40 % decrease of vitality was observed just in DA neurons upon administration of high doses of GlcSph (10 μ M) (Figure 23b).

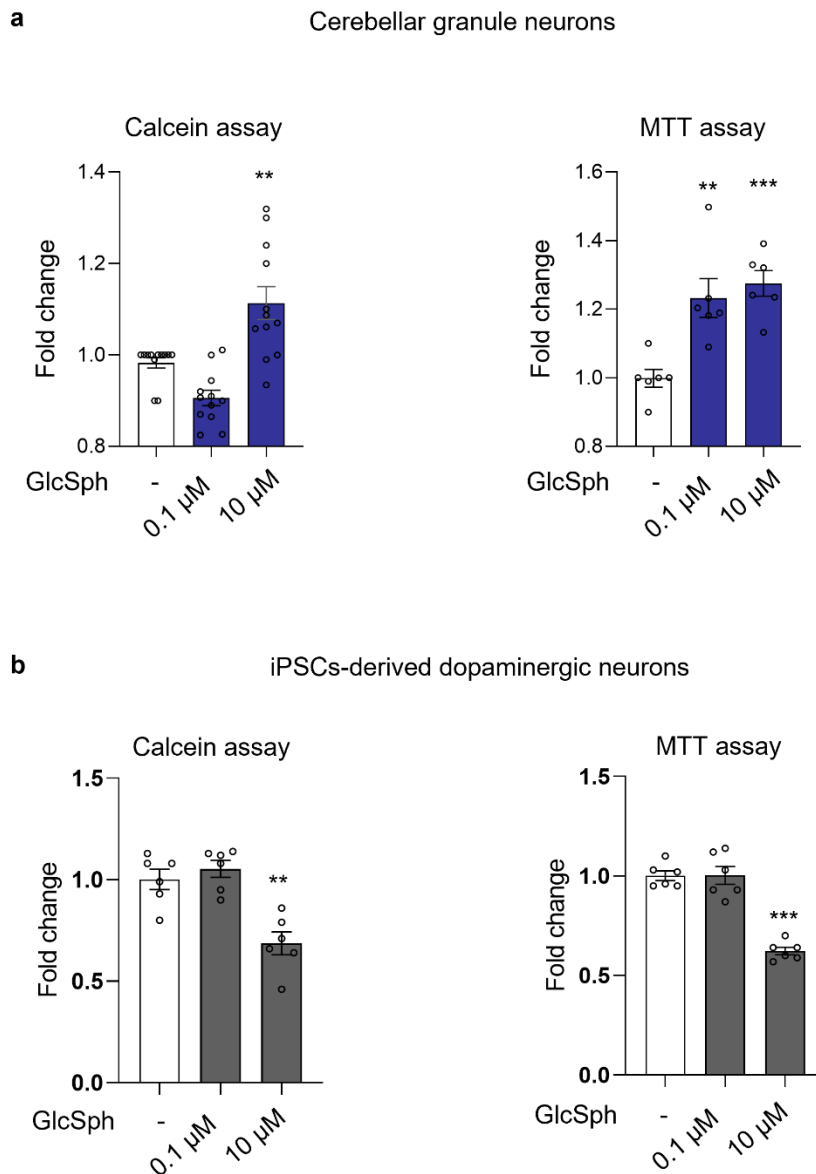


Figure 23. Effect of GlcSph administration on cell viability

Glucosylsphingosine (GlcSph) was administered to **a**) cerebellar granule neurons and **b**) human iPSC-derived dopaminergic neurons at 0,1 and 10 μ M for 24 hours. Cell viability was evaluated by Calcein assay and MTT assay. Data are expressed as fold change with respect to GlcSph- untreated cells (-) and are the mean \pm SEM of at least three experiments; * $p < 0.05$, ** $p < 0.01$, *** $p < 0.001$, One- way ANOVA vs GlcSph- untreated cells.

For what concerns the other lipids, in CGNs a decrease in Cer and SM was observed and became more evident upon long- term CBE treatment showing a reduction of about 50 % and 70 %, respectively (Figure 20a). On the other hand, in DA neurons any significant change was evident, except for SM that presented an increase of about 50 % upon long- term CBE treatment (Figure 20b).

CGNs subjected to long- term CBE treatment revealed a 50 % increase in the content of gangliosides GM3 and GM2 which was paralleled by a slight reduction in the content of GQ1b (Figure 24a). In DA neurons, long- term CBE treatment had a more marked effect on the ganglioside levels, with an increase of about 2- fold in the content of GM3, GM1, and GD1a. GD1b and GQ1b exhibited an increase of about 50 % and 25 % respectively (Figure 24b).

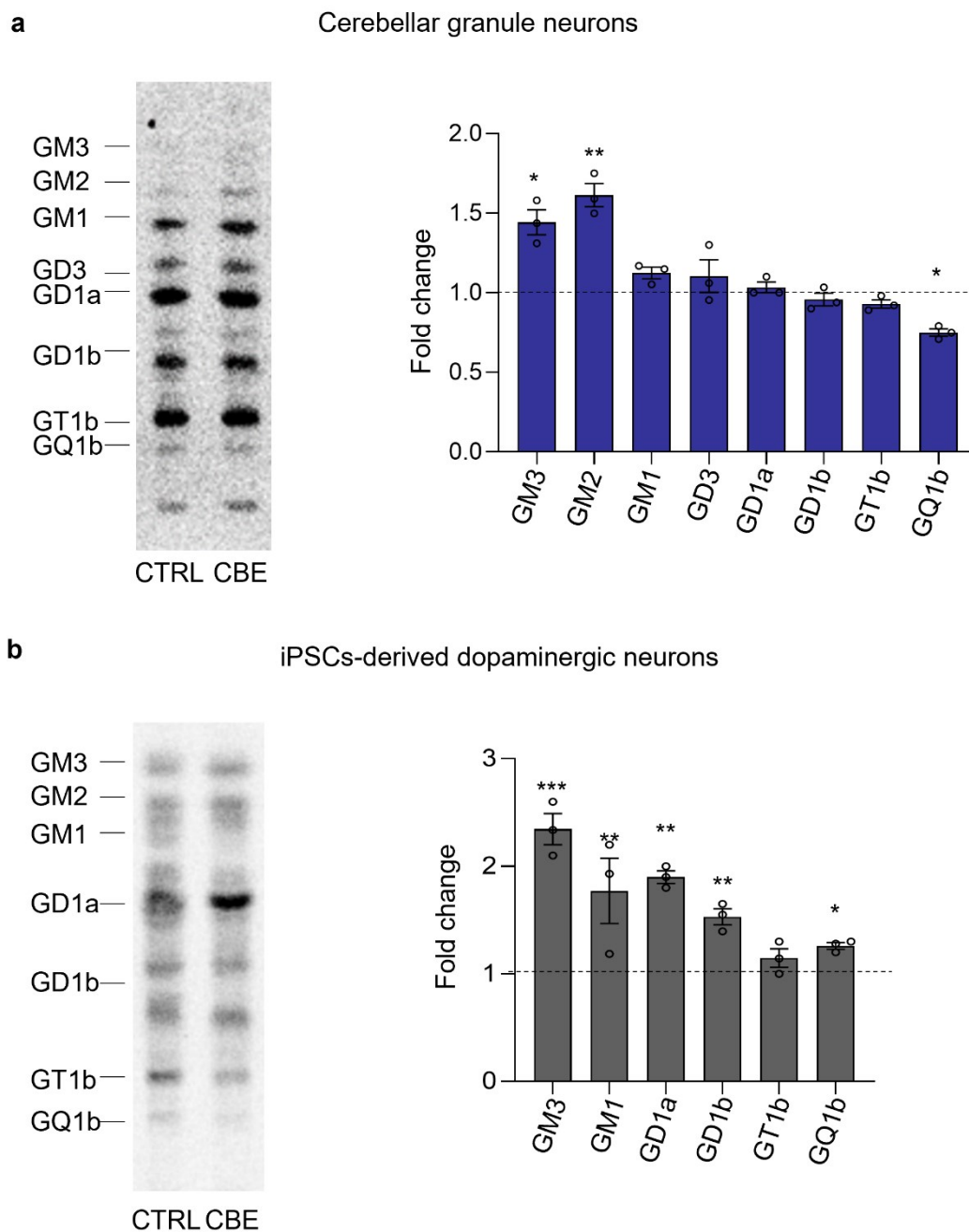


Figure 24. Effect of β -glucocerebrosidase inhibition on ganglioside levels

Representative digital autoradiography of ganglioside pattern and quantification of the radioactivity associated with individual gangliosides in: **a)** mouse cerebellar granule neurons fed with radioactive sphingosine and treated or not (CTRL) with 0.5 mM conduritol B epoxide (CBE) for 14 days, and **b)** human iPSC- derived dopaminergic neurons fed with radioactive sphingosine and treated or not (CTRL) with 0.5 mM CBE for 29 days. Data are expressed as fold change with respect to CBE- untreated cells (dashed line) and are the mean \pm SEM of three different experiments. * $p < 0.05$; ** $p < 0.01$; *** $p < 0.001$, two- tail Student's t- test vs CBE-untreated cells.

The accumulation of uncatabolized SLs is a typical and described feature of lysosomal storage disorders, which implements the impairment of the lysosomal compartment. It is described in literature that upon lysosomal impairment, the nuclear translocation of the transcription factor EB

(TFEB) is enhanced. TFEB is a master regulator of the transcription of genes coding for proteins related to lysosomes, e.g. proteins involved in compensatory processes with the aim to counteract the lysosomal accumulation of uncatabolized material^{112,113}. Upon long- term CBE treatment there was a higher nuclear translocation of TFEB in both cell models (Figure 25).

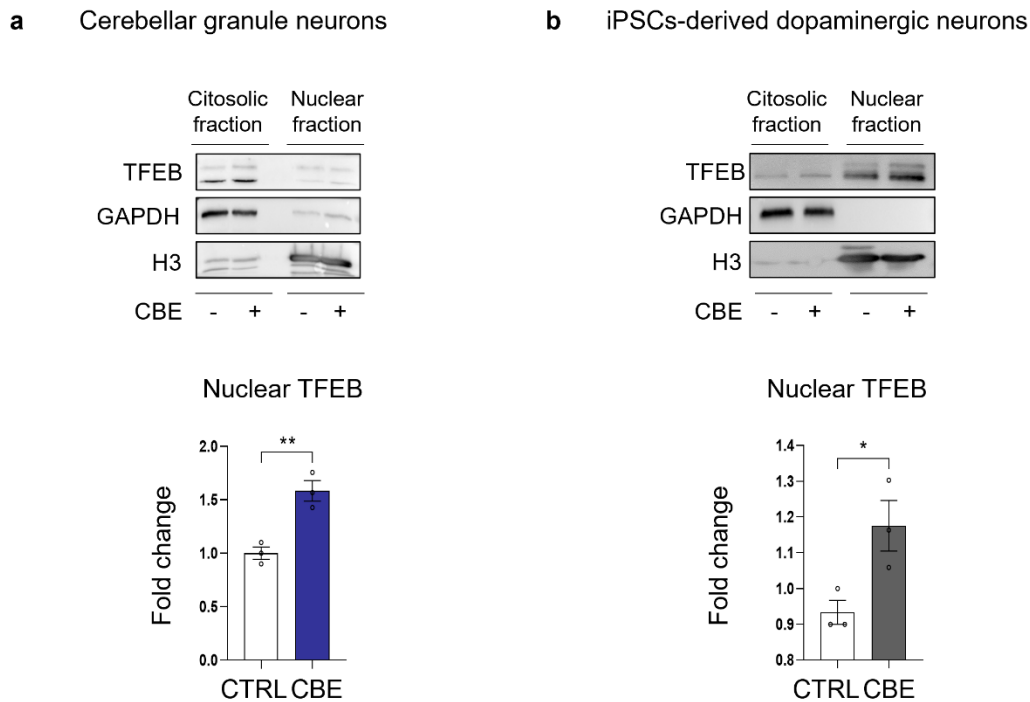


Figure 25. Evaluation of TFEB nuclear translocation

Representative images of the expression of the transcription factor EB (TFEB) in the cytosolic and nuclear fraction of **a)** mouse cerebellar granule neurons **b)** human iPSCs-derived dopaminergic neurons treated or not with 0.5 mM conduritol B epoxide (CBE). Cytosolic and nuclear fraction are represented respectively by the expression of the cytosolic marker GAPDH or the nuclear marker histone 3 (H3).

Quantification of the nuclear amount of TFEB normalized on H3 and expressed as fold change with respect to CBE-untreated cells (CTRL) and are the mean ± SEM of at least three experiments; * p < 0.05; ** p < 0.01, Student's t- test vs CBE-untreated cells.

As mentioned before, the transcription activity of TFEB can lead to the activation of lysosomal biogenesis⁴¹. Therefore, I evaluated the protein levels of the lysosomal marker LAMP1 in both cell models after long- term CBE treatment, which was found to be increased of about 30 % and 50 % in CBE- treated CGNs and DA neurons respectively (Figure 26).

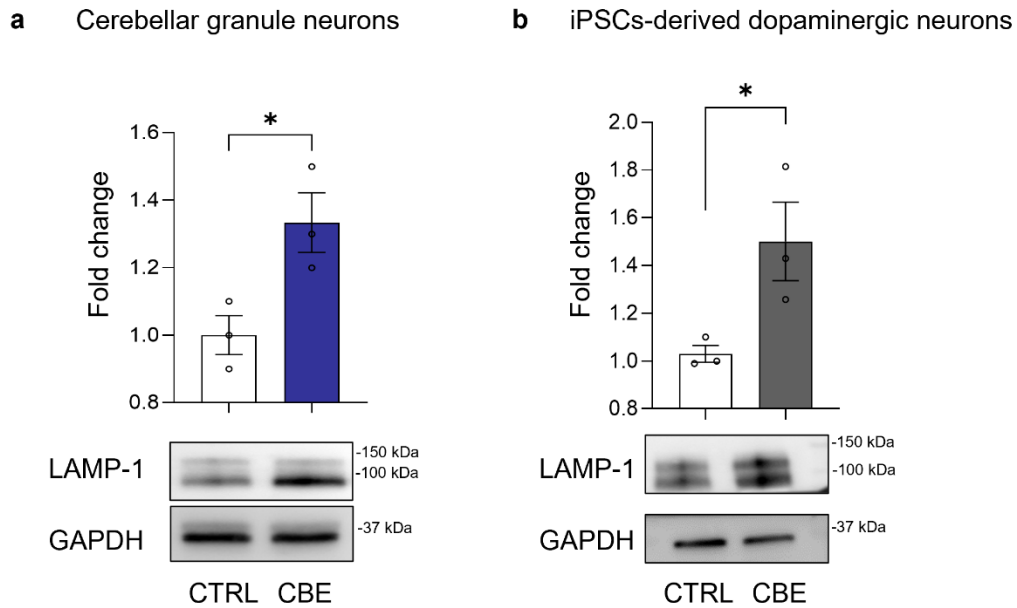


Figure 26. Effect of glucosylceramide accumulation on Lysosomal Associated Membrane Protein- 1 expression

Immunoblotting analyses of Lysosomal associated membrane protein (LAMP- 1) in **a**) mouse cerebellar granule neurons and **b**) human iPSC-derived dopaminergic neurons treated or not with 0.5 mM conduritol B epoxide (CBE) for 14 and 29 days, respectively. Data are expressed as fold change with respect to CBE- untreated cells (CTRL) and are the mean \pm SEM of three experiments; * $p < 0.05$, two- tail Student's t- test vs CBE- untreated cells.

At the end of the CBE treatment I stained CGNs with LysoTracker Red DND- 99, a fluorescent dye which allows to track acidic organelles, which indicated that CBE treatment caused an increase in the relative volume of the endolysosomal compartment (Figure 27a). By indirect immunofluorescence staining of LAMP1 in DA neurons I confirmed the increased expression of the lysosomal marker after CBE treatment, suggesting an increased number of lysosomes (Figure 27b). To corroborate this hypothesis, together with the Advanced Light and Electron Microscopy BiImaging Center IRCCS San Raffaele Hospital and Vita-Salute San Raffaele University of Milan, I carried out electron microscopy analysis of DA neurons subjected to long- term CBE treatment and confirmed the increase in the number and size of lysosomes (Figure 27c).

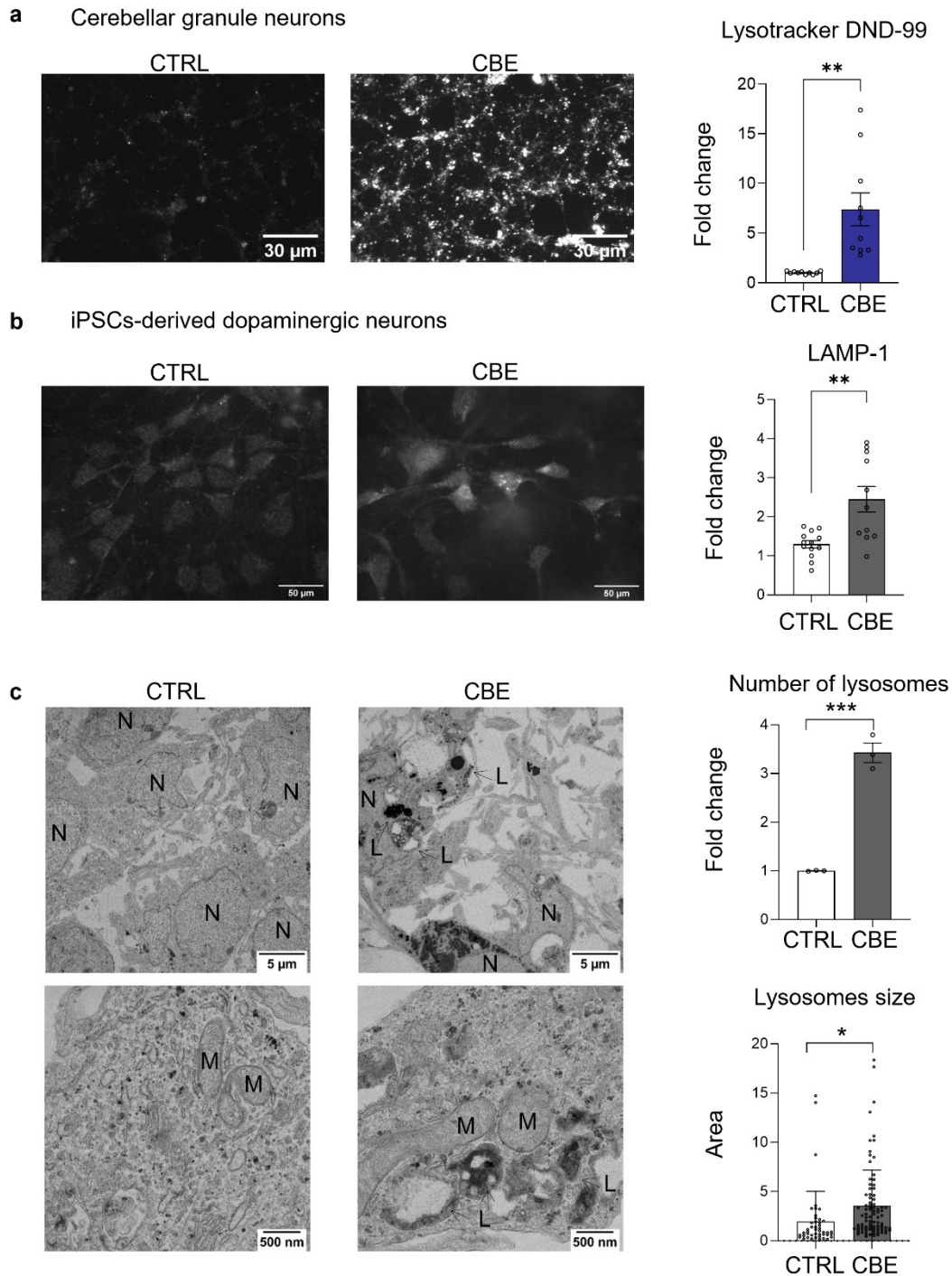


Figure 27. Evaluation of lysosomal biogenesis upon glucosylceramide accumulation

a) Representative image of lysotracker Red DND- 99 staining of mouse cerebellar granule neurons treated or not with 0.5 mM conduritol B epoxide (CBE) for 14 days. Images were acquired at 100x magnification and fluorescence intensity was quantified. **b)** Expression of LAMP- 1 in human iPSC-derived dopaminergic neurons treated or not with 0.5 mM CBE for 29 days, evaluated by immunofluorescence. Images were acquired at 400x magnification and fluorescence intensity was quantified. **c)** Representative electron microscopy images of lysosomes (L) in dopaminergic neurons treated or not (CTRL) with 0.5 mM CBE for 29 days and stained with uranyl acetate and lead citrate. N, nucleus; M, mitochondrion and quantification of the number of lysosomes and their size. Data are expressed as fold change with respect to CBE- untreated cells (CTRL) or as area value of CBE treated and untreated (CTRL) cells and are the mean \pm SEM of at least three experiments; ** $p < 0.01$, Student's t- test vs CBE- untreated cells.

An efficient strategy to split the cargo of accumulated uncatabolized material into more organelles could be to increase lysosomal biogenesis. I therefore investigated the ability of newly produced lysosomes to catabolize SLs by feeding long- term CBE- treated CGNs with radioactive [3-³H(sphingosine)]GM1¹¹⁴. This GM1 derivative presents a radioactive sphingosine moiety and allowed us to follow the production of its catabolites in living cells. As shown in Figure 28, I found a reduced production of radioactive GM1 catabolites, such as GM3, LacCer, GlcCer and Cer in CBE-treated CGNs compared to untreated cells, suggesting an impairment of lysosomal catabolism. I observed also the reduction of radioactive globoside Gb3, whose biosynthesis depends on [3-³H(sphingosine)] salvage pathway, further supporting the lysosomal dysfunction in CGNs treated with CBE.

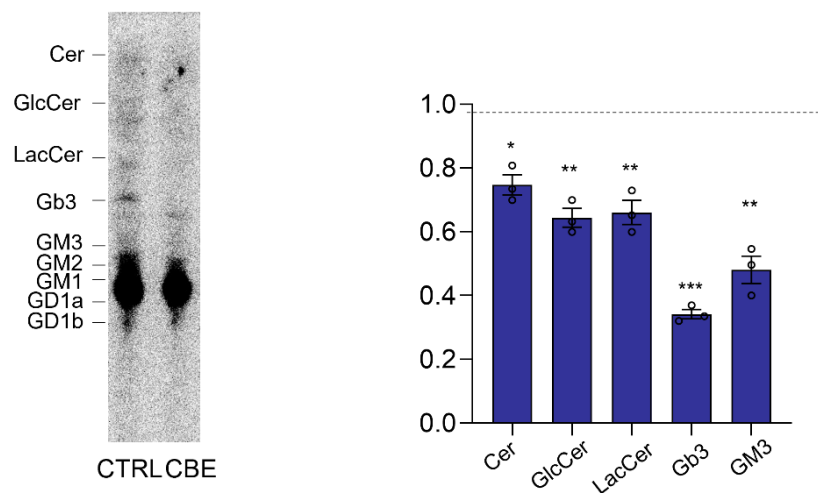


Figure 28. Evaluation of lysosomal catabolism of glycosphingolipids upon glucosylceramide accumulation

Representative HPTLC image and quantification of sphingolipids extracted from mouse cerebellar granule neurons treated or not with 0.5 mM conduritol B epoxide (CBE) for 14 days followed by radioactive GM1 administration (Cer=ceramide; GlcCer= glucosylceramide; LacCer= lactosylceramide; Gb3=globo- triaacylglyceramide; GM3=monosialodihexosylganglioside; GM1= monosialotetrahexosylganglioside). Data are expressed as fold change with respect to CBE- untreated cells (dashed line) and are the mean \pm SEM least of three experiments; * $p < 0.05$, ** $p < 0.01$, *** $p < 0.001$, Student's t- test vs CBE- untreated cells.

Since the lysosomal compartment is an essential component of the cell's catabolic machinery, I evaluated the effect of the lysosomal impairment on the cell proteome to have a general overview of the changes occurring upon GCase inhibition and GlcCer accumulation. Thanks to the collaboration with the group of Dr Armirotti from Genova, Italy, we performed a label- free expression proteomics analysis on DA neurons treated or not with CBE, which allowed the

identification of 70 upregulated (Annex I, table 3) and 71 downregulated (Annex I, Table 4) proteins in CBE treated neurons with respect to untreated ones. Bioinformatics analysis was ran by DAVID software¹¹⁵ (Annex I, Table 5, Figure 29) and showed that, among the upregulated proteins, there was a significant enrichment in proteins involved in the lysosomal structure, in the GSL catabolism, in proteins related to mitochondria activity, and in glycoproteins biosynthesis and trafficking (Figure 29a). Among the significantly enriched pathways, the investigation was further targeted to the “SL metabolism” highlighted by DAVID analysis. Using STRING database to predict functional association between proteins¹¹⁶, I discovered that following GCase inhibition, GalCer catabolism was significantly increases mainly through the overexpression of galactosylcerebrosidase and prosaposin. This result suggested a reaction to GCase inhibition, where cells activate alternative sources for the production of ceramide which is an essential SL for cell homeostasis.

On the other hand, among downregulated proteins there was mainly an enrichment in integral component of membranes and trafficking proteins, such as RAB5, suggesting an impairment in the endocytosis processes, and RAB6, leading to hypothesize an involvement of the endoplasmic reticulum- Golgi- PM vesicular trafficking (Figure 29b). These data indicate that GlcCer accumulation due to GCase inhibition strongly affects the neuronal proteostasis.

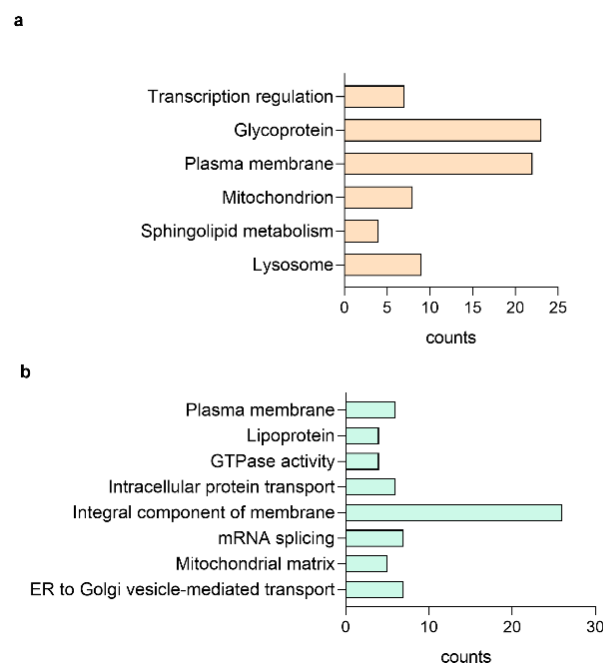


Figure 29. Effect of β - glucocerebrosidase inhibition on proteomic profile

Bar chart showing the cluster enriched annotation groups of proteins **a)** upregulated and **b)** downregulated in CBE treated DA neurons with respect to untreated cells obtained by David bioinformatics analysis. The x axis indicates the number of proteins involved in each term.

It is already well established that the above- described lysosomal impairment and TFEB nuclear translocation lead to the activation of aberrant lysosomal exocytosis⁴¹, which is an alternative process that helps eliminating the accumulated materials by the fusion of the lysosomes with the PM causing the release of lysosomal content in the extracellular environment and the association of lysosomal glycohydrolases with the external leaflet of the PM. To understand the potential effect of this process on the neuronal homeostasis it is necessary to consider how GlcCer accumulates inside lysosomes. GlcCer can be associated with intralysosomal vesicles and can also become part of the inner layer of the lysosomal membrane. Upon lysosomal fusion with the PM, the GlcCer accumulated in the vesicles is released in the extracellular milieu where it can exchange with the GlcCer associated with the PM, while the GlcCer present in the lysosomal membrane can directly become component of the external leaflet of the PM.

To investigate the occurrence of these events, I evaluated the enzymatic activity of specific lysosomal glycohydrolases at PM level exploiting a living cell- based assay³². In long- term CBE-treated CGNs I found an increase of about 50 % in the activity of the PM- associated β - galactosidase (Figure 30a), while in long- term CBE-treated DA neurons the activity of both the PM- associated β - galactosidase and β - hexosaminidase was augmented of about 2- folds (Figure 30b).

Interestingly, I also observed an increase in the release of GlcCer in the extracellular milieu of about 50 % in CBE-treated CGNs and 25 % in DA neurons compared to untreated cells (lower panel Figure 30a and b).

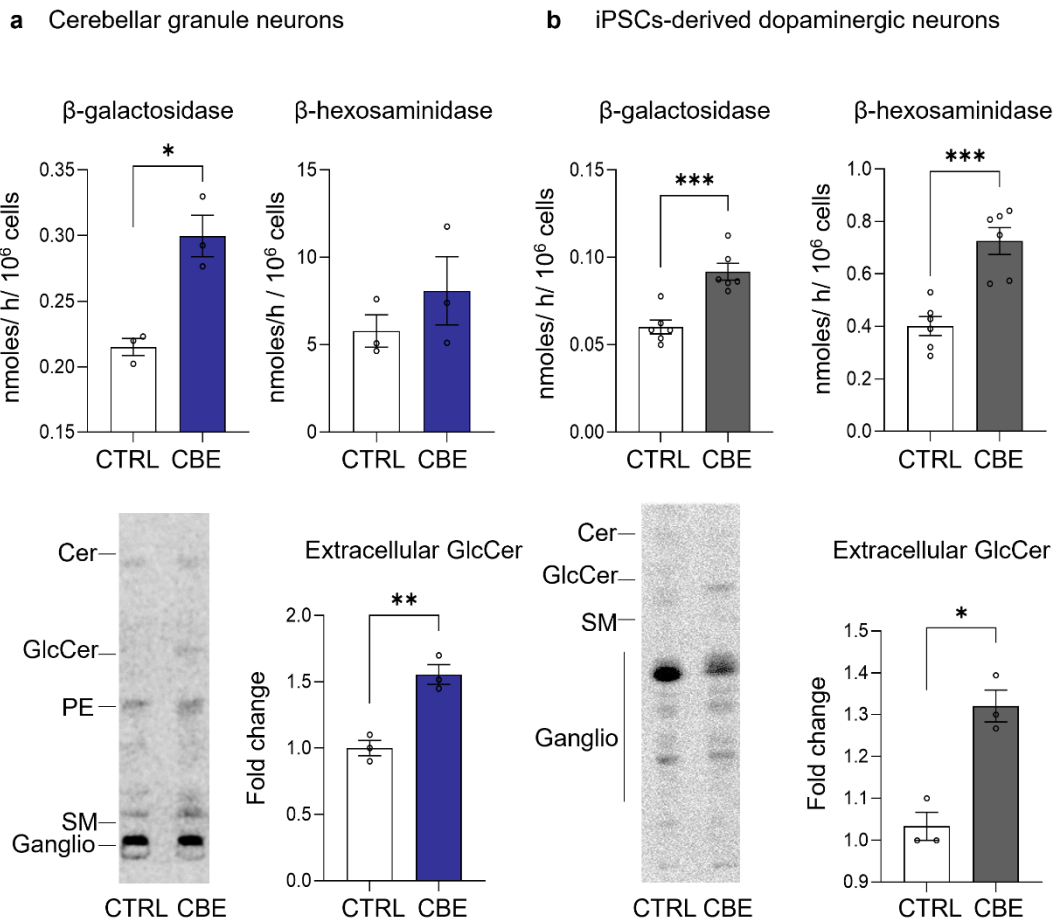


Figure 30. Activity of PM glycohydrolases and extracellular release of glucosylceramide upon its accumulation

Specific enzyme activity of plasma membrane-associated β -galactosidase and β -hexosaminidase and representative images and quantification of extracellular release of glucosylceramide (GlcCer) in **a**) mouse cerebellar granule neurons and **b**) human iPSC-derived dopaminergic neurons fed with radioactive sphingosine followed by treatment in presence or in absence of 0.5 mM conduritol B epoxide (CBE) for 14 and 29 days, respectively. Enzyme activities are expressed as nmoles/h normalized to 10⁶ cells and are the mean \pm SEM of three experiments (* p <0.05, *** p <0.001, two-tail Student's t-test vs CBE-untreated cells (CTRL)). Extracellular release of radioactive GlcCer was determined after lipid extraction of cell culture medium and HPTLC separation (Cer= ceramide, PE= phosphatidylethanolamine, SM= sphingomyelin, ganglio= gangliosides). Data are expressed as fold change with respect to CBE-untreated cells (CTRL) and are the mean \pm SEM of three experiments; * p <0.05, ** p <0.01, *** p <0.001, two-tail Student's t-test vs CBE-untreated cells.

The described processes let hypothesize about the occurrence of modifications in the lipid composition of the PM, already demonstrated to happen in other LSDs⁴¹. To investigate this aspect, I fed CGNs and DA neurons with [1-³H]-sphingosine and after long-term CBE treatment, exploiting a biotin-streptavidin affinity pull-down assay, PM proteins and the surrounding lipids were isolated. The radioactive lipids were extracted from the precipitated portion (P) and from the supernatant obtained after precipitation (SN) and the proteins were denatured to assess the efficiency of precipitation. In CGNs about 80% and in DA neurons about 90% of the biotinylated proteins was

recovered in the P fraction independently from the CBE treatment (Fig 31a). As a confirm of the precipitation purity I evaluated the expression of PM specific proteins and soluble proteins. PM-associated proteins PSD95 or the prion protein Prp were enriched in the P fraction, while the soluble glyceraldehyde 3- phosphate dehydrogenase (GAPDH) was present only in the SN fraction (Figure 31b).

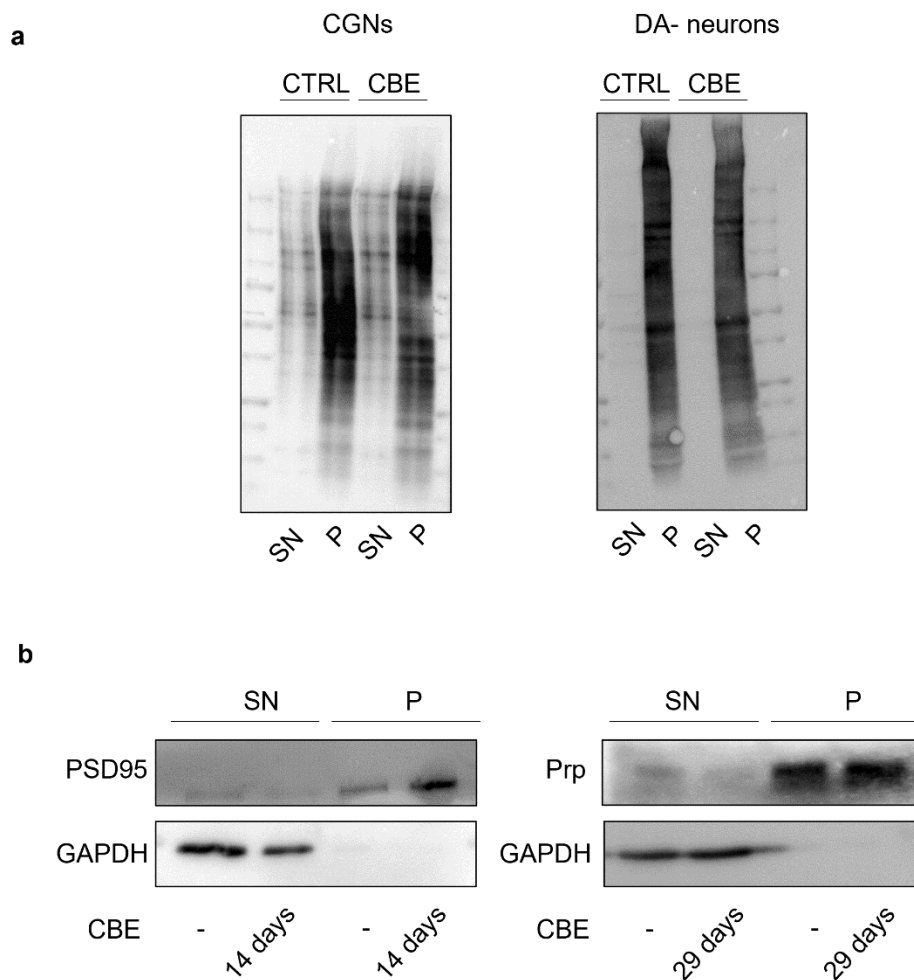


Figure 31. Validation of the efficiency of PM proteins' precipitation

a) Representative image of the biotinylated protein pattern of SN and P fractions of mouse CGNs and human DA-neurons treated or not with CBE respectively for 14- and 29- days **b)** Representative images of cytosolic and PM antigens expression in SN and P fractions of murine CGNs and human DA-neurons treated or not with CBE respectively for 14 and 29 days.

Precipitated proteins were then identified in DA neurons by high resolution mass spectrometry, following digestion with trypsin. 72 proteins were confidently identified as selectively expressed at the PM level of CBE treated neurons (Annex I, Table 5), while 5 proteins as selectively expressed at

the PM level of untreated neurons (Annex I, Table 6). Through an interaction analysis it was revealed that 44 proteins show a significant functional association, as demonstrated in Figure 32. Furthermore, several molecular functions were found to be enriched (Annex I, Table 5). I explored possible known functional associations between this dataset and GCase but no major interactions were highlighted by our analysis.

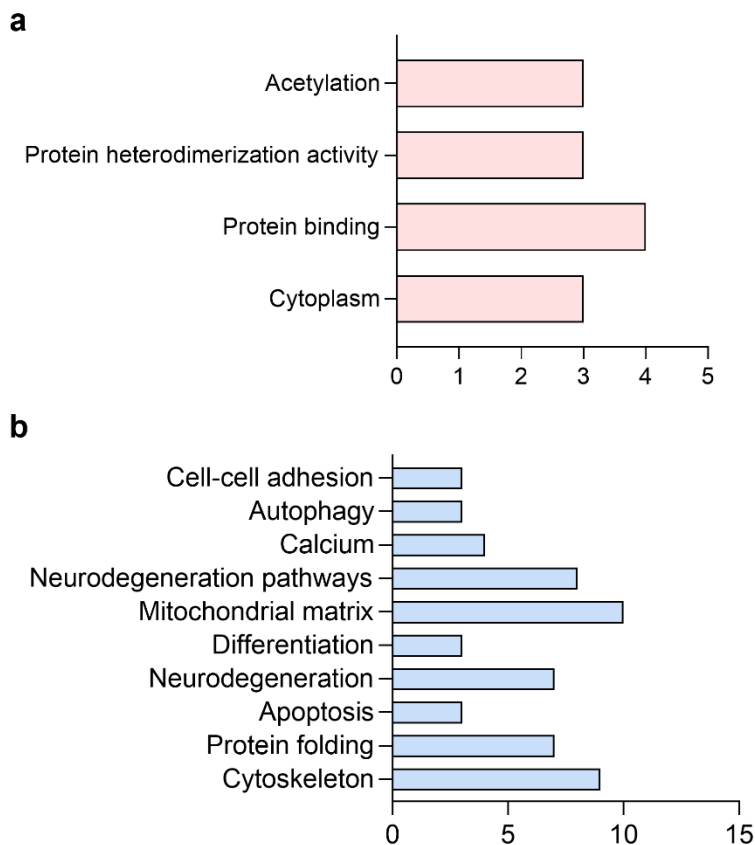


Figure 32. Effect of β - glucocerebrosidase inhibition on PM proteomic profile

Bar chart showing the cluster enriched annotation groups of plasma membrane- associated proteins **a)** repressed and **b)** *de novo* expressed in CBE treated DA neurons obtained by David bioinformatics analysis. The x- axis indicates the number of proteins involved in each term.

For what concerns the lipids, around 40 % was associated with the P fraction of untreated CGNs and DA neurons, which increased up to around 60 % in case of CBE treatment. The accumulation of GlcCer in the SN fraction was about 12- fold and 6- fold in CGNs and DA neurons compared to untreated neurons, respectively. A more intense increase was present in the P fraction, which was approximately 30- fold and 18- fold higher in CBE- treated CGNs and DA neurons, respectively (Figure 33).

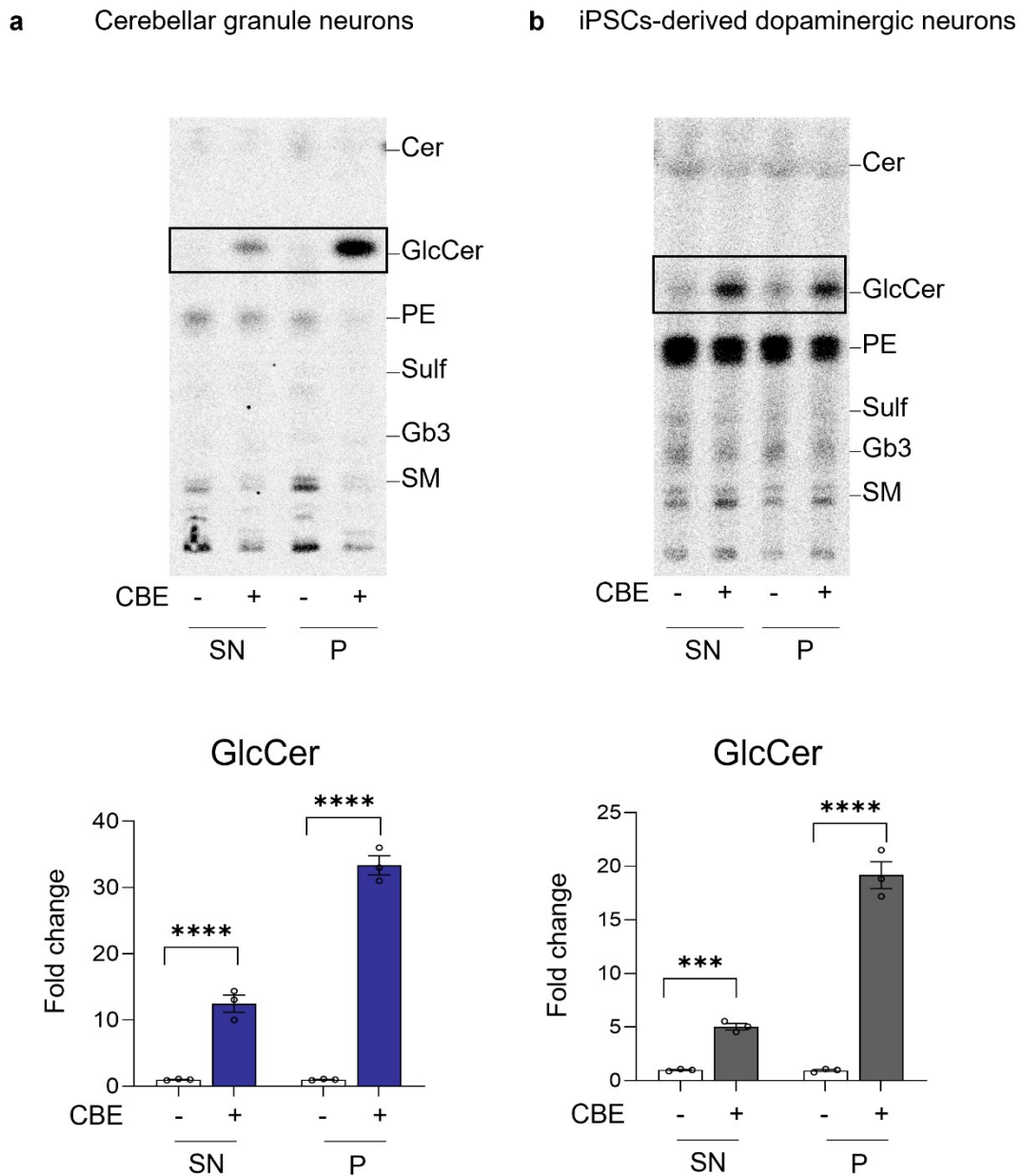


Figure 33. Accumulation of glucosylceramide at the cell surface

Representative HPTLC image of radioactive lipids of cell fractions obtained after selective cell surface protein biotinylation followed by magnetic separation using Dynabeads™ streptavidin magnetic beads; lipids were extracted from the supernatants containing non biotinylated proteins (SN) and the pellets containing the biotinylated cell surface proteins (P); **a**) mouse cerebellar granule neurons and **b**) human iPSC- derived dopaminergic neurons treated or not (-) with 0.5 mM conduritol B epoxide (CBE), for 14 and 29 days, respectively.

(Cer= ceramide; GlcCer= glucosylceramide; PE= phosphatidylethanolamine; SM= sphingomyelin). Data are expressed as fold change of GlcCer with respect to CBE-untreated cell fraction (-) and are the mean ± SEM of three experiments (**p<0.001; ****p<0.0001; one- way two- tail Student's t- test vs CBE- untreated cells). GlcCer content was normalized nCi/ mg of proteins of the sample.

It is known that in the cell membranes and in particularly in the PM, SLs, together with cholesterol and a selected number of proteins, organize macromolecular complexes, defined as detergent resistant membrane portions (DRM), which beside having structural functions, also play a role in the control of signalling cascades^{117,118}.

I proceeded with the isolation and analyses of these PM microdomains in DA neurons subjected to long- term CBE treatment, exploiting their resistance to detergents, in order to evaluate whether lysosomal exocytosis occurs causing GlcCer accumulation in PM- DRMs.

By loading the same protein amount of cell lysates on a sucrose density gradient I was able to separate DRMs based on their low- density, from the high- density fractions (HD) containing all the remaining cell components. The 12 collected fractions of both untreated and CBE- treated DA neurons were assessed for the presence of DRM marker flotillin, and a typical non- DRM-associated protein, calnexin, as well as for the radioactivity content. As shown in Figure 34a, DRM markers were enriched in fractions 5 and 6, whereas non- DRM- associated proteins were only detectable in HD fractions 10, 11, and 12 (Figure 34a).

The radioactivity associated with SLs was particularly abundant in fractions 5 and 6 with respect to the fractions 10, 11, and 12 (Figure 34b) and based on the above- mentioned evidence fractions 5 and 6 represented the DRM, while fractions 10, 11, and 12 were considered as HD.

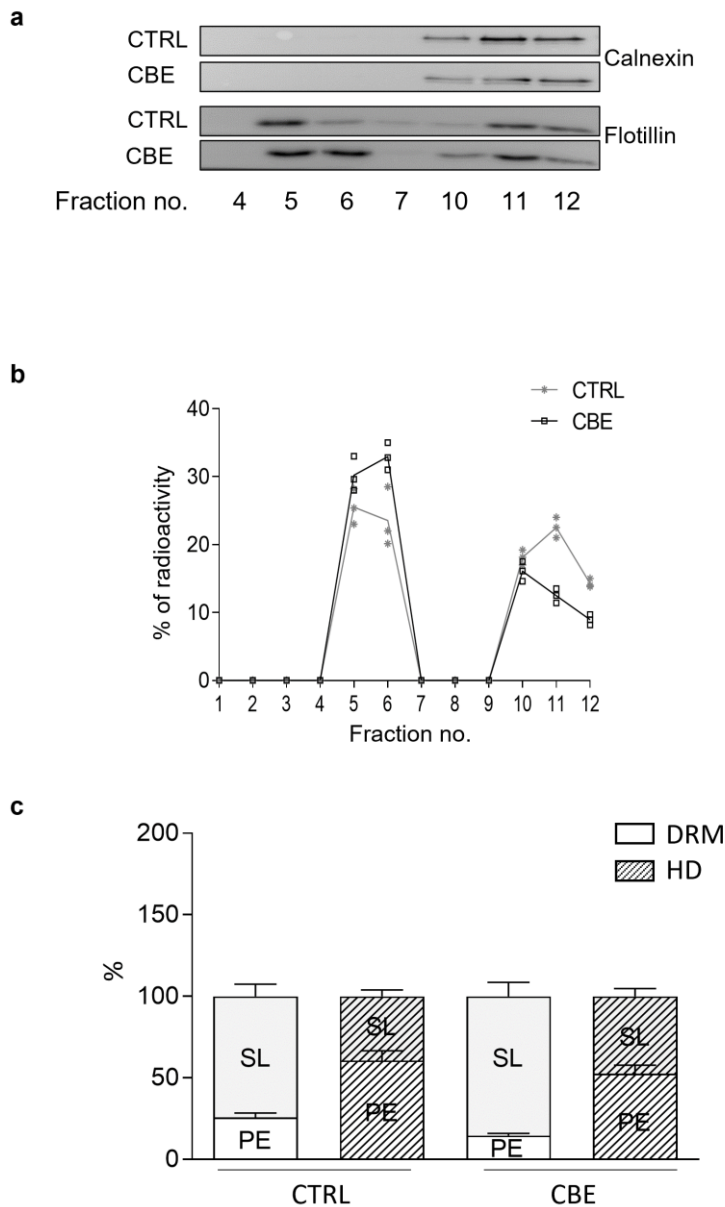


Figure 34. Characterization of Detergent Resistant Membrane fractions

Detergent Resistant Membrane fractions (DRM) were isolated from human iPSCs- derived dopaminergic neurons treated or not with 0.5 mM conduritol B epoxide (CBE) for 29 days after metabolic labelling with [1-³H]- sphingosine. Fractions were collected and either counted for radioactivity or subjected to lipid extraction or immunoblotting with anti- DRM- specific marker antibodies. **a)** Representative image of the expression of protein markers in the fractions 5- 6 and in fractions 10 -12 **b)** Percentage distribution of radioactivity associated with sphingolipids in the sucrose-gradient density fractions. **c)** Percentage distribution of sphingolipids (SL) and phosphatidylethanolamine (PE) in DRM and HD fractions of CBE- untreated (CTRL) and treated DA neurons.

Interestingly, DRM of untreated DA neurons presented about 41 % of the total radioactivity, which increased up to 66 % in CBE- treated neurons (Figure 34b). Furthermore, the DRM fraction was enriched in SLs at the expense of PE when compared to HD (Fig 34c). In addition, the SL pattern

analysis clearly indicated that in CBE-treated DA neurons the increased radioactivity was mainly due to an augmented content of GlcCer (Figure 35a).

To exclude any contribution of DRM from intracellular membranes, I submitted DRM to biotin-streptavidine affinity pull-down assay in conditions preserving DRM integrity. The radioactive lipids were extracted from the P and SN fractions obtained after precipitation, and the proteins were denatured to assess the efficiency of precipitation. About 90 % of the biotinylated proteins were recovered in the P, independently from the CBE treatment. In addition, the P fraction of untreated and CBE-treated neurons contained, respectively, 95 % and 90 % of the total amount of radioactive lipids associated with DRM.

PM- DRM of CBE-treated DA neurons presented a 11-fold increase in GlcCer content, and the halving of Cer levels compared to untreated DA neurons (Figure 35b).

The interaction of SLs and proteins is a widely described feature at PM level and therefore I investigated whether the GlcCer accumulation could also affect the PM proteome. Obtained data indicate that GCCase inhibition was able to block or induce *de novo* expression of several classes of proteins inducing important changes in terms of PM protein composition. In particular, the expression of proteins responsible for exosome release, protein binding, and cytoplasm formation or stability (i.e. tubulin beta-4A chain) were repressed upon GCCase inhibition while a list of 72 proteins was confidently identified as exclusively expressed at the PM level of CBE-treated neurons. CBE treatment induced the expression of proteins involved in cell-to-cell adhesion, autophagy, apoptosis, differentiation, and neurodegeneration suggesting an important effect mediated by the PM on neuronal homeostasis. An interaction analysis revealed that 44 out of 72 proteins show significant functional association but no functional association existed between this dataset and the target GCCase (Figure 32).

From our preliminary analyses it emerged that in DRM of CBE-treated DA neurons there was a 2-fold enrichment in the phosphorylated form of c-Src (pTyr416-Src) with respect to untreated cells (Figure 35c).

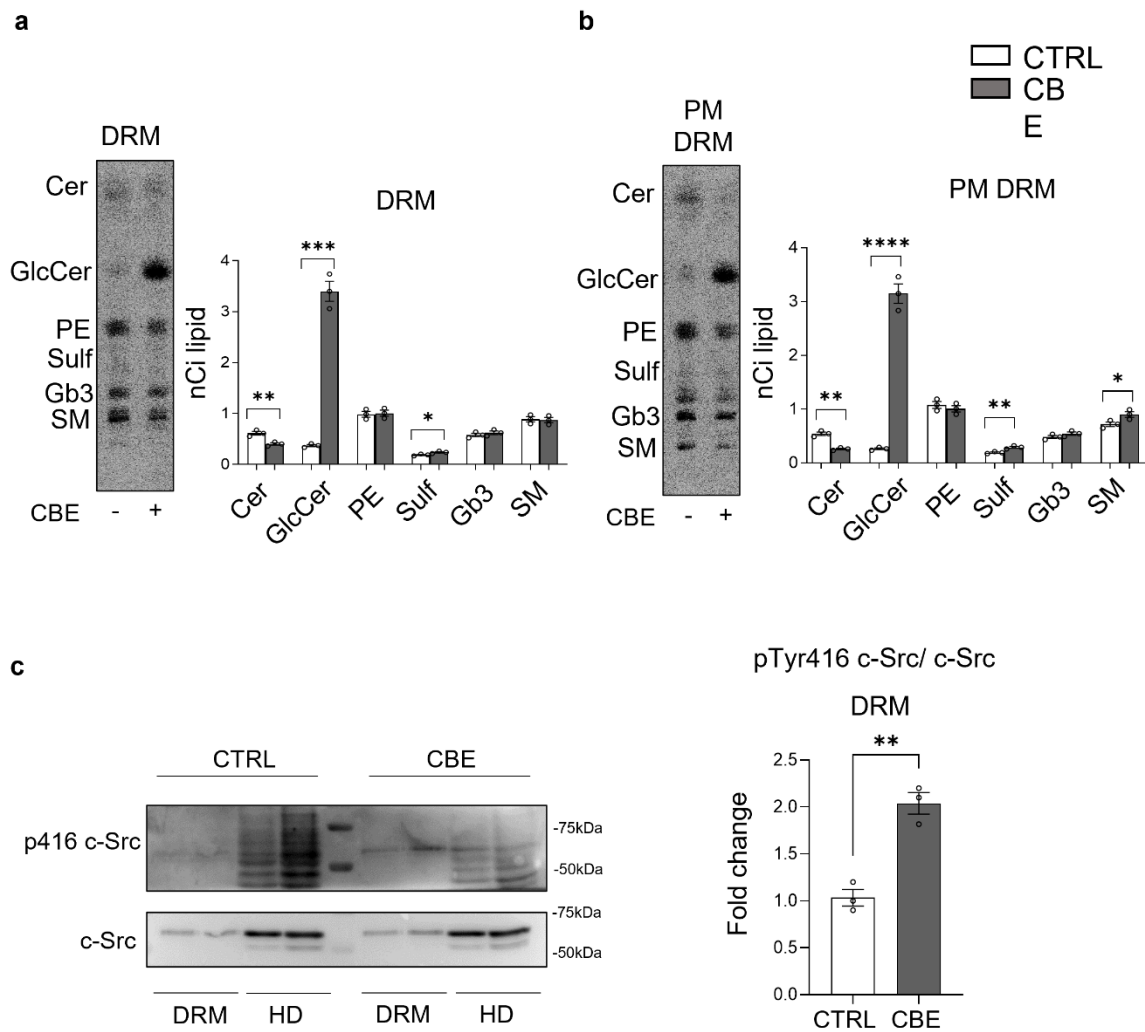


Figure 35. p416 c- Src expression and lipid distribution in detergent- resistant PM fractions of iPSCs- derived dopaminergic neurons treated or not with conduritol B epoxide

a) Representative image of HPTLC of radioactive lipids of detergent- resistant membrane domain fraction (DRM) of human iPSCs-derived dopaminergic neurons treated or not (-) with 0.5 mM conduritol B epoxide (CBE) for 29 days. **b)** Representative image of HPTLC of radioactive lipids of detergent- resistant membrane domain fraction (DRM) after cell surface biotinylation of human iPSCs- derived dopaminergic neurons treated or not (-) with 0.5 mM conduritol B epoxide (CBE) for 29 days. Detergent-resistant PM domain fraction (PM- DRM) was obtained from DRM by streptavidine magnetic beads separation. Data are expressed as nCi and are the mean \pm SEM from at least three experiments (* $p < 0.05$; ** $p < 0.01$; *** $p < 0.001$, **** $p < 0.0001$; two- tail Student's t- test).

(Cer=ceramide; GlcCer= glucosylceramide; PE= phosphatidylethanolamine; Sulf= sulphatides; Gb3= globo- triaoylceramide; SM= sphingomyelin). **c)** Immunoblotting analysis of Src and pTyr416 c- Src expression in DRM fraction and non- DRM high density fractions (HD) of dopaminergic neurons treated or not with CBE for 29 days; analysis of pTyr416 c- Src activation: pTyr416 c- Src band intensity was normalized to c- Src signal of the same sample. Data are expressed as fold change with respect to CBE-untreated cell fraction and are the mean \pm SEM of at least three experiments; ** $p < 0.01$; two- tail Student's t- test.

5.2.2. Analysis of metabolites and ATP production in *iPSCs* derived dopaminergic neurons

Considering the main role of lysosomes as cell degradation hubs involved in the catabolism and recycling of macromolecules, it can be easily imagined that lysosomal impairment could have negative consequences on lysosomal catabolic and recycling ability which could reflect on the overall cell's metabolic flow. To examine how the cell metabolism changes upon lysosomal impairment due to GlcCer accumulation, in collaboration with the group of Prof Nico Mitro of the Department of Pharmacological and Biomolecular Sciences of the University of Milan, liquid chromatography- tandem mass spectrometry (LC- MS/ MS)- based metabolomic profiling on long-term- treated and untreated DA neurons was carried out.

As shown by the principal component analysis in Figure 36, the metabolic profile underwent significant changes upon CBE treatment, depicting a clear separation between long- term CBE- treated and untreated DA neurons. Based on PCA, 61.6 % of the data variability was attributed to the main plane (PC1 and 2). As shown in Figure 36, the areas of origin of long- term CBE- treated and untreated DA neurons were clearly separated according to the PC1 of the plot (46.9 %), suggesting that GCase inhibition induces several changes in the metabolite composition.

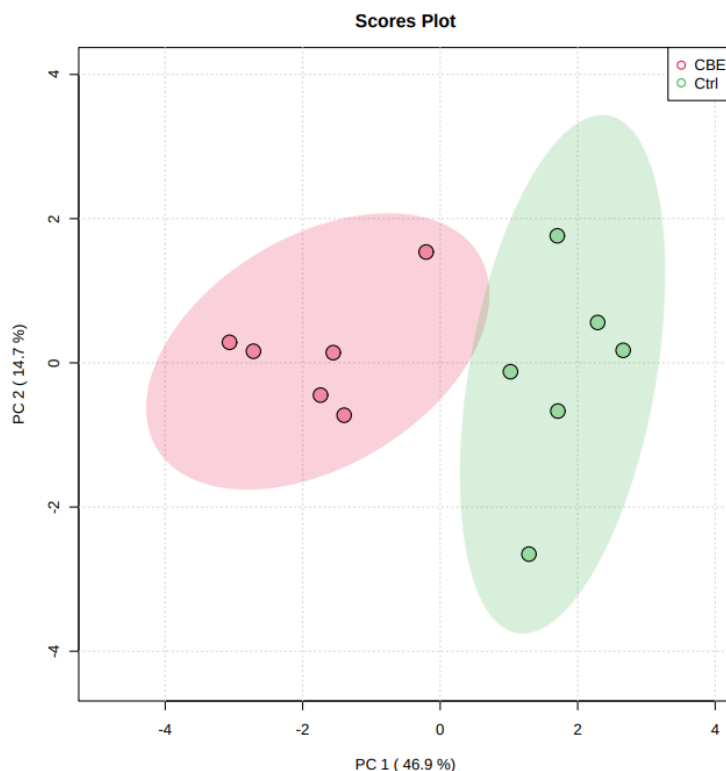


Figure 36. Principal component analysis (PCA) of metabolomics analysis obtained by the liquid chromatography- tandem mass spectrometry (LC- MS/ MS)- based profiling on long- term treated and untreated dopaminergic neurons

Indeed, among the 87 analyzed metabolites, 66 were differentially represented upon CBE treatment. As depicted in the heatmap in Figure 37 changes particularly hit glycolysis, TCA cycle, amino acids, and fatty acid oxidation. In particular, upon the 57 upregulated metabolites there were GSH, aspartate, Dihydroxyacetone phosphate (DHAP/ GAP), fructose bis-phosphate, glutamate, serine, C18: 1-carnitine, C3- carnitine, threonine, C14-carnitine, C16: 1- carnitine, glutamine, glycine, methionine, N- acetylmethionine, sarcosine, guanosine- 5'- triphosphate (GTP), alanine, C16- carnitine, tryptophan, 3', 5'- cyclic guanosine phosphate (GMP), inosine monophosphate (IMP), C5- carnitine, adenosine 5'- triphosphate (ATP), adenosine monophosphate (AMP), dGMP, proline, citrate, isoleucine, deoxyguanosine- 5'- triphosphate (dGTP), tyrosine, lysine, histidine, valine, asparagine, phenylalanine, uridine monophosphate (UMP), S- Adenosyl- L- Methionine (S- AME), leucine, malate, agmatine, isocitrate, free carnitines, arginine, nicotinamide adenine dinucleotide (NAD), putrescine, lactate, and C2- carnitine. Downregulated metabolites were 9 and comprised glucose, glucose- 6- phosphate, norepinephrine, cysteine, gluconate- 6- phosphate, phosphoenolpyruvate, succinate, deoxyadenosine monophosphate (dAMP), and deoxyinosine monophosphate (dIMP).

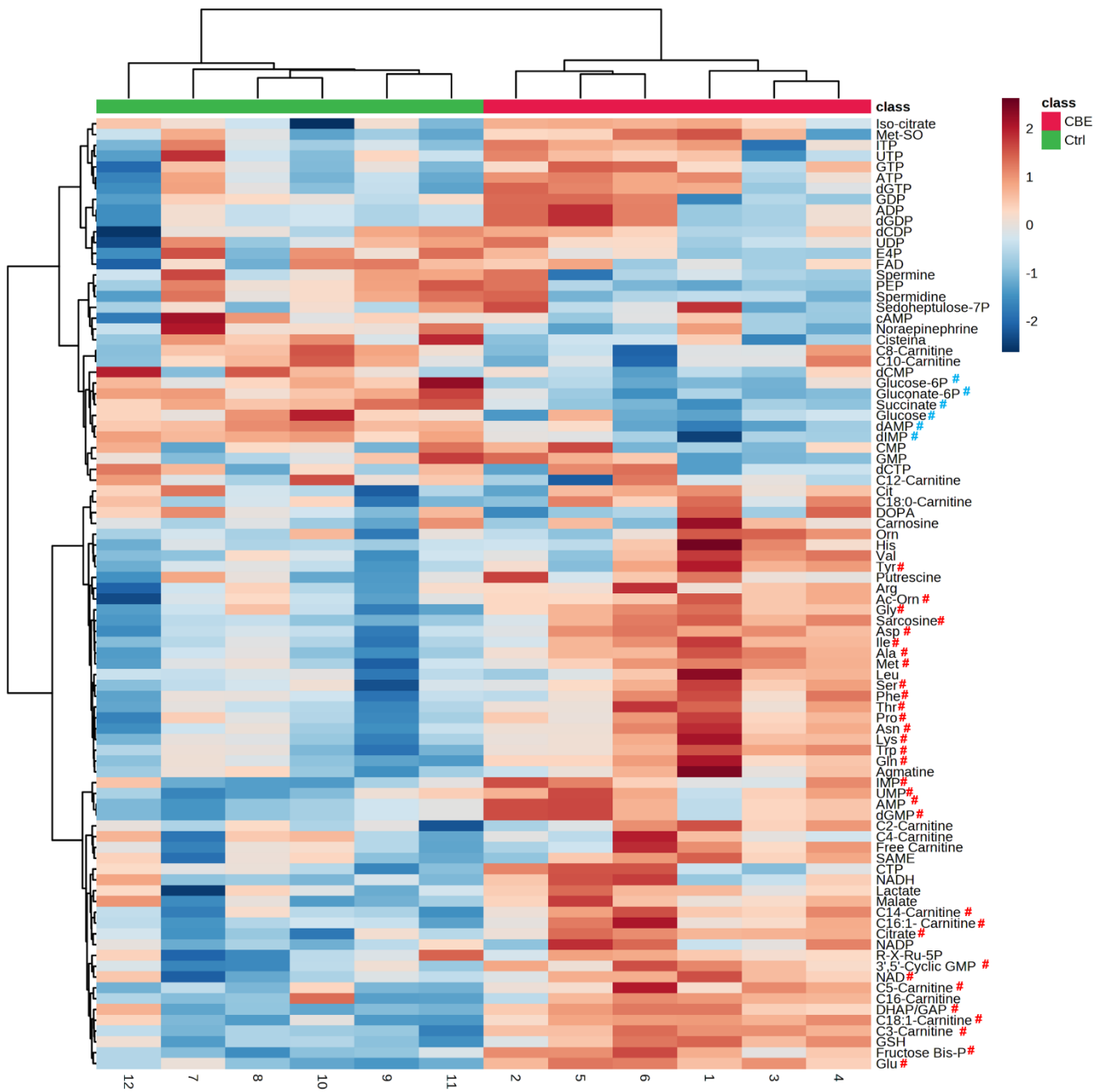


Figure 37. Heatmap of metabolites detected liquid chromatography- tandem mass spectrometry (LC- MS/ MS)- based profiling on long- term CBE- treated and untreated dopaminergic neurons

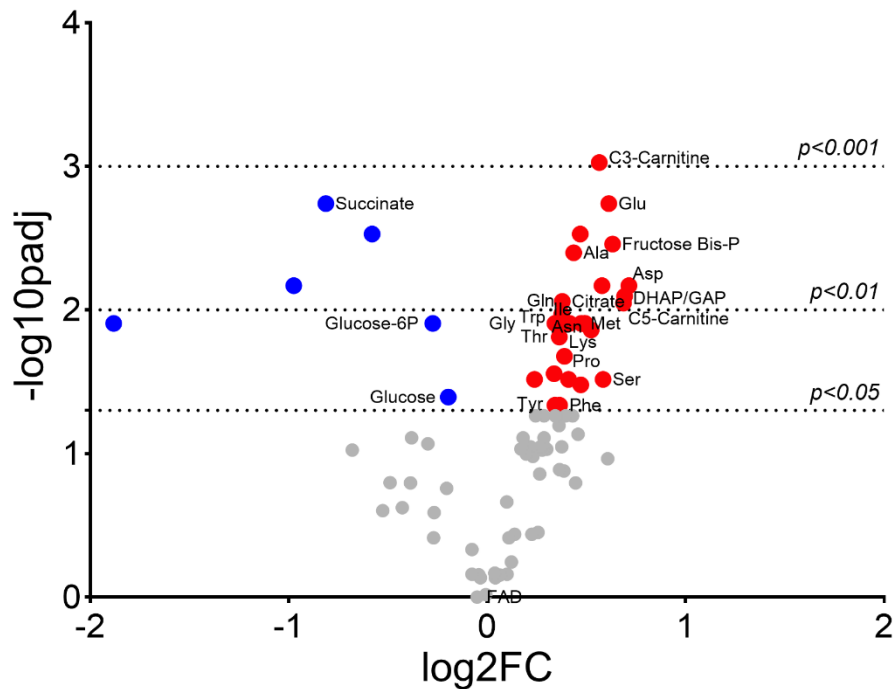


Figure 38. Volcano plot of metabolites detected by mass spectrometry in long- term CBE- treated and untreated dopaminergic neurons

In red are presented metabolites that increase after CBE treatment, in blue are presented those metabolites that decrease after CBE treatment, and in grey those metabolites that do not undergo significant changes. Significant changes are considered starting by adjusted p value (false discovery rate) < 0.05.

Focusing on the energetic metabolism of the cells, CBE- treated neurons showed reduced glucose uptake and conversion to glucose- 6- P which reflected on alterations in both the glycolysis and TCA cycle. In detail, in CBE- treated neurons glucose and glucose 6-P content was reduced of about 15 and 20 % respectively, while succinate content was halved. Citrate, isocitrate, and malate content was increased of about 30 %, which becomes 50 % in case of fructose 1,6- bisphosphate, and DHAP/ GAP ratio. Lactate content also increased upon CBE treatment of about 20 % with respect to the content present in untreated neurons (Figure 38, 39).

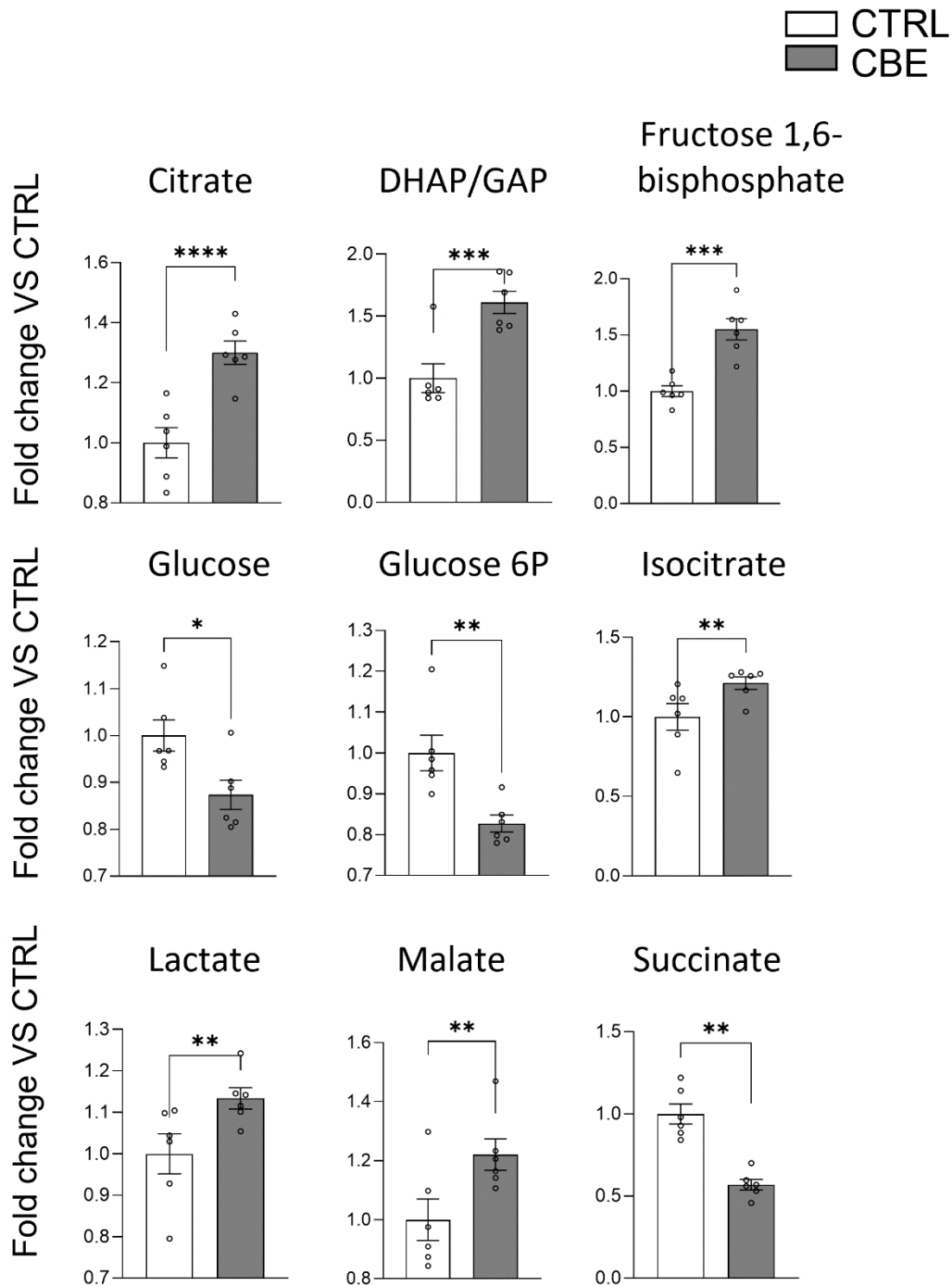


Figure 39. Effect of β -glucocerebrosidase inhibition on glucose metabolism

CBE-treatment induces an impairment in amino acids with respect to non-treated neurons. Data expressed as fold change of CBE-treated neurons (black) with respect to non-treated neurons (-white, CTRL. . (Glucose-6-P= glucose-6-phosphate; DHAP/G3P= dihydroxyacetone phosphate /glyceraldehyde-3-phosphate Data are expressed as fold change with respect to untreated cells (CTRL) and are the mean \pm SEM of at least three experiments (* $p < 0.05$; ** $p < 0.01$; *** $p < 0.001$, **** $p < 0.0001$; two- tail Student's t- test).

Further analysis concerning amino acid content, revealed that upon GCase inhibition there was an intracellular increment of several amino acids, including branched- chained ones. In particular, CBE-

treated neurons show an increased content of alanine, aspartate, glycine, glutamine, glutamate, methionine, serine, threonine, and tryptophan of about 40 % with respect to non- treated neurons. The content of arginine, asparagine, histidine, leucine, lysine, phenylalanine, proline, tyrosine, and valine increased of about 20 % in CBE- treated with respect to untreated DA neurons (Figure 38, 40).

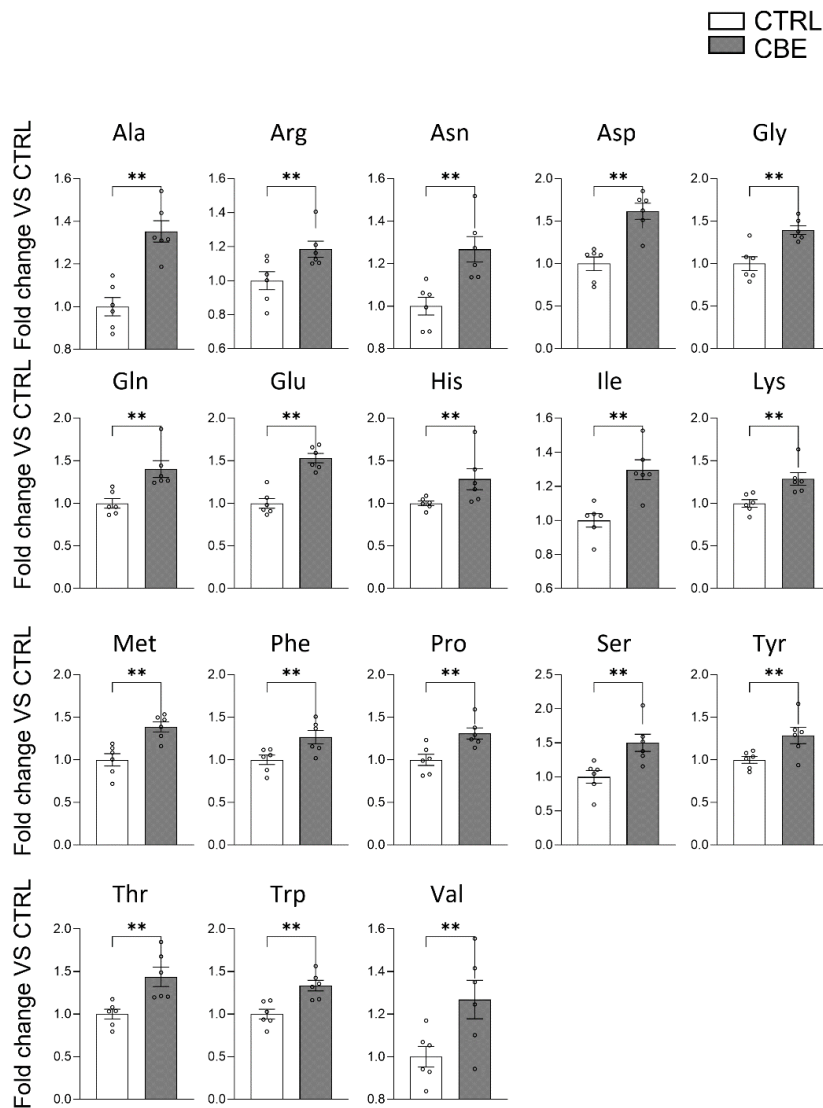


Figure 40. Effect of β -glucocerebrosidase inhibition on free aminoacids' content

CBE-treatment induces an impairment in amino acids with respect to untreated neurons. Data expressed as fold change of CBE- treated neurons (black) with respect to untreated neurons (white, CTRL). (Glucose- 6- P= glucose- 6- phosphate; DHAP/ G3P= dihydroxyacetone phosphate/ glyceraldehyde- 3- phosphate. Data are expressed as fold change with respect to untreated cells (CTRL) and are the mean \pm SEM of at least three experiments (* p <0.05; ** p <0.01; *** p <0.001, **** p <0.0001; two- tail Student's t- test).

In order to evaluate whether the observed metabolic changes had an effect on the cellular rate of ATP demand and production, the ATP content of long-term CBE treated DA neurons was quantified using the Agilent Seahorse XF Real-Time ATP Rate Assay. Through the serial injection of metabolic modulators, I was able to measure the total ATP production rate in living cells. The ATP production rate was not changed upon long-term CBE treatment nor did the amount of ATP produced from mitochondrial oxidative phosphorylation or glycolysis (Figure 41a) or the repartition of ATP production among mitochondria and glycolysis (Figure 41b).

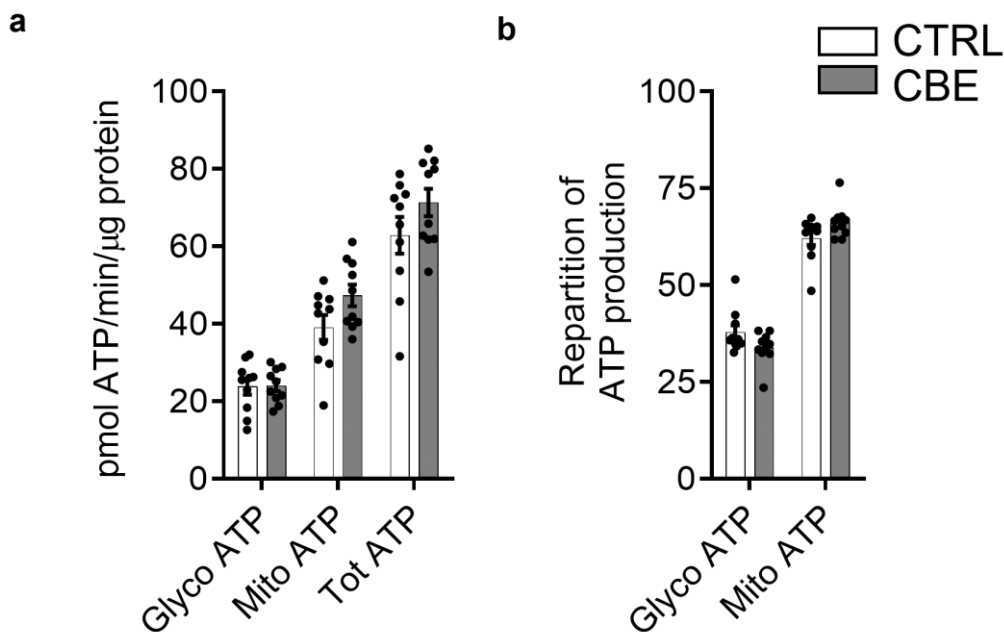


Figure 41. Effect of β - glucocerebrosidase inhibition on ATP production rate and repartition

Seahorse analysis of **a)** the total ATP production, the one derived from glycolysis or from mitochondria respiration and **b)** the ATP production repartition between mitochondria respiration and glycolysis. Data are the mean \pm SEM of at least three experiments (* $p < 0.05$; ** $p < 0.01$; *** $p < 0.001$, **** $p < 0.0001$; two-tail Student's t- test). expressed as pmols of ATP produced/ minute/ μ g of sample proteins.

Using Seahorse analyzer, I performed also Mito stress test assays and as shown in Figure 42 in untreated DA neurons the mean basal oxygen consumption rate (OCR) was 11,1 pmol/ min/ μ g proteins. Oligomycin reduced the OCR to about 21 % of basal rates, indicating that about 79 % of oxygen consumption of the cell was coupled to ATP synthesis while 21 % of basal respiration was coupled to proton leak. FCCP increases OCR to its maximum (21,09 pmol/ min/ μ g proteins) underlining that the spare respiratory capacity of untreated DA neurons is about 9,97 pmol/ min/

µg proteins. No significant alterations were observed upon long- term CBE treatment beside that the basal OCR tended to be about 12 % higher with respect to untreated DA neurons and they presented 17 % higher spare respiratory capacity (14,63 pmol/ min/ µg proteins). Indeed, respiration in CBE- treated DA neurons was near their theoretical maximal OCR (Figure 42).

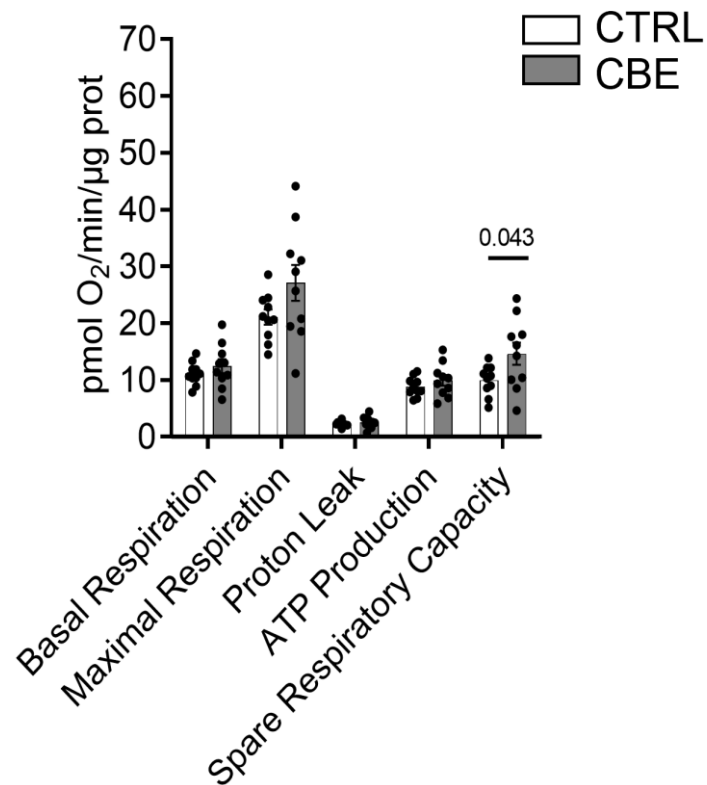


Figure 42. Effect of β-glucocerebrosidase inhibition on mitochondrial respiration

Oxygen consumption rate (OCR) of long-term CBE treated and untreated dopaminergic neurons was measured and expressed as pmols of O₂ consumed/ minutes/ cell protein content.

6. DISCUSSION

Mutations in *GBA1* gene are causative for many neurodegenerative disorders^{84,119–122}. Nevertheless, the role of mutated *GBA1* in pathogenesis is still under debate. Increasing evidence supports GCase deficiency and the impairment of GlcCer metabolism as the basis of neurodegeneration⁸⁶. The fact that several patients affected by GD develop in late stages also parkinsonism and *vice versa* PD patients manifest typical features of GD, strengthens the correlation between *GBA1* mutations and degeneration of neuronal cells.

Neurons are post- mitotic cells characterized by a dynamic membrane architecture, which allows modulation of the synapse interconnection or excitability in response to the different stimuli. The plasticity of the geometry of the neuronal membrane could be considered as a continuum of positive and negative curvatures, branching of neurites, axonal elongation, and synapse formation. All these modifications are basically due to two different actors: the cytoskeleton proteins and the membrane lipids. The human brain and specifically neurons, are particularly enriched in SLs, amphipathic molecules composed by a lipophilic backbone and a hydrophilic head group of different origin that protrudes in the extracellular milieu. During CNS development SLs undergo both quantitative and qualitative modifications. Particularly present at brain level are the gangliosides, a family of GSLs carrying in the hydrophilic head one or more residues of sialic acid. Interestingly, during the neuronal development the ganglioside content increases of 10- fold. In the neural progenitors the ganglioside pattern is composed mainly by the simple gangliosides such as GM3 and GD3 which are converted into complex gangliosides GM1, GD1a, GD1b, and GT1b along the neuronal differentiation to fulfill diverse functions. For instance, GM1 ganglioside stabilizes TrkA- NGF complex and directly activates TrkA- MAPK pathway inducing neuritogenesis and conferring neuroprotection¹²³. GM1, GD1a, and GT1b are activators of the Ca²⁺/ Calmodulin-dependent protein kinase II, which is relevant for neuronal development but also for long- term memory formation and neuronal plasticity^{124,125}. GD1b has been demonstrated to reduce apoptosis suppressing caspase- 3 activity¹²⁶.

Based on these considerations related to the close connection between ganglioside pattern and neuronal function and plasticity, it is expected that each neuronal family is characterized by a peculiar lipid pattern. Up to date, in literature it is reported about lipid pattern of the brain *in toto* while the information related to the single brain areas is scant.

For this reason, as part of my PhD project, I took care of the lipid characterization of several different brain areas derived from a patient affected by *GBA*- PD, carrying a monoallelic mutation in *GBA1*

gene, and compared them to those of healthy subjects. In particular, the analyzed brain areas were the frontal and parietal cortex, the *substantia nigra*, the *cerebellum*, and the *hippocampus*.

In the areas derived from a *GBA*- PD patient, GCCase activity is decreased more than to the expected 50 % residual activity in the parietal cortex, *substantia nigra*, and the *hippocampus*.

In addition, *GBA*- PD areas show a possible impairment of the endolysosomal compartment as demonstrated by the decreased activity of α - and β - mannosidase and to some extent also of the other main glycohydrolytic enzymes.

Surprisingly, by the analyses of the lipid profile I found an accumulation of GlcCer only in the *cerebellum*. GlcCer reduction, despite the reduced GCCase activity, could be attributed to the slightly increased activity of NLGase found in the frontal cortex and *substantia nigra* suggesting a sort of compensatory mechanism to counteract the GCCase deficiency.

Indeed, looking at the overall NLGase activity in brain areas derived from the *GBA*- PD patient, I observed that the entity of activity is higher in all areas with respect to GCCase (Figure 10). Interestingly, the increased activity of NLGase was also observed in several lines of human fibroblasts derived from patients affected by the different forms of GD⁴² and also in the brain and leucocytes derived from a GD mouse model¹²⁷.

For what concerns the ganglioside pattern composition, I found that in the *cerebellum* and frontal cortex *GBA*- PD areas, there is a general increase of the ganglioside content, except for GM1. GM1 increases in the *substantia nigra* and the *hippocampus* of about 1.4- folds with respect to healthy subjects, whereas in the frontal cortex and *cerebellum* I observed a 0.5- fold decrease in its content and the parietal cortex shows a 1.6- folds decrease. Obviously, the parietal and frontal cortices give a much more massive contribution to the whole brain GM1 content with respect to the *substantia nigra* or the *hippocampus*, resulting in a loss of the greatest amount of GM1 ganglioside when PD brain is analysed *in toto*¹²⁸

A typical feature of aging, which is anticipated in neurodegenerative diseases such as PD, is demyelination. Generally, a shrinkage of the white matter is observed in PD patients¹²⁹. Considering sulfatides and LacCer content (Figure 11) of the different analysed areas, it is remarkable how it is reduced in the PD areas with exception for the *cerebellum*, and with a particular entity in the frontal cortex, sustaining the possible demyelination of these areas.

Taken together these results allow to describe a phenotypical characterization of *GBA*- PD brain areas nevertheless, they don't allow to understand the molecular mechanisms relating the decrease in GCCase activity with the onset of neurodegeneration.

The consequences of GCase deficiency were initially studied on primary fibroblast cultures derived from GD or PD patients skin biopsies, but since they don't store GlcCer they are not considered a correct model of the disease. The main problem of studying the link between GlcCer accumulation and neuronal damage is the lack of suitable *in vitro* or *in vivo* models. Studies on *post-mortem* human brains derived from GD patients are limited by their low availability and do not allow to perform analyses on the involved molecular mechanisms. Moreover, *GBA1* knock-out mice with complete enzyme deficiency die within 24 hours after birth, while single-allele knockout mice do not show nigrostriatal degeneration or PD-like features. Another possibility is the use of immortalized cells, but they carry intrinsic artefacts, undergoing continuous mutations during the different passages in culture, presenting an unstable genotype and consequently a variable phenotype. In addition, patient-derived iPSCs do not display a sufficient accumulation of GlcCer and are influenced by the donor patient's genotype. Indeed, the development of a suitable *in vitro* model for the study of GD and *GBA*-PD represents one of the main challenges for the scientific community. Today, mostly used neuronal cell models include neuroblastoma cell lines and primary rodent neurons, such as cerebellar granule neurons, hippocampal, and cortical neurons. GCase alterations are mimicked by pharmacological inhibition of the enzyme by conduritol B epoxide (CBE) administration, siRNA transfection or overexpression of plasmids encoding mutant GCase proteins^{86,130}.

As PhD project I took care of the development of new *in vitro* models able to recapitulate, in an acceptable timeframe, the phenotype of neurons affected by GCase deficiency. In particular, I exploited two different neuron cultures: one represented by CGNs derived from WT C57BL/6 mice pups and the other represented by human DA neurons differentiated starting from iPSCs. The advent of iPSCs technology, discovered by Yamanaka and Takahashi in 2006¹³¹, and thus the possibility to derive stem cells from completely differentiated cells has revolutionized the field of the research in neurodegenerative diseases¹⁰⁹. Indeed, neurons derived from iPSCs represent the only way to obtain human neurons characterized by the same genetic background of the patients. Both models were treated with CBE to suppress GCase activity¹³². The choice of using two neuronal populations derived from different species helped me in understanding that the effect of GCase inhibition on neuronal homeostasis is shared by neurons with unlike activity and origin and that it is conserved among species.

The neurons treated with CBE showed a time-dependent accumulation of GlcCer that is associated with the impairment of the endolysosomal compartment and the onset of neurodegeneration.

Long- term GCase inhibition is necessary to induce a sufficient GlcCer accumulation to cause neurodegeneration, which suggests the presence of a tolerance threshold to cell toxicity. In GD patients the GlcCer accumulation at lysosomal level causes also the aberrant production of GlcSph through GlcCer degradation by the acid ceramidase¹³³. GlcSph has peculiar detergent- like properties which let hypothesize about its role in the onset of neurodegeneration¹¹¹. I confirmed the absence of a toxic effect of GlcSph in our *in vitro* models even if administered at high concentrations.

I observed that our models beside accumulating GlcCer present also storage of secondary uncatabolized complex SLs, such as gangliosides, which is a characteristic described in LSDs and caused by the impairment of the catabolic activity of the endolysosomal compartment^{134,135}.

Thanks to the activation of compensatory mechanisms, which include the nuclear translocation of the transcription factor EB, responsible for the promotion of lysosomal biogenesis and exocytosis, cells try to counteract the lysosomal impairment. These two events help reducing the accumulated material and restore the correct lysosomal function^{41,112}. I have demonstrated that the accumulation of uncatabolized material induces the promotion of lysosomal exocytosis, a process by which lysosomes fuse with the PM and release their content in the extracellular milieu. This is a usual feature of cells belonging to organs with an intense vascularization or to a parenchyma that can recycle or store the released material, but for sure it is not a peculiar feature of neurons. Indeed, in the brain of patients the release of material by affected neurons could be not correctly absorbed by the endothelial cells and could activate surrounding microglia and astrocytes, activating inflammatory processes and inducing the self- propagation of the disease to other brain areas¹³⁶.

In our model of GCase- deficient neurons the aberrant lysosomal exocytosis is also responsible for changes in the PM structure. Indeed, I found that GlcCer accumulation is not only confined to lysosomes. In particular, I demonstrated for the first time in my knowledge that the GlcCer accumulation is not just at lysosomal level but that it occurs also on the PM (Figure 35a) opening a new scenario for the study of the etiopathology of GD and possibly also for the *GBA*- PD. GSLs are particularly abundant in membrane portions called “DRM” often defined also “lipid rafts”^{137–139}. These fractions of the PM are essential structures for signalling events, for the regulation of extracellular stimuli, and for the modulation of signal transduction^{31,140}. Alterations in the DRM have been previously described in organs of GD animal models and in *in vitro* models of GD represented by immortalized cell lines^{134,141}, but no data is available on the effect of GCase deficiency in DRM of neurons. Therefore, I analysed PM- DRM of long- term CBE-treated and untreated DA neurons, and

I discovered the accumulation of GlcCer. DRM are characterized by the spontaneous segregation of SLs, which are enriched at the expense of glycerophospholipids. Therefore, the GlcCer inserted in the PM, is mainly localized in DRM and could explain the variable GlcCer enrichment observed analysing the entire PM or just PM- DRM.

DRM are important in maintaining cell homeostasis and alterations can be associated with alterations in the cell phenotype and function^{118,142}. I showed that the accumulation of GlcCer occurs in the PM- DRM of CBE-treated neurons, altering DRM protein composition. In detail, accumulation of GlcCer is associated with a local hyperactivation of the non- receptor tyrosine kinase c- Src, which is involved in many intracellular signalling pathways important for the neuronal homeostasis^{143,144}. In fact, in physiological conditions the activation of c- Src makes it translocate outside the DRM, where it can exert its functions. The enrichment in ceramide in DRM is a factor promoting this translocation^{145,146}, but in CBE- treated neurons, the accumulation of GlcCer reduces the amount of available ceramide causing the sequestration of c- Src inside PM- DRM and inhibiting its functioning. I need to better investigate this aspect, but it could be a possible future therapeutic target.

Another hot topic for what concerns the definition of new therapeutic strategies in neurodegenerative disorders is represented by the modulation of metabolism. In particular, neurons account for about 90 % of the energetic metabolism of the brain. Considering that lysosomes are central organelles for cell metabolic pathways due to their involvement in the degradation and recycling of substrates, I investigated whether the long- term treatment with CBE and the following impairment of the endolysosomal compartment could have consequences on the overall neuronal metabolism. As previously demonstrated neuronal and in particular iPSC- derived DA neurons' energetic metabolism relies mainly on glucose rather than on the oxidation of other macromolecules but in case of need, neurons can use also other substrates¹⁴⁷. This is of particular value in *in vitro* experiments where neurons cannot draw substrates from the blood and need therefore to take care by themselves of the high energetic demands.

Even if the oxidative phosphorylation pathway of glucose produces about 30– 32 molecules of ATP, and the anaerobic oxidation of glucose to lactate produces just 2 ATP molecules, the anaerobic glycolysis is particularly sustained in DA neurons *in vitro* models. I also discovered that the metabolic profile of long- term CBE- treated DA neurons is significantly distinct from the one of untreated cells. The chronic treatment with CBE seems to increase the ability of the cells to respond to energetic demands as if they had adapted to the stressor CBE. In fact, CBE- treated neurons have the ability to exploit variable substrates for energy production rather than just glucose which renders them

more adaptable to changes. It is interesting to notice, that even if neurons show the ability to increase respiration for energy production, any change can be observed in the amount of produced ATP, neither ATP derived from the anaerobic glycolysis, nor ATP derived from the oxidative phosphorylation.

Overall, the data I've presented so far, indicate a direct role of GlcCer accumulation in the onset of neuronal damage. Beside the impairment of the endolysosomal compartment, the developed models present GlcCer accumulation also in PM- DRM, strengthening the existence of a pathogenic lysosome- PM crosstalk, and alterations in cell energetic metabolism which could contribute to the neurodegenerative phenotype (Figure 43).

This work defines two reliable neuronal models to study the impact of GCase deficiency in neurons and opens a new scenario for the study of GCase- related neurodegenerative disorders.

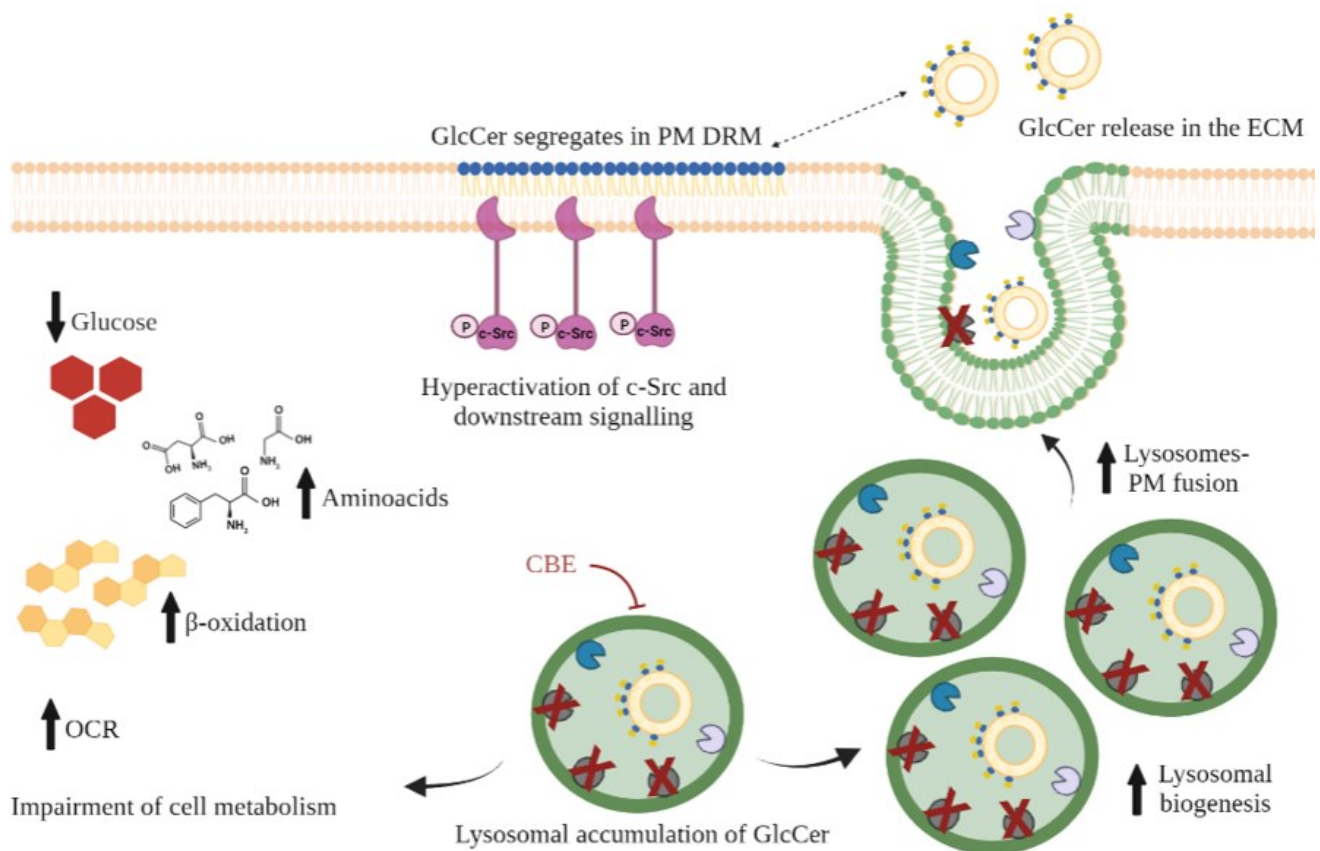


Figure 43. Schematic representation of the events occurring upon long- term conduritol b epoxide treatment (CBE= conduritol b epoxide; GlcCer= glucosylceramide; PM= plasma membrane; ECM= extracellular matrix; DRM= detergent- resistant membrane portions; OCR= oxygen consumption rate)

7. BIBLIOGRAPHY

1. Kim, H. Y., Huang, B. X. & Spector, A. A. Phosphatidylserine in the brain: metabolism and function. *Prog. Lipid Res.* **56**, 1–18 (2014).
2. Vance, J. E. Phospholipid Synthesis and Transport in Mammalian Cells. *Traffic* **16**, 1–18 (2015).
3. El-Sayyad, H. I. H. Cholesterol overload impairing cerebellar function: The promise of natural products. *Nutrition* **31**, 621–630 (2015).
4. Parasassi, T. *et al.* Cholesterol protects the phospholipid bilayer from oxidative damage. *Free Radic. Biol. Med.* **19**, 511–516 (1995).
5. Svennerholm, L., Boström, K., Jungbjer, B. & Olsson, L. Membrane lipids of adult human brain: lipid composition of frontal and temporal lobe in subjects of age 20 to 100 years. *J. Neurochem.* **63**, 1802–1811 (1994).
6. Saher, G. & Stumpf, S. K. Cholesterol in myelin biogenesis and hypomyelinating disorders. *Biochim. Biophys. Acta* **1851**, 1083–1094 (2015).
7. Astudillo, L. *et al.* Glucosylceramidases and malignancies in mammals. *Biochimie* **125**, 267–280 (2016).
8. SVENNERHOLM, L. THE GANGLIOSIDES. *J. Lipid Res.* **5**, 145–155 (1964).
9. Hakomori, S. Glycosphingolipids in cellular interaction, differentiation, and oncogenesis. *Annu. Rev. Biochem.* **50**, 733–764 (1981).
10. Suchański, J. & Ugorski, M. [The biological role of sulfatides]. *Postepy Hig. Med. Dosw. (Online)* **70**, 489–504 (2016).
11. Stoffel, W. Studies on the biosynthesis and degradation of sphingosine bases. *Chem. Phys. Lipids* **5**, 139–158 (1970).
12. Sribney, M. Enzymatic synthesis of ceramide. *Biochim. Biophys. Acta (BBA)/Lipids Lipid Metab.* **125**, 542–547 (1966).
13. Merrill, A. H. Cell regulation by sphingosine and more complex sphingolipids. *J. Bioenerg. Biomembr.* **23**, 83–104 (1991).
14. Rother, J., Echten, G. van, Schwarzmann, G. & Sandhoff, K. Biosynthesis of sphingolipids: dihydroceramide and not sphinganine is desaturated by cultured cells. *Biochem. Biophys. Res. Commun.* **189**, 14–20 (1992).
15. Singh, I. & Kishimoto, Y. Ceramide synthesis in rat brain: characterization of the synthesis requiring pyridine nucleotide. *Arch. Biochem. Biophys.* **202**, 93–100 (1980).
16. Tettamanti, G., Bassi, R., Viani, P. & Riboni, L. Salvage pathways in glycosphingolipid metabolism. *Biochimie* **85**, 423–437 (2003).
17. Rodriguez-Cuenca, S., Barbarroja, N. & Vidal-Puig, A. Dihydroceramide desaturase 1, the gatekeeper of ceramide induced lipotoxicity. *Biochim. Biophys. Acta* **1851**, 40–50 (2015).
18. Perry, R. J. & Ridgway, N. D. Molecular mechanisms and regulation of ceramide transport. *Biochimica et Biophysica Acta - Molecular and Cell Biology of Lipids* vol. 1734 220–234 (2005).

19. Lannert, H., Gorgas, K., Meißner, I., Wieland, F. T. & Jeckel, D. Functional organization of the Golgi apparatus in glycosphingolipid biosynthesis. Lactosylceramide and subsequent glycosphingolipids are formed in the lumen of the late Golgi. *J. Biol. Chem.* **273**, 2939–2946 (1998).
20. Merrill, A. H. Sphingolipid and glycosphingolipid metabolic pathways in the era of sphingolipidomics. *Chemical Reviews* vol. 111 6387–6422 (2011).
21. Sundberg, E. L., Deng, Y. & Burd, C. G. Monitoring Sphingolipid Trafficking in Cells using Fluorescence Microscopy. *Curr. Protoc. cell Biol.* **82**, (2019).
22. Kolter, T., Doering, T., Wilkening, G., Werth, N. & Sandhoff, K. Recent advances in the biochemistry of glycosphingolipid metabolism. *Biochem. Soc. Trans.* **27**, 409–415 (1999).
23. Kolter, T. & Sandhoff, K. Principles of lysosomal membrane digestion: stimulation of sphingolipid degradation by sphingolipid activator proteins and anionic lysosomal lipids. *Annu. Rev. Cell Dev. Biol.* **21**, 81–103 (2005).
24. Inui, K. *et al.* The gene coding for a sphingolipid activator protein, SAP-1, is on human chromosome 10. *Hum. Genet.* **69**, 197–200 (1985).
25. Li, Y. T. & Li, S. C. Enzymatic hydrolysis of glycosphingolipids. *Anal. Biochem.* **273**, 1–11 (1999).
26. Yamamoto, Y. *et al.* Isolation, characterization, and mapping of a human acid beta-galactosidase cDNA. *DNA Cell Biol.* **9**, 119–127 (1990).
27. D’Azzo, A., Hoogeveen, A., Reuser, A. J., Robinson, D. & Galjaard, H. Molecular defect in combined beta-galactosidase and neuraminidase deficiency in man. *Proc. Natl. Acad. Sci. U. S. A.* **79**, 4535–4539 (1982).
28. Nanba, E., Tsuji, A., Omura, K. & Suzuki, Y. GM1-gangliosidosis: abnormalities in biosynthesis and early processing of beta-galactosidase in fibroblasts. *Biochem. Biophys. Res. Commun.* **152**, 794–800 (1988).
29. Morreau, H. *et al.* Human lysosomal protective protein. Glycosylation, intracellular transport, and association with beta-galactosidase in the endoplasmic reticulum. *J. Biol. Chem.* **267**, 17949–17956 (1992).
30. Severino, J., Allen, R. G., Balin, S., Balin, A. & Cristofalo, V. J. Is beta-galactosidase staining a marker of senescence in vitro and in vivo? *Exp. Cell Res.* **257**, 162–171 (2000).
31. Aureli, M. *et al.* Activity of plasma membrane beta-galactosidase and beta-glucosidase. *FEBS Lett.* **583**, 2469–2473 (2009).
32. Aureli, M., Loberto, N., Chigorno, V., Prinetti, A. & Sonnino, S. Remodeling of sphingolipids by plasma membrane associated enzymes. *Neurochem. Res.* **36**, 1636–1644 (2011).
33. Valaperta, R. *et al.* Plasma membrane production of ceramide from ganglioside GM3 in human fibroblasts. *FASEB J.* **20**, 1227–1229 (2006).
34. Aureli, M. *et al.* Cell surface sphingolipid glycohydrolases in neuronal differentiation and aging in culture. *J. Neurochem.* **116**, 891–899 (2011).
35. Coates, P. J. Markers of senescence? *J. Pathol.* **196**, 371–373 (2002).

36. Dimri, G. P. *et al.* A biomarker that identifies senescent human cells in culture and in aging skin in vivo. *Proc. Natl. Acad. Sci. U. S. A.* **92**, 9363–9367 (1995).
37. Triggs-Raine, B., Mahuran, D. J. & Gravel, R. A. Naturally occurring mutations in GM2 gangliosidosis: a compendium. *Adv. Genet.* **44**, 199–224 (2001).
38. Bearpark, T. M. & Stirling, J. L. A difference in the specificities of human liver N-acetyl-beta-hexosaminidases A and B detected by their activities towards glycosaminoglycan oligosaccharides. *Biochem. J.* **173**, 997–1000 (1978).
39. Mencarelli, S. *et al.* Identification of plasma membrane associated mature beta-hexosaminidase A, active towards GM2 ganglioside, in human fibroblasts. *FEBS Lett.* **579**, 5501–5506 (2005).
40. Reddy, A., Caler, E. V. & Andrews, N. W. Plasma membrane repair is mediated by Ca(2+)-regulated exocytosis of lysosomes. *Cell* **106**, 157–169 (2001).
41. Samarani, M. *et al.* A lysosome–plasma membrane–sphingolipid axis linking lysosomal storage to cell growth arrest. *FASEB J.* **32**, 5685–5702 (2018).
42. Aureli, M. *et al.* Cell surface associated glycohydrolases in normal and Gaucher disease fibroblasts. *J. Inherit. Metab. Dis.* **35**, 1081–1091 (2012).
43. Kawecki, C. *et al.* Identification of CD36 as a new interaction partner of membrane NEU1: potential implication in the pro-atherogenic effects of the elastin receptor complex. *Cell. Mol. Life Sci.* **76**, 791–807 (2019).
44. Glanz, V. Y., Myasoedova, V. A., Grechko, A. V. & Orekhov, A. N. Sialidase activity in human pathologies. *Eur. J. Pharmacol.* **842**, 345–350 (2019).
45. Miyagi, T., Wada, T. & Yamaguchi, K. Roles of plasma membrane-associated sialidase NEU3 in human cancers. *Biochim. Biophys. Acta* **1780**, 532–537 (2008).
46. Kopitz, J., Von Reitzenstein, C., Mühl, C. & Cantz, M. Role of plasma membrane ganglioside sialidase of human neuroblastoma cells in growth control and differentiation. *Biochem. Biophys. Res. Commun.* **199**, 1188–1193 (1994).
47. Monti, E., Preti, A., Venerando, B. & Borsani, G. Recent development in mammalian sialidase molecular biology. *Neurochem. Res.* **27**, 649–663 (2002).
48. Miyagi, T., Wada, T., Yamaguchi, K., Hata, K. & Shiozaki, K. Plasma membrane-associated sialidase as a crucial regulator of transmembrane signalling. *J. Biochem.* **144**, 279–285 (2008).
49. Ueno, S. *et al.* Plasma membrane-associated sialidase is up-regulated in renal cell carcinoma and promotes interleukin-6-induced apoptosis suppression and cell motility. *J. Biol. Chem.* **281**, 7756–7764 (2006).
50. Valaperta, R. *et al.* Induction of axonal differentiation by silencing plasma membrane-associated sialidase Neu3 in neuroblastoma cells. *J. Neurochem.* **100**, 708–719 (2007).
51. Proshin, S., Yamaguchi, K., Wada, T. & Miyagi, T. Modulation of neuritogenesis by ganglioside-specific sialidase (Neu 3) in human neuroblastoma NB-1 cells. *Neurochem. Res.* **27**, 841–846 (2002).

52. Von Reitzenstein, C., Kopitz, J., Schuhmann, V. & Cantz, M. Differential functional relevance of a plasma membrane ganglioside sialidase in cholinergic and adrenergic neuroblastoma cell lines. *Eur. J. Biochem.* **268**, 326–333 (2001).
53. Rodriguez, J. A., Piddini, E., Hasegawa, T., Miyagi, T. & Dotti, C. G. Plasma membrane ganglioside sialidase regulates axonal growth and regeneration in hippocampal neurons in culture. *J. Neurosci.* **21**, 8387–8395 (2001).
54. Kalka, D., Von Reitzenstein, C., Kopitz, J. & Cantz, M. The plasma membrane ganglioside sialidase cofractionates with markers of lipid rafts. *Biochem. Biophys. Res. Commun.* **283**, 989–993 (2001).
55. Papini, N. *et al.* The plasma membrane-associated sialidase MmNEU3 modifies the ganglioside pattern of adjacent cells supporting its involvement in cell-to-cell interactions. *J. Biol. Chem.* **279**, 16989–16995 (2004).
56. van Weely, S., Brandsma, M., Strijland, A., Tager, J. M. & Aerts, J. M. F. G. Demonstration of the existence of a second, non-lysosomal glucocerebrosidase that is not deficient in Gaucher disease. *Biochim. Biophys. Acta* **1181**, 55–62 (1993).
57. Körschen, H. G. *et al.* The non-lysosomal β -glucosidase GBA2 is a non-integral membrane-associated protein at the endoplasmic reticulum (ER) and Golgi. *J. Biol. Chem.* **288**, 3381–3393 (2013).
58. Henrissat, B. *et al.* Conserved catalytic machinery and the prediction of a common fold for several families of glycosyl hydrolases. *Proc. Natl. Acad. Sci. U. S. A.* **92**, 7090–7094 (1995).
59. Yildiz, Y. *et al.* Mutation of beta-glucosidase 2 causes glycolipid storage disease and impaired male fertility. *J. Clin. Invest.* **116**, 2985–2994 (2006).
60. Matern, H., Boermans, H., Lottspeich, F. & Matern, S. Molecular cloning and expression of human bile acid beta-glucosidase. *J. Biol. Chem.* **276**, 37929–37933 (2001).
61. Walden, C. M. *et al.* Accumulation of glucosylceramide in murine testis, caused by inhibition of beta-glucosidase 2: implications for spermatogenesis. *J. Biol. Chem.* **282**, 32655–32664 (2007).
62. Hammer, M. B. *et al.* Mutations in GBA2 cause autosomal-recessive cerebellar ataxia with spasticity. *Am. J. Hum. Genet.* **92**, 245–251 (2013).
63. Martin, E. *et al.* Loss of function of glucocerebrosidase GBA2 is responsible for motor neuron defects in hereditary spastic paraplegia. *Am. J. Hum. Genet.* **92**, 238–244 (2013).
64. Beccari, T., Stinchi, S. & Orlacchio, a. Lysosomal alpha-D-mannosidase. *Biosci. Rep.* **19**, 157–62 (1999).
65. Percheron, F., Foglietti, M. J., Bernard, M. & Ricard, B. Mammalian beta-D-mannosidase and beta-mannosidosis. *Biochimie* **74**, 5–11 (1992).
66. Liang, Y. J. *et al.* Changes in glycosphingolipid composition during differentiation of human embryonic stem cells to ectodermal or endodermal lineages. *Stem Cells* **29**, 1995–2004 (2011).
67. Jennemann, R. *et al.* Cell-specific deletion of glucosylceramide synthase in brain leads to severe neural defects after birth. *Proc. Natl. Acad. Sci. U. S. A.* **102**, 12459–12464 (2005).

68. Yu, R. K., Macala, L. J., Taki, T., Weinfeld, H. M. & Yu, F. S. Developmental Changes in Ganglioside Composition and Synthesis in Embryonic Rat Brain. *J. Neurochem.* **50**, 1825–1829 (1988).
69. Palmano, K., Rowan, A., Guillermo, R., Guan, J. & McJarrow, P. The role of gangliosides in neurodevelopment. *Nutrients* **7**, 3891–3913 (2015).
70. Yu, R. K., Nakatani, Y. & Yanagisawa, M. The role of glycosphingolipid metabolism in the developing brain. *J. Lipid Res.* **50 Suppl**, (2009).
71. Ngamukote, S., Yanagisawa, M., Ariga, T., Ando, S. & Yu, R. K. Developmental changes of glycosphingolipids and expression of glycogenes in mouse brains. *J. Neurochem.* **103**, 2327–2341 (2007).
72. Svennerholm, L., Boström, K., Jungbjer, B. & Olsson, L. Membrane Lipids of Adult Human Brain: Lipid Composition of Frontal and Temporal Lobe in Subjects of Age 20 to 100 Years. *J. Neurochem.* **63**, 1802–1811 (2002).
73. Barrier, L. *et al.* Genotype-related changes of ganglioside composition in brain regions of transgenic mouse models of Alzheimer's disease. *Neurobiol. Aging* **28**, 1863–1872 (2007).
74. Pfeiffer, S. E., Warrington, A. E. & Bansal, R. The oligodendrocyte and its many cellular processes. *Trends Cell Biol.* **3**, 191–197 (1993).
75. Jiang, P. *et al.* The HOPS complex mediates autophagosome-lysosome fusion through interaction with syntaxin 17. *Mol. Biol. Cell* **25**, 1327–1337 (2014).
76. Peng, C. *et al.* Vps18 deficiency inhibits dendritogenesis in Purkinje cells by blocking the lysosomal degradation of Lysyl Oxidase. *Biochem. Biophys. Res. Commun.* **423**, 715–720 (2012).
77. Sidransky, E. & Lopez, G. The link between the GBA gene and parkinsonism. *Lancet Neurol.* **11**, 986–998 (2012).
78. Sidransky, E. Gaucher disease and parkinsonism. *Molecular Genetics and Metabolism* vol. 84 302–304 (2005).
79. Weinreb, N. J. *et al.* Effectiveness of enzyme replacement therapy in 1028 patients with type 1 Gaucher disease after 2 to 5 years of treatment: A report from the Gaucher Registry. *Am. J. Med.* **113**, 112–119 (2002).
80. Cox, T. *et al.* Novel oral treatment of Gaucher's disease with N-butyldeoxynojirimycin (OGT 918) to decrease substrate biosynthesis. *Lancet (London, England)* **355**, 1481–1485 (2000).
81. Futerman, A. H., Sussman, J. L., Horowitz, M., Silman, I. & Zimran, A. New directions in the treatment of Gaucher disease. *Trends Pharmacol. Sci.* **25**, 147–151 (2004).
82. Lesage, S. & Brice, A. Parkinson's disease: from monogenic forms to genetic susceptibility factors. *Hum. Mol. Genet.* **18**, (2009).
83. Westbroek, W., Gustafson, A. M. & Sidransky, E. Exploring the link between glucocerebrosidase mutations and parkinsonism. *Trends Mol. Med.* **17**, 485–493 (2011).
84. Sidransky, E. *et al.* Multicenter analysis of glucocerebrosidase mutations in Parkinson's disease. *N. Engl. J. Med.* **361**, 1651–1661 (2009).

85. Gegg, M. E. *et al.* Glucocerebrosidase deficiency in substantia nigra of parkinson disease brains. *Ann. Neurol.* **72**, 455–463 (2012).
86. Mazzulli, J. R. *et al.* Gaucher disease glucocerebrosidase and α -synuclein form a bidirectional pathogenic loop in synucleinopathies. *Cell* **146**, 37–52 (2011).
87. Zhang, P., Xia, N. & Reijo Pera, R. A. Directed dopaminergic neuron differentiation from human pluripotent stem cells. *J. Vis. Exp.* 1–8 (2014) doi:10.3791/51737.
88. Lancaster, M. A. *et al.* Cerebral organoids model human brain development and microcephaly. *Nature* **501**, 373–379 (2013).
89. Howarth, C., Gleeson, P. & Attwell, D. Updated energy budgets for neural computation in the neocortex and cerebellum. *J. Cereb. Blood Flow Metab.* **32**, 1222–1232 (2012).
90. Jensen, N. J., Wodschow, H. Z., Nilsson, M. & Rungby, J. Effects of Ketone Bodies on Brain Metabolism and Function in Neurodegenerative Diseases. *Int. J. Mol. Sci.* **21**, 1–17 (2020).
91. Barros, L. F. *et al.* Aerobic Glycolysis in the Brain: Warburg and Crabtree Contra Pasteur. *Neurochem. Res.* **46**, 15–22 (2021).
92. HYDEN, H. & LANGE, P. W. A kinetic study of the neuronglia relationship. *J. Cell Biol.* **13**, 233–237 (1962).
93. HAMBERGER, A. & HYDEN, H. Inverse enzymatic changes in neurons and glia during increased function and hypoxia. *J. Cell Biol.* **16**, 521–525 (1963).
94. Camandola, S. & Mattson, M. P. Brain metabolism in health, aging, and neurodegeneration. *EMBO J.* **36**, 1474–1492 (2017).
95. Mergenthaler, P., Lindauer, U., Dienel, G. A. & Meisel, A. Sugar for the brain: the role of glucose in physiological and pathological brain function. *Trends Neurosci.* **36**, 587 (2013).
96. Lunghi, G. *et al.* β -Glucocerebrosidase Deficiency Activates an Aberrant Lysosome-Plasma Membrane Axis Responsible for the Onset of Neurodegeneration. *Cells* **11**, (2022).
97. Zhang, P., Xia, N. & Reijo Pera, R. A. Directed dopaminergic neuron differentiation from human pluripotent stem cells. *J. Vis. Exp.* (2014).
98. Di Biase, E. *et al.* Gangliosides in the differentiation process of primary neurons: the specific role of GM1-oligosaccharide. *Glycoconj. J.* 329–343 (2020).
99. Pang, Z. *et al.* MetaboAnalyst 5.0: narrowing the gap between raw spectra and functional insights. *Nucleic Acids Res.* **49**, W388–W396 (2021).
100. Settembre, C. & Medina, D. L. TFEB and the CLEAR network. *Methods Cell Biol.* **126**, 45–62 (2015).
101. FOLCH, J., LEES, M. & SLOANE STANLEY, G. H. A simple method for the isolation and purification of total lipides from animal tissues. *J. Biol. Chem.* **226**, 497–509 (1957).
102. Li, Y. T. *et al.* Selective extraction and effective separation of galactosylsphingosine (psychosine) and glucosylsphingosine from other glycosphingolipids in pathological tissue samples. *Neurochem. Res.* **36**, 1612–1622 (2011).
103. Shaner, R. L. *et al.* Quantitative analysis of sphingolipids for lipidomics using triple

- quadrupole and quadrupole linear ion trap mass spectrometers. *J. Lipid Res.* **50**, 1692–1707 (2009).
104. Svennerholm, L. Quantitative estimation of sialic acids. II. A colorimetric resorcinol-hydrochloric acid method. *Biochim. Biophys. Acta* **24**, 604–611 (1957).
 105. Lunghi, G. *et al.* Modulation of calcium signaling depends on the oligosaccharide of GM1 in Neuro2a mouse neuroblastoma cells. *Glycoconj. J.* **37**, 713–727 (2020).
 106. Ghaffari, M. H. *et al.* Metabolomics meets machine learning: Longitudinal metabolite profiling in serum of normal versus overconditioned cows and pathway analysis. *J. Dairy Sci.* (2019).
 107. Durbin, B. P., Hardin, J. S., Hawkins, D. M. & Rocke, D. M. A variance-stabilizing transformation for gene-expression microarray data. in *Bioinformatics* (2002).
 108. Chong, J., Wishart, D. S. & Xia, J. Using MetaboAnalyst 4.0 for Comprehensive and Integrative Metabolomics Data Analysis. *Curr. Protoc. Bioinforma.* **68**, (2019).
 109. Takahashi, K. & Yamanaka, S. Induction of Pluripotent Stem Cells from Mouse Embryonic and Adult Fibroblast Cultures by Defined Factors. *Cell* **126**, 663–676 (2006).
 110. Sueyoshi N, Maehara T & Ito M. Apoptosis of Neuro2a cells induced by lysosphingolipids with naturally occurring stereochemical configurations - PubMed. *J Lipid Res* **42**, 1197–202 (2001).
 111. Schueler, U. H. *et al.* Toxicity of glucosylsphingosine (glucopsychosine) to cultured neuronal cells: A model system for assessing neuronal damage in Gaucher disease type 2 and 3. *Neurobiol. Dis.* **14**, 595–601 (2003).
 112. Sardiello, M. *et al.* A gene network regulating lysosomal biogenesis and function. *Science* **325**, 473–477 (2009).
 113. Medina, D. L. *et al.* Transcriptional activation of lysosomal exocytosis promotes cellular clearance. *Dev. Cell* **21**, 421–430 (2011).
 114. Aureli, M. *et al.* Photoactivable sphingosine as a tool to study membrane microenvironments in cultured cells. *J. Lipid Res.* **51**, 798–808 (2010).
 115. Dennis G *et al.* DAVID: Database for Annotation, Visualization, and Integrated Discovery - PubMed. *Genome Biol* **4**, P3 (2003).
 116. Szklarczyk, D. *et al.* The STRING database in 2021: customizable protein-protein networks, and functional characterization of user-uploaded gene/measurement sets. *Nucleic Acids Res.* **49**, D605–D612 (2021).
 117. Lingwood, D. & Simons, K. Lipid rafts as a membrane-organizing principle. *Science* **327**, 46–50 (2010).
 118. Sonnino, S. *et al.* Lipid rafts in neurodegeneration and neuroprotection. *Mol. Neurobiol.* **50**, 130–148 (2014).
 119. Stirnemann, J. Ô. *et al.* A Review of Gaucher Disease Pathophysiology, Clinical Presentation and Treatments. *Int. J. Mol. Sci.* **18**, (2017).
 120. Nalls, M. A. *et al.* A multicenter study of glucocerebrosidase mutations in dementia with

- Lewy bodies. *JAMA Neurol.* **70**, 727–735 (2013).
121. McNeill, A., Duran, R., Hughes, D. A., Mehta, A. & Schapira, A. H. V. A clinical and family history study of Parkinson's disease in heterozygous glucocerebrosidase mutation carriers. *J. Neurol. Neurosurg. Psychiatry* **83**, 853–854 (2012).
 122. Cilia, R. *et al.* Survival and dementia in GBA-associated Parkinson's disease: The mutation matters. *Ann. Neurol.* **80**, 662–673 (2016).
 123. Chiricozzi, E. *et al.* GM1 promotes TrkA-mediated neuroblastoma cell differentiation by occupying a plasma membrane domain different from TrkA. *J. Neurochem.* **149**, 231–241 (2019).
 124. Fukunaga, K., Muller, D. & Miyamoto, E. CaM kinase II in long-term potentiation. *Neurochem. Int.* **28**, 343–358 (1996).
 125. Fukunaga, K., Miyamoto, E. & Soderling, T. R. Regulation of Ca²⁺/calmodulin-dependent protein kinase II by brain gangliosides. *J. Neurochem.* **54**, 102–109 (1990).
 126. Chen, X. *et al.* Inhibitory effect of ganglioside GD1b on K⁺ current in hippocampal neurons and its involvement in apoptosis suppression. *J. Lipid Res.* **46**, 2580–2585 (2005).
 127. Burke, D. G. *et al.* Increased glucocerebrosidase (GBA) 2 activity in GBA1 deficient mice brains and in Gaucher leucocytes. *J. Inherit. Metab. Dis.* **36**, 869–872 (2013).
 128. Wu, G., Lu, Z. H., Kulkarni, N. & Ledeen, R. W. Deficiency of ganglioside GM1 correlates with Parkinson's disease in mice and humans. *J. Neurosci. Res.* **90**, 1997–2008 (2012).
 129. Kim, H. J. *et al.* Alterations of mean diffusivity in brain white matter and deep gray matter in Parkinson's disease. *Neurosci. Lett.* **550**, 64–68 (2013).
 130. Cleeter, M. W. J. *et al.* Glucocerebrosidase inhibition causes mitochondrial dysfunction and free radical damage. *Neurochem. Int.* **62**, 1–7 (2013).
 131. Takahashi, K. & Yamanaka, S. Induction of pluripotent stem cells from mouse embryonic and adult fibroblast cultures by defined factors. *Cell* **126**, 663–676 (2006).
 132. Prence, E. M., Chaturvedi, P. & Newburg, D. S. In vitro accumulation of glucocerebroside in neuroblastoma cells: A model for study of Gaucher disease pathobiology. *J. Neurosci. Res.* **43**, 365–371 (1996).
 133. Orvisky, E. *et al.* Glucosylsphingosine accumulation in tissues from patients with Gaucher disease: Correlation with phenotype and genotype. *Mol. Genet. Metab.* **76**, 262–270 (2002).
 134. Hein, L. K., Duplock, S., Hopwood, J. J. & Fuller, M. Lipid composition of microdomains is altered in a cell model of Gaucher disease. *J. Lipid Res.* **49**, 1725–1734 (2008).
 135. Walkley, S. U. & Vanier, M. T. Secondary lipid accumulation in lysosomal disease. *Biochim. Biophys. Acta* **1793**, 726–736 (2009).
 136. Kim, O. S., Park, E. J., Joe, E. H. & Jou, I. JAK-STAT signaling mediates gangliosides-induced inflammatory responses in brain microglial cells. *J. Biol. Chem.* **277**, 40594–40601 (2002).
 137. Chiricozzi, E. *et al.* Turning the spotlight on the oligosaccharide chain of GM1 ganglioside. *Glycoconj. J.* **38**, 101–117 (2021).

138. Lunghi, G. *et al.* The structure of gangliosides hides a code for determining neuronal functions. *FEBS Open Bio* **11**, 3193–3200 (2021).
139. Sonnino, S., Prinetti, A., Mauri, L., Chigorno, V. & Tettamanti, G. Dynamic and structural properties of sphingolipids as driving forces for the formation of membrane domains. *Chem. Rev.* **106**, 2111–2125 (2006).
140. Svennerholm, L. *et al.* Human brain gangliosides: developmental changes from early fetal stage to advanced age. *Biochim. Biophys. Acta (BBA)/Lipids Lipid Metab.* **1005**, 109–117 (1989).
141. Batta, G. *et al.* Alterations in the properties of the cell membrane due to glycosphingolipid accumulation in a model of Gaucher disease. *Sci. Rep.* **8**, (2018).
142. Piccinini, M. *et al.* Deregulated sphingolipid metabolism and membrane organization in neurodegenerative disorders. *Mol. Neurobiol.* **41**, 314–340 (2010).
143. Roskoski, R. Src protein-tyrosine kinase structure, mechanism, and small molecule inhibitors. *Pharmacol. Res.* **94**, 9–25 (2015).
144. Holzer, R. G. *et al.* Saturated fatty acids induce c-Src clustering within membrane subdomains, leading to JNK activation. *Cell* **147**, 173–184 (2011).
145. Kajiwara, K. *et al.* c-Src-induced activation of ceramide metabolism impairs membrane microdomains and promotes malignant progression by facilitating the translocation of c-Src to focal adhesions. *Biochem. J.* **458**, 81–93 (2014).
146. Wu, C. W. *et al.* Enforced C-Src Activation Causes Compartmental Dysregulation of PI3K and PTEN Molecules in Lipid Rafts of Tongue Squamous Carcinoma Cells by Attenuating Rac1-Akt-GLUT-1-Mediated Sphingolipid Synthesis. *Int. J. Mol. Sci.* **21**, 1–26 (2020).
147. Carsana, E. V. *et al.* Metabolic Profile Variations along the Differentiation of Human-Induced Pluripotent Stem Cells to Dopaminergic Neurons. *Biomedicines* **10** (9), (2022).

8. ANNEX I

Table 3. List of the proteins upregulated in long- term CBE- treated neurons compared to untreated cells.

ID	GENE NAME	PROTEIN NAME	T-VALUE	P-VALUE
P08962	CD63	CD63 antigen	12,36	0,001
P07602	PSAP	Prosaposin (Sphingolipid activator protein)	11,84	0,000
P17900	SAP3	Ganglioside GM2 activator	10,33	0,000
P78310	CXAR	Coxsackievirus and adenovirus receptor	10,00	0,000
Q9H0U6	RM18	39S ribosomal protein L18, mitochondrial	7,31	0,001
O00115	DNS2A	Deoxyribonuclease-2-alpha	7,18	0,004
P43003	EAA1	Excitatory amino acid transporter 1	6,11	0,005
P61916	NPC2	NPC intracellular cholesterol transporter 2	5,46	0,010
Q9C0H2	TTYH3	Protein tweety homolog 3	5,42	0,012
P06753	TPM3	Tropomyosin alpha-3 chain	5,25	0,006
Q9UK22	FBX2	F-box only protein 2	5,19	0,006
O15540	FABP7	Fatty acid-binding protein, brain	5,11	0,004
Q9NWB6	ARGL1	Arginine and glutamate-rich protein 1	5,11	0,011
Q9UPT8	ZC3H4	Zinc finger CCCH domain-containing protein 4	5,06	0,007
Q08722	CD47	Leukocyte surface antigen CD47	4,69	0,006
Q92889	XPF	DNA repair endonuclease XPF	4,67	0,003
P52943	CRIP2	Cysteine-rich protein 2	4,63	0,007
P12956	XRCC6	X-ray repair cross-complementing protein 6	4,35	0,008
Q92542	NICA	Nicastrin	4,27	0,006
P11279	LAMP1	Lysosome-associated membrane glycoprotein 1 (LAMP-1)	4,26	0,009
O15400	STX7	Syntaxin-7	4,09	0,018
Q16850	CP51A	Lanosterol 14-alpha demethylase (LDM)	3,93	0,008
Q9H910	JUPI2	Jupiter microtubule associated homolog 2	3,91	0,008
P51608	MECP2	Methyl-CpG-binding protein 2 (MeCp-2 protein)	3,90	0,020
P34913	HYES	Bifunctional epoxide hydrolase 2	3,87	0,014
P53778	MK12	Mitogen-activated protein kinase 12 (MAP kinase 12)	3,84	0,010
Q96B54	ZN428	Zinc finger protein 428	3,80	0,028
Q16352	AINX	Alpha-internexin	3,71	0,020
P28799	GRN	Progranulin	3,69	0,027
P46821	MAP1B	Microtubule-associated protein 1B (MAP-1B)	3,63	0,033
Q9UHG2	PCS1N	ProSAAS (Proprotein convertase subtilisin/kexin type 1 inhibitor)	3,63	0,019
Q9H1E5	TMX4	Thioredoxin-related transmembrane protein 4	3,58	0,014
Q14197	ICT1	Peptidyl-tRNA hydrolase ICT1, mitochondrial	3,54	0,035
O75781	PALM	Paralemmin-1 (Paralemmin)	3,53	0,022
P62263	RS14	40S ribosomal protein S14	3,51	0,027
Q16880	CGT	2-hydroxyacylsphingosine 1-beta-galactosyltransferase	3,51	0,013
B7ZBB8	PP13G	Protein phosphatase 1 regulatory subunit 3G	3,49	0,021
P54803	GALC	Galactocerebrosidase	3,49	0,016
P46976	GLYG	Glycogenin-1	3,46	0,014
Q6UWZ7	ABRX1	BRCA1-A complex subunit Abraxas 1	3,45	0,033

Q13185	CBX3	Chromobox protein homolog 3	3,42	0,016
P14209	CD99	CD99 antigen	3,35	0,042
O43657	TSN6	Tetraspanin-6	3,23	0,019
Q9P2W1	HOP2	Homologous-pairing protein 2 homolog (Nuclear receptor coactivator GT198)	3,22	0,030
Q01844	EWS	RNA-binding protein EWS	3,20	0,023
Q7Z4V5	HDGR2	Hepatoma-derived growth factor-related protein 2	3,18	0,038
P10620	MGST1	Microsomal glutathione S-transferase 1	3,13	0,025
Q9Y2B9	IPKG	cAMP-dependent protein kinase inhibitor gamma (PKI-gamma)	3,09	0,023
Q15262	PTPRK	Receptor-type tyrosine-protein phosphatase kappa	3,08	0,045
O94811	TPPP	Tubulin polymerization-promoting protein (TPPP)	3,05	0,025
Q14061	COX17	Cytochrome c oxidase copper chaperone	3,05	0,033
P20020	AT2B1	PM calcium-transporting ATPase 1	3,04	0,033
Q8TB36	GDAP1	Ganglioside-induced differentiation-associated protein 1 (GDAP1)	3,02	0,026
O15347	HMGB 3	High mobility group protein B3	2,97	0,025
Q969E2	SCAM4	Secretory carrier-associated membrane protein 4	2,96	0,031
P56211	ARP19	cAMP-regulated phosphoprotein 19	2,95	0,027
P37802	TAGL2	Transgelin-2	2,92	0,031
Q16799	RTN1	Reticulon-1	2,91	0,046
Q9NZ43	USE1	Vesicle transport protein USE1 (Putative MAPK- activating protein PM26)	2,88	0,042
Q9NS86	LANC2	LanC-like protein 2	2,82	0,049
Q9BWM 7	SFXN3	Sideroflexin-3	2,82	0,032
Q6P1L5	F117B	Protein FAM117B	2,80	0,033
P61601	NCALD	Neurocalcin-delta	2,69	0,046
Q96BM9	ARL8A	ADP-ribosylation factor-like protein 8A	2,67	0,048
Q5SQI0	ATAT	Alpha-tubulin N-acetyltransferase 1	2,63	0,040
Q5T7N2	LITD1	LINE-1 type transposase domain-containing protein 1	2,61	0,042
Q9P2B2	FPRP	Prostaglandin F2 receptor negative regulator	2,61	0,045
Q9P0M9	RM27	39S ribosomal protein L27, mitochondrial	2,60	0,044
P18065	IBP2	Insulin-like growth factor-binding protein 2 (IBP- 2)	2,51	0,046
Q8IVM0	CCD50	Coiled-coil domain-containing protein 50	2,50	0,046

Table 4. List of the proteins downregulated in long- term CBE- treated neurons compared to untreated cells.

ID	GENE NAME	PROTEIN NAME	T-VALUE	P-VALUE
P26885	FKBP2	Peptidyl-prolyl cis-trans isomerase FKBP2	-2,50	0,048
Q9Y5L0	TNPO3	Transportin-3 (Importin-12)	-2,54	0,045
P62312	LSM6	U6 snRNA-associated Sm-like protein LSM6	-2,56	0,046
P29373	RABP2	Cellular retinoic acid-binding protein 2	-2,64	0,040
P62942	FKB1A	Peptidyl-prolyl cis-trans isomerase FKBP1A	-2,64	0,039
P56134	ATPK	ATP synthase subunit f, mitochondrial	-2,68	0,037
Q9BVT8	TMUB1	Transmembrane and ubiquitin-like domain-containing protein 1	-2,69	0,048
O15260	SURF4	Surfeit locus protein 4	-2,71	0,047
P61020	RAB5B	Ras-related protein Rab-5B	-2,71	0,035
P62861	RS30	40S ribosomal protein S30	-2,74	0,040
Q96EC8	YIPF6	Protein YIPF6	-2,76	0,034
Q9NR31	SAR1A	GTP-binding protein SAR1a	-2,84	0,030
Q14165	MLEC	Malectin	-2,85	0,035
O95861	BPNT1	3'(2'),5'-bisphosphate nucleotidase 1	-2,86	0,044
O43488	ARK72	Aflatoxin B1 aldehyde reductase member 2	-2,87	0,029
O43324	MCA3	Eukaryotic translation elongation factor 1 epsilon-1	-2,93	0,043
P38117	ETFB	Electron transfer flavoprotein subunit beta	-2,99	0,025
Q9NPJ3	ACO13	Acyl-coenzyme A thioesterase 13	-3,02	0,027
P51991	ROA3	Heterogeneous nuclear ribonucleoprotein A3	-3,02	0,042
P62310	LSM3	U6 snRNA-associated Sm-like protein LSM3	-3,04	0,024
P62318	SMD3	Small nuclear ribonucleoprotein Sm D3	-3,05	0,030
O94766	B3GA3	Galactosylgalactosylxylosylprotein 3-beta-glucuronosyltransferase 3	-3,05	0,023
P25208	NFYB	Nuclear transcription factor Y subunit beta	-3,07	0,034
Q9Y5U9	IR3IP	Immediate early response 3-interacting protein 1	-3,10	0,024
Q6BDS2	URFB1	UHRF1-binding protein 1	-3,12	0,033
P53597	SUCA	Succinate--CoA ligase [ADP/GDP-forming] subunit alpha, mitochondrial	-3,17	0,028
P61960	UFM1	Ubiquitin-fold modifier 1	-3,17	0,020
P22626	ROA2	Heterogeneous nuclear ribonucleoproteins A2/B1	-3,20	0,026
P60468	SC61B	Protein transport protein Sec61 subunit beta	-3,21	0,025
Q6NUQ4	TM214	Transmembrane protein 214	-3,23	0,044
Q16650	TBR1	T-box brain protein 1	-3,34	0,030
Q9H0V9	LMA2L	VIP36-like protein	-3,43	0,039
P24752	THIL	Acetyl-CoA acetyltransferase, mitochondrial	-3,43	0,027
P20340	RAB6A	Ras-related protein Rab-6A (Rab-6)	-3,47	0,014
P61081	UBC12	NEDD8-conjugating enzyme Ubc12	-3,49	0,013
P29762	RABP1	Cellular retinoic acid-binding protein 1	-3,50	0,013
O75396	SC22B	Vesicle-trafficking protein SEC22b	-3,53	0,031
Q96AY3	FKB10	Peptidyl-prolyl cis-trans isomerase FKBP10	-3,60	0,034
Q96EX1	SIM12	Small integral membrane protein 12	-3,62	0,014
Q9Y3D6	FIS1	Mitochondrial fission 1 protein	-3,63	0,013
Q5EB52	MEST	Mesoderm-specific transcript homolog protein	-3,72	0,013

O43772	MCAT	Mitochondrial carnitine/acylcarnitine carrier protein	-3,74	0,012
P61923	COPZ1	Coatomer subunit zeta-1	-3,78	0,009
O75880	SCO1	Protein SCO1 homolog, mitochondrial	-3,85	0,019
P09972	ALDOC	Fructose-bisphosphate aldolase C	-3,86	0,026
O60783	RT14	28S ribosomal protein S14, mitochondrial	-3,98	0,007
P13674	P4HA1	Prolyl 4-hydroxylase subunit alpha-1	-4,00	0,010
Q96DB5	RMD1	Regulator of microtubule dynamics protein 1	-4,00	0,011
Q07955	SRSF1	Serine/arginine-rich splicing factor 1	-4,06	0,023
Q5JWF2	GNAS1	Guanine nucleotide-binding protein G(s) subunit alpha isoforms XLas	-4,10	0,011
O43237	DC1L2	Cytoplasmic dynein 1 light intermediate chain 2	-4,14	0,007
O75323	NIPS2	Protein NipSnap homolog 2	-4,45	0,011
Q969M3	YIPF5	Protein YIPF5 (Five-pass transmembrane protein localizing in the Golgi apparatus and the endoplasmic reticulum 5)	-4,48	0,004
O75347	TBCA	Tubulin-specific chaperone A	-4,50	0,007
P32322	P5CR1	Pyrroline-5-carboxylate reductase 1, mitochondrial	-4,57	0,005
O60831	PRAF2	PRA1 family protein 2	-4,58	0,015
Q13596	SNX1	Sorting nexin-1	-4,65	0,004
P45877	PPIC	Peptidyl-prolyl cis-trans isomerase C	-4,74	0,003
Q9BUJ2	HNRL1	Heterogeneous nuclear ribonucleoprotein U-like protein 1	-4,86	0,007
Q969R2	OSBP2	Oxysterol-binding protein 2	-5,06	0,002
O14832	PAHX	Phytanoyl-CoA dioxygenase, peroxisomal	-5,27	0,009
Q9GZS3	WDR61	WD repeat-containing protein 61	-5,75	0,002
Q8TBQ9	KISHA	Protein kish-A	-5,83	0,002
Q71UI9	H2AV	Histone H2A.V	-5,85	0,001
O15269	SPTC1	Serine palmitoyltransferase 1	-6,27	0,001
Q96GQ5	RUSF1	RUS family member 1	-6,46	0,001
Q9HD45	TM9S3	Transmembrane 9 superfamily member 3	-8,36	0,003
Q13242	SRSF9	Serine/arginine-rich splicing factor 9	-8,41	0,001
P43307	SSRA	Translocon-associated protein subunit alpha (TRAP-alpha)	-9,45	0,000
Q9BRA2	TXD17	Thioredoxin domain-containing protein 17	-9,89	0,000
Q9Y5M8	SRPRB	Signal recognition particle receptor subunit beta	-13,23	0,000

Table 5. List of the proteins only expressed in the precipitate (P) of long- term CBE- treated neurons in the comparison CBE treated vs CBE- untreated neurons

ID	GENE NAME	PROTEIN NAME
P61604	CH10	10 kDa heat shock protein, mitochondrial
P62269	RS18	40S ribosomal protein S18
P15880	RS2	40S ribosomal protein S2
P23396	RS3	40S ribosomal protein S3
P62241	RS8	40S ribosomal protein S8
P48047	ATPO	ATP synthase subunit O, mitochondrial
P27824	CALX	Calnexin OS=Homo sapiens
Q15417	CNN3	Calponin-3 OS=Homo sapiens
P13861	KAP2	cAMP-dependent protein kinase type II-alpha regulatory subunit
P35221	CTNA1	Catenin alpha-1 OS=Homo sapiens
P26232	CTNA2	Catenin alpha-2 OS=Homo sapiens
Q00610	CLH1	Clathrin heavy chain 1 OS=Homo sapiens
Q14204	DYHC1	Cytoplasmic dynein 1 heavy chain 1
P13639	EF2	Elongation factor 2 OS=Homo sapiens
P14625	ENPL	Endoplasmin OS=Homo sapiens
P47756	CAPZB	F-actin-capping protein subunit beta
P21333	FLNA	Filamin-A OS=Homo sapiens
Q14315	FLNC	Filamin-C OS=Homo sapiens
P00367	DHE3	Glutamate dehydrogenase 1, mitochondrial
P04899	GNAI2	Guanine nucleotide-binding protein G(i) subunit alpha-2
Q9UBI6	GBG12	Guanine nucleotide-binding protein G(I)/G(S)/G(O) subunit gamma
P09471	GNAO	Guanine nucleotide-binding protein G(o) subunit alpha
P16401	H15	Histone H1.5
Q92522	H1X	Histone H1x
P68431	H31	Histone H3.1
Q16695	H31T	Histone H3.1t
Q71DI3	H32	Histone H3.2
P84243	H33	Histone H3.3
P50502	F10A1	Hsc70-interacting protein
Q14974	IMB1	Importin subunit beta-1
Q9NZI8	IF2B1	Insulin-like growth factor 2 mRNA-binding protein 1
Q12906	ILF3	Interleukin enhancer-binding factor 3
Q9UK76	JUPI1	Jupiter microtubule associated homolog 1
P35908	K22E	Keratin, type II cytoskeletal 2 epidermal
P42166	LAP2A	Lamina-associated polypeptide 2, isoform alpha
P42167	LAP2B	Lamina-associated polypeptide 2, isoforms beta/gamma
P11137	MTAP2	Microtubule-associated protein 2
P60660	MYL6	Myosin light polypeptide 6
P29966	MARCS	Myristoylated alanine-rich C-kinase substrate
O95865	DDAH2	N(G)N(G)-dimethylarginine dimethylaminohydrolase 2
P13591	NCAM1	Neural cell adhesion molecule 1
P07196	NFL	Neurofilament light polypeptide

P07197	NFM	Neurofilament medium polypeptide
O43602	DCX	Neuronal migration protein doublecortin
P19338	NUCL	Nucleolin
P06748	NPM	Nucleophosmin
P62937	PPIA	Peptidyl-prolyl cis-trans isomerase A
Q06830	PRDX1	Peroxiredoxin-1
P30086	PEBP1	Phosphatidylethanolamine-binding protein 1
P18669	PGAM1	Phosphoglycerate mutase 1
Q15365	PCBP1	Poly(rC)-binding protein 1
Q15366	PCBP2	Poly(rC)-binding protein 2
Q92841	DDX17	Probable ATP-dependent RNA helicase DDX17
P07737	PROF1	Profilin-1
Q99623	PHB2	Prohibitin-2
Q99497	PARK7	Protein/nucleic acid deglycase DJ-1
P31150	GDIA	Rab GDP dissociation inhibitor alpha
O15075	DCLK1	Serine/threonine-protein kinase DCLK1
Q04837	SSBP	Single-stranded DNA-binding protein, mitochondrial
Q13813	SPTN1	Spectrin alpha chain, non-erythrocytic 1
Q7KZF4	SND1	Staphylococcal nuclease domain-containing protein 1
P78371	TCPB	T-complex protein 1 subunit beta
Q9UI15	TAGL3	Transgelin-3
P55072	TERA	Transitional endoplasmic reticulum ATPase
P29401	TKT	Transketolase
P55084	ECHB	Trifunctional enzyme subunit beta, mitochondrial
Q13748	TBA3C	Tubulin alpha-3C/D chain
Q3ZCM	TBB8	Tubulin beta-8 chain
7		
P09936	UCHL1	Ubiquitin carboxyl-terminal hydrolase isozyme L1
P21796	VDAC1	Voltage-dependent anion-selective channel protein 1
O75083	WDR1	WD repeat-containing protein 1
P12956	XRCC6	X-ray repair cross-complementing protein 6

Table 6. List of the proteins only expressed in the precipitate (P) of CBE- untreated neurons in the comparison long-term CBE treated vs CBE- untreated neurons

ID	GENE NAME	PROTEIN NAME
Q14011	CIRBP	Cold-inducible RNA-binding protein
Q71UI9	H2AV	Histone H2A.V
P0C0S5	H2AZ	Histone H2A.Z
P35232	PHB	Prohibitin
P04350	TBB4A	Tubulin beta-4A chain

9. PUBLISHED MANUSCRIPT

The following pages represent the manuscript published on *Cells* journal on the 29th of July 2022, where I am first co- author together with Dr Giulia Lunghi⁹⁶.

The following manuscript and the related supplementary material are the main core of my PhD work and are described in *section 5.2.1* of this PhD thesis.

Article

β -Glucocerebrosidase Deficiency Activates an Aberrant Lysosome-Plasma Membrane Axis Responsible for the Onset of Neurodegeneration

Giulia Lunghi ^{1,†}, Emma Veronica Carsana ^{1,†}, Nicoletta Loberto ¹, Laura Cioccarelli ¹, Simona Prioni ¹, Laura Mauri ¹, Rosaria Bassi ¹, Stefano Duga ^{2,3}, Letizia Straniero ^{2,3}, Rosanna Asselta ^{2,3}, Giulia Soldà ^{2,3}, Alessio Di Fonzo ⁴, Emanuele Frattini ⁴, Manuela Magni ⁴, Nara Liessi ⁵, Andrea Armirotti ⁵, Elena Ferrari ⁶, Maura Samarani ^{7,‡} and Massimo Aureli ^{1,*,‡}

- ¹ Department of Medical Biotechnology and Translational Medicine, University of Milan, 20054 Milan, Italy; giulia.lunghi@unimi.it (G.L.); emma.carsana@unimi.it (E.V.C.); nicoleta.loberto@unimi.it (N.L.); laura.cioccarelli@hotmail.it (L.C.); simona.prioni@unimi.it (S.P.); laura.mauri@unimi.it (L.M.); rosaria.bassi@unimi.it (R.B.)
- ² Department of Biomedical Sciences, Humanitas University, 20090 Milan, Italy; stefano.duga@hunimed.eu (S.D.); letizia.straniero@humanitasresearch.it (L.S.); rosanna.asselta@hunimed.eu (R.A.); giulia.solda@hunimed.eu (G.S.)
- ³ Humanitas Clinical and Research Center—IRCCS, Via Manzoni 56, 20072 Milan, Italy
- ⁴ IRCCS Foundation Ca' Granda Ospedale Maggiore Policlinico, Dino Ferrari Center, Neuroscience Section, Department of Pathophysiology and Transplantation, University of Milan, 20122 Milan, Italy; alessio.difonzo@policlinico.mi.it (A.D.F.); emanuele.frattini@unimi.it (E.F.); manuelamagni90@gmail.com (M.M.)
- ⁵ Analytical Chemistry Facility, Fondazione Istituto Italiano di Tecnologia, Via Morego 30, 16163 Genoa, Italy; nara.liessi@iit.it (N.L.); andrea.armirotti@iit.it (A.A.)
- ⁶ Department of Pharmacological and Biomolecular Sciences, University of Milan, 20133 Milan, Italy; elena.ferrari2@unimi.it
- ⁷ Department of Cell Biology and Infection, Institut Pasteur, 75015 Paris, France; maura.samarani@pasteur.fr
- * Correspondence: massimo.aureli@unimi.it; Tel.: +39-025-033-0364
- † These authors contributed equally to this work.
- ‡ These authors share the senior position.



Citation: Lunghi, G.; Carsana, E.V.; Loberto, N.; Cioccarelli, L.; Prioni, S.; Mauri, L.; Bassi, R.; Duga, S.; Straniero, L.; Asselta, R.; et al. β -Glucocerebrosidase Deficiency Activates an Aberrant Lysosome-Plasma Membrane Axis Responsible for the Onset of Neurodegeneration. *Cells* **2022**, *11*, 2343. <https://doi.org/10.3390/cells11152343>

Academic Editors: Illana Gozes and Carmen Laura Sayas

Received: 21 June 2022

Accepted: 27 July 2022

Published: 29 July 2022

Publisher's Note: MDPI stays neutral with regard to jurisdictional claims in published maps and institutional affiliations.



Copyright: © 2022 by the authors. Licensee MDPI, Basel, Switzerland. This article is an open access article distributed under the terms and conditions of the Creative Commons Attribution (CC BY) license (<https://creativecommons.org/licenses/by/4.0/>).

Abstract: β -glucocerebrosidase is a lysosomal hydrolase involved in the catabolism of the sphingolipid glucosylceramide. Biallelic loss of function mutations in this enzyme are responsible for the onset of Gaucher disease, while monoallelic β -glucocerebrosidase mutations represent the first genetic risk factor for Parkinson's disease. Despite this evidence, the molecular mechanism linking the impairment in β -glucocerebrosidase activity with the onset of neurodegeneration is still unknown. In this frame, we developed two in vitro neuronal models of β -glucocerebrosidase deficiency, represented by mouse cerebellar granule neurons and human-induced pluripotent stem cells-derived dopaminergic neurons treated with the specific β -glucocerebrosidase inhibitor conduritol B epoxide. Neurons deficient for β -glucocerebrosidase activity showed a lysosomal accumulation of glucosylceramide and the onset of neuronal damage. Moreover, we found that neurons react to the lysosomal impairment by the induction of their biogenesis and exocytosis. This latter event was responsible for glucosylceramide accumulation also at the plasma membrane level, with an alteration in lipid and protein composition of specific signaling microdomains. Collectively, our data suggest that β -glucocerebrosidase loss of function impairs the lysosomal compartment, establishing a lysosome–plasma membrane axis responsible for modifications in the plasma membrane architecture and possible alterations of intracellular signaling pathways, leading to neuronal damage.

Keywords: GBA1; glucosylceramide; Gaucher disease; lysosomes; plasma membrane; lipid rafts

1. Introduction

β -glucocerebrosidase (GCCase) is a lysosomal hydrolase encoded by *GBA1* gene that catalyzes the hydrolysis of the glycosphingolipid (GSL) glucosylceramide (GlcCer) to ceramide and glucose. The severe deficiency of GCCase results in the accumulation of GlcCer, which is classically linked to the multi-organ clinical manifestations typical of Gaucher disease (GD), the most common lysosomal storage disorder (LSD) [1,2].

Mutations in *GBA1* are associated with an increased incidence of Parkinson's disease (PD), both in GD patients and in heterozygous carriers, representing the main genetic risk factor for the development of PD [3–7]. Interestingly, a deficiency of GCCase activity in the substantia nigra pars compacta has been demonstrated not only in PD patients carrying *GBA1* mutations, but also in PD subjects with a wild-type *GBA1* [8,9]. Furthermore, Murphy and co-workers analyzed brain tissues from sporadic PD patients without *GBA1* mutations and discovered that deficits in GCCase are positively correlated with the levels of accumulated alpha-synuclein. Interestingly, the accumulation of alpha-synuclein within lysosomes has been associated with a chronic reduction in lysosomal function [10,11].

Different theories have been formulated to explain how and to which extent GCCase deficiency contributes to neurodegeneration [12]. It has been hypothesized that a central role could be played by the endolysosomal compartment where GlcCer accumulation could directly influence the abnormal lysosomal storage of alpha-synuclein oligomers, thus resulting in a further inhibition of GCCase activity. These findings suggest the establishment of a positive feedback loop between GCCase deficiency and alpha-synuclein accumulation, which may lead to a self-propagation of the disease [13]. In line with this evidence, the rescue of GCCase activity ameliorates the neurodegenerative phenotype, suggesting a possible direct involvement of the accumulated GlcCer in neurodegeneration [14,15]. Despite these findings, the molecular mechanism linking GCCase impairment with neurodegeneration remains unclear and still debated in the scientific community. A major obstacle in the understanding of the molecular mechanism linking GCCase impairment with neurodegeneration is represented by the lack of suitable *in vitro* and *in vivo* models.

In this study, we developed two different neuronal *in vitro* models of GCCase deficiency represented by murine cerebellar granule neurons (CGN) and human-induced pluripotent stem cell (iPSC)-derived dopaminergic (DA) neurons, both treated with conduritol B epoxide (CBE) a selective inhibitor of GCCase activity [16]. Our data highlight the existence of a pathogenic lysosome–plasma membrane (PM) axis that participates in the onset of neurodegeneration upon GCCase deficiency, thus adding a new piece to the already multifaceted research on GCCase-related pathologies.

2. Materials and Methods

2.1. Materials

Commercial chemicals were of the highest purity available, common solvents were distilled before use and water was doubly distilled in a glass apparatus. Phosphate-buffered saline (PBS) and calcium magnesium free (CMF)-PBS, glucose, sodium orthovanadate (Na_3VO_4), phenylmethanesulfonyl fluoride (PMSF), aprotinin, protease inhibitor cocktail (IP), Triton X-100, bovine serum albumin, rabbit polyclonal anti-GAPDH antibody (RRID: AB_796208), DNase I, Trypsin, Conduritol B epoxide (CBE), Rock inhibitor, SB431542, SAG, pumorphamine, CHIR99021, cAMP and L-ascorbic acid, mono-dimensional HPTLC were obtained from Sigma-Aldrich (St. Louis, MO, USA). L-Glutamine, penicillin/streptomycin (10,000 Units/mL) and D-MEM were purchased from EuroClone (Paignton, UK). Mouse anti-Neurofilament H (RRID: AB_10694081), rabbit anti-MAP2 (RRID: AB_10693782), mouse anti-Tau (RRID: AB_10695394), rabbit anti-PSD95 (RRID: AB_561221), mouse anti- β 3-tubulin (RRID: AB_1904176), rabbit anti-c-Src (RRID: AB_2106059), rabbit anti-phospho-c-Src (p-Src Tyr416) (RRID: AB_331697) and goat-anti-rabbit HRP-conjugated antibodies were obtained from Cell Signalling Technology (Danvers, MA, USA). Mouse anti-TH (RRID: AB_628422) antibody was obtained from Santa Cruz Biotechnology. Mouse anti-LAMP1 (RRID: AB_2296838) antibody was purchased from Developmental Studies Hybridoma

Bank (Iowa City, Iowa, USA). The chemiluminescence kit for immunoblotting was obtained from Cyanagen (Bologna, Italy). Neurobasal medium A 1x, Neurobasal medium 1x, B27 Supplement, N2 supplement, KSR supplement, Geltrex, Essential 8 medium, Accutase, 100X non-essential amino acid, 100X 2-mercaptoethanol, 100X Glutamax, EZ-Link Sulfo-NHS-biotin, Dynabeads M-280 Streptavidin and goat-anti-mouse HRP conjugated (RRID: 31430) were obtained from ThermoFisher Scientific (Waltham, MA, USA). Liquid scintillation cocktail Ultima Gold™ was from Perkin Elmer (Waltham, MA, USA). A total of 4–20% Mini-PROTEAN® TGX™ Precast Protein Gels, Turbo Polyvinylidene difluoride (PVDF) Mini-Midi membrane and DC™ protein assay kit were from BioRad (Hercules, CA, USA). High-performance thin-layer chromatography (HPTLC) plate and Triton X-100 were from Merck Millipore (Frankfurt, Germany). LDN-193189 was from Reprorcell. FGF-8b, BDNF, GDNF, TGF-3β were from Peprotech (London, UK). 4-Methylumbelliferyl-b-D-galactopyranoside (MUB-Gal), 4-methylumbelliferyl-b-D-glucopyranoside (MUB-Glc) and 4-methylumbelliferone were obtained from Glycosynth (Warrington, UK).

2.2. Generation of Murine Cerebellar Granule Neurons

Pregnant C57BL/6J mice were provided by Charles River—Research Models and Services (Calco, Lecco, Italy). All animal procedures were approved by the Ethics Committee of the University of Milano, Italy and were performed in accordance with the National Institute of Health Guide for the Care and Use of Laboratory Animals (Directive 2010/63/EU) (project numbers FD611.N.TAQ). CGN were prepared as previously described [17]. Briefly, 5-day-old pups were sacrificed by decapitation to extract the cerebellum. CGN were dissociated from pooled cerebella by mechanic trituration with blade (70 times in perpendicular directions), followed by incubation with Trypsin 1% (*w/v*) plus DNase I 0.1% (*w/v*) in CMF-PBS-Glucose 0.2% (*w/v*) (1 mL every 5 cerebella) for 3.5 min at 23 °C. The reaction was stopped by centrifugation of the cell mixture at 1000× *g* for 10 s and the supernatant was removed. The cell pellet was suspended in Trypsin inhibitor 0.04% (*w/v*) plus DNase I 0.1% (*w/v*) in CMF-PBS-glucose 0.2% (*w/v*) (1 mL every 5 cerebella). The cells were definitively dissociated by repeated passages through descending caliber glass Pasteur pipettes. The solution was removed by centrifugation (1000× *g*, 5 min) and the cells were washed with 0.2% (*w/v*) glucose in CMF-PBS before being resuspended in Neurobasal A medium containing 25 mM KCl, 1% B27 Supplement, 2 mM L-glutamine, 100 U/mL penicillin, and 100 µg/mL streptomycin. Cells were plated at a density of 3.15×10^5 cells/cm² on plastic supports pre-coated with poly-L-lysine (10 µg/mL for 2 h at 37 °C) and maintained in culture in standard conditions. Then, 24h after plating, the culture medium was supplemented with 0.25 mg/mL Cytarabine. Half of the medium was changed every 2 days.

2.3. iPSC Culture

Human iPSC lines derived from fibroblasts of a healthy subject were obtained from the IRCCS Foundation Ca' Granda Ospedale Maggiore Policlinico. The use of iPSCs was approved by the IRB of Fondazione IRCCS Ca' Granda Ospedale Maggiore Policlinico. Fibroblasts were derived from a 2 mm diameter skin punch biopsy and cultured in DMEM supplemented with 15% fetal bovine serum and 1% penicillin/streptomycin. Fibroblasts were reprogrammed with a commercial kit (CytoTune™-iPS 2.0 Sendai Reprogramming Kit, Thermo Fisher Scientific, Waltham, MA, USA), following the manufacturer's instructions. Then, 3 weeks after the transfection, colonies were manually picked and individual clones of iPSCs were isolated. The karyotype analysis of selected clones of reprogrammed iPSCs showed no major chromosomal rearrangements (data not shown) and one single clone was further expanded for experiments. Cells showed typical stem cell-like morphology and stained positive for stem cell markers (data not shown). iPSCs were grown in geltrex-coated (1% for 1h at 37 °C) 6-well plates and cultured in Essential 8 Medium. At 80–90% confluence (i.e., every 3–4 days), cells were passaged using Accutase (3 min 37 °C) and plated at a density of 10⁴ cells/cm² in Essential 8 Medium supplemented with 10 µM Rock inhibitor for 24 h.

2.4. Differentiation of iPSC into Dopaminergic Neurons

iPSCs were differentiated into DA neurons according to the protocol described by Zhang et al. [18]. Cells were cultured in proper media supplemented with specific factors at proper concentrations as follows. Day 0: KSR differentiation medium (81% DMEM, 15% KSR, 100X 1% non-essential amino acids, 100X 1% 2-mercaptoethanol, 100 U/mL penicillin, and 100 µg/mL streptomycin) supplemented with 10 µM SB431542 and 100 µM LDN-193189. Days 1 and 2: KSR differentiation medium supplemented with 10 µM SB431542, 100 nM LDN-193189, 0.25 µM SAG, 2 µM purmorphamine and 50 ng/mL FGF8b. Days 3 and 4: KSR differentiation medium supplemented with 10 µM SB431542, 100 nM LDN-193189, 0.25 µM SAG, 2 µM purmorphamine, 50 ng/mL FGF8b and 3 µM CHIR99021. Days 5 and 6: 75% KSR differentiation medium and 25% N2 differentiation medium (97% DMEM, 100X 1% N2 supplement, 100 U/mL penicillin, and 100 µg/mL streptomycin) supplemented with 100 nM LDN-193189, 0.25 µM SAG, 2 µM purmorphamine, 50 ng/mL FGF8b and 3 µM CHIR99021. Days 7 and 8: 50% KSR differentiation medium and 50% N2 differentiation medium supplemented with 100 nM LDN-193189 and 3 µM CHIR99021. Days 9 and 10: 25% KSR differentiation medium and 75% N2 differentiation medium supplemented with 100 nM LDN-193189 and 3 µM CHIR99021. Days 11 and 12: B27 differentiation medium (95% Neurobasal medium, 50X 2% B27 supplement, 1% Glutamax, 100X, 100 U/mL penicillin, and 100 µg/mL streptomycin) supplemented with 3 µM CHIR99021, 10 ng/mL BDNF, 10 ng/mL GDNF, 1 ng/mL TGF-β3, 0.2 mM ascorbic acid and 0.1 mM cyclic AMP. From day 13 to the end of differentiation: B27 differentiation medium supplemented with 10 ng/mL BDNF, 10 ng/mL GDNF, 1 ng/mL TGF-β3, 0.2 mM ascorbic acid and 0.1 mM cyclic AMP. After 20 days of differentiation, cells were split using Accutase (3 min 37 °C) on geltrex-coated plates at a density of 2×10^5 cells/cm². The medium was changed every day.

2.5. Cell Sphingolipid Labelling with [1-³H]-Sphingosine

Mature DA neurons at 29 days in culture (DIC) and CGN at 2 DIC were fed with 36 nM [1-³H]-sphingosine to metabolically label cell sphingolipids as previously described [19]. Briefly, [1-³H]-sphingosine dissolved in methanol was transferred into a sterile glass tube, dried under a nitrogen stream, and then solubilized in an appropriate volume of medium to obtain a final concentration of 36 nM. The correct solubilization was verified by measuring the radioactivity associated with an aliquot of the medium by beta-counter (PerkinElmer, Waltham, MA, USA). After 24 h of incubation the medium was removed and the cells were incubated in a fresh culture medium without radioactive sphingosine.

2.6. CBE Treatment

CGN were treated with CBE starting from 3 DIC for 7 and 14 days. Mature DA neurons were treated with CBE starting from 31 DIC for 14 and 29 days. CBE was dissolved in water at a concentration of 100 mM and diluted in culture medium at the final concentration of 0.5 mM [20]. CBE was re-added at every change of the culture medium. Untreated cells were incubated under the same experimental conditions without CBE.

2.7. Protein Determination

The protein concentration of samples was assessed with the DC™ protein assay kit according to the manufacturer's instructions, using BSA at different concentrations as standard.

2.8. Cell Surface Protein Biotinylation and Isolation of Plasma Membrane Proteins by Streptavidin Pulldown Assay

At the end of CBE treatment, the control and treated cells were washed with PBS and incubated with 4.7 mg/mL of EZ-Link Sulfo-NHS-biotin in PBS for 30 min at 4 °C. Cells were rinsed with 100 mM glycine in PBS at 4 °C and then mechanically harvested in PBS and centrifuged at 270× g for 10 min. Pellets were lysed in 2 mL of 1% Triton X-100, 50 mM

Tris-HCl pH 7.4, 150 mM NaCl, 2 mM NaF, 1 mM EDTA, 1 mM EGTA supplemented with Protease Inhibitor Cocktail and 1 mM Na_3VPO_4 for 30 min in ice and then passed 11 times in a Dounce homogenizer with tight pestle. The lysates were centrifuged at $1300\times g$ for 5 min at 4°C to remove nuclei and cellular debris and obtain a post nuclear supernatant (PNS). To separate the biotinylated protein fractions, equal amounts of PNS proteins from CBE-treated and untreated cells were mixed with streptavidin-coated magnetic beads (DynabeadsTM M-280 Streptavidin, Thermo Fisher Scientific), stirred overnight at 4°C , and then recovered by magnet precipitation. Radioactive lipids were extracted from the pellets containing the biotinylated cell surface proteins (P) with chloroform: methanol (2:1, *v:v*, 400 μL twice), whereas radioactive lipids from the supernatants containing non-biotinylated proteins (SN) were extracted as described in the lipid analysis paragraph. Radioactivity associated with both fractions was determined by liquid scintillation counting. Lipid separation and quantification were performed as described in the lipid analysis paragraph.

2.9. Cell Surface Protein Biotinylation and Isolation of Detergent-Resistant Membrane Fractions

At the end of CBE treatment, the treated and untreated cells were biotinylated as described in the previous paragraph and then mechanically harvested in PBS and centrifuged at $270\times g$ for 10 min. Pellets were then lysed in 2 mL of 1% Triton X-100 in 19 mM TNEV buffer (10 mM Tris-HCl, 150 mM NaCl, 5 mM EDTA (pH 7.5)) supplemented with Protease Inhibitor Cocktail and 1mM Na_3VPO_4 for 30 min in ice and then lysed 11 times using a tight Dounce. The lysates were centrifuged at $1300\times g$ for 5 min at 4°C to remove nuclei and cellular debris and obtain the PNS. A total of 1 mL of PNS was mixed with an equal volume of 85% sucrose (*w/v*) in TNEV buffer containing 1 mM Na_3VO_4 , loaded at the bottom of a discontinuous sucrose gradient (30–5%) and centrifuged at $200,000\times g$ at 4°C for 17 h. After ultracentrifugation, 12 fractions were collected starting from the top of the tube. The light scattering band, corresponding to the detergent-resistant membrane domain (DRM) fraction, was collected in corresponding fractions 5 and 6, whereas fractions 10, 11 and 12 correspond to high-density fractions (HD). The entire procedure was performed at $0\text{--}4^\circ\text{C}$ in ice immersion. Radioactivity associated with PNS and with gradient fractions (HD and DRM) was determined by liquid scintillation counting [21]. DRM fractions from the CBE-treated and untreated cells were subjected to precipitation of cell surface biotinylated protein and lipids extraction as described in the previous paragraph. In this case, the pellets containing the biotinylated cell surface proteins represent the detergent-resistant plasma membrane domain fractions (PM-DRM). Radioactivity associated with PM-DRM and SN was determined by liquid scintillation counting. Lipid separation and quantification were performed as described in the lipid analysis paragraph. Equal volumes of each fraction were diluted with Laemmli buffer and used for immunoblotting analysis.

2.10. Immunoblotting

Immunoblotting for CGN or DA neurons total cell lysates, HD, and DRM fractions were performed using standard protocols. Aliquots of proteins were mixed with Laemmli buffer (0.15 M DTT, 94 mM Tris-HCl pH 6.8, 15% glycerol, 3% *w/v* SDS, 0.015% blue bromophenol) and heated for 5 min at 95°C . Proteins were separated on 4–20% polyacrylamide gradient gels and transferred to PVDF membranes by electroblotting. PVDF membranes were incubated in a blocking solution with (5% non-fat dry milk (*w/v*) in TBS-0.1% tween-20 (*v/v*)) at 23°C for 1 h under gentle shaking. Subsequently, PVDF membranes were incubated overnight at 4°C with primary antibodies diluted in blocking solution. The day after, PVDF membranes were incubated for 1 h at 23°C with secondary HRP-conjugated antibodies diluted in blocking solution. PVDF were scanned using the chemiluminescence system Alliance Mini HD9 (Uvitec, Cambridge, UK) and band intensity was quantified using ImageJ software (v2.1.0/1.53c) (National Institutes of Health, Bethesda, USA). The following primary antibodies were used for immunoblotting: Polyclonal rabbit anti-PSD95 (dilution: 1:1000), polyclonal rabbit anti-MAP2 (dilution: 1:1000), monoclonal mouse anti-Tau (dilution: 1:1000), monoclonal mouse anti-Neurofilament H

(dilution: 1:1000), monoclonal mouse anti-LAMP1 (dilution: 1:100), monoclonal mouse non-phospho-Src Tyr416 (dilution 1:1000), monoclonal mouse phospho-Src family Tyr416 (dilution 1:1000), polyclonal rabbit anti-GAPDH (dilution: 1:7000) and monoclonal mouse anti- β 3-tubulin (dilution: 1:1000).

The following secondary antibodies were used: goat-anti-rabbit HRP-conjugated (1:1000) and goat-anti-mouse HRP conjugated (dilution: 1:2000).

2.11. Evaluation of Enzymatic Activities in Cell Lysates

GCCase activity in total cell lysates was determined as previously described [22,23] using the 4-Methylumbelliferone (MUB)-derived fluorogenic substrate MUB- β -Glc.

Aliquots of cell lysates corresponding to 20 μ g of proteins were pre-incubated for 30 min at 23 °C in a 96-well microplate with a reaction mixture composed of: 25 μ L of McIlvaine buffer 4X (0.4 M citric acid, 0.8 M Na₂HPO₄) pH 5.2, the specific inhibitor of the non-lysosomal β -glucocereamidase AMP-DNM (Adamantane-pentyl-dNM;N-(5-adamantane-1-yl-methoxy-pentyl)-Deoxynojirimycin) at the final concentration of 5 nM and water to a final volume of 75 μ L. At the end of pre-incubation, the reaction was started adding 25 μ L of MUB- β -Glc at a final concentration of 6 mM. The reaction mixtures were incubated at 37 °C under gentle shaking. At different time points, 10 μ L of the reaction mixtures were transferred to a black microplate (Black, 96-well, OptiPlate-96 F, Perkin Elmer) and 190 μ L of 0.25 M glycine pH 10.7 were added. The fluorescence associated with MUB was detected by a Victor microplate reader (Perkin Elmer) (ex/em 365/460 nm). Data were expressed as nanomoles of converted substrate/h and normalized to milligrams of cell proteins.

2.12. Evaluation of Plasma Membrane Enzymatic Activities in Living Cells

Cells were plated in 96-well microplate at a density of 3.15×10^5 cells/cm² for CGN and 2×10^5 cells/cm² for DA neurons to assay the activity of β -galactosidase and β -hexosaminidase according to a high throughput cell lived-based assay as previously described [22]. After the removal of the culture medium, cells were rinsed with DMEM-F12 without phenol red and artificial substrates (MUB-Gal and MUG), solubilized in DMEM-F12 without phenol red at pH 6 to a final concentration of 1 mM and 6 mM, respectively, which were added to the cells. Reactions occurred at 37 °C for 2 h. At the end of the incubation, 10 μ L of the reaction mixtures were transferred to a black microplate (Black, 96-well, OptiPlate-96 F, Perkin Elmer) and 190 μ L of 0.25 M glycine pH 10.7 were added. The fluorescence associated with MUB was detected by a Victor microplate reader (Perkin Elmer) (ex/em 365/460 nm). Since substrates are not able to cross the PM, under these experimental conditions, the observed fluorescence is exclusively associated with the PM glycohydrolases. Enzymatic activity was expressed as nanomoles of product/h and normalized to 10⁶ cells.

2.13. Lipid Analysis

At the end of CBE treatment, cells were harvested and lysed with H₂O supplemented with proteinase and phosphatase inhibitors and the cell lysates were subjected to lyophilization. Total lipids were extracted from lyophilized cell lysates with chloroform: methanol: water (2:1:0.1, *v:v:v*) and separated from the pellet by centrifugation at $13,000 \times g$ for 15 min, followed by a second and third extraction with chloroform: methanol, 2:1 by vol. Total lipid extracts (TLEs) were subjected to a two-phase partitioning by adding 20% water, resulting in the separation of an aqueous phase (AP) containing gangliosides and an organic phase (OP) containing the other lipids. The radioactivity associated with TLE, AP and OP was determined by liquid scintillation counting by beta-counter (PerkinElmer). Lipids were resolved by mono-dimensional HPTLC using different solvent systems: chloroform: methanol: CaCl₂ (50:42:11, *v:v:v*) for the ganglioside analysis of TLE and AP, chloroform: methanol: NH₄OH (70:30:3, *v:v:v*) for the glucosylsphingosine analysis of OP and chloroform: methanol: water (110:40:6, *v:v:v*) for the neutral glycolipid analysis of TLE and

OP. Lipids were identified after separation by comigration with authentic standards. Radioactive lipids were detected by radioactivity imaging (Beta-Imager[†]Racer Betaimager, BioSpace Laboratory, Paris, France) and quantified using the M3 Vision software (BioSpace Laboratory, Paris, France).

2.14. Evaluation of GlcCer Release

Cell culture medium was collected daily, centrifuged at $211\times g$ to remove cells and filtered through $0.22\ \mu\text{m}$ filtering units. The medium of the CBE-treated and untreated neurons was subjected to dialysis to remove salts and lyophilized and then lipids were extracted. GlcCer released in culture medium was evaluated by HPTLC as described in the lipid analysis section using the solvent system chloroform: methanol: CaCl_2 (50:42:11, *v:v:v*).

2.15. Proteomic Analysis

All chemicals and reagents used for sample preparation and LC-MS/MS analysis were purchased from Aldrich (Milano, Italy). Digestion buffer was obtained by dissolving NH_4HCO_3 in MilliQ water at the final concentration of 50 mM. The reducing solution was 100 mM DTT (dithiothreitol) in digestion buffer, and the alkylating solution was 100 mM IAA (iodoacetamide) in digestion buffer. Trypsin from porcine pancreas was used for protein digestion: the powder was reconstituted in $40\ \mu\text{L}$ of water +0.1% formic acid (FA).

2.15.1. Protein Digestion

A volume corresponding to $50\ \mu\text{g}$ of proteins was transferred to a new Eppendorf tube. Disulfide bonds were reduced by adding $10\ \mu\text{L}$ of reducing solution and incubating samples at $56\ ^\circ\text{C}$ for 30 min. Cysteine residues were alkylated by adding $30\ \mu\text{L}$ of alkylating solution, vortexing and incubating at RT for 20 min in the dark. After spinning the tubes, proteins were precipitated by adding 1 mL of cold acetone and incubating samples at $-20\ ^\circ\text{C}$ overnight. Samples were then centrifuged at $20,000\times g$ for 30 min at $4\ ^\circ\text{C}$, the supernatant was removed and the pellet was washed with $100\ \mu\text{L}$ of cold methanol, vortexed for 10 min and centrifuged at $20,000\times g$ for 30 min at $4\ ^\circ\text{C}$. The supernatant was discarded and protein pellets dried under the fume hood. The pellet was then redissolved in $200\ \mu\text{L}$ of digestion buffer (50 mM NH_4HCO_3), and $2\ \mu\text{L}$ of Trypsin ($0.5\ \mu\text{g}/\mu\text{L}$) was added. The samples were incubated at $37\ ^\circ\text{C}$ in a shaker at 600 rpm overnight for protein digestion. Sample tubes, now containing peptides, were then centrifuged at $20,000\times g$ for 30 min at $4\ ^\circ\text{C}$. The supernatant was transferred to new Eppendorf tubes and dried down in a speed-vac under vacuum. Peptides were then resuspended in $50\ \mu\text{L}$ of 3% acetonitrile to which was added 0.1% formic acid for LC-MS analysis.

2.15.2. LC-MS/MS Analysis

Tryptic peptides were analyzed by high-resolution LC-MS using a UPLC NanoAcquity chromatographic system (Waters, Milford, MA, USA) coupled with a TripleTof 5600+ mass spectrometer (Sciex, Warrington, UK) equipped with an electrospray ion source. Peptides were desalted using a trapping column (Guard column YMC-Triart C18, $3\ \mu\text{m}$ particle size, $0.5\times 5\ \text{mm}$, $1/32''$), then moved on a reversed-phase C18 column (Eksigent C18, $3\ \mu\text{m}$ particle size, $0.3\times 150\ \text{mm}$ format) and eluted with a gradient of acetonitrile (ACN) in water. Both eluents were added with 0.1% formic acid. Samples were acquired both in DIA (data-independent acquisition) and DDA (data-dependent acquisition) modes.

2.15.3. Peptide Chromatography

The eluents used were: A (water + 0.1% formic acid) and B (acetonitrile + 0.1% formic acid). Injection volume was $5\ \mu\text{L}$ (Full Loop), the flow rate was set to $5\ \mu\text{L}/\text{min}$, and the column temperature was kept at $45\ ^\circ\text{C}$. After trapping the sample on the trap column (at 1% ACN for 5 min), samples were eluted with the following gradient program: 0.0–1.0 min 5% B; 1.0–60.0 min 5 to 40% B; 60.0–63.0 min 40 to 95% B; 63.0–68.0 min 95% B;

and 68.0–68.1 min 95 back to 5% B. The column was then reconditioned for 11.9 min. The total run time was 80 min.

2.15.4. SWATH Acquisition

Acquisition in SWATH DIA (data-independent acquisitions), ESI+ was performed. A TOF MS scan was set from 350 to 1250 m/z . Then, 100 SWATH experiments were collected in the high sensitivity mode, each with an accumulation time of 25 ms, from 100 to 1500 m/z . The total cycle time was ~2.8 s. Collision energy for each window was automatically calculated by the acquisition software using the equation: $CE = 0.063 (m/z) - 3.24$ (parameter recommended by the vendor). The ion source parameters were: ion spray voltage floating at 5300 V, ion source gas 1 at 30, curtain gas at 30, and declustering potential at 80 V.

2.15.5. Data-Dependent Acquisition

The spectra were acquired in ESI+. The scan range was set from 300 to 1250 m/z for MS and from 100 to 1500 m/z for MS/MS. Precursor ions with charge states 2 and 5 with intensity greater than 150 counts were selected for MS/MS. Collision energy profiles were set according to SCIEX recommended settings. The ion source parameters were: ion spray voltage floating at 5000 V, ion source gas 1 at 20, curtain gas at 30, and declustering potential at 80 V.

2.16. Data Analysis

2.16.1. SWATH—Data Analysis

The raw data files were analyzed by using the SWATH Acquisition MicroApp 2.0.1.2133 of PeakView software 2.2 (SCIEX). The quantification was performed applying the following filters: number of peptides per protein at 6, number of transition per peptide at 6, peptide confidence threshold at 99%, FDR threshold at 1%, maximum mass tolerance at 50 ppm, and maximum RT tolerance at 20 min. The modified peptides were excluded. Multivariate data analysis and other statistics were performed by using the free online software MetaboAnalyst [24].

2.16.2. DDA—Data Analysis

Raw data were analyzed using Protein Pilot software (SCIEX). The Paragon Method used for protein identification employed a UniProt-reviewed human database; the confidence cut-off was set on 0.05, running the false discovery rate (FDR) analysis. Only protein identified with at least two peptides were retained.

2.17. Statistical Analyses

All statistical analyses were performed using GraphPad Prism 7 (GraphPad Software Inc., La Jolla, CA, USA). Data are expressed as mean \pm SEM. For normally distributed data, two-tailed unpaired Student's *t*-test was used. A *p*-value < 0.05 was considered significant.

3. Results

3.1. GCase Inhibition Induces a Neurodegenerative Phenotype

We developed two different in vitro neuronal models of GCase deficiency represented by CGN and human iPSCs-derived DA neurons treated with CBE.

The first experimental model is represented by CGN obtained upon the spontaneous differentiation of neuronal precursors isolated from postnatal day 5 C57BL/6 mouse cerebella. After 2 days in culture (DIC), cells were fed with [$1\text{-}^3\text{H}$]-sphingosine in order to label all cell sphingolipids (SLs) at the steady state. When cells reached the stage of CGN (4 DIC), they were treated with 0.5 mM CBE either for 7 days (short-term treatment) or 14 days (long-term treatment) (Figure S1a).

The second experimental model exploited the use of human iPSCs (Figure S2) obtained from fibroblasts of a healthy subject and differentiated for 29 days into a neuronal

population enriched in DA neurons, according to Zhang P. [18]. As reported in Figure S3, the protocol of neuronal differentiation allows to obtain, with a high yield, cells positive for the neuron-specific class III β -tubulin (Tuj1) and about 35% of cells positive for the DA marker tyrosine hydroxylase (TH). To perform the SL analyses, [^3H]-sphingosine was administered to mature DA neurons (29 DIC). At 31 DIC, cells were treated with 0.5 mM CBE for either 14 days (short-term treatment) or 29 days (long-term treatment) (Figure S1b).

Both short- and long-term CBE treatment were able to strongly reduce GCCase activity with a residual activity of 4% and 1% in CGN and DA neurons, respectively (Figure 1).

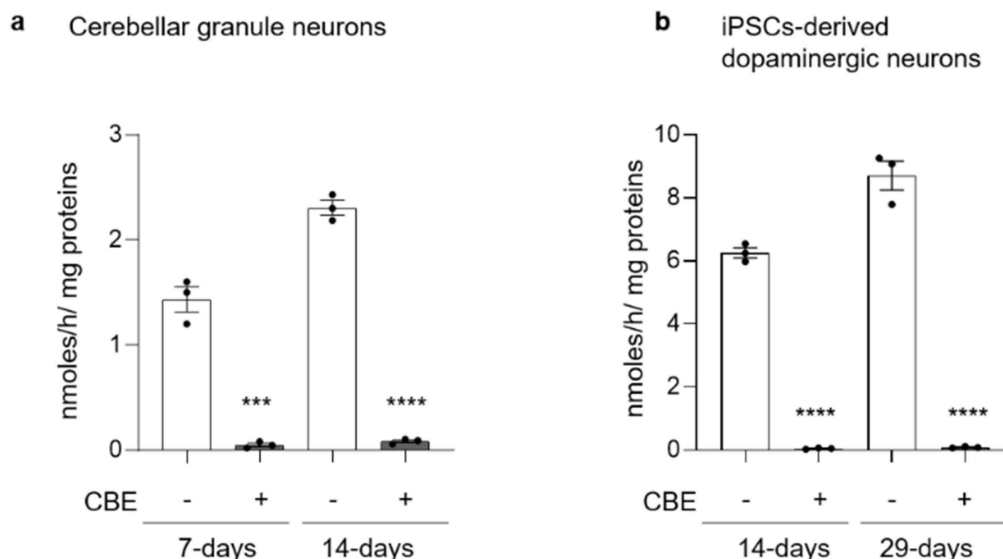


Figure 1. Effect of conduritol B epoxide treatment on β -glucocerebrosidase activity. β -glucocerebrosidase activity was evaluated in (a) mouse cerebellar granule neurons treated or not with 0.5 mM CBE for 7 or 14 days and (b) in human iPSC-derived dopaminergic neurons treated or not with 0.5 mM CBE for 14 or 29 days. β -glucocerebrosidase activity is expressed as nmoles of formed product/hour/mg cell proteins. All data are shown as mean \pm SEM of three different experiments. *** $p < 0.001$, **** $p < 0.0001$, two-tailed Student's t -test vs. CBE-untreated cells.

We evaluated the onset of neuronal damage assessing the expression of neuronal-specific markers by immunoblotting analysis both in CGN and in DA neurons after CBE treatment. As shown in Figure 2a, CGN subjected to short-term treatment with CBE did not show any significant variation in the protein levels of the neuronal markers NF-H, MAP2, TAU and PSD95. On the other hand, long-term treated CGN were characterized by a reduction in the protein levels of about 50% for NF-H, 60% for MAP2, 50% for TAU and 30% for PSD95. On the other side, DA neurons showed the onset of neurodegeneration at both time points. Upon short-term treatment with CBE, they were characterized by a reduced expression of about 40% of MAP2 and 70% of TAU (Figure 2b). Upon long-term treatment, the neuronal markers underwent a more evident decrease, with a reduction of 50% for NF-H, 60% for MAP2, 65% for TAU and 35% for PSD95 (Figure 2b). Moreover, we confirmed the degeneration of DA neurons treated with CBE (long-term treatment) by immunofluorescence analyses against MAP2 and Tuj1, showing neuritis fragmentation and degeneration (Figure S4a), and by the halving of the cell number compared to the untreated cells (Figure S4b).

These data indicate that a long-term inhibition of GCCase in CGN and human iPSCs-derived DA neurons resulted in a significant reduction in neuronal markers.

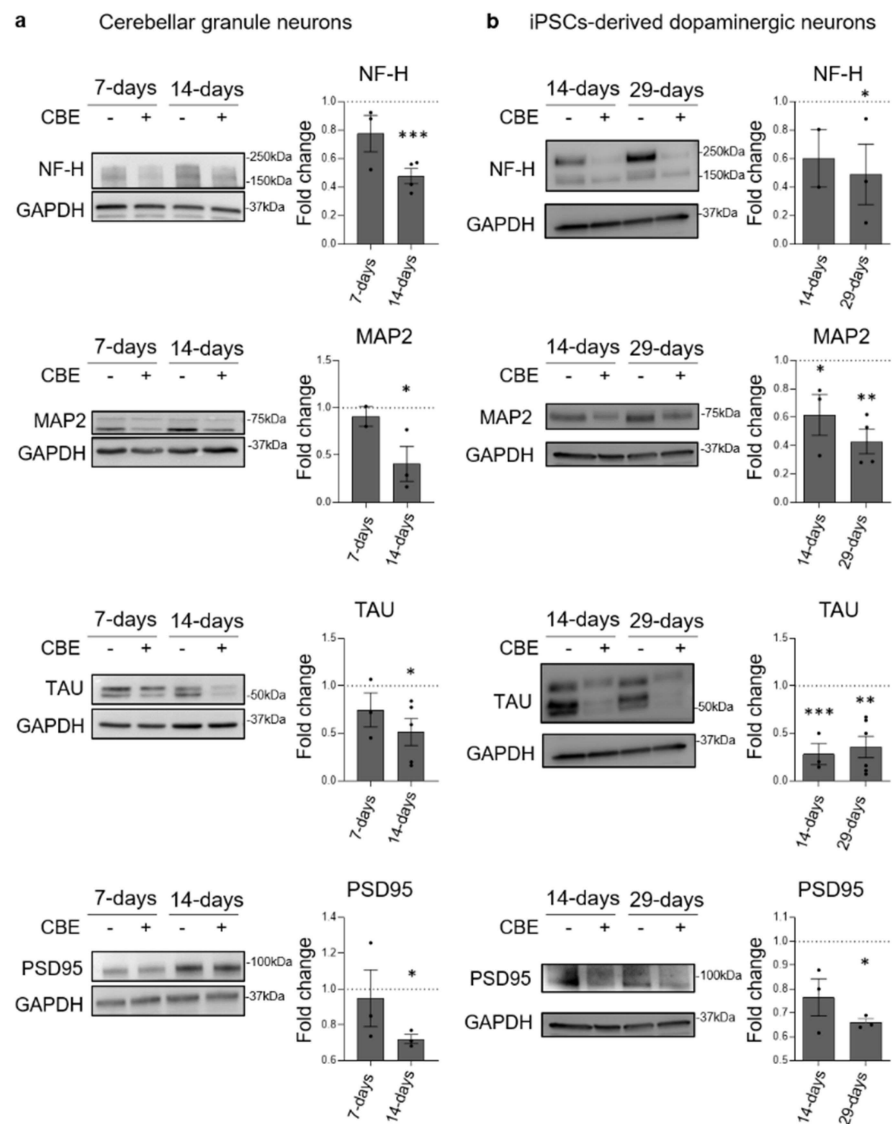


Figure 2. Effect of β -glucocerebrosidase inhibition on neuronal markers' expression. Immunoblotting analysis of the expression of Neurofilament H (NF-H), MAP2, TAU and PSD95 in: (a) mouse cerebellar granule neurons (CGN) treated or not with conduritol B epoxide (CBE) 0.5 mM for 7 and 14 days and (b) human iPSC-derived dopaminergic neurons treated or not with CBE 0.5 mM for 14 and 29 days. Optical densities of the individual bands were quantified using NIH ImageJ and normalized to GAPDH. Data are expressed as fold change with respect to CBE-untreated cells (dashed lined) and are the mean \pm SEM of three different experiments. * $p < 0.05$; ** $p < 0.01$; *** $p < 0.001$. Two-tailed Student's t -test vs. CBE-untreated cells.

3.2. GCase Inhibition Alters the SL Pattern

The radioactive lipids of CGN and DA neurons, untreated or treated with CBE, were analyzed by HPTLC. As shown in Figure 3, both cell models presented a significant and time-dependent accumulation of GlcCer compared to untreated cells. Specifically, short-term CBE-treated CGN and DA neurons showed an increase in GlcCer of seven- and five-fold compared to untreated cells, respectively. The analyses performed after long-term CBE treatment revealed a 10-times higher GlcCer content with respect to untreated cells in both cell models. To validate these data, we analyzed the endogenous counterpart by HPTLC and HPLC elution profile followed by ESI-MS analysis (Figures S5 and S6). Moreover, as shown in Figure 3 and Figure S7, upon the accumulation of GlcCer in CBE-treated neurons, we observed an increased production of its deacylated form glucosylsphingosine (GlcSph)

in both cell models. The role of GlcSph in the onset of cell toxicity is widely discussed in the literature [25–27]; therefore, we decided to investigate its effect on the viability of CGN and DA neurons by its exogenous administration. As shown in Figure S8a, no toxic effect was found in CGN upon administration of GlcSph even at high concentrations. DA neurons did not show the onset of cell toxicity at the lower concentration, whereas a 40% decrease of vitality was observed at the higher concentration of GlcSph (Figure S8b).

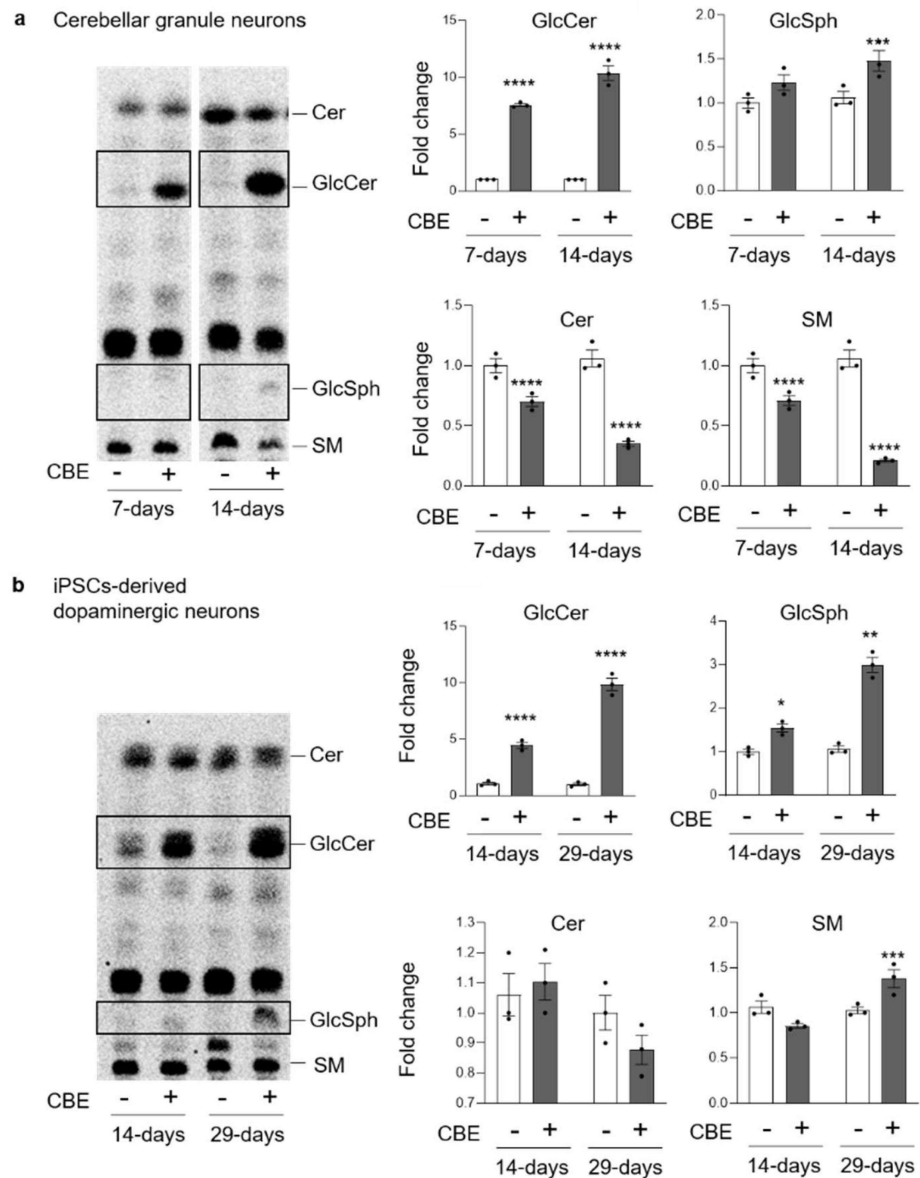


Figure 3. Effect of β -glucocerebrosidase inhibition on glucosylceramide and glucosylsphingosine levels. Representative digital autoradiography of sphingolipid pattern and quantification of the radioactivity associated with glucosylceramide (GlcCer), glucosylsphingosine (GlcSph), ceramide (Cer) and sphingomyelin (SM) in: (a) mouse cerebellar granule neurons fed with radioactive sphingosine and treated or not (–) with 0.5 mM conduritol B epoxide (CBE) for 7 and 14 days and (b) human iPSC-derived dopaminergic neurons fed with radioactive sphingosine and treated or not with CBE for 14 and 29 days. Data are expressed as fold change with respect to CBE-untreated cells (–) and are the mean \pm SEM of three different experiments. * $p < 0.05$; ** $p < 0.01$; *** $p < 0.001$; **** $p < 0.0001$. Two-tailed Student's t -test vs. CBE-untreated cells.

In CGN, we observed a decrease in Cer and SM content, which was more evident upon long-term CBE treatment with a reduction of about 50% and 70%, respectively (Figure 3a).

On the other hand, in DA neurons, we did not observe any significant change, except for SM that presented an increase of about 50% upon long-term CBE treatment (Figure 3b).

The analyses of the ganglioside pattern of CGN subjected to long-term CBE treatment revealed a 50% increase in the content of GM3 and GM2 accompanied by a slight reduction in the content of GQ1b (Figure S9a). In DA neurons, the effect of long-term CBE treatment on the ganglioside levels was more marked, with an increase of about two-fold in the content of GM3, GM1, and GD1a. Moreover, GD1b and GQ1b exhibited an increase of about 50% and 25%, respectively (Figure S9b).

Overall, these results show that, in both cell models, long-term GCase inhibition induced a time-dependent accumulation of GlcCer and GlcSph, together with an increased content of gangliosides.

3.3. GCase Inhibition Alters the Proteomic Profile

We performed a label-free expression proteomics analysis on DA neurons subjected or not to long-term CBE treatment. The proteomic analysis identified 70 upregulated (Table S1) and 71 downregulated (Table S2) proteins in CBE-treated neurons with respect to untreated ones. The bioinformatics analyses by DAVID software [28] (Data S1) showed that, among the upregulated proteins, there was a significant enrichment in proteins involved in the lysosomal structure and in the glycosphingolipids catabolism. In addition, we observed also an enrichment in proteins related to mitochondria activity and glycoproteins biosynthesis and trafficking (Figure 4a). Among the significantly enriched pathways, we further refined the investigation on the “sphingolipid metabolism” highlighted by DAVID. By using STRING, a database for interaction analysis and gene enrichment [29], we found that galactosylceramide catabolism is significantly enhanced following inhibition of GCase, mainly through the overexpression of galactosylcerebrosidase and prosaposin (Data S2). This result comes with little surprise, with the cell reacting to GCase inhibition by activating alternative sources for ceramide production.

On the other hand, the downregulated proteins were mainly integral component of membranes and trafficking proteins, such as RAB5, which suggested an impairment in the endocytosis processes, and RAB6, which is involved in the ER-Golgi-PM vesicular trafficking (Figure 4b). These data indicate that GlcCer accumulation due to GCase inhibition strongly affects neuronal proteostasis.

3.4. GlcCer Accumulation Affects the Lysosomal Compartment

A widely described mechanism occurring upon lysosomal impairment is the nuclear translocation of the transcription factor EB (TFEB), which is a master regulator of the expression of genes coding for proteins involved in compensatory processes aimed at counteracting the lysosomal accumulation of uncatabolized substrates [30,31]. We found that the nuclear translocation of TFEB was enhanced in both cell models after long-term CBE treatment (Figure S10). One of the described consequences of TFEB transcription activity is the activation of lysosomal biogenesis [30]. We evaluated the protein levels of the lysosomal marker LAMP1 in both cell models after long-term CBE treatment. As shown in Figure 5, LAMP1 expression was found to be increased of about 30% and 50% in CBE-treated CGN and DA neurons, respectively.

The staining of CGN with LysoTracker Red DND-99 indicated that CBE treatment caused an increase in the relative volume of the endo-lysosomal compartment (Figure S11a). The indirect immunofluorescence staining of LAMP1 in DA neurons corroborated the increased expression of the lysosomal marker after CBE treatment, suggesting an augmented number of lysosomes (Figure S11b). Electron microscopy analysis of DA neurons subjected to long-term CBE treatment confirmed the increase in the number of lysosomes and also suggested an increase in their size (Figure S11c). Furthermore, we investigated the lysosomal catabolic potential by feeding untreated and long-term CBE-treated CGN with radioactive [3-³H(sphingosine)]GM1 [32]. The use of GM1 derivative, which is radioactive on the sphingosine moiety, allowed to follow the production of its

catabolites in living cells, giving an indication of lysosomal catabolic activity. The uptake of the radioactive ganglioside was the same in both untreated and CBE-treated CGN (data not shown). As shown in Figure S12, we found a reduced production of radioactive GM1 catabolites, such as GM3, lactosylceramide, GlcCer and Cer in CBE-treated CGN, suggesting an impairment of lysosomal catabolism. Of note, the reduction in radioactive globoside Gb3, whose biosynthesis depends on 3-³H(sphingosine) salvage pathway, further supported lysosomal dysfunction in CBE-treated neurons.

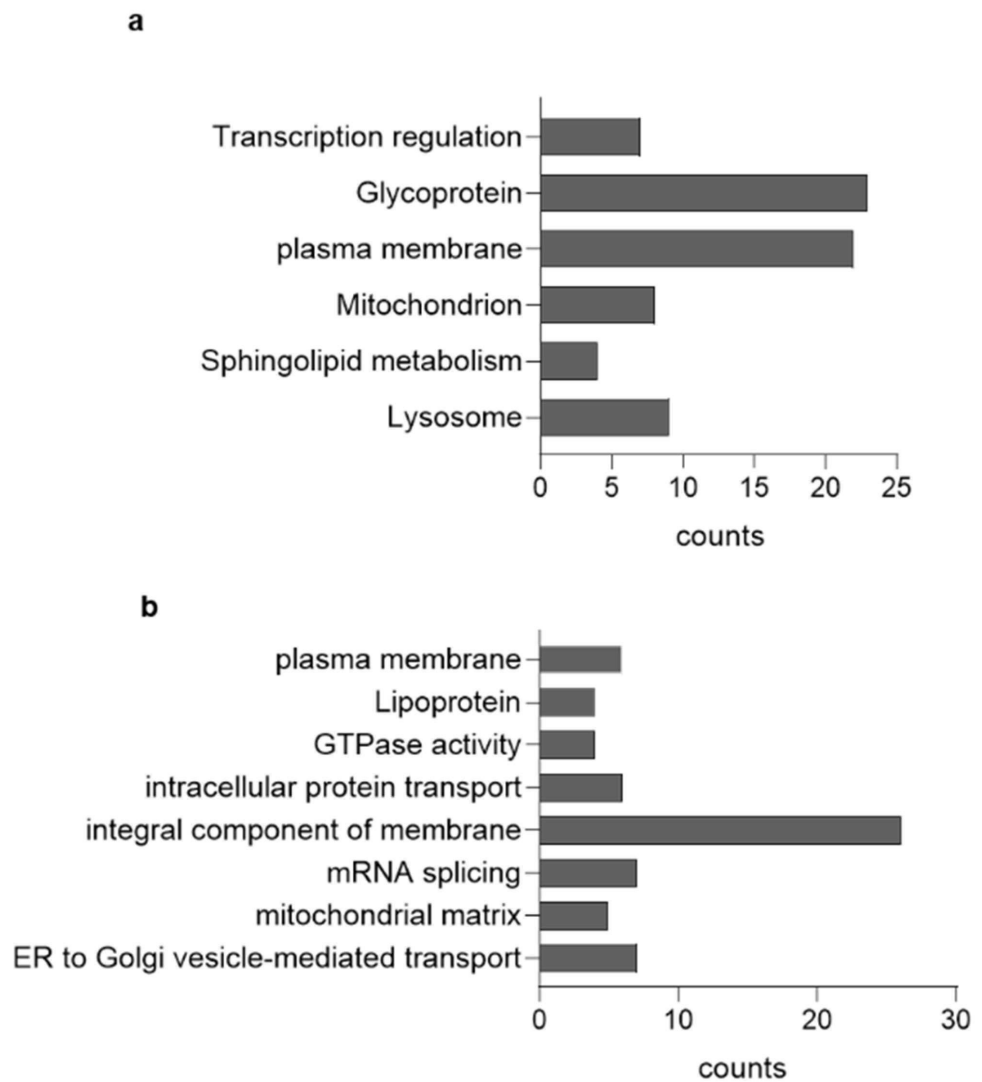


Figure 4. Effect of β -glucocerebrosidase inhibition on proteomic profile. Bar chart showing the cluster enriched annotation groups of proteins (a) upregulated and (b) downregulated in CBE-treated DA neurons with respect to untreated cells obtained by David bioinformatics analysis. The x-axis indicates the number of proteins involved in each term.

Taken together, these results indicate that long-term GCase inhibition induced the biogenesis of lysosomes, which in turn presented a reduced catabolic potential, suggesting an impairment of lysosomal activity.

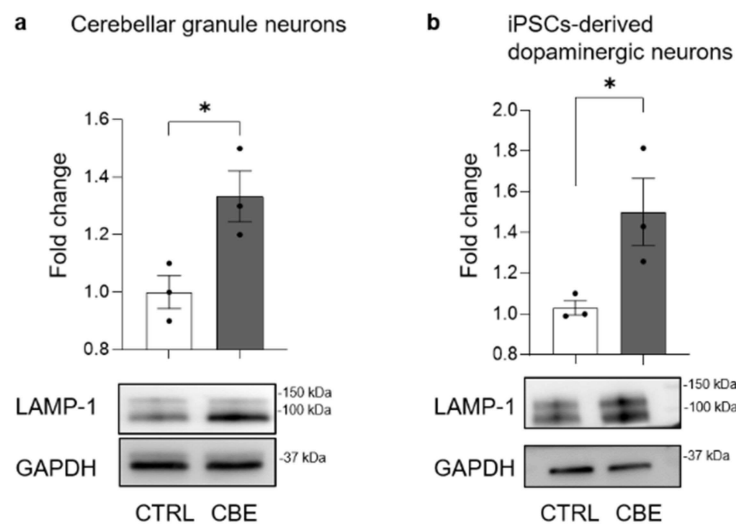


Figure 5. Effect of glucosylceramide accumulation on lysosomal-associated membrane protein-1 expression. Immunoblotting analyses of lysosomal-associated membrane protein (LAMP-1) in (a) mouse cerebellar granule neurons and (b) human iPSC-derived dopaminergic neurons treated or not with 0.5 mM conduritol B epoxide (CBE) for 14 and 29 days, respectively. Data are expressed as fold change with respect to CBE-untreated cells (CTRL) and are the mean \pm SEM of three experiments; * $p < 0.05$, two-tailed Student's *t*-test vs. CBE-untreated cells.

3.5. GCCase-Inhibited Neurons Are Characterized by Aberrant Lysosomal Exocytosis

It is already well established that lysosomal impairment and TFEB transcription activity lead to the activation of aberrant lysosomal exocytosis [30]. The fusion of lysosomes with the PM induces the release of lysosomal content in the extracellular environment and the association of lysosomal glycohydrolases with the external leaflet of the PM. To investigate this process, the enzymatic activity of specific lysosomal glycohydrolases was evaluated at PM level [22]. As shown in Figure 6a, in long-term CBE-treated CGN we found an increase of about 50% in the activity of the PM-associated β -galactosidase. In long-term CBE-treated DA neurons, there was an increase of about two-fold in the activity of both the PM-associated β -galactosidase and β -hexosaminidase (Figure 6b).

Subsequently, we observed an increase in the release of GlcCer in the extracellular milieu of about 50% in CBE-treated CGN and 25% in DA neurons compared to untreated cells (lower panel Figure 6a,b).

These data demonstrate that long-term GCCase inhibition in CGN and DA neurons caused an increased lysosomal exocytosis and consequently led to the release of the uncatabolized GlcCer in the extracellular milieu.

3.6. GlcCer Accumulation Is Not Confined to Lysosomes

In other LSDs, the impairment of the lysosomal compartment due to the accumulation of uncatabolized substrates is accompanied by modifications in the lipid composition of the PM [30]. To investigate this aspect, we fed CGN and DA neurons with [1-³H]-sphingosine that was equally incorporated by neurons (data not shown).

At the end of long-term CBE treatment, PM proteins and the surrounding lipids were isolated exploiting a biotin–streptavidin affinity pull-down assay. The radioactive lipids were extracted from the precipitate (P) and from the supernatant (SN) obtained after precipitation and the corresponding proteins were denatured to assess the efficiency of precipitation. The biotinylated proteins recovered in the P fraction were about 80% in CGN and 90% in DA neurons independently from the CBE treatment (data not shown). In DA neurons, precipitated proteins were then identified by high resolution mass spectrometry, following digestion with trypsin. A list of 72 proteins was confidently identified as exclusively expressed at the PM level of CBE treated neurons (Table S3). An interaction analysis

reveals that 44 out of 72 proteins show significant functional association, as demonstrated in Figure S13. Furthermore, several molecular functions were found to be significantly enriched in this organic insoluble fraction (Data S3). We then explored possible known functional associations between this dataset and the target GCase. No major molecular interactions were highlighted by our analysis.

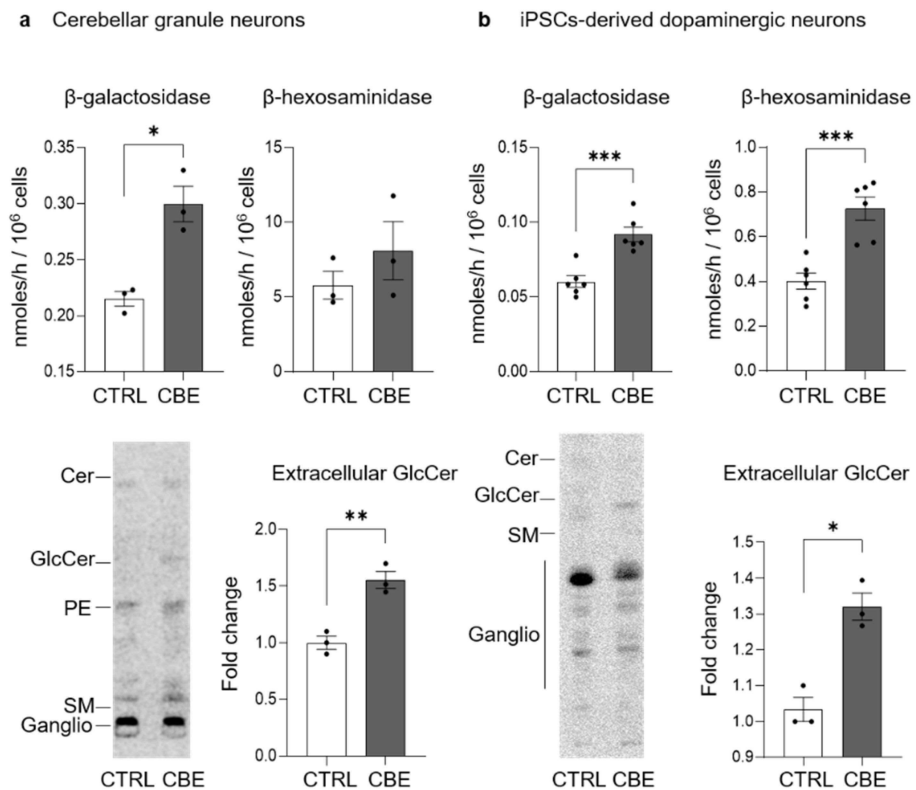


Figure 6. Activity of plasma membrane glycohydrolases and extracellular release of glucosylceramide upon its accumulation. Specific enzyme activity of plasma membrane-associated β -galactosidase and β -hexosaminidase and representative image and quantification of extracellular release of glucosylceramide (GlcCer) in (a) mouse cerebellar granule neurons and (b) human iPSC-derived dopaminergic neurons fed with radioactive sphingosine followed by treatment in presence or in absence of 0.5 mM conduritol B epoxide (CBE) for 14 and 29 days, respectively. Enzyme activities are expressed as nmoles/h normalized to 10^6 cells and are the mean \pm SEM of three experiments (* $p < 0.05$, *** $p < 0.001$, two-tailed Student's t -test vs. CBE-untreated cells (CTRL)). Extracellular release of radioactive GlcCer was determined after the lipid extraction of cell culture medium and HPTLC separation (Cer = ceramide, PE = phosphatidylethanolamine, SM = sphingomyelin, ganglio = gangliosides). Data are expressed as fold change with respect to CBE-untreated cells (CTRL) and are the mean \pm SEM of three experiments; * $p < 0.05$, ** $p < 0.01$, *** $p < 0.001$, two-tailed Student's t -test vs. CBE-untreated cells.

Regarding the radioactive lipids, 41% was associated with the P fraction of untreated CGN, while 61% was recovered in the P fraction obtained from CBE-treated CGN. Similarly, in the P of untreated DA neurons, we found 40% of radioactivity which increased up to 60% in case of CBE treatment (data not shown). As shown in Figure 7, the analyses of the radioactive lipids of the SN and P revealed that in CBE-treated CGN and DA neurons, the accumulation of GlcCer in the SN was about 12-fold and 6-fold compared to untreated neurons, respectively. Interestingly, a more marked increase was observed in the P fraction, which was approximately 30-fold and 18-fold higher in CBE-treated CGN and DA neurons, respectively (Figure 7).

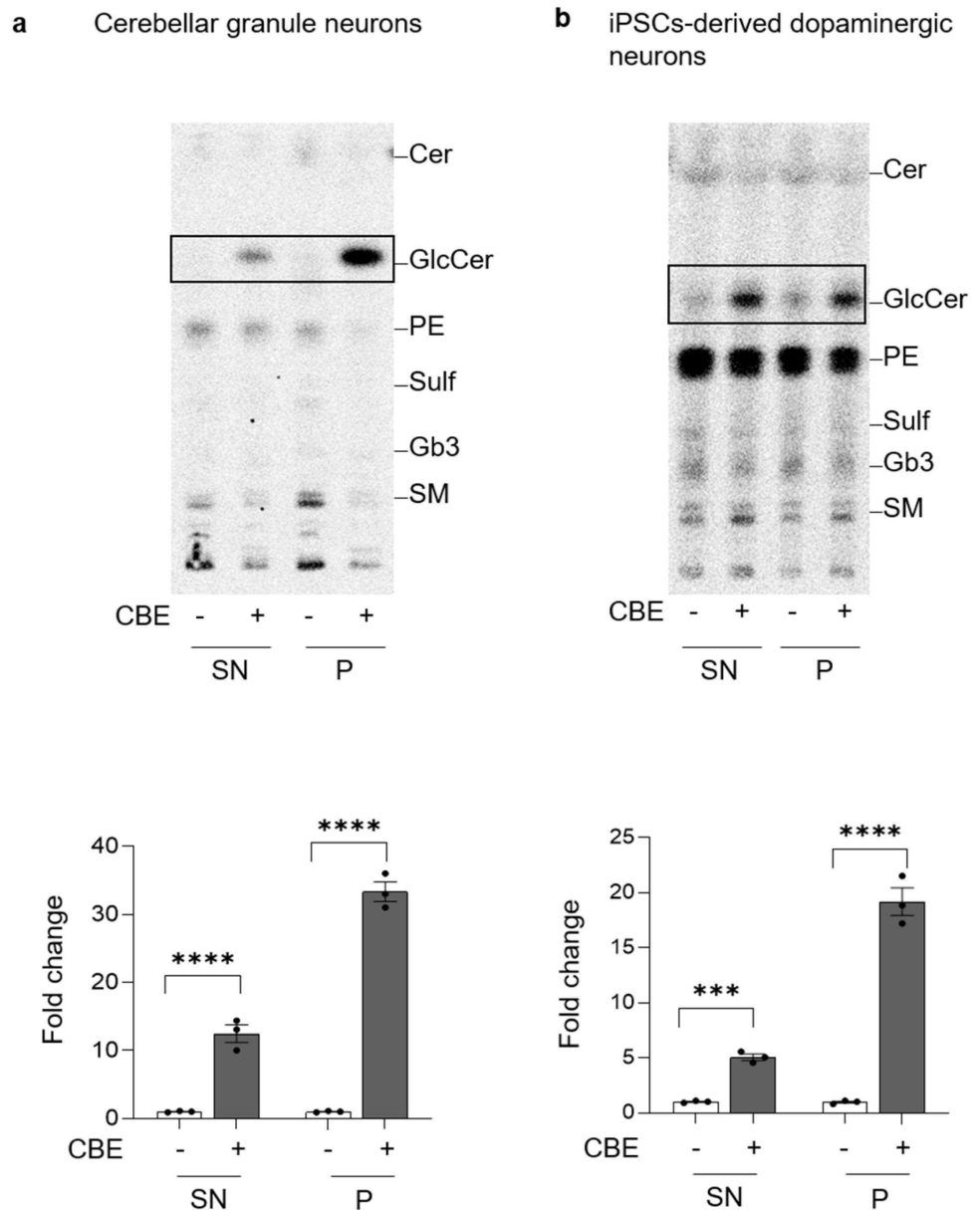


Figure 7. Accumulation of glucosylceramide at the cell surface. Representative HPTLC image of radioactive lipids of cell fractions obtained after selective cell surface protein biotinylation followed by magnetic separation using Dynabeads™ streptavidin magnetic beads; lipids were extracted from the supernatants containing non biotinylated proteins (SN) and the pellets containing the biotinylated cell surface proteins (P); (a) mouse cerebellar granule neurons and (b) human iPSC-derived dopaminergic neurons treated or not (–) with 0.5 mM conduritol B epoxide (CBE), for 14 and 29 days, respectively. (Cer = ceramide; GlcCer = glucosylceramide; PE = phosphatidylethanolamine; SM = sphingomyelin). Data are expressed as fold change of GlcCer with respect to CBE-untreated cell fraction (–) and are the mean ± SEM of three experiments (***p* < 0.001; *****p* < 0.0001; one-way two-tailed Student’s *t*-test vs. CBE-untreated cells). GlcCer content was normalized nCi/ mg of proteins of the sample.

These data show that the chronic inhibition of GCase induced changes in the PM protein composition and accumulation of GlcCer.

3.7. GCase Inhibition Induces Changes in PM Microdomains

In the PM, SLs together with cholesterol and a selected number of proteins organize macromolecular complexes involved in the control of signaling cascades [33,34]. Based on these considerations, we analyzed these microdomains (DRM) in DA neurons treated or not with CBE [33].

To this purpose, DRM domains were isolated from DA neurons subjected to long-term CBE-treatment. DRM represented the low-density detergent insoluble fractions (fraction 5 and 6) obtained by loading the same protein amount of cell lysates on a sucrose density gradient, while the high-density fractions (HD) contained all the remaining cell components. The 12 collected fractions of both CBE-treated and -untreated DA neurons were assessed for the presence of flotillin, a DRM marker, and calnexin, a typical non-DRM-associated protein, as well as for the radioactivity content. As shown in Figure S14a, flotillin was enriched in fractions 5 and 6, whereas calnexin was detectable only in HD fractions 10, 11 and 12.

The radioactivity associated with SLs was enriched in fractions 5 and 6 with respect to the fractions 10, 11 and 12 (Figure S14b). Based on these data, fractions 5 and 6 were pooled together as DRM, while fractions 10, 11 and 12 were considered as HD.

Interestingly, the radioactivity associated with DRM of untreated DA neurons was about 41% of the total and increased up to 66% in CBE-treated cells (Figure S14b). The analyses of the radioactive lipids revealed that DRM fractions were enriched in SLs at the expense of phosphatidylethanolamine (PE) when compared to HD (Figure S14c).

From the SL pattern of DRM, it clearly emerged that in CBE-treated DA neurons the increased radioactivity was mainly due to an augmented content of GlcCer (Figure 8a). To evaluate the effect of CBE only in PM-DRM excluding any contribute of DRM from intracellular membranes, we submitted DRM to biotin–streptavidine affinity pull-down assay in conditions preserving DRM integrity. The radioactive lipids were extracted from the P and SN fractions obtained after precipitation, and the corresponding proteins were denatured to assess the efficiency of precipitation. About 90% of the biotinylated proteins were recovered in the P, independently from the CBE treatment (data not shown). In addition, the P fraction of untreated and CBE-treated neurons contained, respectively, 95% and 90% of the total amount of radioactive lipids associated with DRM (data not shown).

The analyses of the radioactive lipid pattern showed that PM-DRM of CBE-treated DA neurons were characterized by a 11-fold increase in GlcCer content and by the halving of Cer levels compared to untreated DA neurons (Figure 8b). Conversely, a two-fold enrichment in the active form of c-Src (pTyr416-Src) was found in DRM of CBE-treated DA neurons with respect to untreated cells (Figure 8c).

Overall, these results show that GlcCer accumulated in specific PM signaling microdomains, altering their SL and protein pattern.

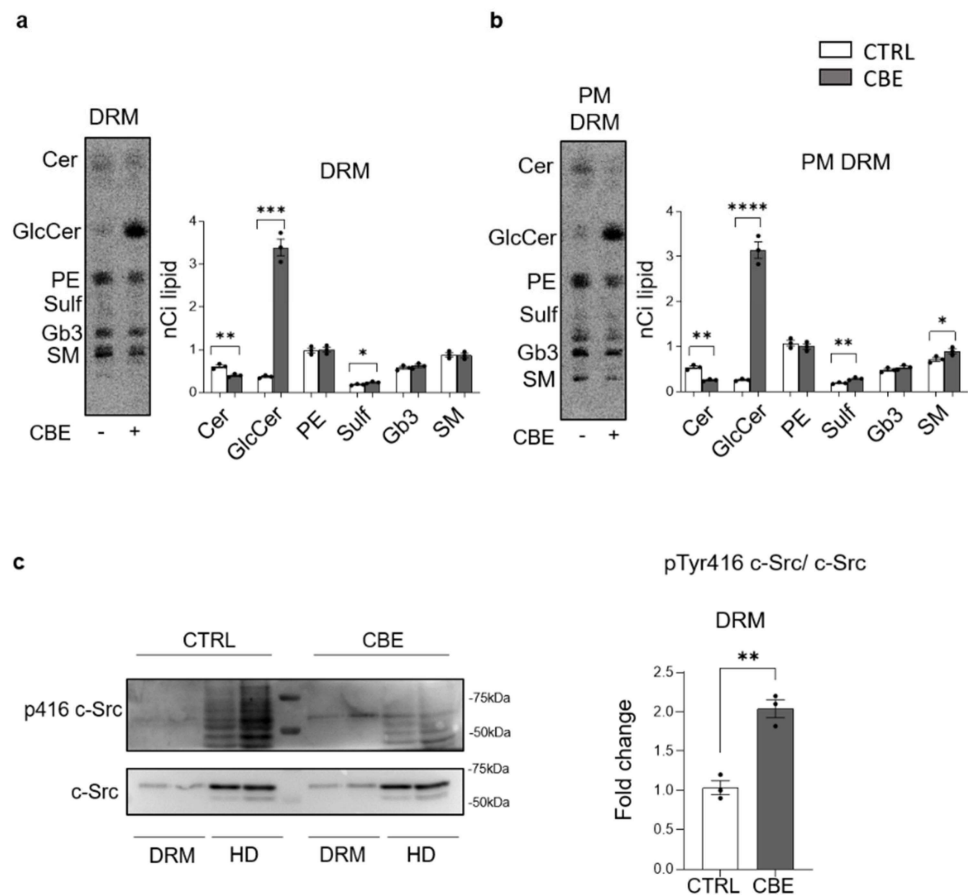


Figure 8. p416 c-Src expression and lipid distribution in detergent-resistant plasma membrane fractions of iPSCs-derived dopaminergic neurons treated or not with conduritol B epoxide. (a) Representative image of HPTLC of radioactive lipids of detergent-resistant membrane domain fraction (DRM) of human iPSCs-derived dopaminergic neurons treated or not (–) with 0.5 mM conduritol B epoxide (CBE) for 29 days. (b) Representative image of HPTLC of radioactive lipids of detergent-resistant membrane domain fraction (DRM) after cell surface biotinylation of human iPSCs-derived dopaminergic neurons treated or not (–) with 0.5 mM conduritol B epoxide (CBE) for 29 days. Detergent-resistant plasma membrane domain fraction (PM-DRM) was obtained from DRM by streptavidine magnetic beads separation. Data are expressed as nCi and are the mean \pm SEM from at least three experiments (* $p < 0.05$; ** $p < 0.01$; *** $p < 0.001$; **** $p < 0.0001$; two-tailed Student's *t*-test). (Cer = ceramide; GlcCer = glucosylceramide; PE = phosphatidylethanolamine; Sulf = sulphatides; Gb3 = globo-triaosylceramide; SM = sphingomyelin). (c) Immunoblotting analysis of Src and pTyr416 c-Src expression in DRM fraction and non-DRM high density fractions (HD) of dopaminergic neurons treated or not with CBE for 29 days; analysis of pTyr416 c-Src activation: pTyr416 c-Src band intensity was normalized to c-Src signal of the same sample. Data are expressed as fold change with respect to CBE-untreated cell fraction of and are the mean \pm SEM of at least three experiments; ** $p < 0.01$; two-tailed Student's *t*-test.

4. Discussion

Mutations in the *GBA1* gene are associated with several neurodegenerative disorders, such as Gaucher disease, Parkinson's disease, dementia with Lewy bodies, rapid eye movement disorder, and sleep behavior disorders [1,35–39]. Nevertheless, the pathogenic role of mutated *GBA1* is still a cause of debate in the scientific community. An increasing amount of evidence supports GCase loss of function and the consequent impairment of GlcCer metabolism at the basis of the onset of neurodegenerative phenotypes [13,40]. The main limitation of the study of the molecular mechanisms linking GlcCer accumulation to the onset of neuronal damage is the lack of suitable in vitro or in vivo models. Indeed,

studies on post-mortem human brain derived from GD patients are limited by their low availability, rapid deterioration, and impossibility to perform analyses on the involved molecular pathways. Moreover, *GBA1* knock-out mice with complete enzyme deficiency die within 24 h after birth, while single-allele knockout mice do not show nigrostriatal degeneration or PD-like phenotype. Finally, immortalized cells carry intrinsic artefacts, undergoing continuous mutations during the different passages in culture, thus presenting an unstable genotype and consequently a variable phenotype. In addition, patient-derived iPSCs are influenced by the donor patient's genotype [41–43].

Here, we proposed to develop novel in vitro models able to recapitulate, in a reasonable timing, the phenotype of neurons affected by GCase deficiency. In particular, we took advantage of two different neuronal cultures: one represented by CGN derived from pups of WT C57BL/6 mice and the other consisting of human DA neurons differentiated from iPSCs derived from a healthy subject. Both neuronal models were treated with CBE to induce GCase deficiency [16]. We selected two different neuronal populations derived from distinct species to test whether the effect of GCase inhibition on neuronal homeostasis was shared by neurons with different activity and origin.

Interestingly, we discovered that long-term GCase inhibition is required to induce a sufficient GlcCer accumulation able to cause a neurodegenerative phenotype, suggesting the existence of a tolerance threshold that, once overcome, leads to cell toxicity. In GD patients, the lysosomal accumulation of GlcCer causes the aberrant production of GlcSph by the action of the acid ceramidase [44]. Of note, considering the detergent-like physical-chemical properties of GlcSph, a possible role of this catabolite in the onset of neurodegeneration has been hypothesized [25,27]. To exclude its involvement in the onset of neuronal damage in our model, we verified that GlcSph does not exert any toxic effect at the concentration found in GD patients, whereas the treatment with high concentration of GlcSph partially affects the viability of DA neurons only. In addition, we can exclude the toxic effect of another sphingolipid known to be involved in the activation of the apoptotic process, the ceramide. In particular, we found that its level decreased in CGN, probably because cells do not activate a compensatory mechanism involved in its de novo biosynthesis in order to deal with the reduced availability of sphingosine due to the block of glucosylceramide catabolism. Conversely, we can speculate that such mechanism was activated in DA neurons, since the levels of ceramide are the same in treated and untreated neurons.

Interestingly, label-free expression proteomic analysis identified changes in the expression of 141 proteins in CBE treated DA neurons with respect to untreated cells. In particular, the expression of 70 proteins was upregulated, while 71 proteins were downregulated, suggesting that the GlcCer accumulation due to GCase inhibition has a general impact on neuronal proteostasis.

Our models also recapitulate the secondary accumulation of uncatabolized complex SLs, such as gangliosides, which is a common feature observed in several LSDs due to an impairment in the catabolic activity of the endo-lysosomal compartment [45,46]. Nowadays, we know that cells can counteract this impairment by activating a compensatory mechanism, which includes the activation of the transcriptional factor EB, responsible for the promotion of lysosomal biogenesis and exocytosis. These two evolutionary conserved events are activated to reduce as much as possible the accumulated material and restore the proper lysosomal function [29,30,46]. In particular, the release of material in the extracellular milieu could be attributed to cells belonging to organs characterized by an intense vascularization or by a parenchyma formed by cells that can recycle or store the released material. Notably, we demonstrated that the accumulation of uncatabolized substrate induces the promotion of lysosomal exocytosis. This observation suggests a new pathogenic mechanism, since in patient's brain the material released by impaired neurons could be poorly absorbed by the endothelial cells and could activate astrocytes and glial cells, turning on neuronal inflammation and allowing the self-propagation of the disease to other brain areas [47].

In addition, we found that, in GCCase-deficient neurons, which accumulate high levels of GlcCer, the aberrant activation of lysosomal exocytosis is also responsible for alterations in the PM architecture. Indeed, we found that GlcCer accumulation is not only confined to lysosomes but occurs also at PM level, affecting also its protein composition. In particular, by high resolution mass spectrometry we found a list of 72 proteins that were only expressed at the PM of CBE treated neurons.

GSLs are particularly enriched in membrane domains called “lipid rafts” or “DRM” [48–50]. These discontinuous portions of the PM are fundamental signaling platforms through which cells can regulate extracellular stimuli and modulate the signal transduction [51,52]. Structural alterations have been described in DRM derived from organs of GD animals and from in vitro GD models represented by immortalized cell lines [53,54]. Conversely, no data exist on the effect of GCCase deficiency in DRM of neurons.

Based on these premises, we focused our analysis on PM DRM obtained from CBE-treated and untreated DA neurons, where we observed the accumulation of GlcCer. In these domains, SLs spontaneously segregate, determining their enrichment at the expense of glycerophospholipids. For this reason, the GlcCer inserted in the PM, preferentially localizes in these specific areas. This could explain the different GlcCer enrichment observed by the analysis of the entire PM or PM DRM.

An increasing amount of evidence has shown the importance of DRM in the maintenance of cell homeostasis and modifications in their structure are often associated with important changes in cell functioning and phenotype [34,55]. Remarkably, we demonstrated for the first time that, in pathological neurons, the accumulation of GlcCer occurs also in the PM DRM, causing alterations of the protein composition of these domains. In particular, we found a local hyperactivation of c-Src, a non-receptor protein kinase involved in several intracellular signaling pathways, fundamental for the neuronal homeostasis [56,57].

Usually, the activation of c-Src induces its own translocation outside the DRM, event necessary to exert its functions. In particular, the translocation of the active form of c-Src is promoted by the enrichment of ceramide in DRM [58,59]. In our models, the reduction in ceramide due to the accumulation of GlcCer within PM DRM could sequester the activated c-Src, avoiding its functioning.

Even though this aspect needs to be further investigated, it opens a new perspective on putative targets for novel therapeutic strategies.

Taken together, our data indicate a direct role of the accumulated GlcCer in the onset of neuronal damage (Figure S12). Interestingly, we observed GlcCer accumulation also at the PM level, in particular in DRM domains. In addition, our observations strengthened the existence of a pathogenic lysosome–PM axis that determines alterations of the PM architecture, contributing to the establishment of the neurodegenerative phenotype. Our work establishes two reliable neuronal models to study the impact of GCCase deficiency in neurons and opens a new scenario on the study of GCCase-related neurodegenerative disorders.

Supplementary Materials: The following supporting information can be downloaded at: <https://www.mdpi.com/article/10.3390/cells11152343/s1>, Figure S1: Generation of in vitro neuronal models of β -glucocerebrosidase deficiency; Figure S2: Evaluation of the differentiation of iPSC-derived dopaminergic neurons by immunofluorescence analysis; Figure S3: Effect of CBE treatment on dopaminergic neurons differentiation; Figure S4: Effect of GCCase inhibition on GlcCer level; Figure S5: HPLC elution profiles of total lipid extracts and ESI-MS analyses of glucosylceramide; Figure S6: HPLC elution profiles of total lipid extracts and ESI-MS analyses of glucosylsphingosine; Figure S7: Effect of GlcSph administration on cell viability of mouse cerebellar granule neurons; Figure S8: Effect of β -glucocerebrosidase inhibition on ganglioside levels; Figure S9: Evaluation of lysosomal biogenesis upon glucosylceramide accumulation; Figure S10: Evaluation of lysosomal catabolism of glycosphingolipids upon glucosylceramide accumulation; Figure S11: Interactome of plasma membrane proteins isolated from CBE-treated neurons; Figure S12: Characterization of Detergent Resistant Membrane fractions; Table S1: List of the proteins upregulated in CBE-treated neurons compared to untreated cells; Table S2: List of the proteins down-regulated in CBE-treated

neurons compared to untreated cells; Table S3: List of the proteins only expressed in the IP of CBE-treated neurons in the comparison CBE-treated vs. CBE-untreated neurons; Data S1: DAVID enrichment analyses; Data S2: STRING enrichment analyses; Data S3: STRING enrichment analyses on precipitated proteins.

Author Contributions: G.L. and E.V.C. performed the experiments, analyzed the data and participated in writing the manuscript; N.L. (Nicoletta Loberto) performed endogenous lipid analyses; L.C. performed the immunoblotting analyses; S.P. prepared the cerebellar granule neurons; L.M. performed the mass spectrometry analyses and prepared radioactive lipid derivatives; A.D.F., E.F. (Emanuele Frattini) and M.M. contributed in iPSC generation and characterization and in iPSCs differentiation toward neurons; M.S. and E.F. (Elena Ferrari) performed the experiments on cerebellar granule neurons; S.D., L.S., G.S., R.A. and R.B., equally contributed in the interpretation of data and in editing the content of this manuscript; A.A. and N.L. (Nara Liessi) performed the proteomic analysis; M.S. and M.A. designed and coordinated the study, analyzed the data and wrote the manuscript. All authors have read and agreed to the published version of the manuscript.

Funding: This research was funded by Ministero dell'Università e della Ricerca (PRIN 2017) and by Cariplo foundation (cariplo2015) to Massimo Aureli.

Institutional Review Board Statement: The animal study protocol was approved by the Ethics Committee of the University of Milano (protocol code FD611.N.TAQ of 04/12/2017).

Informed Consent Statement: Not applicable.

Data Availability Statement: The data sets generated and analyzed during the current study are available from the corresponding author on reasonable request.

Acknowledgments: The authors thank Maria Carla Panzeri (Advanced Light and Electron Microscopy BioImaging Center, an advanced microscopy laboratory established by IRCCS San Raffaele Hospital and Vita-Salute San Raffaele University, Milan, Italy) for expert assistance in electron microscopy imaging. We would like to honor the memory of Stefano Duga by dedicating this manuscript to him.

Conflicts of Interest: The authors declare no conflict of interest.

Abbreviations

GCase	β -glucocerebrosidase;
GSL	glycosphingolipid;
GlcCer	glucosylceramide;
GD	Gaucher disease;
LSD	lysosomal storage disorder;
PD	Parkinson's disease;
CGN	cerebellar granule neurons;
iPSC	induced pluripotent stem cell;
DA	dopaminergic;
CBE	conduritol B epoxide;
PM	plasma membrane;
SL	sphingolipid;
DIC	days in culture;
TH	tyrosine hydroxylase;
GlcSph	glucosylsphingosine;
P	precipitate;
SN	supernatant;
HD	high-density fractions;
DRM	detergent resistant membrane.

References

1. Stirnemann, J.; Belmatoug, N.; Camou, F.; Serratrice, C.; Froissart, R.; Caillaud, C.; Levade, T.; Astudillo, L.; Serratrice, J.; Brassier, A.; et al. A Review of Gaucher Disease Pathophysiology, Clinical Presentation and Treatments. *Int. J. Mol. Sci.* **2017**, *18*, 441. [[CrossRef](#)] [[PubMed](#)]
2. Chiricozzi, E.; Aureli, M.; Mauri, L.; Di Biase, E.; Lunghi, G.; Fazzari, M.; Valsecchi, M.; Carsana, E.V.; Loberto, N.; Prinetti, A.; et al. Glycosphingolipids. *Adv. Exp. Med. Biol.* **2021**, *1325*, 61–102. [[CrossRef](#)] [[PubMed](#)]
3. Lwin, A.; Orvisky, E.; Goker-Alpan, O.; LaMarca, M.E.; Sidransky, E. Glucocerebrosidase mutations in subjects with parkinsonism. *Mol. Genet. Metab.* **2004**, *81*, 70–73. [[CrossRef](#)] [[PubMed](#)]
4. Goker-Alpan, O.; Schiffmann, R.; LaMarca, M.E.; Nussbaum, R.L.; McInerney-Leo, A.; Sidransky, E. Parkinsonism among Gaucher disease carriers. *J. Med. Genet.* **2004**, *41*, 937–940. [[CrossRef](#)] [[PubMed](#)]
5. Eblan, M.J.; Walker, J.M.; Sidransky, E. The glucocerebrosidase gene and Parkinson's disease in Ashkenazi Jews. *N. Engl. J. Med.* **2005**, *352*, 728–731, author reply 728–731. [[CrossRef](#)]
6. Sidransky, E. Heterozygosity for a Mendelian disorder as a risk factor for complex disease. *Clin. Genet.* **2006**, *70*, 275–282. [[CrossRef](#)]
7. Straniero, L.; Asselta, R.; Bonvegna, S.; Rimoldi, V.; Melistaccio, G.; Solda, G.; Aureli, M.; Della Porta, M.; Lucca, U.; Di Fonzo, A.; et al. The SPID-GBA study: Sex distribution, Penetrance, Incidence, and Dementia in GBA-PD. *Neurol. Genet.* **2020**, *6*, e523. [[CrossRef](#)]
8. Gegg, M.E.; Burke, D.; Heales, S.J.; Cooper, J.M.; Hardy, J.; Wood, N.W.; Schapira, A.H. Glucocerebrosidase deficiency in substantia nigra of parkinson disease brains. *Ann. Neurol.* **2012**, *72*, 455–463. [[CrossRef](#)]
9. Seo, B.A.; Kim, D.; Hwang, H.; Kim, M.S.; Ma, S.X.; Kwon, S.H.; Kweon, S.H.; Wang, H.; Yoo, J.M.; Choi, S.; et al. TRIP12 ubiquitination of glucocerebrosidase contributes to neurodegeneration in Parkinson's disease. *Neuron* **2021**, *109*, 3758–3774.e3711. [[CrossRef](#)]
10. Dilsizoglu Senol, A.; Samarani, M.; Syan, S.; Guardia, C.M.; Nonaka, T.; Liv, N.; Latour-Lambert, P.; Hasegawa, M.; Klumperman, J.; Bonifacino, J.S.; et al. alpha-Synuclein fibrils subvert lysosome structure and function for the propagation of protein misfolding between cells through tunneling nanotubes. *PLoS Biol.* **2021**, *19*, e3001287. [[CrossRef](#)]
11. Murphy, K.E.; Gysbers, A.M.; Abbott, S.K.; Tayebi, N.; Kim, W.S.; Sidransky, E.; Cooper, A.; Garner, B.; Halliday, G.M. Reduced glucocerebrosidase is associated with increased alpha-synuclein in sporadic Parkinson's disease. *Brain* **2014**, *137*, 834–848. [[CrossRef](#)] [[PubMed](#)]
12. Goker-Alpan, O.; Hruska, K.S.; Orvisky, E.; Kishnani, P.S.; Stubblefield, B.K.; Schiffmann, R.; Sidransky, E. Divergent phenotypes in Gaucher disease implicate the role of modifiers. *J. Med. Genet.* **2005**, *42*, e37. [[CrossRef](#)] [[PubMed](#)]
13. Mazzulli, J.R.; Xu, Y.H.; Sun, Y.; Knight, A.L.; McLean, P.J.; Caldwell, G.A.; Sidransky, E.; Grabowski, G.A.; Krainc, D. Gaucher disease glucocerebrosidase and alpha-synuclein form a bidirectional pathogenic loop in synucleinopathies. *Cell* **2011**, *146*, 37–52. [[CrossRef](#)] [[PubMed](#)]
14. Richter, F.; Fleming, S.M.; Watson, M.; Lemesre, V.; Pellegrino, L.; Ranes, B.; Zhu, C.; Mortazavi, F.; Mulligan, C.K.; Sioshansi, P.C.; et al. A GCase chaperone improves motor function in a mouse model of synucleinopathy. *Neurotherapeutics* **2014**, *11*, 840–856. [[CrossRef](#)] [[PubMed](#)]
15. Kim, S.; Yun, S.P.; Lee, S.; Umanah, G.E.; Bandaru, V.V.R.; Yin, X.; Rhee, P.; Karuppagounder, S.S.; Kwon, S.H.; Lee, H.; et al. GBA1 deficiency negatively affects physiological alpha-synuclein tetramers and related multimers. *Proc. Natl. Acad. Sci. USA* **2018**, *115*, 798–803. [[CrossRef](#)] [[PubMed](#)]
16. Prence, E.M.; Chaturvedi, P.; Newburg, D.S. In vitro accumulation of glucocerebrosidase in neuroblastoma cells: A model for study of Gaucher disease pathobiology. *J. Neurosci. Res.* **1996**, *43*, 365–371. [[CrossRef](#)]
17. Di Biase, E.; Lunghi, G.; Fazzari, M.; Maggioni, M.; Pome, D.Y.; Valsecchi, M.; Samarani, M.; Fato, P.; Ciampa, M.G.; Prioni, S.; et al. Gangliosides in the differentiation process of primary neurons: The specific role of GM1-oligosaccharide. *Glycocon. J.* **2020**, *37*, 329–343. [[CrossRef](#)]
18. Zhang, P.; Xia, N.; Reijo Pera, R.A. Directed dopaminergic neuron differentiation from human pluripotent stem cells. *J. Vis. Exp.* **2014**, 51737. [[CrossRef](#)]
19. Schiumarini, D.; Loberto, N.; Mancini, G.; Bassi, R.; Giussani, P.; Chiricozzi, E.; Samarani, M.; Munari, S.; Tamanini, A.; Cabrini, G.; et al. Evidence for the Involvement of Lipid Rafts and Plasma Membrane Sphingolipid Hydrolases in Pseudomonas aeruginosa Infection of Cystic Fibrosis Bronchial Epithelial Cells. *Mediat. Inflamm.* **2017**, *2017*, 1730245. [[CrossRef](#)]
20. Schondorf, D.C.; Aureli, M.; McAllister, F.E.; Hindley, C.J.; Mayer, F.; Schmid, B.; Sardi, S.P.; Valsecchi, M.; Hoffmann, S.; Schwarz, L.K.; et al. iPSC-derived neurons from GBA1-associated Parkinson's disease patients show autophagic defects and impaired calcium homeostasis. *Nat. Commun.* **2014**, *5*, 4028. [[CrossRef](#)] [[PubMed](#)]
21. Lunghi, G.; Fazzari, M.; Di Biase, E.; Mauri, L.; Sonnino, S.; Chiricozzi, E. Modulation of calcium signaling depends on the oligosaccharide of GM1 in Neuro2a mouse neuroblastoma cells. *Glycocon. J.* **2020**, *37*, 713–727. [[CrossRef](#)] [[PubMed](#)]
22. Aureli, M.; Loberto, N.; Lanteri, P.; Chigorno, V.; Prinetti, A.; Sonnino, S. Cell surface sphingolipid glycohydrolases in neuronal differentiation and aging in culture. *J. Neurochem.* **2011**, *116*, 891–899. [[CrossRef](#)] [[PubMed](#)]
23. Loberto, N.; Lunghi, G.; Schiumarini, D.; Samarani, M.; Chiricozzi, E.; Aureli, M. Methods for Assay of Ganglioside Catabolic Enzymes. *Methods Mol. Biol.* **2018**, *1804*, 383–400. [[CrossRef](#)]

24. Schueler, U.H.; Kolter, T.; Kaneski, C.R.; Blusztajn, J.K.; Herkenham, M.; Sandhoff, K.; Brady, R.O. Toxicity of glucosylsphingosine (glucopsychosine) to cultured neuronal cells: A model system for assessing neuronal damage in Gaucher disease type 2 and 3. *NeuroBiol. Dis* **2003**, *14*, 595–601. [[CrossRef](#)]
25. Sueyoshi, N.; Maehara, T.; Ito, M. Apoptosis of Neuro2a cells induced by lysosphingolipids with naturally occurring stereochemical configurations. *J. Lipid Res.* **2001**, *42*, 1197–1202. [[CrossRef](#)]
26. Liu, J.; Halene, S.; Yang, M.; Iqbal, J.; Yang, R.; Mehal, W.Z.; Chuang, W.L.; Jain, D.; Yuen, T.; Sun, L.; et al. Gaucher disease gene GBA functions in immune regulation. *Proc. Natl. Acad. Sci. USA* **2012**, *109*, 10018–10023. [[CrossRef](#)] [[PubMed](#)]
27. Dennis, G., Jr.; Sherman, B.T.; Hosack, D.A.; Yang, J.; Gao, W.; Lane, H.C.; Lempicki, R.A. DAVID: Database for Annotation, Visualization, and Integrated Discovery. *Genome Biol.* **2003**, *4*, P3. [[CrossRef](#)] [[PubMed](#)]
28. Szklarczyk, D.; Gable, A.L.; Nastou, K.C.; Lyon, D.; Kirsch, R.; Pyysalo, S.; Doncheva, N.T.; Legeay, M.; Fang, T.; Bork, P.; et al. The STRING database in 2021: Customizable protein-protein networks, and functional characterization of user-uploaded gene/measurement sets. *Nucleic Acids Res.* **2021**, *49*, D605–D612. [[CrossRef](#)] [[PubMed](#)]
29. Samarani, M.; Loberto, N.; Solda, G.; Straniero, L.; Asselta, R.; Duga, S.; Lunghi, G.; Zucca, F.A.; Mauri, L.; Ciampa, M.G.; et al. A lysosome-plasma membrane-sphingolipid axis linking lysosomal storage to cell growth arrest. *FASEB J.* **2018**, *32*, 5685–5702. [[CrossRef](#)]
30. Sardiello, M.; Palmieri, M.; di Ronza, A.; Medina, D.L.; Valenza, M.; Gennarino, V.A.; Di Malta, C.; Donaudy, F.; Embrione, V.; Polishchuk, R.S.; et al. A gene network regulating lysosomal biogenesis and function. *Science* **2009**, *325*, 473–477. [[CrossRef](#)]
31. Aureli, M.; Prioni, S.; Mauri, L.; Loberto, N.; Casellato, R.; Ciampa, M.G.; Chigorno, V.; Prinetti, A.; Sonnino, S. Photoactivable sphingosine as a tool to study membrane microenvironments in cultured cells. *J. Lipid Res.* **2010**, *51*, 798–808. [[CrossRef](#)] [[PubMed](#)]
32. Lingwood, D.; Simons, K. Lipid rafts as a membrane-organizing principle. *Science* **2010**, *327*, 46–50. [[CrossRef](#)] [[PubMed](#)]
33. Sonnino, S.; Aureli, M.; Grassi, S.; Mauri, L.; Prioni, S.; Prinetti, A. Lipid rafts in neurodegeneration and neuroprotection. *Mol. NeuroBiol.* **2014**, *50*, 130–148. [[CrossRef](#)]
34. Riboldi, G.M.; Di Fonzo, A.B. GBA, Gaucher Disease, and Parkinson’s Disease: From Genetic to Clinic to New Therapeutic Approaches. *Cells* **2019**, *8*, 364. [[CrossRef](#)] [[PubMed](#)]
35. Cilia, R.; Tunesi, S.; Marotta, G.; Cereda, E.; Siri, C.; Tesi, S.; Zecchinelli, A.L.; Canesi, M.; Mariani, C.B.; Meucci, N.; et al. Survival and dementia in GBA-associated Parkinson’s disease: The mutation matters. *Ann. Neurol.* **2016**, *80*, 662–673. [[CrossRef](#)]
36. Sidransky, E.; Nalls, M.A.; Aasly, J.O.; Aharon-Peretz, J.; Annesi, G.; Barbosa, E.R.; Bar-Shira, A.; Berg, D.; Bras, J.; Brice, A.; et al. Multicenter analysis of glucocerebrosidase mutations in Parkinson’s disease. *N. Engl. J. Med.* **2009**, *361*, 1651–1661. [[CrossRef](#)]
37. McNeill, A.; Duran, R.; Hughes, D.A.; Mehta, A.; Schapira, A.H. A clinical and family history study of Parkinson’s disease in heterozygous glucocerebrosidase mutation carriers. *J. Neurol. Neurosurg. Psychiatry* **2012**, *83*, 853–854. [[CrossRef](#)]
38. Nalls, M.A.; Duran, R.; Lopez, G.; Kurzawa-Akanbi, M.; McKeith, I.G.; Chinnery, P.F.; Morris, C.M.; Theuns, J.; Crosiers, D.; Cras, P.; et al. A multicenter study of glucocerebrosidase mutations in dementia with Lewy bodies. *JAMA Neurol.* **2013**, *70*, 727–735. [[CrossRef](#)]
39. Johnson, P.H.; Weinreb, N.J.; Cloyd, J.C.; Tuite, P.J.; Kartha, R.V. GBA1 mutations: Prospects for exosomal biomarkers in alpha-synuclein pathologies. *Mol. Genet. Metab.* **2020**, *129*, 35–46. [[CrossRef](#)] [[PubMed](#)]
40. Farfel-Becker, T.; Vitner, E.B.; Futerman, A.H. Animal models for Gaucher disease research. *Dis. Model. Mech.* **2011**, *4*, 746–752. [[CrossRef](#)]
41. Enquist, I.B.; Lo Bianco, C.; Ooka, A.; Nilsson, E.; Mansson, J.E.; Ehinger, M.; Richter, J.; Brady, R.O.; Kirik, D.; Karlsson, S. Murine models of acute neuronopathic Gaucher disease. *Proc. Natl. Acad. Sci. USA* **2007**, *104*, 17483–17488. [[CrossRef](#)] [[PubMed](#)]
42. Sillence, D.J.; Puri, V.; Marks, D.L.; Butters, T.D.; Dwek, R.A.; Pagano, R.E.; Platt, F.M. Glucosylceramide modulates membrane traffic along the endocytic pathway. *J. Lipid Res.* **2002**, *43*, 1837–1845. [[CrossRef](#)] [[PubMed](#)]
43. Orvisky, E.; Park, J.K.; LaMarca, M.E.; Ginns, E.I.; Martin, B.M.; Tayebi, N.; Sidransky, E. Glucosylsphingosine accumulation in tissues from patients with Gaucher disease: Correlation with phenotype and genotype. *Mol. Genet. Metab.* **2002**, *76*, 262–270. [[CrossRef](#)]
44. Hein, L.K.; Meikle, P.J.; Hopwood, J.J.; Fuller, M. Secondary sphingolipid accumulation in a macrophage model of Gaucher disease. *Mol. Genet. Metab.* **2007**, *92*, 336–345. [[CrossRef](#)]
45. Walkley, S.U.; Vanier, M.T. Secondary lipid accumulation in lysosomal disease. *Biochim. Biophys. Acta* **2009**, *1793*, 726–736. [[CrossRef](#)]
46. Medina, D.L.; Fraldi, A.; Bouche, V.; Annunziata, F.; Mansueto, G.; Spampinato, C.; Puri, C.; Pignata, A.; Martina, J.A.; Sardiello, M.; et al. Transcriptional activation of lysosomal exocytosis promotes cellular clearance. *Dev. Cell* **2011**, *21*, 421–430. [[CrossRef](#)]
47. Kim, O.S.; Park, E.J.; Joe, E.H.; Jou, I. JAK-STAT signaling mediates gangliosides-induced inflammatory responses in brain microglial cells. *J. Biol. Chem.* **2002**, *277*, 40594–40601. [[CrossRef](#)]
48. Sonnino, S.; Prinetti, A.; Mauri, L.; Chigorno, V.; Tettamanti, G. Dynamic and structural properties of sphingolipids as driving forces for the formation of membrane domains. *Chem. Rev.* **2006**, *106*, 2111–2125. [[CrossRef](#)]
49. Chiricozzi, E.; Di Biase, E.; Lunghi, G.; Fazzari, M.; Loberto, N.; Aureli, M.; Mauri, L.; Sonnino, S. Turning the spotlight on the oligosaccharide chain of GM1 ganglioside. *Glycoconj. J.* **2021**, *38*, 101–117. [[CrossRef](#)]
50. Lunghi, G.; Fazzari, M.; Di Biase, E.; Mauri, L.; Chiricozzi, E.; Sonnino, S. The structure of gangliosides hides a code for determining neuronal functions. *FEBS Open Bio.* **2021**, *11*, 3193–3200. [[CrossRef](#)]

51. Aureli, M.; Masilamani, A.P.; Illuzzi, G.; Loberto, N.; Scandroglio, F.; Prinetti, A.; Chigorno, V.; Sonnino, S. Activity of plasma membrane beta-galactosidase and beta-glucosidase. *FEBS Lett.* **2009**, *583*, 2469–2473. [[CrossRef](#)] [[PubMed](#)]
52. Svennerholm, L.; Bostrom, K.; Fredman, P.; Mansson, J.E.; Rosengren, B.; Rynmark, B.M. Human brain gangliosides: Developmental changes from early fetal stage to advanced age. *Biochim. Biophys. Acta* **1989**, *1005*, 109–117. [[CrossRef](#)]
53. Batta, G.; Soltesz, L.; Kovacs, T.; Bozo, T.; Meszar, Z.; Kellermayer, M.; Szollosi, J.; Nagy, P. Alterations in the properties of the cell membrane due to glycosphingolipid accumulation in a model of Gaucher disease. *Sci. Rep.* **2018**, *8*, 157. [[CrossRef](#)] [[PubMed](#)]
54. Hein, L.K.; Duplock, S.; Hopwood, J.J.; Fuller, M. Lipid composition of microdomains is altered in a cell model of Gaucher disease. *J. Lipid Res.* **2008**, *49*, 1725–1734. [[CrossRef](#)] [[PubMed](#)]
55. Piccinini, M.; Scandroglio, F.; Prioni, S.; Buccinna, B.; Loberto, N.; Aureli, M.; Chigorno, V.; Lupino, E.; DeMarco, G.; Lomartire, A.; et al. Deregulated sphingolipid metabolism and membrane organization in neurodegenerative disorders. *Mol. Neurobiol.* **2010**, *41*, 314–340. [[CrossRef](#)] [[PubMed](#)]
56. Roskoski, R., Jr. Src protein-tyrosine kinase structure, mechanism, and small molecule inhibitors. *Pharmacol. Res.* **2015**, *94*, 9–25. [[CrossRef](#)] [[PubMed](#)]
57. Holzer, R.G.; Park, E.J.; Li, N.; Tran, H.; Chen, M.; Choi, C.; Solinas, G.; Karin, M. Saturated fatty acids induce c-Src clustering within membrane subdomains, leading to JNK activation. *Cell* **2011**, *147*, 173–184. [[CrossRef](#)] [[PubMed](#)]
58. Kajiwara, K.; Yamada, T.; Bamba, T.; Fukusaki, E.; Imamoto, F.; Okada, M.; Oneyama, C. c-Src-induced activation of ceramide metabolism impairs membrane microdomains and promotes malignant progression by facilitating the translocation of c-Src to focal adhesions. *Biochem. J.* **2014**, *458*, 81–93. [[CrossRef](#)] [[PubMed](#)]
59. Wu, C.W.; Wang, S.G.; Lee, C.H.; Chan, W.L.; Lin, M.L.; Chen, S.S. Enforced C-Src Activation Causes Compartmental Dysregulation of PI3K and PTEN Molecules in Lipid Rafts of Tongue Squamous Carcinoma Cells by Attenuating Rac1-Akt-GLUT-1-Mediated Sphingolipid Synthesis. *Int. J. Mol. Sci.* **2020**, *21*, 5812. [[CrossRef](#)]

Supporting information

β -glucocerebrosidase deficiency activates an aberrant lysosome-plasma membrane axis responsible for the onset of neurodegeneration

Giulia Lunghi^{1*}, Emma Veronica Carsana^{1*}, Nicoletta Loberto¹, Laura Cioccarelli¹, Simona Prioni¹, Laura Mauri¹, Rosaria Bassi¹, Stefano Duga^{2,3}, Letizia Straniero^{2,3}, Rosanna Asselta^{2,3}, Giulia Soldà^{2,3}, Alessio Di Fonzo⁴, Emanuele Frattini⁴, Nara Liessi⁵, Andrea Armirotti⁵, Elena Ferrari⁶, Maura Samarani^{7†}, Massimo Aureli^{1†}

¹Department of Medical Biotechnology and Translational Medicine, University of Milan, Milan, Italy

²Department of Biomedical Sciences, Humanitas University, Via Rita Levi Montalcini 4, 20090 Pieve Emanuele, Milan, Italy

³Humanitas Clinical and Research Center, IRCCS, Via Manzoni 56, 20072 Rozzano, Milan, Italy

⁴IRCCS Foundation Ca' Granda Ospedale Maggiore Policlinico, Dino Ferrari Center, Neuroscience Section, Department of Pathophysiology and Transplantation, University of Milan, Milan, Italy

⁵ Analytical Chemistry Facility, Fondazione Istituto Italiano di Tecnologia, Via Morego 30, 16163, Genoa, Italy

⁶Department of Pharmacological and Biomolecular Sciences, University of Milan, Milan, Italy

⁶Department of Cell Biology and Infection, Institut Pasteur, Paris, France

* These authors equally contributed

† These authors share the senior position

Corresponding author:

Massimo Aureli, Department of Medical Biotechnology and Translational Medicine, University of Milan, Milan, Italy, Tel: 0250330364, massimo.aureli@unimi.it

Methods

Glucosylsphingosine treatment

Glucosylsphingosine (GlcSph) was solubilized directly in the culture medium of CGN and DA neurons at 100 nM and 10 μ M (final concentration) of and administered to CGN at 14 DIC for 24 h. Untreated cells were incubated under the same experimental conditions without GlcSph.

Calcein assay

Cells were plated in 96-well microplate at a density of 3.15×10^5 cells/cm² for CGN and 2×10^5 cells/cm² for DA neurons. After the removal of culture medium, cells were washed with PBS and then incubated with 5 μ g/ml Calcein-AM solution in of PBS (15 min, 37°C). At the end of incubation, Calcein-AM solution was discarded and cells were lysed with 1% Triton X-100 in TNEV buffer in mild agitation (10 min, 23°C). The cell lysates were transferred to a black microplate (Black, 96-well, OptiPlate-96 F, Perkin Elmer) and fluorescence intensity (ex/em 495/515 nm) was measured by a Victor microplate reader (Perkin Elmer).

MTT assay

CGNs and DA neurons were plated in 96-well microplate at a density of 3.15×10^5 cells/cm² and 2×10^5 cells/cm² respectively. Cells were incubated in culture medium containing 1 mg/ml MTT at 37°C. After 2 hours, MTT solution was discarded and the blue MTT–formazan product was extracted with 2-propanol: formic acid, 95: 5 (v:v). After 15 min of gentle agitation at room temperature, the absorbance of the formazan solution was read at 570 nm by a microplate spectrophotometer (Wallac 1420 VICTOR2 TM; Perkin Elmer).

Mass spectrometry and data analysis

The analysis of GlcCer content was carried out on aliquots of the organic phase, subjected to alkaline treatment to remove glycerophospholipids¹. The analysis of GlcSph content was carried out as previously described². Lyophilized cell lysates were extracted with acetone, the extracts were dried under nitrogen flow and then resuspended in chloroform: methanol 2: 1 (v: v). GlcCer and GlcSph were analysed by LC ESI-MS/MS according to Merrill, A. H., Jr., 2011³ with proper modifications⁴. Mass spectrometry analyses were carried out using LCQDeca ion trap mass spectrometer (Thermo Fisher Scientific) equipped with an electrospray ionization source, an Xcalibur data system and a Jasco PU980 Pump HPLC. GlcCer and GlcSph were separated and detected using an HPLC system (JASCO; Tokyo, Japan) equipped with a normal phase column LC-Si (Supelco 2.1 mm x 250 mm x 5µm). Elution was carried out at a flow rate of 0.700 ml/min, with a gradient formed by solvent system A: CH₃CN: CH₃OH: H₃CCOOH 97: 2: 1 (v: v: v) with 5 mM ammonium acetate and solvent system B: CH₃OH containing 5 mM ammonium acetate. MS analyses were carried out at a positive ion mode MS/MS, sheath gas flow of 60 arbitrary units, spray voltage of 5 kV, capillary voltage of 70 eV and capillary temperature of 300°C. Mass spectra were acquired over a range of m/z 200–2 000.

Immunofluorescence staining

DA neurons were plated at a density of 10⁵ cells/cm² on 24 mm cover glasses precoated with geltrex (1%, 1 h 37°C). Neurons were fixed in 4% paraformaldehyde in PBS for 20 min at 23°C. Cells were then permeabilized in 0.2 % Triton X-100 in PBS for 10 min at 23°C and blocked in 1% BSA/ 2% Donkey serum in PBS for 1 h at 23°C. Cells were incubated 2 h at 23°C with primary antibodies diluted in 0.25% BSA/ 0.5% Donkey serum in PBS and 1 h at 23°C with secondary antibodies conjugated to Alexa Fluor, diluted in the same solution. Nuclei were stained by incubation with Hoechst solution (2 µg/ml in PBS) for 5 min at 23°C. The following antibodies were used: monoclonal mouse anti-β3-tubulin (4466; CellSignaling Technology; dilution: 1:200), monoclonal mouse anti-TH (F-11) (25269; SantaCruz; dilution: 1:50), mouse anti-LAMP1 (AB_2296838; dilution: 1:50; DSHB), polyclonal anti-mouse AlexaFluor488 (A21202; ThermoFisher Scientific) and anti-mouse AlexaFluor568 (A10037; ThermoFisher Scientific). Coverslips were mounted with Dako Fluorescent

Mounting Medium (Agilent Technologies, Santa Cruz, CA, USA). Images were taken using an Olympus BX50 Upright Fluorescence Microscope fluorescence with a fast-high resolution camera (Colorview 12).

Analysis of endogenous lipid pattern by HPTLC

Lipids were extracted from CBE-treated and untreated CGNs and DA neurons and subjected to two-phase partitioning, as described in the Methods section.

For each sample, equal amounts in terms of cell proteins were loaded on HPTLC and lipids were separated using the solvent system chloroform: methanol: H₂O 110:40:6 (v:v:v).

Endogenous lipid content was detected by spraying the HPTLC with anisaldehyde reagent. Identification of lipids after separation was assessed by comigration with authentic standards. The relative amounts of lipids were determined by densitometry analysis using ImageJ software.

Lysotracker staining

CGNs were plated in 24-well plate at a density of 3.15×10^5 cells/cm² and were treated or not with CBE for 17 days. At 20 DIC LysoTracker Red DND-99 (Molecular Probes) was directly diluted in the culture medium at 50 nM final concentration (30 minutes, 37°C, 5% CO₂). Cells were then washed with PBS and images were acquired with Olympus IX50 Inverted Fluorescence Microscope equipped with a halogen lamp directly on live cells at 100x magnification.

Transmission electron microscopy

Cell monolayers were fixed in 2.5% glutaraldehyde, 0.1 M sodium cacodylate buffer pH 7.4 for 1 h at 23°C, washed three times with cacodylate buffer and post-fixed with 1% osmium tetroxide, 1.5% potassium ferrocyanide in 0.1 M cacodylate for 1 h on ice.

After several washes in distilled water, samples were "en bloc" stained with 0.5% uranyl acetate in water overnight at 4°C. Samples were dehydrated in a graded ethanol series (30%, 50%, 70%, 80%, 90%, 96%, 5 minutes each followed by 3 washes with absolute ethanol, 10 min each). The

samples were then infiltrated in a 1:1 ethanol: Epon 812 solution for 2 hours and in 100% Epon twice for 1 h each. The Epon-embedded cell monolayers were then polymerized in an oven at 60°C for 48 hours. At the end of the polymerization the plastic was separated from the Epon block mechanically breaking the plastic, leaving the cell monolayer facing up on the resin block.

A portion of the specimen was glued on top of an Epon block and mounted on a Leica Ultracut UCT ultramicrotome. Ultrathin (70-90nm) sections were then collected on copper grids and stained with uranyl acetate and lead citrate. Grids were examined with a transmission electron microscope (TALOS L120C ThermoScientific) at 120 kv.

Treatment of cell cultures with [3-³H(sphingosine)] -GM1

Isotopically labeled [3-³H(sphingosine)]-GM1 dissolved in propanol: H₂O 7:3 (v:v) was transferred into a sterile glass tube, dried under a nitrogen stream, solubilized in an appropriate volume of culture medium (0,067 μCi /ml of medium) and administered to cells. After 4 h, cells were harvested with PBS and processed for lipid extraction and analysis as already described. TLE were then separated by HPTLC (MilliporeSigma) with the solvent system chloroform: methanol: CaCl₂ (50: 42: 11 v: v: v). Radioactive lipids were detected by digital autoradiography (TRacer betaimager; BioSpace Laboratory) and quantified using M3 Vision software. Lipids were identified after separation by comigration with radioactive lipid standards.

Immunoblotting analysis of SN and P fractions after cell surface biotinylation

Proportional amounts of SN and P fractions from CGN or DA neurons were separated on 4–20% polyacrylamide gradient gel and transferred to PVDF membranes by electroblotting. Membranes were blocked in 5 % non-fat dry milk solution. Subsequently PVDFs were incubated overnight at 4°C with the primary antibody and secondary HRP-conjugated antibodies in 5 % non-fat dry milk solution for 1 h at 23°C. Biotinylated proteins were detected with HRP-conjugated streptavidin using the chemiluminescent system Alliance Mini HD9 (Uvitec, Cambridge, United Kingdom). Band intensity was quantified using ImageJ software (v2.1.0/1.53c). The following primary antibodies were used for

immunoblotting: Polyclonal rabbit anti-PSD95 (25072; Cell Signaling Technology; dilution: 1:1 000), polyclonal rabbit anti-GAPDH (G9535, MilliporeSigma; dilution: 1: 7 000).

The following secondary antibodies were used: Goat-anti-rabbit HRP-conjugated (7074; CellSignaling Technology; 1: 2 000) and Goat-anti-mouse HRP conjugated (31430; ThermoFisher; dilution: 1: 5 000) Streptavidin HRP-conjugated (HRP; SA-5004; Vector Laboratories, Burlingame, CA, USA).

Immunofluorescence of iPSCs

iPSCs were grown on suitable culture imaging plates to allow visualization of the cells following immunofluorescence by inverted wide field and confocal microscopes. Cells were fixed with 4% paraformaldehyde (PFA) for 30 minutes. Then cells were rinsed twice with PBS 1X, permeabilized and quenched with wash-buffer (PBS 1X + BSA 3% + Goat serum (Vector) 5% + Triton X-100 (Euroclone) 0.3%), blocked for 30 minutes at room temperature (RT). Plates were subsequently incubated with primary antibodies overnight at 4°C (for primary antibodies dilution, see antibody Table), washed three times in wash buffer (PBS + 0.1% Triton X-100) for 5 minutes each, then incubated with secondary antibodies (Alexa 488, 568, 647, Molecular Probes; 1:500) and DAPI (1:1000) nuclear counterstain for 10 minutes at room temperature, and finally washed as previously described. Plates were then mounted on imaging slides (Thermo Fisher Scientific). Cells were stored at 4°C in dark until image acquisition through confocal microscope.

Antibody table

Primary Antibody	Host	Vendor	Dilution
OCT4	Rabbit	Cell Signaling	1:100
SSEA4	Mouse	Cell Signaling	1:200
SOX2	Rabbit	Cell Signaling	1:200
NANOG	Rabbit	Cell Signaling	1:200

TRA160	Mouse	Cell Signaling	1:500
TRA181	Mouse	Cell Signaling	1:500

Real-time PCR (qPCR)

RNA extraction

RNA extraction was achieved by TRIzol™ Reagent (Invitrogen). After a mechanical homogenization of the sample with 1 mL of TRIzol™ Reagent, 200 µL of ice-cold chloroform (Sigma-Aldrich) was added. Samples were vortexed until the two phases mixed together to form an emulsion. After that, samples were centrifuged for 10 min at 4°C at 13'500 rpm. RNA phase was collected in a new tube and ice-cold isopropanol (Sigma-Aldrich) was added in 1:1 ratio, mixing gently. The RNA was precipitated overnight at -20°C. Samples were then centrifuged for 20 minutes at 4°C at 13,500 rpm. RNA pellets were then washed two or three times with 1 mL of ice-cold 70% ethanol (Sigma-Aldrich). For every wash, samples were centrifuged for 5 minutes at 6,000 rpm at 4°C. After the last one, RNA pellets were dried in fume hood for a few minutes until they become transparent. RNA pellets were resuspended in RNase-free water based on the RNA pellet dimension (usually 20-30 µL for a medium-sized pellet) and kept at -80 degrees until further use.

Quantification of extracted RNA by UV absorption

RNA was quantified using UV absorption and the absorbance was measured at RNA's maximum absorption wavelength (260 nm) through a spectrophotometer. The linear relationship between absorbance and concentration of an absorbing specie was determinate by the Beer-Lambert law, $A = \log(I_0/I) = \epsilon cl$, which predicts a linear change in absorbance with concentration. The NanoDrop 1000 Spectrophotometer (Thermo Fisher Scientific) was used to perform the analyses. The ratios of the absorbance 260/280nm (~2.0) and 260/230 (~1.8-2.2) were used to assess the RNA purity. RNA

samples were diluted to reach 500 ng/μL and after every dilution the RNA concentrations were quantified again.

RT-PCR: Retrotranscription of RNA into cDNA

The iScript cDNA Synthesis Kit (Bio-Rad) was used to perform the retrotranscription. This kit contains oligo (dT), random hexamer primers and a reverse transcriptase enzyme. To perform retrotranscription, 500 ng of RNA were transferred in a PCR RNase-free tube and nuclease-free water was added up to 15 μL volume. Then 5 μL of mix solution (4 μL 5X iScript Reaction Mix/Buffer, 1 μL iScript Reverse Transcriptase) were added and the PCR tube containing complete reaction mix was incubated in a thermal cycler using the RT-PCR protocol. cDNA was stored at -20°C until use.

qPCR

The qPCR mix used was the SsoFast™ EvaGreen® Supermix 2X (Bio-Rad). Retrotranscribed cDNA from RT-PCR was further diluted (1:10) and 5 μL of diluted cDNA for each sample was loaded in triplicate in a Hard-Shell® 96-Well PCR Plates (Bio-Rad).

15 μL of SsoFast™ EvaGreen® Supermix diluted with nuclease-free water and with the specific primers (see primer Table) for the target of interest, were added. In this final qPCR reaction volume, Supermix reaches the right dilution and primers get 10 μM concentration. Routine qPCR negative controls were included in the plate and the qPCR protocol was performed using a CFX96™ Real-Time System (Bio-Rad) coupled with a C1000™ Thermal Cycler (Bio-Rad).

Once qPCR was carried out, data were analyzed with the CFX Manager Software (BioRad) and excel data sheet tool. Gene expression was achieved through the use of ΔCT as relative gene expression analysis using a reference gene. ΔCT was calculated through Ct normalization of the target gene to the reference YWHAZ gene.

$$2^{(Ct(\text{ref})-Ct(\text{sample}))} = \text{Expression}$$

Primer table

PRIMER	SEQUENCE 5'>3'
YWHAZ-FW	ACTTTTGGTACATTGTGGCTTCAA
YWHAZ-RV	CCGCCAGGACAAACCAGTAT
OCT4-FW	AGGCTCTGAGGTGTGGGGGAT
OCT4-RV	TGAGAGGTCTCCAAGCCGCCT
NANOG-FW	CATGAGTGTGGATCCAGCTTG
NANOG-RV	CCTGAATAAGCAGATCCATGG

Karyotype analysis

Following incubation with colchicine for 3 hours, iPSCs were incubated with 0.6% sodium citrate and 0.13% potassium chloride, fixed with methanol/acetic acid, and incubated with Quinacrine solution to obtain Q-banding. Acquired metaphases were analyzed with MetaSystem-Ikaros.

Statistical analyses

All statistical analyses were performed using GraphPad Prism 7 (GraphPad Software Inc., La Jolla, CA, USA). Data are expressed as mean \pm SEM. For normally distributed data, two-tailed unpaired Student's *t* test, one-way ANOVA or two-way ANOVA tests were used. A p-value < 0.05 was considered significant.

Figure Legends

Supplementary Figure S1. Generation of in vitro neuronal models of β -glucocerebrosidase deficiency Schematic diagrams of the experimental protocols to induce β -glucocerebrosidase deficiency in two neuronal models: a primary cultures of granule neurons from the post-natal mouse cerebellum (CGN); b dopaminergic neurons from human-induced pluripotent stem cells (iPSCs). During differentiation of both the neuronal cultures, cell sphingolipids were metabolically labeled at the steady state with radioactive sphingosine; at the stage of mature neurons, cells were then treated with 0.5 mM conduritol B epoxide (CBE) to inhibit β -glucocerebrosidase. After different time points of CBE treatment, neurons were analyzed for β -glucocerebrosidase activity, neuronal marker expression and sphingolipid levels. DIC: days in culture; DOT: days of CBE treatment.

Supplementary Figure S2. Characterization of iPSCs. a. Representative immunofluorescence images of iPSC colonies showing expression of stem cell markers (OCT4, SSEA4, SOX2, TRA181, TRA160, and NANOG). Images were acquired at 20X magnification. b. qPCR showing expression levels of stem cell genes OCT4 and NANOG in iPSCs compared with fibroblasts. Data are shown as absolute normalized amount of mRNA ($2^{-\Delta Ct}$) \pm s.e.m. (iPSCs N=8, Fibroblasts N=2; ***P < 0.001, *P < 0.05, Student's *t*-test). c. Karyotype analysis of a selected clone of the generated iPSC line.

Supplementary Figure S3. Evaluation of differentiation of iPSC-derived dopaminergic neurons by immunofluorescence analysis. Representative immunofluorescence images of human iPSCs-derived dopaminergic neurons after 29 days of differentiation. Cells were positive for neuron-specific class III β -tubulin (TUJ1) and for the dopaminergic marker Tyrosine Hydroxylase (TH). Cell nuclei were stained with Hoechst. Images were acquired at 400x magnification.

Supplementary figure S4. Effect of CBE treatment on dopaminergic neurons differentiation. a Representative immunofluorescence images of human iPSCs-derived dopaminergic neurons treated or not with 0.5 mM CBE for 29 days. Cells were positive for the neuronal markers β -III-tubulin (TUJ1) and microtubule associated protein 2 (MAP2). Cell nuclei were stained with Hoechst. Images were acquired at 200x magnification. b Cell counting of dopaminergic neurons derived from human iPSCs treated or not (CTRL) with CBE 0.5 mM for 29 days. The graph shows the mean \pm SEM of the fold change over control from three different experiments; **** p < 0.001, Student's *t*-test vs CBE-untreated cells.

Supplementary figure S5 Effect of GCase inhibition on GlcCer level. Representative HPTLC separation of endogenous lipids of the organic phases extracted from: **a** mouse cerebellar granule neurons and **b** human iPSCs-derived dopaminergic neurons treated or not with 0.5 mM CBE for 14 days and 29 days, respectively. Cer=ceramide; GlcCer= glucosylceramide; PE=phosphatidylethanolamine; Sulf=sulphatides; SM= sphingomyelin); GlcCer content was quantified by densitometric analysis; data are expressed as fold change with respect to CBE-untreated cells and are the mean \pm SEM of three different experiments; *** $p < 0.001$; **** $p < 0.0001$. Student's t-test vs CBE-untreated cells.

Supplementary figure S6. HPLC elution profiles of total lipid extracts and ESI-MS analyses of glucosylceramide. **a** Representative chromatogram of the HPLC elution profile of total lipid extracts from mouse cerebellar granule neurons treated or not (CTRL) with 0.5 mM CBE; in grey is highlighted the peak corresponding to glucosylceramide (GlcCer) **b** Mass spectrum of GlcCer content of mouse cerebellar granule neurons treated or not (CTRL) with 0.5 mM CBE.

Supplementary figure S7 HPLC elution profiles of total lipid extracts and ESI-MS analyses of glucosylsphingosine. **a** Representative chromatogram of the HPLC elution profile of total lipid extracts from mouse cerebellar granule neurons treated or not (CTRL) with 0.5 mM conduritol B epoxide (CBE); in grey is highlighted the peak corresponding to glucosylsphingosine (GlcSph) **b** Mass spectrum of GlcSph content of mouse cerebellar granule neurons treated or not (CTRL) with 0.5 mM CBE.

Supplementary figure S8. Effect of GlcSph administration on cell viability. Glucosylsphingosine (GlcSph) was administered to **a** cerebellar granule neurons and **b** human iPSC-derived dopaminergic neurons at 0,1 and 10 μ M for 24 hours. Cell viability was evaluated by Calcein assay and MTT assay. Data are expressed as fold change with respect to GlcSph-untreated cells (-) and are the mean \pm SEM of at least three experiments; * $p < 0.05$, ** $p < 0.01$, *** $p < 0.001$, One-way ANOVA vs GlcSph-untreated cells.

Supplementary figure S9. Effect of β -glucocerebrosidase inhibition on ganglioside levels. Representative digital autoradiography of ganglioside pattern and quantification of the radioactivity associated with individual gangliosides in: **a** mouse cerebellar granule neurons fed with radioactive sphingosine and treated or not (CTRL) with 0.5 mM conduritol B epoxide (CBE) for 14 days, and **b** human iPSC-derived dopaminergic neurons fed with radioactive sphingosine and treated or not

(CTRL) with 0.5 mM CBE for 29 days. Data are expressed as fold change with respect to CBE-untreated cells (dashed line) and are the mean \pm SEM of three different experiments. * $p < 0.05$; ** $p < 0.01$; *** $p < 0.001$, two-tail Student's t-test vs CBE-untreated cells.

Supplementary figure S10. Evaluation of TFEB nuclear translocation

Representative images of the expression of the transcription factor EB (TFEB) in the cytosolic and nuclear fraction of **a** mouse cerebellar granule neurons and **b** human iPSCs-derived dopaminergic neurons treated or not with 0.5 mM conduritol B epoxide (CBE). Cytosolic and nuclear fraction are represented respectively by the expression of the cytosolic marker GAPDH or the nuclear marker histone 3 (H3). Quantification of the nuclear amount of TFEB normalized on H3 and expressed as fold change with respect to CBE-untreated cells (CTRL) and are the mean \pm SEM of at least three experiments; * $p < 0.05$; ** $p < 0.01$, Student's t-test vs CBE-untreated cells.

Supplementary figure S11. Evaluation of lysosomal biogenesis upon glucosylceramide accumulation.

a Representative images of lysotracker Red DND-99 staining of mouse cerebellar granule neurons treated or not with 0.5 mM conduritol B epoxide (CBE) for 14 days. Images were acquired at 100x magnification and fluorescence intensity was quantified. **b** Expression of LAMP-1 in human iPSC-derived dopaminergic neurons treated or not with 0.5 mM CBE for 29 days, evaluated by immunofluorescence. Images were acquired at 400x magnification and fluorescence intensity was quantified. **c** Representative electron microscopy images of lysosomes (L) in dopaminergic neurons treated or not (CTRL) with 0.5 mM CBE for 29 days and stained with uranyl acetate and lead citrate. N, nucleus; M, mitochondrion and quantification of the number of lysosomes and their size. Data are expressed as fold change with respect to CBE-untreated cells (CTRL) or as area value of CBE treated and untreated (CTRL) cells and are the mean \pm SEM of at least three experiments; ** $p < 0.01$, Student's t-test vs CBE-untreated cells.

Supplementary figure S12. Evaluation of lysosomal catabolism of glycosphingolipids upon glucosylceramide accumulation.

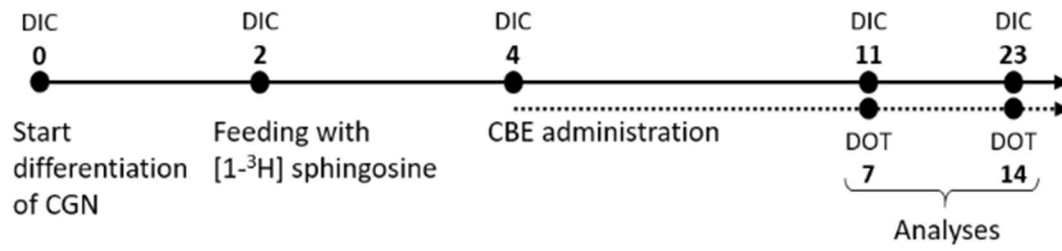
Representative HPTLC image and quantification of sphingolipids extracted from mouse cerebellar granule neurons treated or not with 0.5 mM conduritol B epoxide (CBE) for 14 days followed by radioactive GM1 administration (Cer=ceramide; GlcCer=glucosylceramide; LacCer=lactosylceramide; Gb3=globo-triaosylceramide; GM3=monosialodihexosylganglioside; GM1= monosialo). Data are expressed as fold change with respect to CBE untreated cells (dashed line) and are the mean \pm SEM of the from at least three experiments; * $p < 0.05$, ** $p < 0.01$, *** $p < 0.001$, Student's t-test vs CBE-untreated cells.

Supplementary figure S13. Interactome of plasma membrane proteins isolated from CBE treated neurons. Representation of functional interactions between precipitated plasma membrane proteins exclusively present in DA neurons treated with 0.5 mM CBE compared to untreated neurons. Interactions were obtained by analysis with STRING.

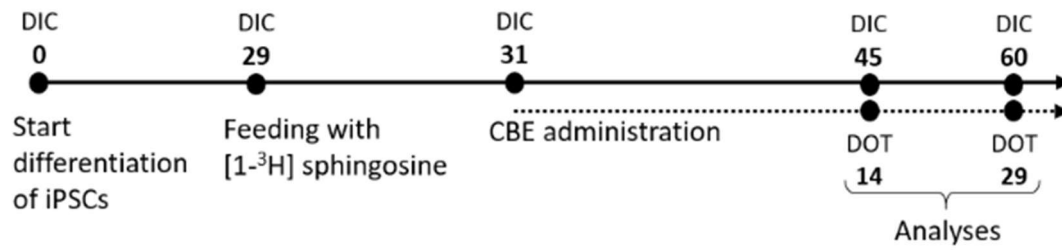
Supplementary figure S14. Characterization of Detergent Resistant Membrane fractions. Detergent Resistant Membrane fractions (DRM) were isolated from human iPSCs-derived dopaminergic neurons treated or not with 0.5 mM conduritol B epoxide (CBE) for 29 days after metabolic labelling with [1-³H]-sphingosine. Fractions were collected and either counted for radioactivity or subjected to lipid extraction or immunoblotting with anti-DRM-specific marker antibodies. **a** Representative image of the expression of protein markers in the fractions no. 5-6 and in fractions 10 -12 **b** Percentage distribution of radioactivity associated with sphingolipids in the sucrose-gradient density fractions. **c** Percentage distribution of sphingolipids (SL) and phosphatidylethanolamine (PE) in DRM and HD fractions of CBE- untreated (CTRL) and treated DA neurons

Supplementary figure S1

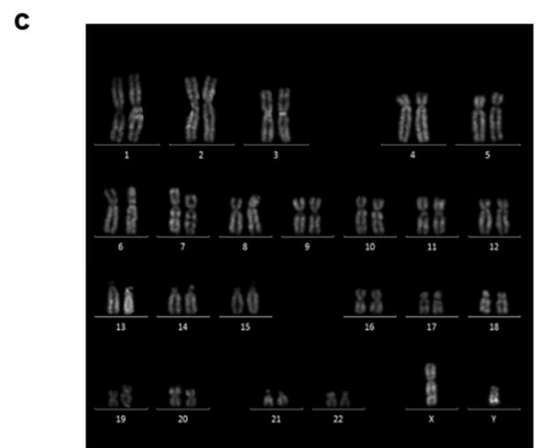
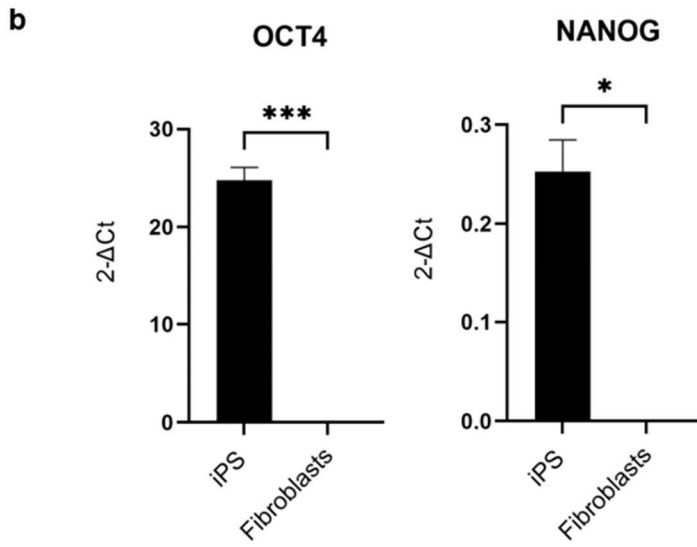
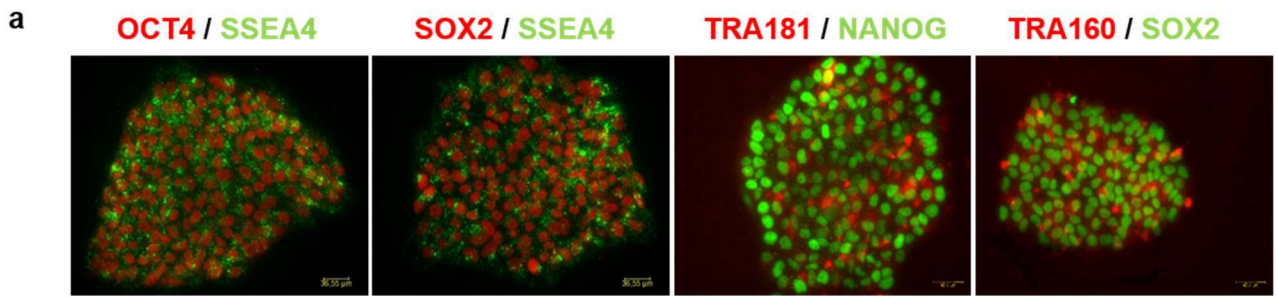
a



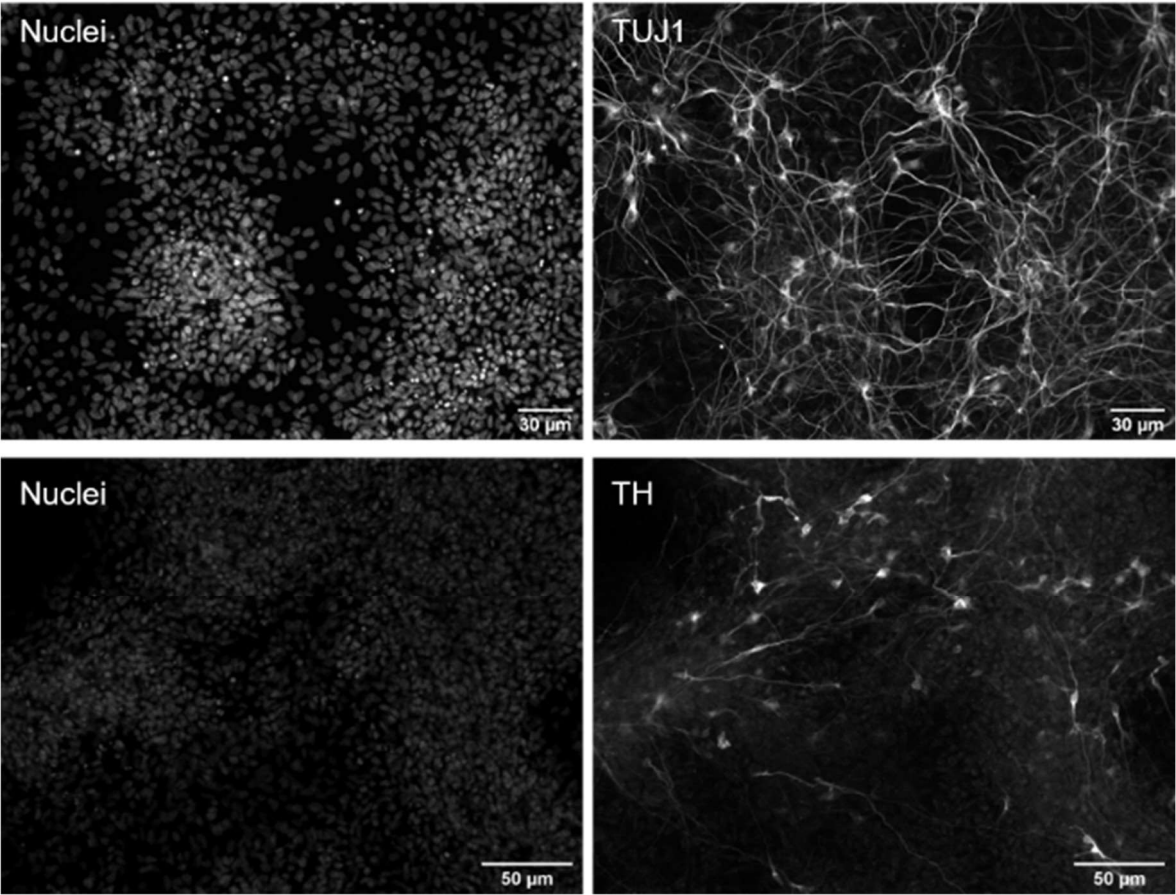
b



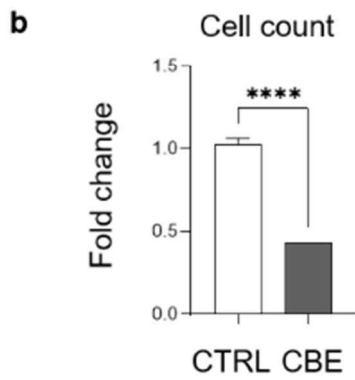
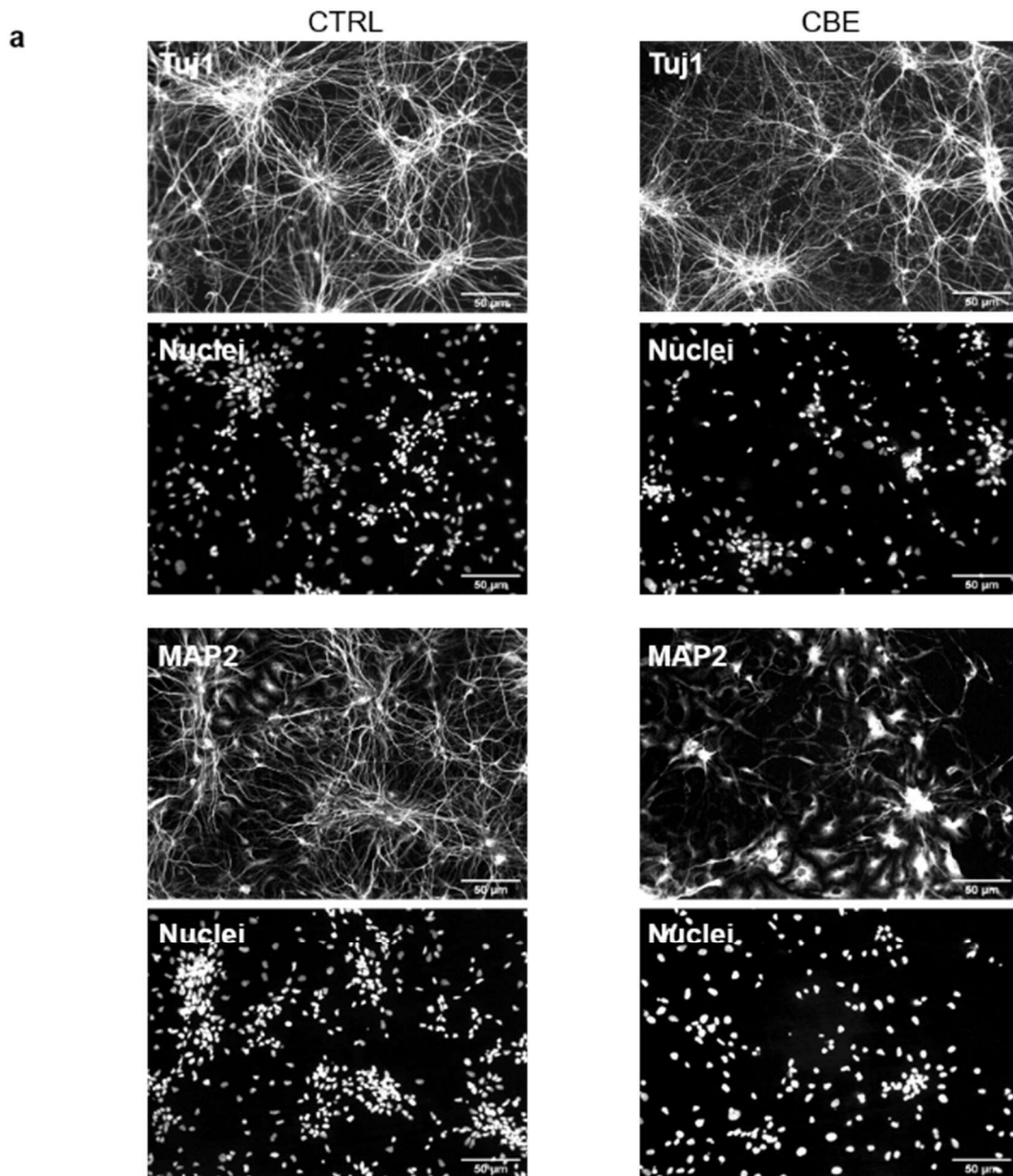
Supplementary figure S2



Supplementary figure S3



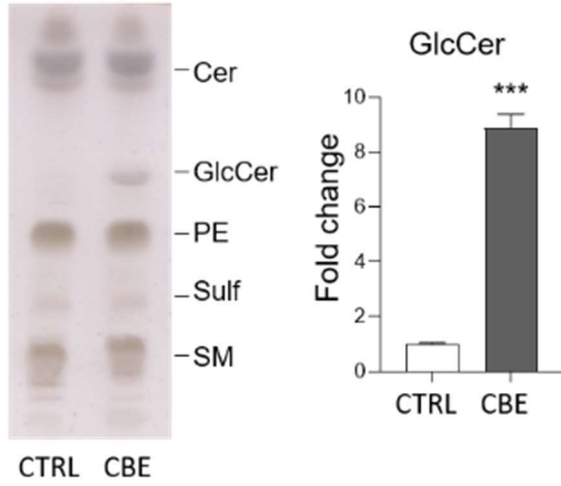
Supplementary figure S4



Supplementary figure S5

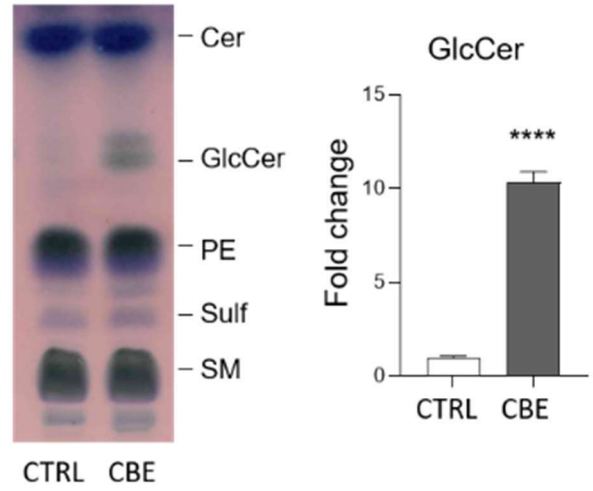
a

Cerebellar granule neurons

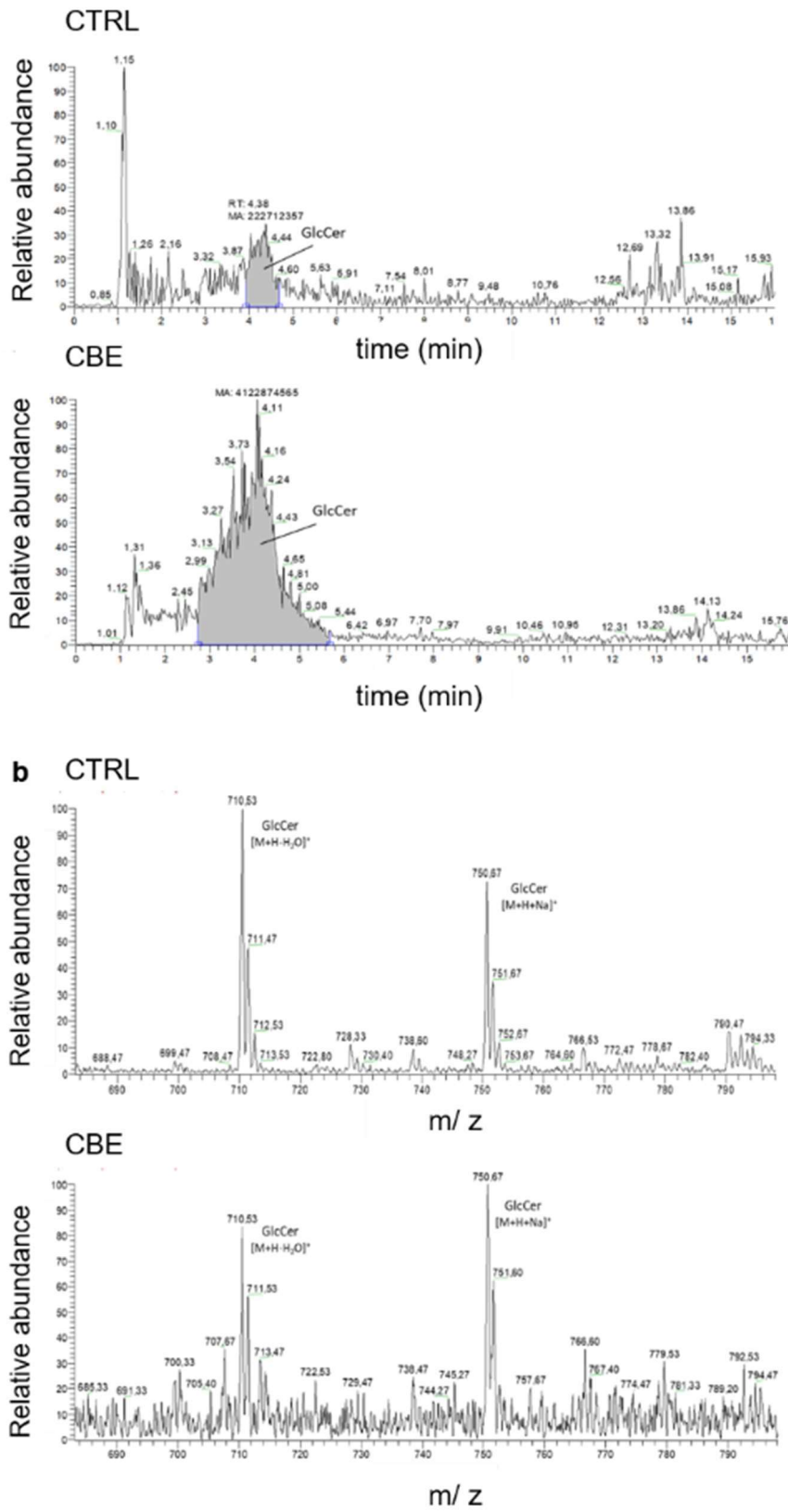


b

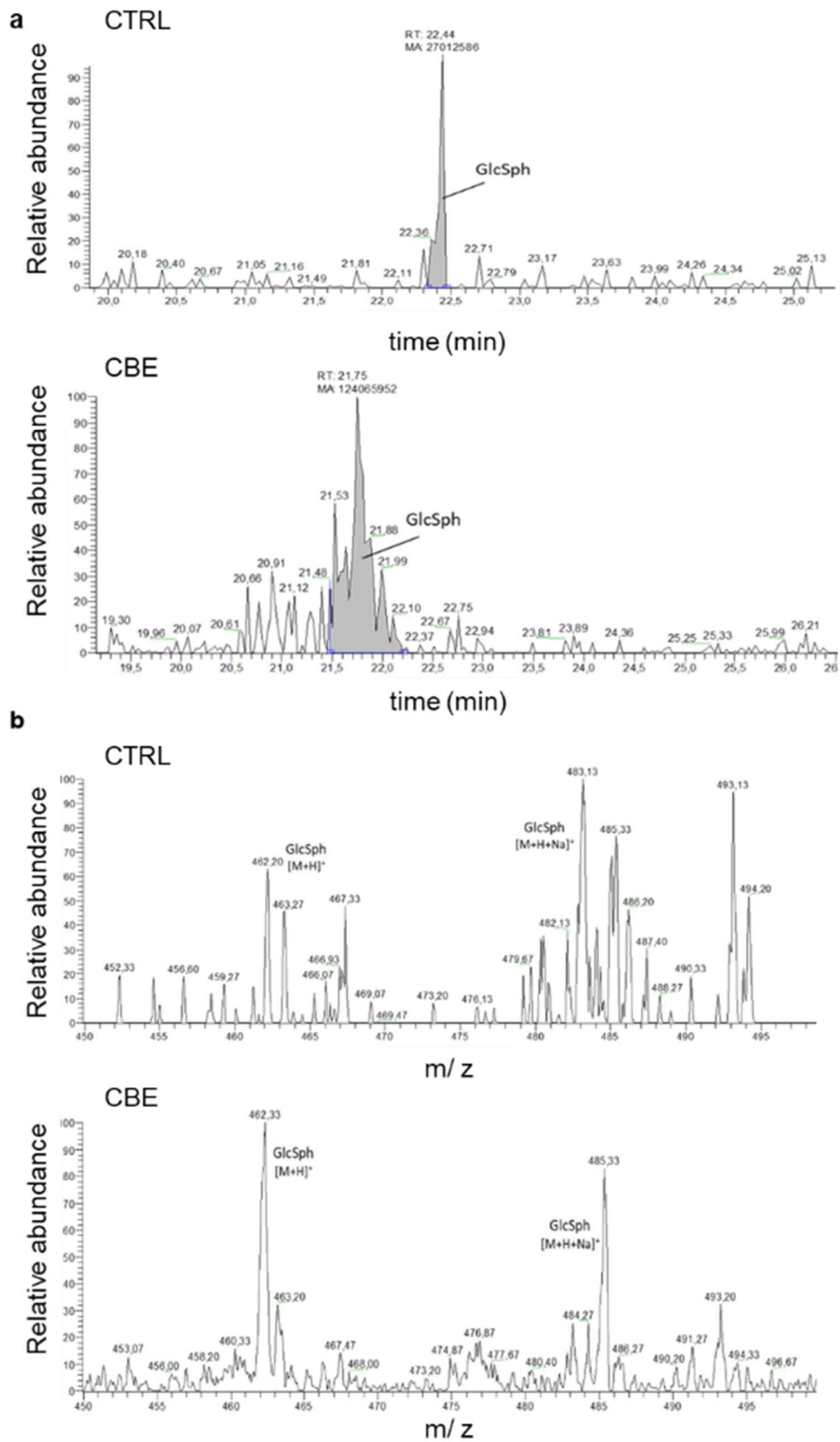
iPSCs-derived dopaminergic neurons



Supplementary figure S6

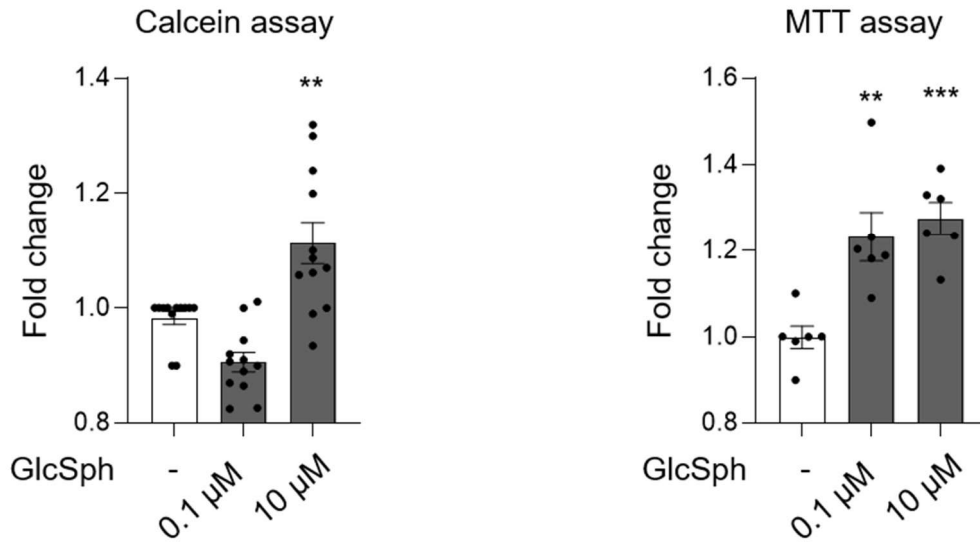


Supplementary figure S7

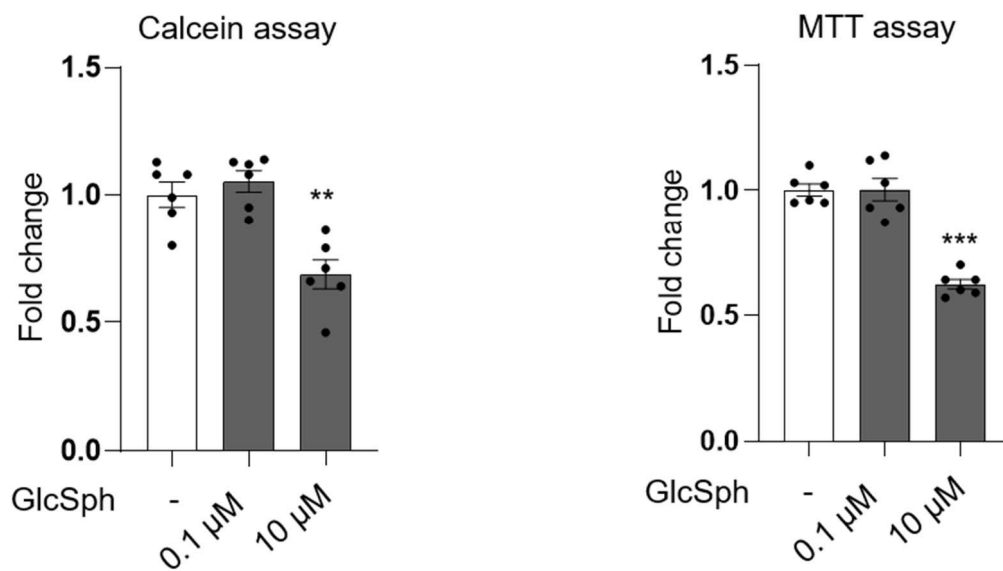


Supplementary figure S8

a Cerebellar granule neurons



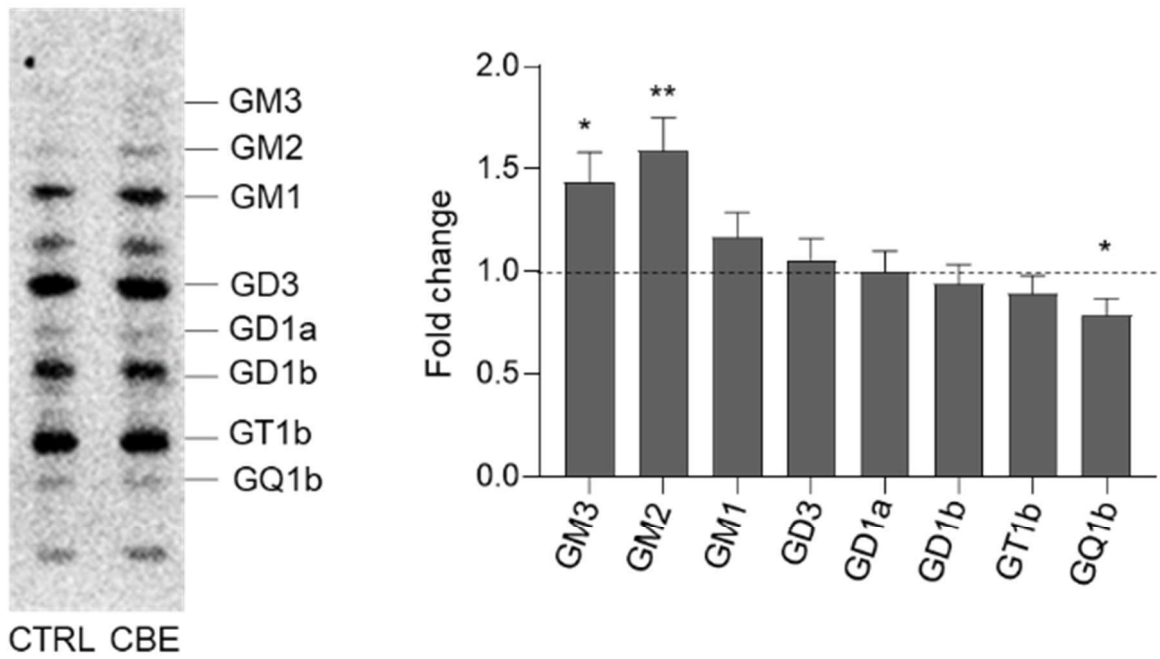
b iPSCs-derived dopaminergic neurons



Supplementary figure S9

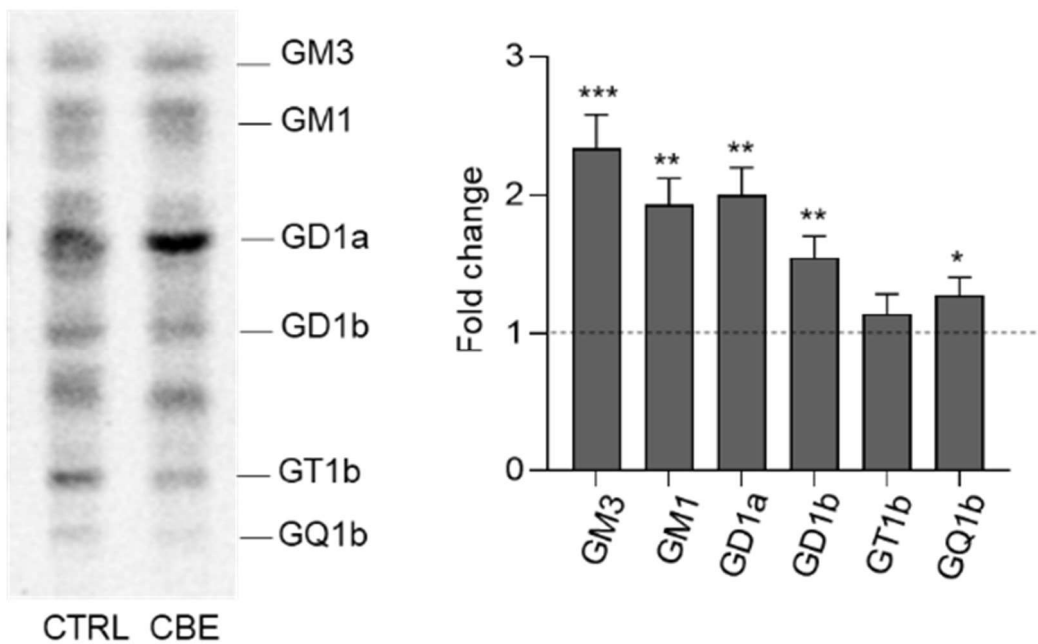
a

Cerebellar granule neurons



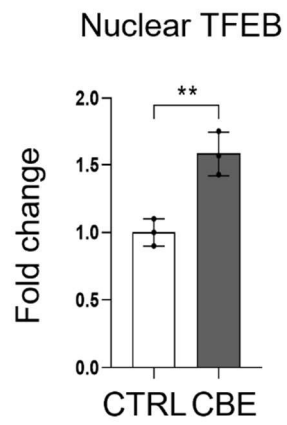
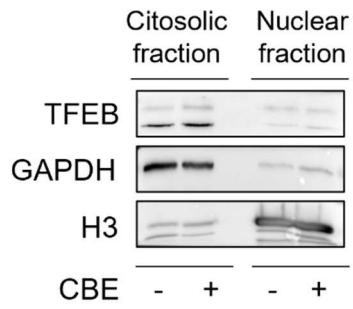
b

iPSCs-derived dopaminergic neurons

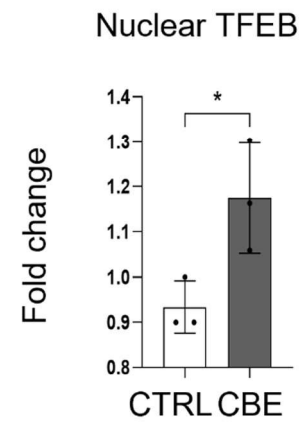
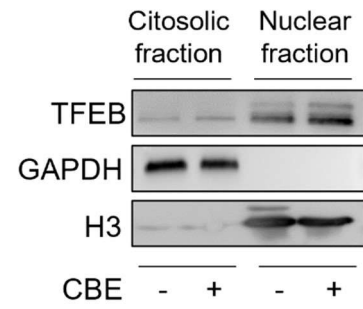


Supplementary figure S10

a Cerebellar granule neurons

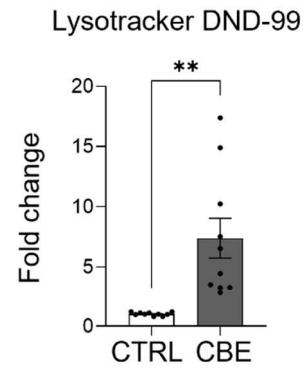
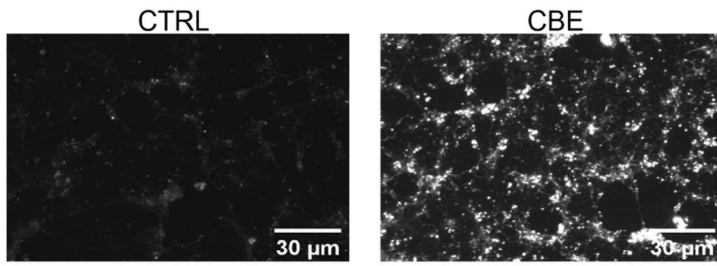


b iPSCs-derived dopaminergic neurons

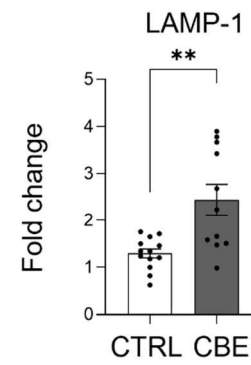
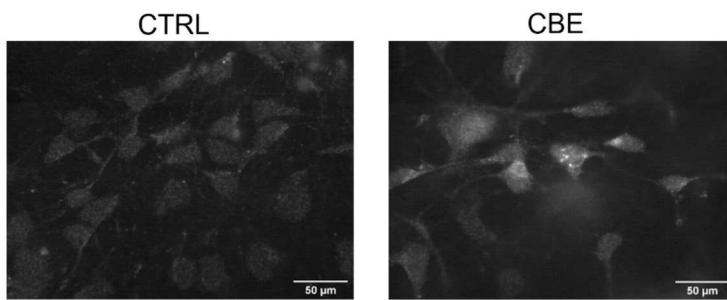


Supplementary figure S11

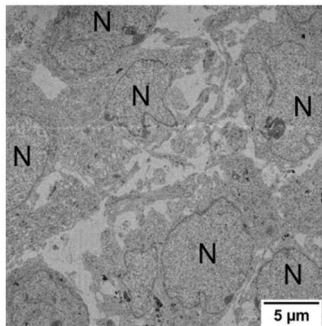
a Cerebellar granule neurons



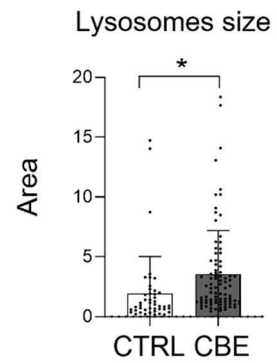
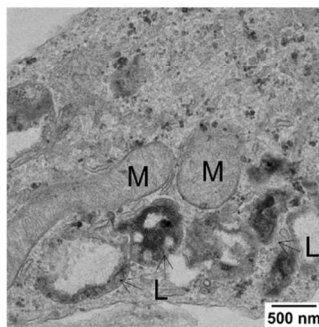
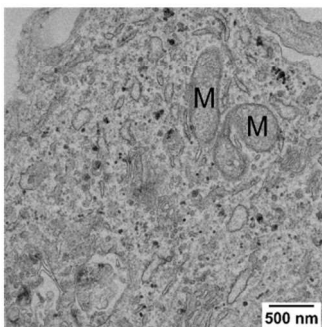
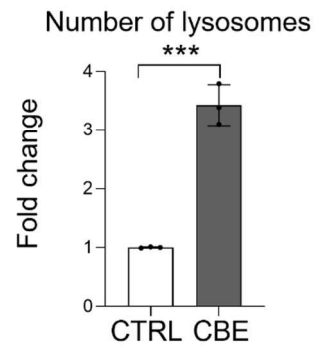
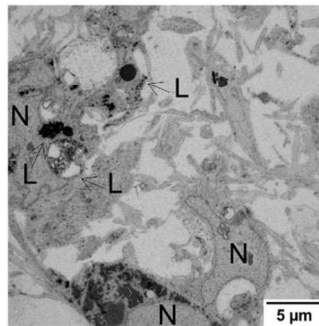
b iPSCs-derived dopaminergic neurons



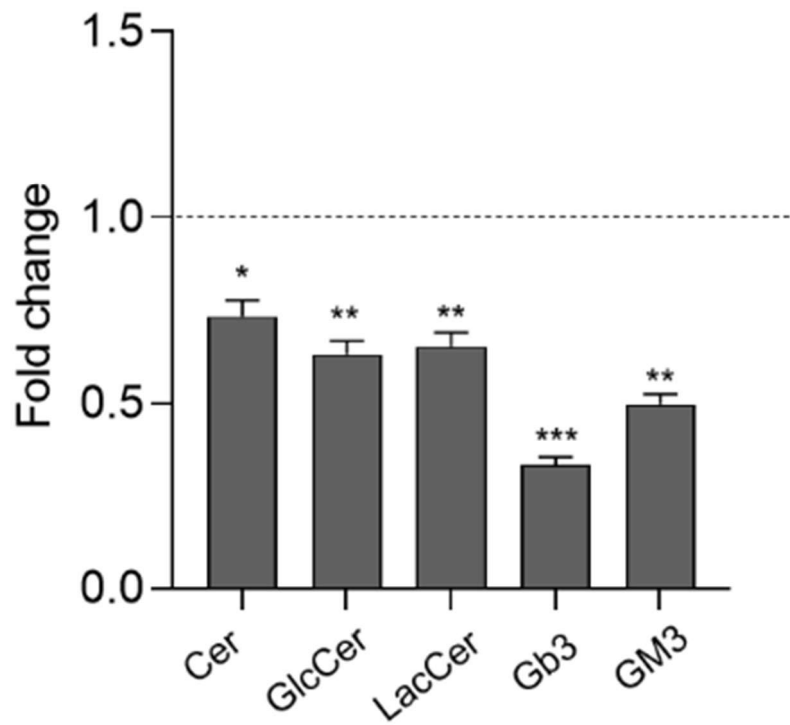
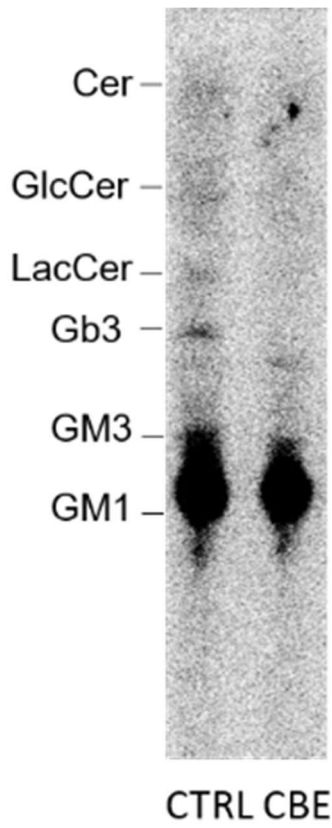
c CTRL



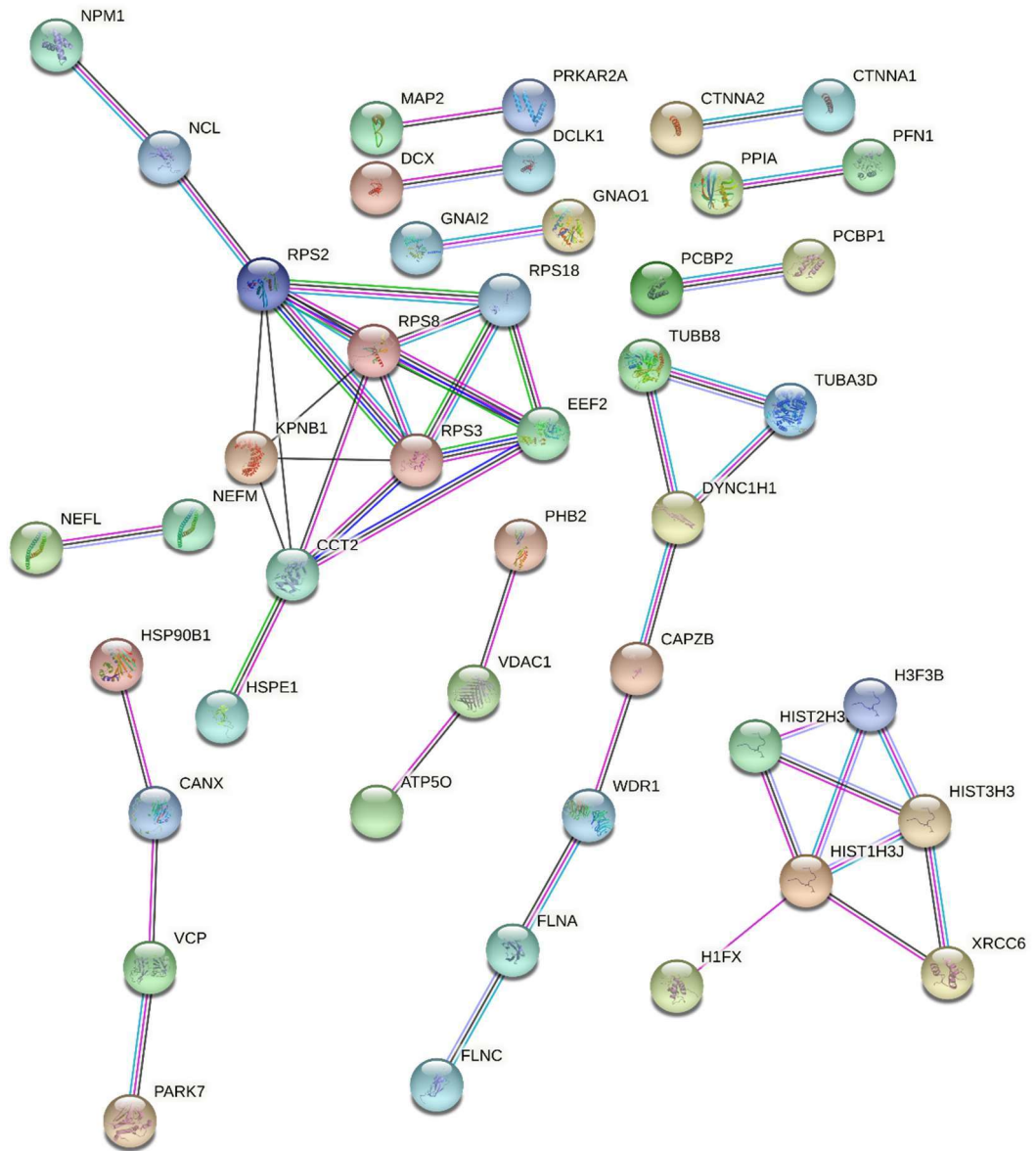
CBE



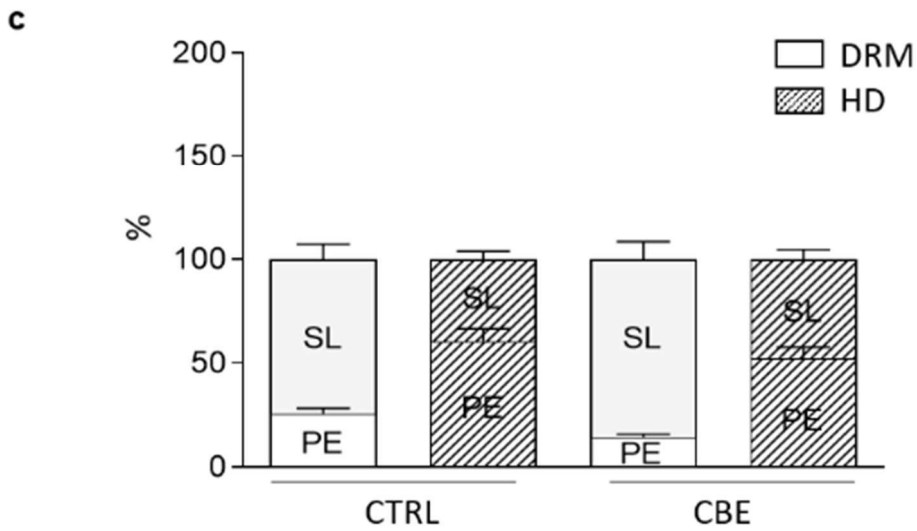
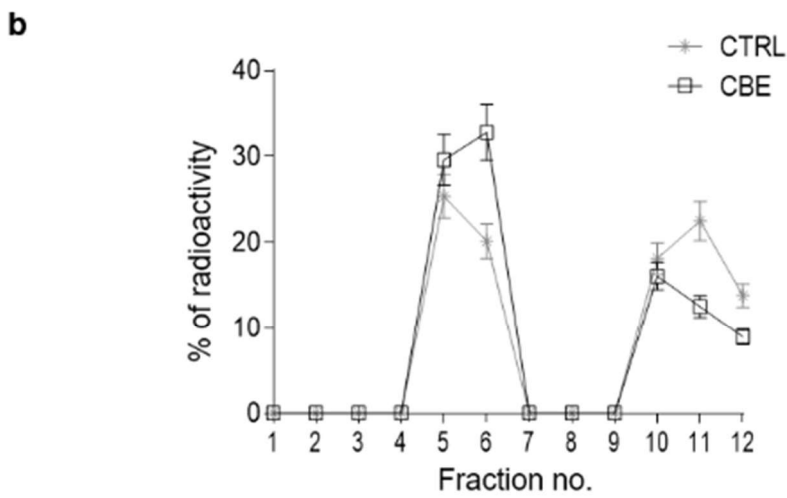
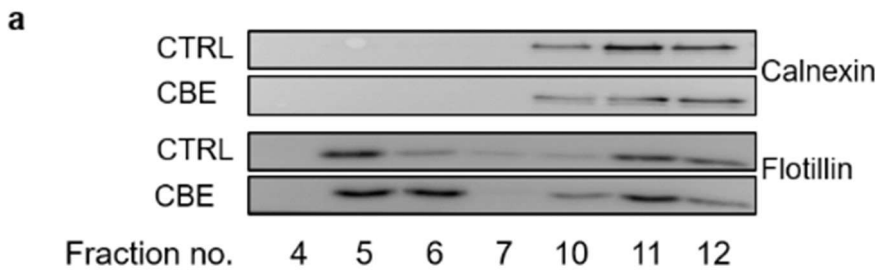
Supplementary figure S12



Supplementary figure S13



Supplementary figure S14



Supplementary table S1 List of the proteins upregulated in CBE-treated neurons compared to untreated cells.

ID	Gene name	Protein name	t-value	p-value
P08962	CD63	CD63 antigen	12,36	0,001
P07602	PSAP	Prosaposin (Sphingolipid activator protein)	11,84	0,000
P17900	SAP3	Ganglioside GM2 activator	10,33	0,000
P78310	CXAR	Coxsackievirus and adenovirus receptor	10,00	0,000
Q9H0U6	RM18	39S ribosomal protein L18, mitochondrial	7,31	0,001
O00115	DNS2A	Deoxyribonuclease-2-alpha	7,18	0,004
P43003	EAA1	Excitatory amino acid transporter 1	6,11	0,005
P61916	NPC2	NPC intracellular cholesterol transporter 2	5,46	0,010
Q9C0H2	TTYH3	Protein tweety homolog 3	5,42	0,012
P06753	TPM3	Tropomyosin alpha-3 chain	5,25	0,006
Q9UK22	FBX2	F-box only protein 2	5,19	0,006
O15540	FABP7	Fatty acid-binding protein, brain	5,11	0,004
Q9NWB6	ARGL1	Arginine and glutamate-rich protein 1	5,11	0,011
Q9UPT8	ZC3H4	Zinc finger CCCH domain-containing protein 4	5,06	0,007
Q08722	CD47	Leukocyte surface antigen CD47	4,69	0,006
Q92889	XPF	DNA repair endonuclease XPF	4,67	0,003
P52943	CRIP2	Cysteine-rich protein 2	4,63	0,007
P12956	XRCC6	X-ray repair cross-complementing protein 6	4,35	0,008
Q92542	NICA	Nicastrin	4,27	0,006
P11279	LAMP1	Lysosome-associated membrane glycoprotein 1 (LAMP-1)	4,26	0,009
O15400	STX7	Syntaxin-7	4,09	0,018
Q16850	CP51A	Lanosterol 14-alpha demethylase (LDM)	3,93	0,008
Q9H910	JUPI2	Jupiter microtubule associated homolog 2	3,91	0,008
P51608	MECP2	Methyl-CpG-binding protein 2 (MeCp-2 protein)	3,90	0,020
P34913	HYES	Bifunctional epoxide hydrolase 2	3,87	0,014
P53778	MK12	Mitogen-activated protein kinase 12 (MAP kinase 12)	3,84	0,010
Q96B54	ZN428	Zinc finger protein 428	3,80	0,028
Q16352	AINX	Alpha-intermexin	3,71	0,020
P28799	GRN	Progranulin	3,69	0,027
P46821	MAP1B	Microtubule-associated protein 1B (MAP-1B)	3,63	0,033
Q9UHG2	PCS1N	ProSAAS (Proprotein convertase subtilisin/kexin type 1 inhibitor)	3,63	0,019
Q9H1E5	TMX4	Thioredoxin-related transmembrane protein 4	3,58	0,014
Q14197	ICT1	Peptidyl-tRNA hydrolase ICT1, mitochondrial	3,54	0,035
O75781	PALM	Paralemmin-1 (Paralemmin)	3,53	0,022
P62263	RS14	40S ribosomal protein S14	3,51	0,027
Q16880	CGT	2-hydroxyacylsphingosine 1-beta-galactosyltransferase	3,51	0,013
B7ZBB8	PP13G	Protein phosphatase 1 regulatory subunit 3G	3,49	0,021
P54803	GALC	Galactocerebrosidase	3,49	0,016
P46976	GLYG	Glycogenin-1	3,46	0,014
Q6UWZ7	ABRX1	BRCA1-A complex subunit Abraxas 1	3,45	0,033
Q13185	CBX3	Chromobox protein homolog 3	3,42	0,016
P14209	CD99	CD99 antigen	3,35	0,042

Q43657	TSN6	Tetraspanin-6	3,23	0,019
Q9P2W1	HOP2	Homologous-pairing protein 2 homolog (Nuclear receptor coactivator GT198)	3,22	0,030
Q01844	EWS	RNA-binding protein EWS	3,20	0,023
Q7Z4V5	HDGR2	Hepatoma-derived growth factor-related protein 2	3,18	0,038
P10620	MGST1	Microsomal glutathione S-transferase 1	3,13	0,025
Q9Y2B9	IPKG	cAMP-dependent protein kinase inhibitor gamma (PKI-gamma)	3,09	0,023
Q15262	PTPRK	Receptor-type tyrosine-protein phosphatase kappa	3,08	0,045
O94811	TPPP	Tubulin polymerization-promoting protein (TPPP)	3,05	0,025
Q14061	COX17	Cytochrome c oxidase copper chaperone	3,05	0,033
P20020	AT2B1	Plasma membrane calcium-transporting ATPase 1	3,04	0,033
Q8TB36	GDAP1	Ganglioside-induced differentiation-associated protein 1 (GDAP1)	3,02	0,026
O15347	HMGB3	High mobility group protein B3	2,97	0,025
Q969E2	SCAM4	Secretory carrier-associated membrane protein 4	2,96	0,031
P56211	ARP19	cAMP-regulated phosphoprotein 19	2,95	0,027
P37802	TAGL2	Transgelin-2	2,92	0,031
Q16799	RTN1	Reticulon-1	2,91	0,046
Q9NZ43	USE1	Vesicle transport protein USE1 (Putative MAPK-activating protein PM26)	2,88	0,042
Q9NS86	LANC2	LanC-like protein 2	2,82	0,049
Q9BWM7	SFXN3	Sideroflexin-3	2,82	0,032
Q6P1L5	F117B	Protein FAM117B	2,80	0,033
P61601	NCALD	Neurocalcin-delta	2,69	0,046
Q96BM9	ARL8A	ADP-ribosylation factor-like protein 8A	2,67	0,048
Q5SQI0	ATAT	Alpha-tubulin N-acetyltransferase 1	2,63	0,040
Q5T7N2	LITD1	LINE-1 type transposase domain-containing protein 1	2,61	0,042
Q9P2B2	FPRP	Prostaglandin F2 receptor negative regulator	2,61	0,045
Q9P0M9	RM27	39S ribosomal protein L27, mitochondrial	2,60	0,044
P18065	IBP2	Insulin-like growth factor-binding protein 2 (IBP-2)	2,51	0,046
Q8IVM0	CCD50	Coiled-coil domain-containing protein 50	2,50	0,046

Supplementary table S2 List of the proteins down-regulated in CBE-treated neurons compared to untreated cells.

ID	Gene name	Protein name	t-value	p-value
P26885	FKBP2	Peptidyl-prolyl cis-trans isomerase FKBP2	-2,50	0,048
Q9Y5L0	TNPO3	Transportin-3 (Importin-12)	-2,54	0,045
P62312	LSM6	U6 snRNA-associated Sm-like protein LSm6	-2,56	0,046
P29373	RABP2	Cellular retinoic acid-binding protein 2	-2,64	0,040
P62942	FKB1A	Peptidyl-prolyl cis-trans isomerase FKBP1A	-2,64	0,039
P56134	ATPK	ATP synthase subunit f, mitochondrial	-2,68	0,037
Q9BVT8	TMUB1	Transmembrane and ubiquitin-like domain-containing protein 1	-2,69	0,048
O15260	SURF4	Surfeit locus protein 4	-2,71	0,047
P61020	RAB5B	Ras-related protein Rab-5B	-2,71	0,035
P62861	RS30	40S ribosomal protein S30	-2,74	0,040
Q96EC8	YIPF6	Protein YIPF6	-2,76	0,034
Q9NR31	SAR1A	GTP-binding protein SAR1a	-2,84	0,030
Q14165	MLEC	Malectin	-2,85	0,035
O95861	BPNT1	3'(2'),5'-bisphosphate nucleotidase 1	-2,86	0,044
O43488	ARK72	Aflatoxin B1 aldehyde reductase member 2	-2,87	0,029
O43324	MCA3	Eukaryotic translation elongation factor 1 epsilon-1	-2,93	0,043
P38117	ETFB	Electron transfer flavoprotein subunit beta	-2,99	0,025
Q9NPJ3	ACO13	Acyl-coenzyme A thioesterase 13	-3,02	0,027
P51991	ROA3	Heterogeneous nuclear ribonucleoprotein A3	-3,02	0,042
P62310	LSM3	U6 snRNA-associated Sm-like protein LSm3	-3,04	0,024
P62318	SMD3	Small nuclear ribonucleoprotein Sm D3	-3,05	0,030
O94766	B3GA3	Galactosylgalactosylxylosylprotein 3-beta-glucuronosyltransferase 3	-3,05	0,023
P25208	NFYB	Nuclear transcription factor Y subunit beta	-3,07	0,034
Q9Y5U9	IR3IP	Immediate early response 3-interacting protein 1	-3,10	0,024
Q6BDS2	URFB1	UHRF1-binding protein 1	-3,12	0,033
P53597	SUCA	Succinate--CoA ligase [ADP/GDP-forming] subunit alpha, mitochondrial	-3,17	0,028
P61960	UFM1	Ubiquitin-fold modifier 1	-3,17	0,020
P22626	ROA2	Heterogeneous nuclear ribonucleoproteins A2/B1	-3,20	0,026
P60468	SC61B	Protein transport protein Sec61 subunit beta	-3,21	0,025
Q6NUQ4	TM214	Transmembrane protein 214	-3,23	0,044
Q16650	TBR1	T-box brain protein 1	-3,34	0,030
Q9H0V9	LMA2L	VIP36-like protein	-3,43	0,039
P24752	THIL	Acetyl-CoA acetyltransferase, mitochondrial	-3,43	0,027
P20340	RAB6A	Ras-related protein Rab-6A (Rab-6)	-3,47	0,014
P61081	UBC12	NEDD8-conjugating enzyme Ubc12	-3,49	0,013
P29762	RABP1	Cellular retinoic acid-binding protein 1	-3,50	0,013
O75396	SC22B	Vesicle-trafficking protein SEC22b	-3,53	0,031
Q96AY3	FKB10	Peptidyl-prolyl cis-trans isomerase FKBP10	-3,60	0,034
Q96EX1	SIM12	Small integral membrane protein 12	-3,62	0,014
Q9Y3D6	FIS1	Mitochondrial fission 1 protein	-3,63	0,013
Q5EB52	MEST	Mesoderm-specific transcript homolog protein	-3,72	0,013

Q43772	MCAT	Mitochondrial carnitine/acylcarnitine carrier protein	-3,74	0,012
P61923	COPZ1	Coatomeer subunit zeta-1	-3,78	0,009
O75880	SCO1	Protein SCO1 homolog, mitochondrial	-3,85	0,019
P09972	ALDOC	Fructose-bisphosphate aldolase C	-3,86	0,026
O60783	RT14	28S ribosomal protein S14, mitochondrial	-3,98	0,007
P13674	P4HA1	Prolyl 4-hydroxylase subunit alpha-1	-4,00	0,010
Q96DB5	RMD1	Regulator of microtubule dynamics protein 1	-4,00	0,011
Q07955	SRSF1	Serine/arginine-rich splicing factor 1	-4,06	0,023
Q5JWF2	GNAS1	Guanine nucleotide-binding protein G(s) subunit alpha isoforms XLas	-4,10	0,011
O43237	DC1L2	Cytoplasmic dynein 1 light intermediate chain 2	-4,14	0,007
O75323	NIPS2	Protein NipSnap homolog 2	-4,45	0,011
Q969M3	YIPF5	Protein YIPF5 (Five-pass transmembrane protein localizing in the Golgi apparatus and the endoplasmic reticulum 5)	-4,48	0,004
O75347	TBCA	Tubulin-specific chaperone A	-4,50	0,007
P32322	P5CR1	Pyrroline-5-carboxylate reductase 1, mitochondrial	-4,57	0,005
O60831	PRAF2	PRA1 family protein 2	-4,58	0,015
Q13596	SNX1	Sorting nexin-1	-4,65	0,004
P45877	PPIC	Peptidyl-prolyl cis-trans isomerase C	-4,74	0,003
Q9BUJ2	HNRL1	Heterogeneous nuclear ribonucleoprotein U-like protein 1	-4,86	0,007
Q969R2	OSBP2	Oxysterol-binding protein 2	-5,06	0,002
O14832	PAHX	Phytanoyl-CoA dioxygenase, peroxisomal	-5,27	0,009
Q9GZS3	WDR61	WD repeat-containing protein 61	-5,75	0,002
Q8TBQ9	KISHA	Protein kish-A	-5,83	0,002
Q71UI9	H2AV	Histone H2A.V	-5,85	0,001
O15269	SPTC1	Serine palmitoyltransferase 1	-6,27	0,001
Q96GQ5	RUSF1	RUS family member 1	-6,46	0,001
Q9HD45	TM9S3	Transmembrane 9 superfamily member 3	-8,36	0,003
Q13242	SRSF9	Serine/arginine-rich splicing factor 9	-8,41	0,001
P43307	SSRA	Translocon-associated protein subunit alpha (TRAP-alpha)	-9,45	0,000
Q9BRA2	TXD17	Thioredoxin domain-containing protein 17	-9,89	0,000
Q9Y5M8	SRPRB	Signal recognition particle receptor subunit beta	-13,23	0,000

Supplementary table S3 List of the proteins only expressed in the IP of CBE treated neurons in the comparison CBE treated vs CBE untreated neurons

ID	Gene name	Protein name
P61604	CH10	10 kDa heat shock protein, mitochondrial
P62269	RS18	40S ribosomal protein S18
P15880	RS2	40S ribosomal protein S2
P23396	RS3	40S ribosomal protein S3
P62241	RS8	40S ribosomal protein S8
P48047	ATPO	ATP synthase subunit O, mitochondrial
P27824	CALX	Calnexin OS=Homo sapiens
Q15417	CNN3	Calponin-3 OS=Homo sapiens
P13861	KAP2	cAMP-dependent protein kinase type II-alpha regulatory subunit
P35221	CTNA1	Catenin alpha-1 OS=Homo sapiens
P26232	CTNA2	Catenin alpha-2 OS=Homo sapiens
Q00610	CLH1	Clathrin heavy chain 1 OS=Homo sapiens
Q14204	DYHC1	Cytoplasmic dynein 1 heavy chain 1
P13639	EF2	Elongation factor 2 OS=Homo sapiens
P14625	ENPL	Endoplasmin OS=Homo sapiens
P47756	CAPZB	F-actin-capping protein subunit beta
P21333	FLNA	Filamin-A OS=Homo sapiens
Q14315	FLNC	Filamin-C OS=Homo sapiens
P00367	DHE3	Glutamate dehydrogenase 1, mitochondrial
P04899	GNAI2	Guanine nucleotide-binding protein G(i) subunit alpha-2
Q9UBI6	GBG12	Guanine nucleotide-binding protein G(I)/G(S)/G(O) subunit gamma
P09471	GNAO	Guanine nucleotide-binding protein G(o) subunit alpha
P16401	H15	Histone H1.5
Q92522	H1X	Histone H1x
P68431	H31	Histone H3.1
Q16695	H31T	Histone H3.1t
Q71DI3	H32	Histone H3.2
P84243	H33	Histone H3.3
P50502	F10A1	Hsc70-interacting protein
Q14974	IMB1	Importin subunit beta-1
Q9NZI8	IF2B1	Insulin-like growth factor 2 mRNA-binding protein 1
Q12906	ILF3	Interleukin enhancer-binding factor 3
Q9UK76	JUPI1	Jupiter microtubule associated homolog 1
P35908	K22E	Keratin, type II cytoskeletal 2 epidermal
P42166	LAP2A	Lamina-associated polypeptide 2, isoform alpha
P42167	LAP2B	Lamina-associated polypeptide 2, isoforms beta/gamma
P11137	MTAP2	Microtubule-associated protein 2
P60660	MYL6	Myosin light polypeptide 6
P29966	MARCS	Myristoylated alanine-rich C-kinase substrate
O95865	DDAH2	N(G),N(G)-dimethylarginine dimethylaminohydrolase 2
P13591	NCAM1	Neural cell adhesion molecule 1

P07196	NFL	Neurofilament light polypeptide
P07197	NFM	Neurofilament medium polypeptide
O43602	DCX	Neuronal migration protein doublecortin
P19338	NUCL	Nucleolin
P06748	NPM	Nucleophosmin
P62937	PPIA	Peptidyl-prolyl cis-trans isomerase A
Q06830	PRDX1	Peroxiredoxin-1
P30086	PEBP1	Phosphatidylethanolamine-binding protein 1
P18669	PGAM1	Phosphoglycerate mutase 1
Q15365	PCBP1	Poly(rC)-binding protein 1
Q15366	PCBP2	Poly(rC)-binding protein 2
Q92841	DDX17	Probable ATP-dependent RNA helicase DDX17
P07737	PROF1	Profilin-1
Q99623	PHB2	Prohibitin-2
Q99497	PARK7	Protein/nucleic acid deglycase DJ-1
P31150	GDIA	Rab GDP dissociation inhibitor alpha
O15075	DCLK1	Serine/threonine-protein kinase DCLK1
Q04837	SSBP	Single-stranded DNA-binding protein, mitochondrial
Q13813	SPTN1	Spectrin alpha chain, non-erythrocytic 1
Q7KZF4	SND1	Staphylococcal nuclease domain-containing protein 1
P78371	TCPB	T-complex protein 1 subunit beta
Q9UI15	TAGL3	Transgelin-3
P55072	TERA	Transitional endoplasmic reticulum ATPase
P29401	TKT	Transketolase
P55084	ECHB	Trifunctional enzyme subunit beta, mitochondrial
Q13748	TBA3C	Tubulin alpha-3C/D chain
Q3ZCM7	TBB8	Tubulin beta-8 chain
P09936	UCHL1	Ubiquitin carboxyl-terminal hydrolase isozyme L1
P21796	VDAC1	Voltage-dependent anion-selective channel protein 1
O75083	WDR1	WD repeat-containing protein 1
P12956	XRCC6	X-ray repair cross-complementing protein 6

References

- 1 Valsecchi, M. *et al.* Ceramide and sphingomyelin species of fibroblasts and neurons in culture. *J Lipid Res* **48**, 417-424, doi:10.1194/jlr.M600344-JLR200 (2007).
- 2 Li, Y. T. *et al.* Selective extraction and effective separation of galactosylsphingosine (psychosine) and glucosylsphingosine from other glycosphingolipids in pathological tissue samples. *Neurochem Res* **36**, 1612-1622, doi:10.1007/s11064-010-0348-3 (2011).
- 3 Merrill, A. H., Jr. Sphingolipid and glycosphingolipid metabolic pathways in the era of sphingolipidomics. *Chem Rev* **111**, 6387-6422, doi:10.1021/cr2002917 (2011).
- 4 Shaner, R. L. *et al.* Quantitative analysis of sphingolipids for lipidomics using triple quadrupole and quadrupole linear ion trap mass spectrometers. *J Lipid Res* **50**, 1692-1707, doi:10.1194/jlr.D800051-JLR200 (2009).